A new free-wave technique for ~~dielectric~~ measuring materials ~~and ferrite measurement~~ dielectric and magnetic properties at millimetre wavelengths

by

Abolfazl Khosrowbeygi Borchalooei

A thesis submitted to the University of London for the Degree of Doctor of Philosophy in Electronic Engineering

Department of Electronic and Electrical Engineering
UNIVERSITY COLLEGE LONDON

1994

ProQuest Number: 10045558

All rights reserved

INFORMATION TO ALL USERS
The quality of this reproduction is dependent upon the quality of the copy submitted.

In the unlikely event that the author did not send a complete manuscript
and there are missing pages, these will be noted. Also, if material had to be removed,
a note will indicate the deletion.

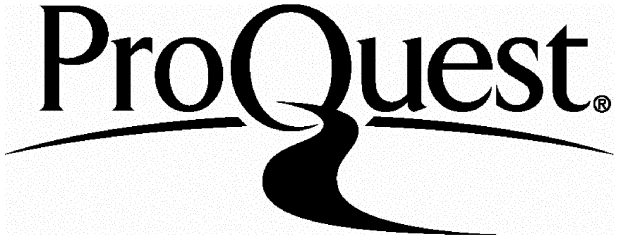

ProQuest 10045558

Published by ProQuest LLC(2016). Copyright of the Dissertation is held by the Author.

All rights reserved.
This work is protected against unauthorized copying under Title 17, United States Code.
Microform Edition © ProQuest LLC.

ProQuest LLC
789 East Eisenhower Parkway
P.O. Box 1346
Ann Arbor, MI 48106-1346

Abstract

The complex permittivity and permeability of materials can be measured by different techniques, but none of the conventional methods is appropriate for measuring lossy materials at millimetre wavelengths. In this thesis a new free-wave technique for measuring the properties of lossy materials at these frequencies is introduced.

Free-wave and conventional measurement techniques are reviewed. The sources of error in free-wave measurements are explained, and ways to reduce their impact from the measurement results are discussed. Various methods for calculating the sample properties from the measured parameters are introduced, and the dependence of the sample properties on these parameters are studied. The total error in the sample properties is investigated, and the optimum way of using the measured data is presented.

The use of time gating for removing unwanted reflections from the measurement results is explained, and the gating error due to discarding higher order terms of multiple reflections within the slab for an ideal time domain gate is calculated. The gating error for a real gate is simulated and compared with the calculated values for an ideal gate. Removing multiple reflections within the sample by the time gating technique is introduced, and the minimum electrical length of the sample is estimated. It is also shown that ignoring multiple reflections within the sample improves the total accuracy.

An angular spectrum model considering the measurement in the near-field region is introduced. The accuracy improvement delivered by this model is demonstrated by simulation techniques, and the minimum antenna distance to ignore the wavefront curvature error is estimated. The key parameters in constructing a compact single-pass system for measuring material properties in the range of 26.5-40 GHz are presented, and examples of the results obtained from measurements of ferrite and dielectric samples are presented and discussed. Finally the achievements obtained in this project are summarised, and further work to improve free-wave measurement techniques is suggested.

. . . To my mother and father

Whose patience, understanding and encouragements helped me to complete this research

Acknowledgements

I would like to express my sincere gratitude to Professor H.D. Griffiths for expert supervision and advice throughout the course of this work. As Head of the Antennas and Radar Group, he provided the friendly environment in which this research flourished. His positive attitude and assistance in providing the required hardware and also in solving my personal and academic problems will never be forgotten.

My very sincere gratitude to Professor A.L. Cullen, who has been my co-supervisor, for his invaluable kindly lessons of life and engineering. His broad and profound knowledge of electromagnetics and microwave engineering and also his ability to simplify complicated problems deserve the admiration of any microwave engineer, including myself. As the initiator of this research, Prof. Cullen's contribution in directing this research has been invaluable. It has been my honour to carry out this research under his supervision.

I am specially grateful to Dr. A.L. Lynch for sharing with me his invaluable theoretical knowledge and practical experience. I am indebted to him for taking an active interest in this project and for many fruitful discussions and invaluable suggestions.

Thanks also go to Dr. K. Milne and Dr. R. Benjamin, both Visiting Professors at UCL. Their invaluable discussions and periodic comments are gratefully acknowledged. I would like to thank Mr. K. Pitman, Dr. S. Appleton, Mr. I. Youngs and Dr. D. Simkin of DRA (Holton Heath) for providing the required ferrite samples and the hardware during the main course of this project

Thanks are also due to all members of the Antennas and Radar Group, and in particular, Dr. A. Khanifar and Dr. B. Pourseyyed for many fruitful discussions, invaluable advice and assistance. The help of Dr. P.V. Brennan in correcting the script of this thesis is also gratefully acknowledged.

I am also indebted to my ex-colleagues at ITRC, M.H. Entezari, B. Ghanbari, H. Shakeri, M. Khosravi, N. Jahangard and Dr. M. Hakkak without whose help this research would not have been completed.

Finally, I would like to thank the following institutions for providing financial assistance during this research:

The Ministry of Culture and Higher Education (Iran)
Edmond Davis Scholarship (University of London)
Overseas Research Scholarship (UK)
DRA(Holton Heath)

Table of contents

4. Sources of error

5 Time gating

List of symbols

Symbol	Definition
Γ	Reflection coefficient of a semi-infinite slab.
Γ_t	Reflection coefficient of a slab of finite thickness
$\Gamma_{\parallel}$	Reflection coefficient from of a semi-infinite at parallel polarisation.
$\Gamma_{\perp}$	Reflection coefficient of a semi-infinite slab at perpendicular polarisation.
$\Gamma_{t\parallel}$	Reflection coefficient of a slab of finite thickness at parallel polarisation.
$\Gamma_{t\perp}$	Reflection coefficient of a slab of finite thickness at perpendicular polarisation.
T_t	Transmission coefficient of a slab of finite thickness at perpendicular polarisation.
$T_{t\parallel}$	Transmission coefficient of a slab of finite thickness at parallel polarisation.
P	Propagation coefficient.
λ_o	Wavelength in free space.
λ	Wavelength within the sample.
CF	Correction factor, transmission measurement.
θ	Incident angle with respect to the normal to the sample surface.
ε_r	Relative complex permittivity ($\varepsilon_r=\varepsilon'+j\varepsilon''$).
ε'	Real part of the relative permittivity.
ε''	Imaginary part of the relative permittivity.
μ_r	Relative complex permeability ($\mu_r=\mu'+j\mu''$).
μ'	Real part of the relative permeability.
μ''	Imaginary part of the relative permeability.
Z_S	Wave impedance within the sample.

Z_C	Characteristic impedance of transmission line.
R	Resistance per unit length.
L	Inductance per unit length.
G	Conductance per unit length.
C	Capacitance per unit length.
ω	Angular frequency
Φ_{Rmax}	Maximum phase error in reflection measurement.
Φ_{Tmax}	Maximum phase error in transmission measurement.
M_{Rmax}	Maximum magnitude error in reflection measurement.
M_{Tmax}	Maximum magnitude error in reflection measurement.

List of figures

List of Tables

1 Introduction

1.1 Background

Knowledge of the complex permittivity and permeability of materials is needed for many purposes, and the required measurement accuracy varies in different applications. The design of resonators, lenses, radomes, etc., needs precise measurement of dielectric properties, while in industrial heating applications the loss properties of the materials are of great importance. The magnetic properties of materials should be precisely known in designing isolators, circulators, and radiation absorbing layers.

At millimetre wavelengths, conventional measurement techniques (waveguide and cavity resonator) become inaccurate and difficult to use. The maximum operating frequencies of these techniques are limited by the size of the waveguide or cavity. Open resonators are also inherently appropriate for low-loss materials at these frequencies, but they run into difficulty in measuring lossy materials.

Free-wave measurement techniques use TEM propagation without continuous guiding constraints, and the specimen can be relatively easily introduced into the measurement system. In these techniques, the sample should have flat and parallel surfaces with known thickness, and the sample size in the transverse direction should be large enough to intercept the incident wave adequately. The capability of measuring lossy materials and relatively easy sample preparation make free-wave techniques attractive at millimetre wave frequencies.

Although free-wave techniques are not new, they have not been employed extensively for measuring material properties. Lower accuracy with respect to resonance methods and inaccuracy in measuring the fields are the main factors that have restricted their popularity. The propagation of waves in an unbounded region introduces error in the measured transmission and reflection coefficients which cannot be removed by conventional error correction techniques.

The use of error correction techniques and time domain gating have resulted in improved accuracy in the new generation of automatic vector network analysers. The ability of measuring scattering parameters and removing systematic error over a wide range of frequencies has initiated the idea of using automatic network analysers in free-wave measurements. Regarding the increasing demand for employing mm-wave frequencies in military and civil applications, free-wave methods are considered as potential techniques for measuring the properties of lossy materials at mm-wave frequencies. Since these techniques are non-destructive and contact-less, they can be used for measuring a wide range of materials at different physical conditions. Free-wave methods deliver relatively poor accuracy with respect to resonance methods and are basically appropriate for measuring the properties of materials with high loss tangents. In spite of these intrinsic limitations, they provide a unique technique for measuring complex permittivity and permeability of lossy materials at mm-wave frequencies

1.2 Thesis layout and objectives

The lack of a reliable technique to measure the complex permittivity and permeability of lossy materials at millimetre wavelengths has been one of the main obstacles in developing and testing new materials in this frequency band. The use of multi-layered structures to reduce the radar cross section of ships and aircrafts is one of the main motivations for devising an appropriate measurement technique for characterising lossy ferrites at mm-wave frequencies. The aim of this research is therefore to study free-wave techniques in order to devise a reliable method for measuring the properties of lossy materials at millimetre wavelengths.

This research was indeed initiated by the idea of measuring the magnetic and electrical properties of a sample from the measured reflection coefficient at two polarisations proposed by Cullen [41]. The availability of open resonator as a well established measurement technique for measuring low-loss materials and the potential interest of the industry in measuring lossy ferrites at mm-wave frequencies provided the motivation to devise an appropriate measurement technique for lossy materials and to build a prototype system as the main objectives of this research.

In this research, the development of a practical measurement system and construction of a prototype measurement system have been a high priority. Therefore a great effort has been made to implement and examine the suggested techniques, while also tackling the problems by means of a theoretical approach and simulation techniques have not been put aside throughout this project.

In free-wave techniques, the total error in the sample properties depends on the accuracy of the instrument used for measuring the required parameters. At millimetre wavelengths the measurement instrument and the passive components are extremely expensive, and the required instrument and measurement environment cannot be provided in some cases. Therefore, the effectiveness of different techniques are examined by comparing the results obtained from the measurement of the same sample by different techniques.

The main part of the thesis is devoted to the presentation and discussion of the most important topics such that the reader does not need to go through cumbersome derivations, while the simulation results and derivations can be found in the appendices. Chapter 2 is devoted to reviewing the conventional methods and free-wave measurement techniques, and the basic theory of free-wave measurement methods is presented in chapter 3. In chapter 4 the conventional error terms and the new error sources introduced by the free space paths are studied, and various methods for removing or reducing the impact of the error terms are discussed. The use of time domain gating technique to remove the effect of multiple reflections within the sample and the associated error sources are presented in chapter 5. This chapter continues with a thorough study of this technique and its limitations. In the gating error analysis, the time domain gating error for an ideal gate is calculated and compared with the simulation results. The criteria for considering the sample as thin or thick are presented, and the achieved accuracy improvement is discussed.

In chapter 6, a new mathematical model for calculating transmission and reflection coefficients in the near-field region is introduced, and the use of this model in calculating the material properties is discussed. The error due to the measurement in the near-field and its impact in the calculated material properties are simulated and discussed. Chapter 7 is devoted to the study of the mechanisms contributing to the total error and the mathematical relationships between the measured parameters and the error in permittivity and permeability. In this chapter, the total measurement accuracy for various methods are examined and compared.

In chapter 8, a prototype single-pass free-wave measurement system and the considerations in its design are presented. The measurement procedures are reviewed, and suggestions for improving this system are made. Chapter 9 is devoted to presentation of the results obtained from the measurement of some dielectric and ferrite samples. Chapter 10 completes the thesis by summarizing and reviewing the achievements in this research, and the total accuracy in free-wave methods are discussed and the preferred technique for measuring different types of slabs are recommended. Finally, suggestions for further research in the required areas are presented.

2 Review

2.1 Introduction

Various techniques have been devised for measuring the electric and magnetic properties of material. Although some can be used directly, or modified for measuring magnetic properties, most of the them are appropriate for measuring only dielectric properties. The aim of this chapter is to review different measurement techniques, with an emphasis on free-wave measurement methods.

The techniques for measuring material properties can be categorised into different classes. Each of these methods has its own accuracy, frequency range and limitations. Although there is now complete overlap and coverage from RF to infrared, the description of experimental methods are divided into microwave methods based on microwave hardware, and optical methods which are based, almost but not quite exclusively, on free-space interferometers. As microwave methods are of interest in this project, only these techniques are reviewed in this chapter. The reviews of different measurement techniques by Afsar et al [1], Birch and Clarke [2], Clarke and Rosenberg [3] and Lynch [4] cover virtually all the conventional methods. In the first part of this chapter, conventional techniques are briefly reviewed, then free-wave methods are discussed.

2.2 Low frequency

At frequencies below a few hundred MHz, lumped circuits are used for determining the electric properties of materials, and the classical approach is to treat the sample as a lossy capacitor. The dielectric specimen is placed between two electrodes to form a specimen capacitor, and the complex permittivity of the sample is calculated by measuring this capacitor cell in a bridge or a circuit resonated with an inductor. In this technique, the geometry of the sample is such that its vacuum capacitance can be calculated. The preferred shape is a flat plate with plane and parallel surfaces, either circular or square.

The edge capacitance of the electrodes and the capacitance of the upper electrode to ground introduce error in the measurement. Micrometer electrodes or suitably shielded three-electrode systems can reduce the effect of both the capacitances. Applying electrodes on the sample surfaces increases accuracy in the dielectric constant measurement, but the residual impedances of the electrodes decreases the accuracy in measuring the dissipation factor. At high frequencies, the resistance of the electrodes becomes more significant. In the measurement of low permittivity materials, an intentional air gap may be introduced between the specimen and the electrodes (Lynch [6]).

In the three-electrode technique, one of the measuring electrodes is surrounded by an additional guard electrode. In order to measure the dielectric constant accurately, some type of thin film metallic electrodes must be applied to the specimen. This metallic film improves the contact between the specimen and the electrodes. Air gaps between the sample surface and the electrodes decrease the dissipation factor and cause error in the dielectric constant measurement. There are also some techniques devised to reduce air gaps between the sample surface and electrodes (Von Hippel [5]).

The electrode system can be either fixed or adjustable. In the first case the capacitance changes after inserting the specimen, but in the latter the capacitance is adjusted to the same value before inserting the sample. In the capacitance model of the specimen, the edge capacitance must be taken into account (Lynch [4]). Only in the immersion method, where the specimen is immersed in a liquid of the same permittivity as the specimen, can the edge capacitance be ignored.

The micrometer-controlled electrode system designed by Hartshorn and Ward [7] has low series inductance and resistance, and it yields excellent results whenever two-electrode measurements are acceptable (accuracy of 5 parts in 1000 in permittivity measurement). The electrodes themselves would allow the measurement of loss angles down to 20 microradians or better. In the measurement of specimens larger than electrodes, the correction due to the edge capacitance which is partly in air and partly in the specimen must be considered (Lynch [8]). At frequencies below 1 MHz, a third electrode is used for guarding one of the electrodes. In the frequency range of 1 kHz to 1 MHz accuracies of $\pm 5 \times 10^{-6}$ for power factor and uncertainty of ± 0.1 percent in dielectric measurement can be delivered by this method (Lynch [6]).

In the liquid immersion method, the result is almost independent of the specimen dimensions, provided that the permittivities of the specimen and the liquid are well matched. The advantages of the liquid immersion method apply only in the measurement of permittivity, since the loss tangents of the specimen and liquid are not matched. The main difficulty in measuring the dielectric properties of a liquid is in ensuring their purity. The difficulty of finding a matched liquid for each material is another disadvantage.

Different techniques have been developed to improve the accuracy in bridge measurements (Von Hippel [5] and Lynch [4]). For lossy materials, non-resonant methods using RF bridge are more appropriate. Lynch [9] has described the use of unbalanced bridges for the measurement of dielectric losses up to 100 MHz. A balanced bridge using two different sources locked manually has been reported by Pratt and Smith [10]. This system works from 0.1 Hz to 10 MHz over a temperature range of -200°C to 200°C.

Although bridge methods can be used up to very high frequencies, resonance methods give better accuracy above 1 MHz. The highest frequency of resonant circuits is limited by the smallest inductor that can be built with sufficiently small dissipation factor, to about 200 MHz. At very low frequencies, below 10 Hz, the voltmeter-ammeter method can be used to measure the charging or discharging of a dielectric specimen as a function of time. The measurement may take as long as days, since the current must be observed over a long time at very low frequency, e.g. 10^{-7} Hz. This classical technique needs very sensitive instruments for measuring the voltages or currents. Time domain spectrometry can also be used for measuring dielectric properties of a sample at these frequencies. This is a fast technique but delivers poor accuracy in measuring loss tangents.

At frequencies below 1 MHz electrode systems are usually used, and the capacitance and dissipation factor of the dielectric specimen is measured by a null method in an ac bridge. This method is limited at lower frequencies by the following factors: excessive required time for balancing the bridge, harmonics of the generator and insufficient sensitivity or selectivity of the detectors. After any adjustment, a certain number of cycles must pass to establish equilibrium. Therefore, for frequencies below a few Hertz it becomes too difficult to balance the bridge. The upper frequency of the bridge method is set by the residual impedances in the leads to the specimen, the standards and the bridge components. The bridge method is useful in the frequency range of 10 kHz up to 10 MHz.

In the frequency range of 10 kHz to 200 MHz, the resonant method is usually employed. The capacitance of the specimen is still measured by a substitution method, but loss properties are calculated from the resonance curve. Again, in the resonance method, the upper frequency limit is set by the smallest inductor that can be built with sufficiently low dissipation factor, up to about 200 MHz. The lower frequency limit (10 kHz), which is given by the input impedance of the voltmeter, overlaps the usable frequency in the null methods. The effectiveness of the screening technique decreases rapidly for frequencies above 1 MHz. The unscreened two terminal approach, above 1 MHz, has always delivered large uncertainties (0.5 percent or worse) for permittivity. As this method can measure very low-loss dielectrics (tan $\delta \leq 10$ μrad) in solids by accurate determination of Q-factor, it is still in favour.

A source of error in two-terminal cells is fringing fields, and mathematical correction is usually used to remove it. This technique, as a sensitive method of measuring low-loss polymers, has been the subject of many investigations. At VHF frequencies this technique has been improved for accurate measurement of the complex dielectric constant by Ogawa [11], Kakimoto [12], Kakimoto [13], and Buckingham [14].

At UHF, TEM re-entrant cavities are used for measuring permittivity. In the re-entrant cavity technique, the sample is assumed to have a diameter equal to the resonator metal cores and the fundamental mode (lowest resonant frequency) to be excited. These assumptions introduce some limitations to the measurement method. The maximum value of permittivity is limited up to 20 for the cases where the sample diameter is equal to core diameter, since the off-tuning amount of resonant frequency increases with increasing the permittivity. The second limitation of this method is the maximum loss tangent of the specimen ($\approx 10^{-2}$). This limitation arises from the requirement of filling the area of the cavity where the electric field is high. Kaczkowaski and Milewski [15] reported an uncertainty of ±1 percent in the real part and $\pm(5\% + 5\text{x}10^{-5})$ for loss tangent of a large range of materials by using their computational technique. In their method, the sample size is smaller than the cavity core size. Clarke [16] has used positive feedback to increase the Q-factor of the cavity for measuring of organic liquids. There are also a number of approaches to compute the fields in the re-entrant cavity accurately, e.g., Ciuffini and Sotgiu [17].

2.3 Time domain spectroscopy

In TDS, instead of measuring the response of the sample to a periodic function, the response to a step function is measured. A fast rise voltage is propagated in a coaxial line and the changes in the characteristics of the pulse after reflection from or transmission through a dielectric-filled section are measured. Then, the complex permittivity of the sample is calculated from these measurements in a particular frequency band. The step function approach for measuring material properties was not a new method, but the restriction on the instrumentation to pulse widths of longer than 1 μs had been the main problem in employing this technique. In the late 1960s, the development of fast sampling oscilloscopes together with tunnel-diode step generators having rise times as fast as 35 ps allowed time domain spectrometry to be used widely for material properties measurement.

TDS is used from 10^{-5} Hz up to 10 GHz, but its accuracy decreases rapidly towards the higher end. TDS is a powerful method for obtaining a great deal of information in a short time, but its accuracy in measuring dielectric loss is less than the single frequency techniques. This technique is also used at frequencies above 100 GHz. In the infrared region, single frequency measurement is limited because of the lack of an appropriate source working at a wide range of frequencies. The measurement of liquids in coaxial cells faces with no major problem, but for solid materials machining requirement introduces some restrictions to TDS techniques.

The different type of cells used in TDS measurements are reviewed by Afsar [1]. The bulk of literature on TDS technique is concerned with liquid dielectrics, but techniques for measuring solids have also been devised . For low-loss materials, multiple reflection TDS has been developed, and a transmission TDS method has been used by Sugget [18]. A theoretical view of dielectric behaviour as a purely time domain phenomenon rather than a Fourier transform of frequency response has been developed by Cole [19] and [20]. At low frequencies (below 1 kHz), good results can be achieved from a purpose-built automatic system, and an accuracy of 10 mrad has been reported at 10 kHz by Mopsik [21].

2.4 Frequency domain measurement

Although TDS techniques offer broad band measurement, this is at the cost of lower accuracy. When accurate measurements of complex permittivity are required frequency domain methods are preferred, particularly for low loss materials. At frequencies below 3 GHz, the standard coaxial technique is used. In this method, the locations of maxima and minima of the reflection from a short circuited sample are measured by a probe. In this method, the accuracy is limited to about ±1 percent in permittivity and about ±200 μrad in loss tangent (Lynch [4]). In this method, the losses in the conductors and the air gap between the specimen and short circuit (for solid specimens) are the sources of error. This technique is at its best between 200 MHz to 1 GHz. The use of an automatic network analyser (figure 2.1) can improve the accuracy and automate the measurement procedure (references [23]).

The increasing error with frequency and the difficulties of inserting the sample in the coaxial method limit the use of this technique at frequencies above few GHz. The measurement of the reflection or transmission coefficient from a piece of waveguide containing the sample provides the required data for calculating the sample properties. The waveguide methods are not suitable for specimens having dielectric constants of greater than 4, since over-moding may cause problems. In the waveguide methods, reflection measurements have been more popular than transmission measurements, and the well-known Roberts and Von Hippel [22] method is probably one of the most commonly used techniques at microwave frequencies. In this technique, the location of maxima and minima from a short circuited waveguide containing the specimen are measured.

A fixed probe and a movable short circuit can also be used instead of a movable probe, if the mode is such that a slot in the waveguide is not permissible. A liquid specimen can fill the waveguide completely, but the air gaps between the surfaces of a solid specimen and the waveguide walls is a source of error in this technique. Failure to fill a circular waveguide used in a TE_{01} mode does not introduce a serious error to the result, but failure to fill the smaller dimension of a rectangular waveguide is important. If the reflections from the ends of the sample are not taken into account in the calculations, the multiple reflections within the sample should be made small. Tapering the specimen such that the thin end of the taper lies against the narrow wall of the guide can reduce the multiple reflections. The error due to the air gaps between the sample and the guide surfaces can be reduced by

filling the gaps with a liquid of the same permittivity, if a low loss liquid matched with the sample can be found.

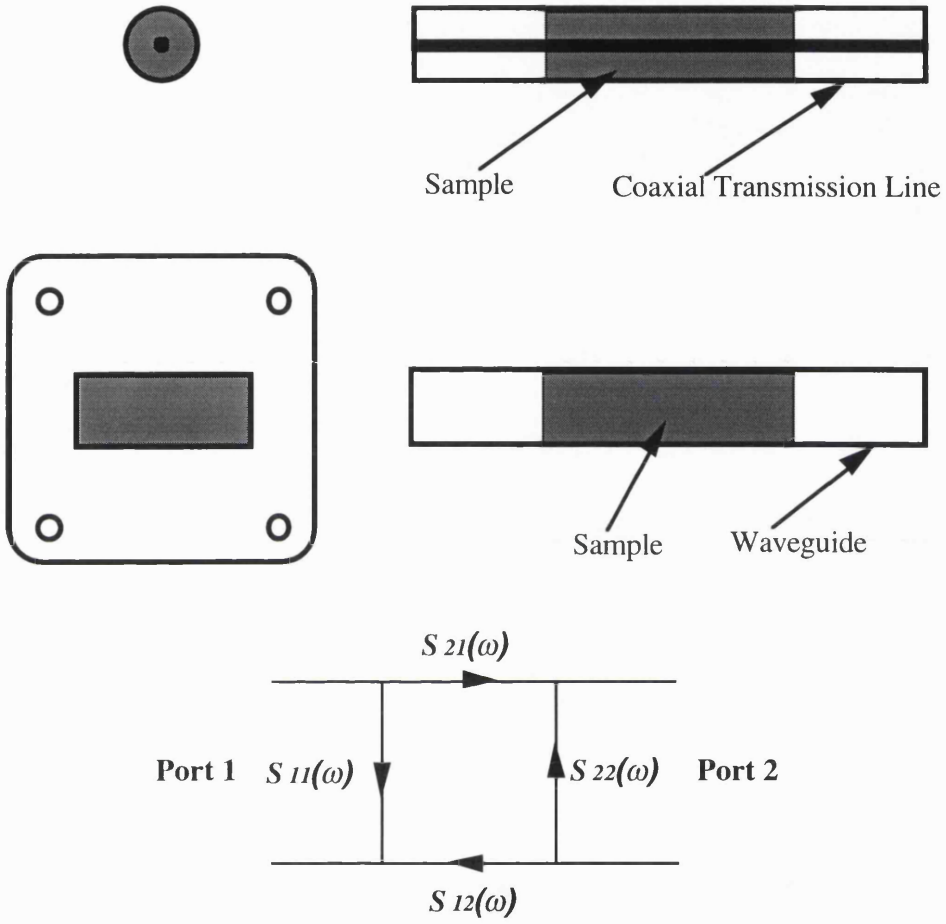

Figure 2.1 Transmission line method (upper), waveguide method (middle) and the associated flowgraph (lower).

2.4.1 Closed cavity

In spite of the greater convenience and easier automation in the waveguide method, resonant methods are more popular. In measuring liquid permittivity, the liquid can be introduced through a small filling hole to the cavity, but the resonator must be taken apart for introducing a solid specimen. The division between two parts of the cavity should be so arranged that no current flows across it, with regard to the chosen mode of resonance. The

size of specimen must be large enough that inserting the sample changes the Q-factor and the resonance frequency significantly. After inserting the specimen, the resonant frequency is restored in adjustable cavities. The mode of resonance can sometimes be chosen so that close fitting of the specimen against the walls is unnecessary.

There are two rather different approaches in closed cavity measurements. The perturbation method can be used for all permittivities, for anisotropic and magnetic materials and for medium and high loss materials. In the perturbation method, the fields in the sample and in the cavity are approximated and the specimen size is small compared with the cavity size. In the other approach, the cavity is partially or completely filled and the fields are derived from Maxwell's equations. In this method, the cavity is filled with a reference material (or vacuum). Then, the reference material is replaced with the specimen, and the second measurement is made with the cavity again resonating in the same mode.

Measurements of low-loss materials require a larger sample which fills a significant proportion of the cavity volume. In order to allow more accurate expressions for the fields to be used without the mathematics becoming too intractable, simple geometries are preferred. The most popular geometry is the TM_{010} cavity, of cylindrical-shape. A tubular cell of liquid or a round-shape specimen is placed along the axis of the cavity. Mathematical approximations and practical difficulties can increase uncertainties in perturbation methods. Numerical analysis can present a more complete description of the fields in the cavity, (Li et al [25]). In fact the exact theory is more commonly applied to the cavities used for measurements on very low loss materials, 300 μrad or less. The requirement of removing the T_{m11} mode has led to cavities being constructed from helical waveguide. Cook [26] has reported an accuracy of about 1 percent in relative permittivity. He has achieved this accuracy without too much difficulty in the measurement of PTFE.

2.4.2 Open resonator

It becomes difficult to use conventional cavity or waveguide methods for the measurement of material properties at the lower millimetric or shorter wavelengths. Metal loss and small sizes of cavity, which are two sources of error in these techniques, become more serious at these frequencies. An open resonator with plane reflectors is the microwave form of the

Fabry-Perot interferometer (Culshaw [27], [28], and [29]). In practice concave open resonators are preferred, since they can keep the radiation more easily within the system which leads to a higher Q-factor and smaller diameter for the specimen (Cullen and Nagenthiram [30], Jones [31]). In open resonators (figure 3.2), the distance between two reflectors are a few wavelengths, therefore the physical size of the cavity is not a problem. The Q-factors offered by open resonators are high enough to measure low-loss samples with high accuracy. The sample is in a sheet form placed between the two reflectors. In the open resonator only the sample thickness must be known accurately and there is no requirement of sample machining, hence this technique has a great advantage over closed cavity methods. Different geometries have been proposed for the reflectors. Bi-concave or plano-concave are the most sensitive type of open resonators.

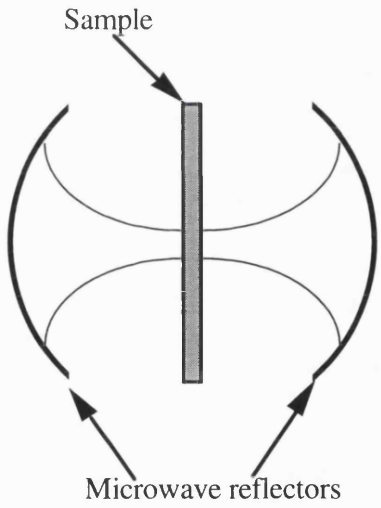

Figure 2.2 Bi-concave open resonator.

Open resonators have been developed to measure homogeneous low-loss materials at millimetre-wave frequencies. TEM resonance, in which the electromagnetic field takes the form of a standing-wave Gaussian beam, is used in the open resonator technique. On the axis, the fields are at a maximum and fall away on a Gaussian curve as one moves from it. Sample sizes of down to six wavelengths are quite adequate for measurements at the waist of the resonator. Open resonators are used in the frequency range of 30 to 300 GHz. They can be used at lower frequencies and are as sensitive as closed cavities, if the larger sample

diameter does not cause a problem. The Q-factor that can be achieved is quite high, about 150000 at 35 GHz (Jones [31]). The high Q-factor allows high sensitivity in the measurements of loss tangent, down to 1 μrad in 100, in open resonators. The properties of magnetic materials can also be measured by open resonators.

2.4.3 Free-wave methods

Free-wave methods for measuring material properties have been used for many years. As a successful measurement of water permittivity, the Saxton and Lane [32] experiment at 1.58 and 1.24 cm is worthy of note. The measured reflection and transmission coefficients are used to calculate the electrical properties of water. The appropriate distances of the antennas from the sample surface is experimentally found by measuring the transmission between the antennas as a function of their distance. In this experiment, the sample size is large enough to ignore diffraction of the wave from its edges and the water absorption is sufficiently high that the multiple reflections can be ignored.

Redheffer [33] discussed the use of free-wave methods for measuring the dielectric properties of solids. He has also suggested possible techniques for reducing the error in the measurement and developed the required formulae for calculating the sample properties from the measurement at the Brewster angle. Later, this method was used by Talpey [34] for determining dielectric properties at 35 GHz from the measured transmission and reflection coefficients at the Brewster angle. The measurement of transmission coefficients at parallel and perpendicular polarisations, as well as the measurement of the ratio of reflection coefficients at the two polarisations at the Brewster angle are used to separate magnetic and electrical losses. He approximated the multiple reflections within the sample and reported an accuracy of ± 6% in measuring some known dielectrics, (Bakelite, Glass, Polystyrene, and Paraffin). Breeden [35] has used a rotated sample to avoid multiple reflections at the two air/dielectric interfaces. For angles the near Brewster angle, he has carried out an error analysis and checked the results by measuring slip-cast fused silica at 94 GHz.

A method for measuring dielectric properties of liquids is presented by Jeyaraj et al [36]. In their method, the reflection coefficient of a metal backed liquid sample is measured for different sample thicknesses. They used a curve fitting algorithm to find the permittivity of

the liquid, and reported a relatively good accuracy in measuring dielectric constant of the liquids with tan $\delta \leq 1$. In their method, the accuracy is slightly better for the lossy liquids. In their experiment, the random error in the measurement is reduced by increasing the number of measurements. The estimated error from the asymptotic standard deviation of the best fitting parameters in ε' is about 0.5% and 1% for medium loss and high loss liquids respectively. Similarly, the estimated error in ε'' is 0.8% and 1.5% for medium loss and low loss liquids respectively.

Campbell [37] has used free-wave transmission methods for measuring permittivity of low-loss solids at 35 GHz, and his measurement method is a modified version of Talpey's technique. He has used reflection measurement at oblique incidence to find the the Brewster angle. In his measurement system, the accuracy in measuring the Brewster angle is about 0.25°, and accuracy of better than ±5 percent in measuring permittivity of low-loss dielectrics is reported. Cook and Rosenberg [38] have used transmission coefficient measurement for calculating complex permittivity of the medium loss isotropic materials at 35 GHz. They used a microwave bridge for their measurements and reported measured properties of an anisotropic material. In their calculations, the multiple reflections within the specimen are taken into account. They also used reflection coefficient measurement to calculate the properties of composite materials. In their transmission method, an uncertainty of ±0.5% in refractive index and ±10 - 15% in absorption index (K), have been reported. In their reflection method for measuring anisotropic specimens, they report an accuracy of 3% and ±5% in the measurements of n and K respectively.

Kadaba [39] has used transmission and reflection coefficient for measuring dielectric and magnetic properties of Plexiglas, Fibreglass, FGM-40, and Teflon at 18, 56 and 94 GHz. He reported accuracies of better than 10% in measuring permittivity and permeability, and suggested the use of a lens antenna for reducing the minimum sample distance from the antenna.

In free-wave techniques, the required data can be acquired by measuring transmission and/or reflection coefficients at different incident angles. Shimabukuro et al [40] used this technique and reported the measurement of complex permittivity at 93.788 GHz. In their technique the amplitude of transmission coefficients at different incident angles and at perpendicular polarisation are used to calculate the sample properties. The sample

properties are calculated by a curve fitting algorithm finding the best matched set of values for the measured parameters. They also used a simple model for correcting the error due to the changes in the effective aperture size after inserting the sample and achieved accuracies of 0.2 and 2.5 percent in calculating of ε_r and tan δ respectively.

Cullen [41] suggested a new method for measuring complex permittivity and permeability of ferrites. His method is based on measuring reflection coefficients at two orthogonal polarisations. In his technique, the material under test is assumed to be lossy enough that the multiple reflections can be ignored. He also suggested an alternative technique in which a thin sample is backed by a metal if the reflection from the front surface is not sufficiently high.

Introducing new techniques such as error correction and time gating has improved the accuracy in free-wave measurement considerably. The use of an automatic network analyser enables us to benefit from the measurement over a wide frequency band and to cancel out unwanted reflections. Ghodgaonkar et al [42] have used an HP-8510B network analyser to measure the reflection coefficient of solid specimens at normal incidence. In their experiments, a pair of lens antennas are used to reduce diffraction from edges of the sample. They also used the *TRL* calibration method to enhance the accuracy in measuring transmission and reflection coefficients. The residual error and the unwanted reflections are also reduced by time domain gating. They measured the properties of Teflon and PVC at frequencies 14 to 18 GHz, and the results confirm the permittivity of these materials measured by the waveguide method. Considering the practical error in measuring S_{11}, they conclude that their technique is more appropriate for medium and high loss materials.

Simultaneous measurement of transmission and reflection coefficients of a slab specimen can provide the required data for calculating permittivity and permeability. Ghodgaonkar et al [43] improved their technique to measure the dielectric and magnetic properties of a slab at normal incidence. In order to prevent the sagging effect of thin flexible samples, they used two quartz plates sandwiching the sample. They have reported the measurement of lossy materials and concluded that a loss tangent of less than 0.1 cannot be measured accurately in their technique.

Baker-Jarvis et al [44] have used transmission and reflection coefficients for determining

the material properties of the non-magnetic materials. They also carried out an error analysis and by measuring extra data managed to remove the phase error in the reflection coefficient measurement.

The measurement at oblique incident has the advantage of reducing the unwanted reflections and possibility of acquiring more independent data at different polarisations. Umari et al [45] have extended free-wave techniques by measuring reflection coefficient of a metal backed sample at oblique incident angle. They have also developed a correction factor for removing the effect of the displacement in the reflected wave.

Free-wave techniques and various methods of measuring liquids, gases and solids are analysed by Musil [46]. In this reference, the analysis of free-wave methods and the required formulae can be found. Although the practical techniques mentioned in this reference are based on rather old fashioned equipment, a useful theory is presented.

Improving free-wave techniques and automating the measurement have been carried out by some researchers. Blackhum [47] reports an automated measurement system based on the *Hewlett Packard* automatic network analyser. In this method, the basic theory has not been changed and the sample properties are calculated from the measured transmission and reflection coefficients at normal incidece. The use of a separate set of antennas for receiving and transmitting and also a purpose made calibration kit (*TRM*) improved total accuracy. In order to focus the beam in a sample surface and minimise the required sample size, a pair of lens antennas are employed and the residual mismatches are removed by a time gating technique. In this experiment, the sample size is 2 inch by 2 inch and the sample is placed at a distance of $2D^2/\lambda$. Good agreement for measuring the properties in non-magnetic materials by this method is reported.

Recently, Nitsche et al [48] has reported very good accuracy in measuring glass samples at 94 GHz. Although they have not referenced to another technique for checking the accuracy in their measurements, the results of the measurement at the different incident angles are consistent. They calculate the sample properties from the simultaneous measurement of transmission and reflection coefficients. They also measured the dielectric properties of acrylic by measuring transmission coefficient at parallel or perpendicular polarisation.

Part of the achievements in this project are also published as a number of papers. References [49] and [50] report mainly the progress in measuring lossy samples at millimetre wavelengths, and the optimum way of using the measured data in calculating the material properties is discussed in reference [51]. The use of time domain gating for removing the multiple reflections within the sample as a new method is introduced by Khosrowbegi, et al [52]. The measurement in the near-field region and its impact on the total accuracy are discussed in Khosrowbegi et al [53]. In this paper, the angular spectrum model is introduced, and the implications associated with using this model in free-wave measurements are presented.

3 Free-wave measurement techniques

3.1 Introduction

In this chapter, free-wave measurements are reviewed and the procedures for measuring transmission and reflection coefficients are presented. The total reflection and transmission coefficients of a slab in the plane wave model are derived. Multiple reflections within the sample are discussed, and criteria for considering a sample as '*thick*' or '*thin*' are defined. Single-pass and double-pass measurement systems are explained, and the general problems in free-wave measurements are briefly reviewed.

3.2 Free-wave measurements

Free-wave measurement techniques can be considered as an extension of transmission line or waveguide methods. At millimetre wavelengths, sample preparation becomes more difficult and conventional techniques run into difficulty. Resonant methods also are not appropriate for lossy materials, therefore free-wave techniques are considered as potential methods for measuring lossy materials at these frequencies. These techniques are non-destructive and can be used for measuring a wide range of materials at different physical conditions. In free-wave methods, the sample preparation is relatively simple and the only requirement is the sample should have flat and parallel surfaces. The sample size should also be large enough to intercept the incident wave adequately. In spite of all these, free-wave techniques have some limitations. The propagation of the wave in an unbounded area and the measurement in the near-field region both cause error in the measured transmission and reflection coefficients. These error terms cannot be removed by conventional error correction methods, and appropriate techniques should be devised for reducing their impact.

3.4 Measurement system

A free-wave measurement system consists of a rigid structure for positioning the sample, and a set of antennas for illuminating the sample and measuring the transmitted and/or reflected waves. The sample is placed in a holder which aligns the desired angle of incidence and the plane of polarisation. Then the magnitude and the phase of transmitted and reflected waves are measured, and the sample properties are calculated.

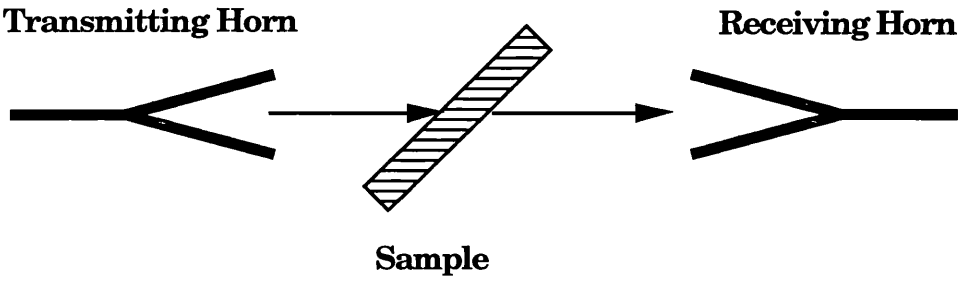

Figure 3.1 Free-wave single-path transmission measurement system.

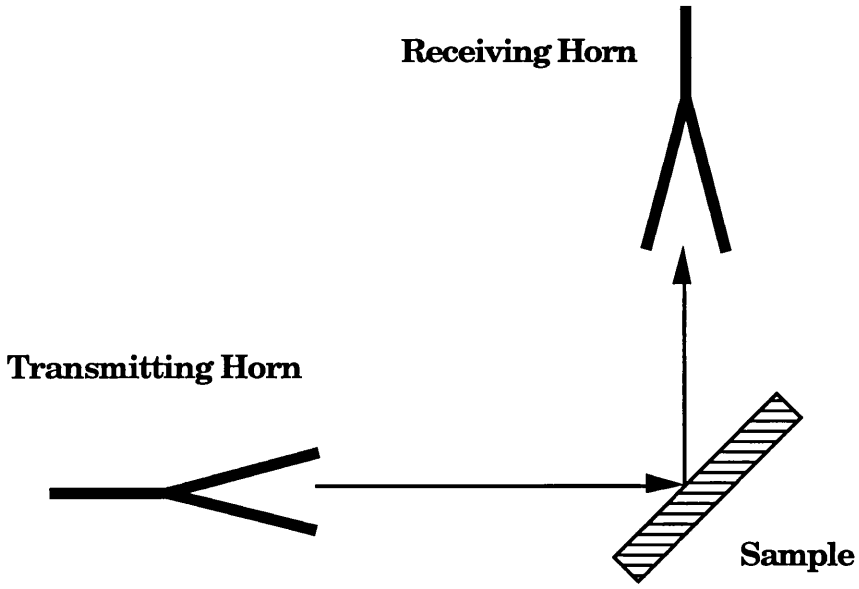

Figure 3.2 Free-wave single-path reflection measurement system.

Free-wave measurement systems can be classified into two categories: single-pass and double-pass. In single-pass systems, the sample surface is illuminated by the transmitting antenna and the reflected or transmitted wave is measured by the receiving antenna (figures 3.1 and 3.2). In a single-pass apparatus a two-port measurement system is required, and the measured parameter is actually the coupling between two antennas. Modelling single-pass measurement systems is relatively simple, but to change the plane of polarisation the geometry of the antennas and the sample position have to be altered.

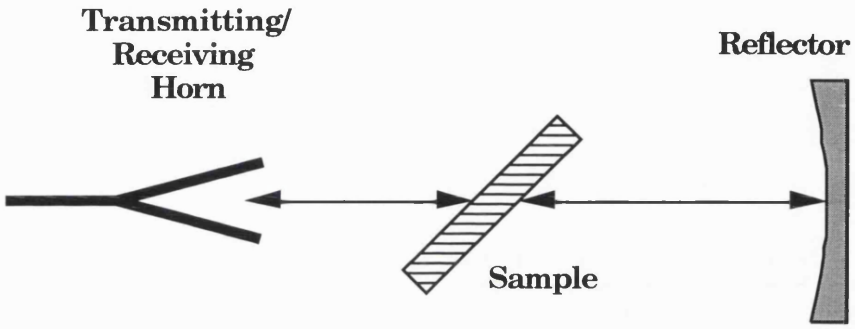

Figure 3.3 Free-wave double-path transmission measurement system.

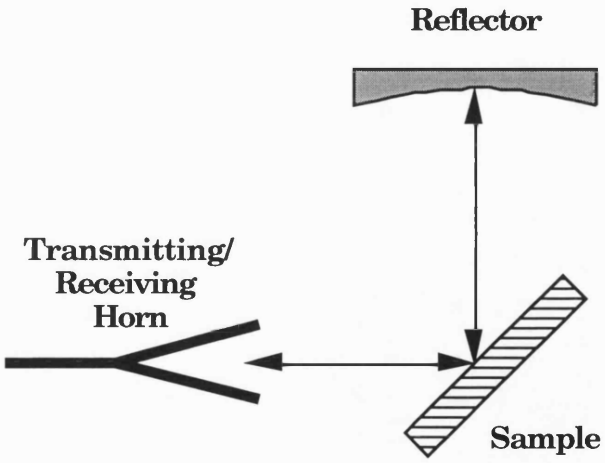

Figure 3.4 Free-wave double-path reflection measurement system.

In the double-pass technique (figures 3.3 and 3.4), a one-port measurement system is used to measure the transmission and reflection coefficients. The transmitted and reflected waves are reflected towards the sample by a reflector or focused by a lens, and the wave is measured after a second transition or reflection. In double-pass measurement systems the plane of polarisation can be changed easily, and the use of a microwave reflector reduces the error associated with diffraction of the wave from the edges of the sample.

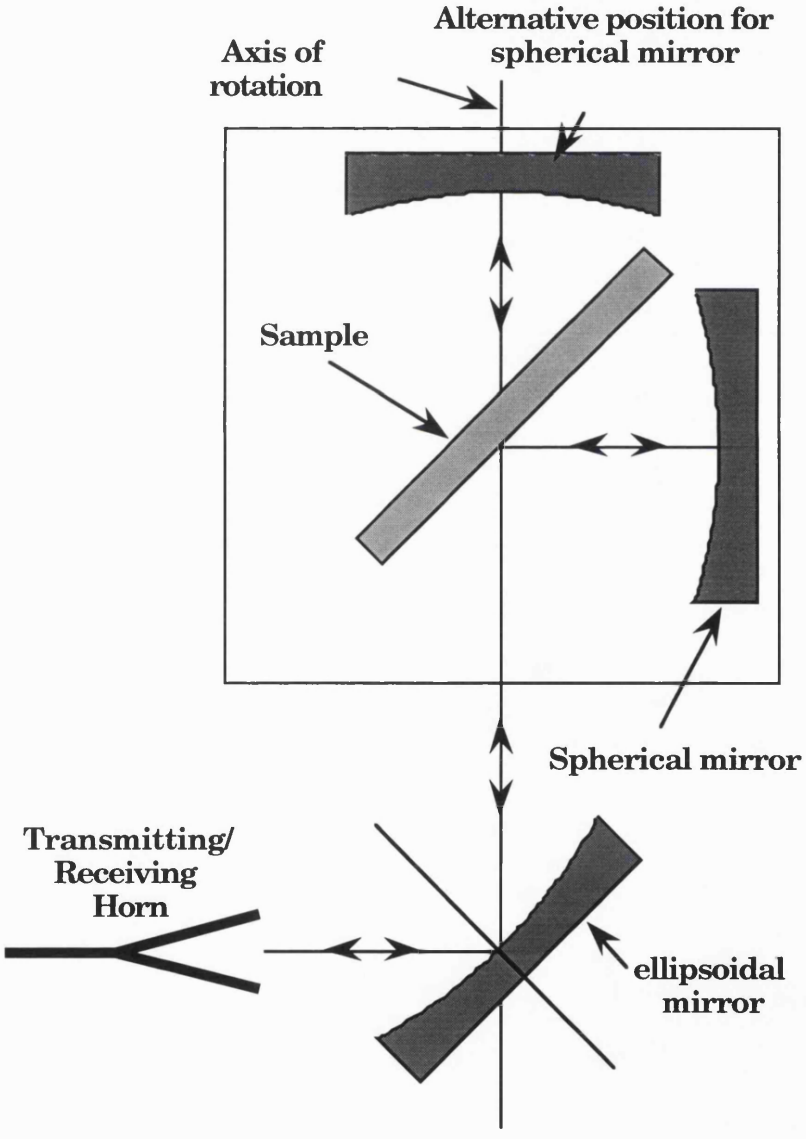

Figure 3.5 A compact free-wave double-pass measurement system.

In double-pass systems, the square of the transmission or reflection coefficients is measured, so there is an ambiguity of 180° in determining the measured phase. Double-pass measurement systems are relatively compact and the sample size can be smaller with respect to one-path systems, but their modelling is relatively more complicated. Figure 3.5 shows a double-pass measurement system in which the plane of polarisation can be changed by rotating the sample holder. In this apparatus, the configuration for transmission and reflection can be set by changing the position of the spherical mirror.

3.4 Measurement techniques

As mentioned, the required data for calculating the material properties can be acquired by measuring a combination of transmission and/or reflection coefficients at different incident angles, sample thicknesses or polarisations. If the sample properties do not change with frequency, measurement at different frequencies can also provide the required data. Therefore, numerous methods for calculating the sample properties can be devised. The different methods of measurement and their relative advantages are discussed in chapter 7. In free-wave techniques, the measurement process includes three stages. In the first step, the measurement system should be calibrated. Then, the required parameters including transmission and/or reflection coefficient and the sample specifications are measured. In the final stage, the complex permittivity and permeability of the sample are calculated.

The relationship between the measured parameters and the sample properties is expressed by a mathematical model. This model plays an important role in estimating the total accuracy. In free-wave techniques, two models can be considered: the plane wave and the angular spectrum models. In the plane wave model, the sample is assumed to be infinitely large and illuminated by a uniform plane wave. This model is simple, but the effects of wavefront curvature and wave diffraction from the edges of the sample are not taken into account. In the angular spectrum model the sample is assumed to be infinitely large, but measurement in the near-field region is taken into account. This model delivers more realistic values for transmission and reflection coefficients of a slab measured in the near-field region. The propagated wave is resolved into an infinite number of uniform plane waves travelling at different angles. The angular spectrum model and its improvement in measurement accuracy are discussed in chapter 6.

3.5 Plane wave model

In the plane wave model, the sample is assumed to be illuminated by a uniform plane wave and diffraction of the wave from its edges is ignored. The wave within the sample is reflected from the sample surfaces and constitutes the multiple reflections. Multiple reflections within the slab play an important role in constituting the total transmitted and reflected waves. In this part, the total transmission and reflection coefficients associated with a sample are calculated.

If a semi-infinite sample is illuminated by a uniform plane wave (figure 3.6), the reflected wave from the front surface can be calculated from the Fresnel equations, (1) and (2). In practice, the wave is reflected an infinite number of times from the sample surfaces and constitute the multiple reflections within the sample.

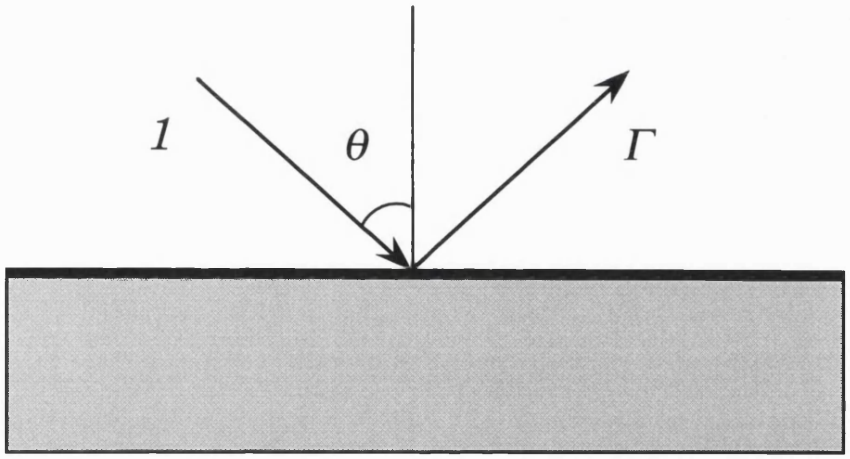

Figure 3.6 Reflection from a semi-infinite sample.

$$\Gamma_{\parallel} = \frac{\sqrt{\varepsilon_r \mu_r - \sin^2\theta} - \varepsilon_r \cos\theta}{\sqrt{\varepsilon_r \mu_r - \sin^2\theta} + \varepsilon_r \cos\theta} \qquad \ldots(1)$$

$$\Gamma_{\perp} = \frac{\mu_r \cos\theta - \sqrt{\varepsilon_r \mu_r - \sin^2\theta}}{\mu_r \cos\theta + \sqrt{\varepsilon_r \mu_r - \sin^2\theta}} \qquad \ldots(2)$$

If the multiple reflections within the sample are not taken into account (figure 3.7), the total transmission and reflection coefficients of a slab can be found from equations (3) to (6). P is the propagation coefficient and is given by (7).

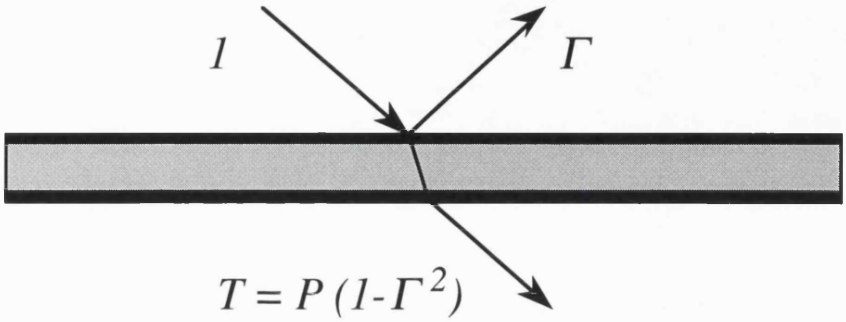

Figure 3.7 Transmission and reflection coefficients in a slab of finite thickness in the absence of the multiple reflections.

$$T_{t\parallel} = P\,(1 - \Gamma_{\parallel}^{2}) \qquad \ldots(3)$$

$$T_{t\perp} = T\,(1 - \Gamma_{\perp}^{2}) \qquad \ldots(4)$$

$$\Gamma_{t\parallel} = \Gamma_{\parallel} \qquad \ldots(5)$$

$$\Gamma_{t\perp} = \Gamma_{\perp} \qquad \ldots(6)$$

$$P = exp\left(\frac{-j\,2\pi d}{\lambda_o}\sqrt{\varepsilon_r\mu_r - sin^{2}\theta}\right) \qquad \ldots(7)$$

In the general case multiple reflections within the sample cannot be ignored, and the wave is reflected an infinite number of times from the sample surfaces within the slab. As the wave travels within the sample its magnitude decreases, and the rate of decay is a function of the sample properties. The propagation coefficient (P) defines the changes in the magnitude and the phase of the wave travelling a distance of d within the sample. In the presence of multiple reflections, the total reflected or transmitted wave can be calculated by summing all the terms of a geometric series expressing reflected or transmitted waves, (Collin [54]).

Throughout this thesis, the plane of polarisation is defined according to the direction of the main component of the electrical field with respect to the plane of incidence. At parallel polarisation, the vector representing the main electrical field is in the plane of incidence, while perpendicular polarisation denotes the case in which the main component of the electrical field is perpendicular to the plane of incidence. In figure 3.8, each uniform plane wave is shown by a line and the arrow shows the direction of propagation. The total transmitted and reflected waves associated with a slab of infinite size illuminated by a plane wave are given by (8) and (9).

$$T_{total} = T_{21}T_{32}P + T_{21}T_{32}P^3\Gamma_2\Gamma_3 + T_{21}T_{32}P^5\Gamma_2^2\Gamma_3^2 + \ldots \quad \ldots(8)$$

$$\Gamma_{total} = \Gamma_1 + \Gamma_3T_{21}T_{12}P^2 + \Gamma_3^2T_{21}T_{12}P^4\Gamma_2 + \Gamma_3^3T_{21}T_{12}P^6\Gamma_2^2 + \ldots \quad \ldots (9)$$

Summing these geometric series, equations (8) and (9) are simplified to (10) and (11).

$$T_{total} = T_{21}T_{32}P\sum_{n=0}^{\infty}\Gamma_3^n\Gamma_2^nP^{2n} \quad \ldots(10)$$

$$\Gamma_{total} = \Gamma_1 + \Gamma_3T_{21}T_{12}P^2\sum_{n=0}^{\infty}\Gamma_3^n\Gamma_2^nP^{2n} \quad \ldots(11)$$

Using the boundary conditions for the reflected and transmitted waves at the air/sample interfaces, the total transmitted and reflected waves simplify to (17) and (18).

$$\Gamma_1 = -\Gamma_2 = -\Gamma_3 = \Gamma \quad \ldots(12)$$

$$T_{12} = 1 + \Gamma_2 = 1 - \Gamma \quad \ldots(13)$$

$$T_{21} = 1 + \Gamma_1 \quad \ldots(14)$$

$$T_{12} = 1 + \Gamma_2 \quad \ldots(15)$$

$$T_{12} = T_{32} \quad \ldots(16)$$

$$\Gamma_{total} = \frac{\Gamma(1-P^2)}{1-P^2\Gamma^2} \quad ...(17)$$

$$T_{total} = \frac{P(1-\Gamma^2)}{1-P^2\Gamma^2} \quad ...(18)$$

Substituting the reflection coefficient from a semi-infinite sample, the total reflection coefficients for a slab illuminated by a plane wave can be given by equations (19) and (20).

$$\Gamma_{t\parallel} = \frac{\Gamma_{\parallel}(1-P^2)}{1-P^2\Gamma_{\parallel}^2} \quad ...(19)$$

$$\Gamma_{t\perp} = \frac{\Gamma_{\perp}(1-P^2)}{1-P^2\Gamma_{\perp}^2} \quad ...(20)$$

In the calibration process, the measured transmission coefficient is normalized with respect to the transmission coefficient of the empty sample holder. In other words, the effect of the slice of air which is replaced by the sample should be taken into account. In the plane wave model, the slice of air is represented by a phase shift in the transmission coefficients. The appropriate factor for correcting the transmission coefficient is given by equation (21). Therefore, the observed transmission coefficients at parallel and perpendicular polarisations are given by equations (22) and (23) respectively.

$$CF = exp\left(\frac{j\,2\pi d}{\lambda_o} COS\ \theta\right) \quad ...(21)$$

$$T_{t\parallel} = \frac{P(1-\Gamma_{\parallel}^2)}{1-P^2\Gamma_{\parallel}^2} CF \quad ...(22)$$

$$T_{t\perp} = \frac{P(1-\Gamma_{\perp}^2)}{1-P^2\Gamma_{\perp}^2} CF \quad ...(23)$$

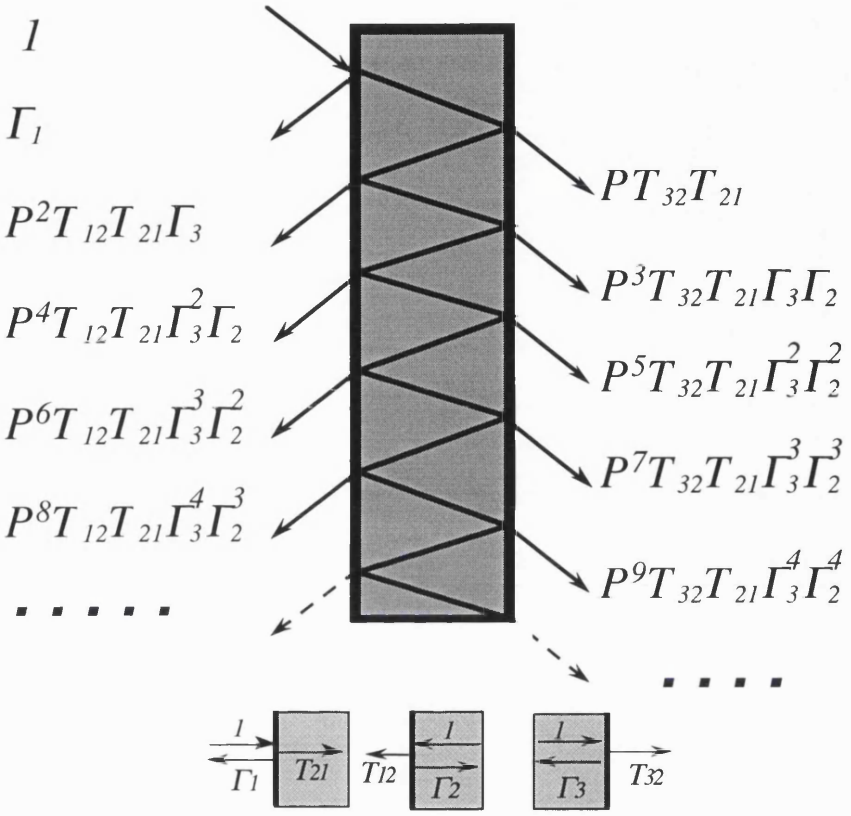

Figure 3.8 Transmitted and reflected waves in the presence of multiple reflections within the slab.

3.6 Multiple reflections within the sample

Multiple reflections within the sample play an important role in constituting the total transmitted and reflected waves. At frequencies such that the sample thickness is a multiple of λ/2 the reflected wave is minimum, and the transmitted wave through the sample is maximum. For a lossless sample there is no reflection at these frequencies. Therefore, the required data cannot be acquired by measuring the reflection coefficient.

In chapter 7, it is shown that total accuracy is also a function of the sample electrical length. If multiple reflections within the sample can be ignored, the calculation becomes less complicated and dependence of total accuracy on the sample electrical length decreases considerably. *Thick* samples refer to the situation where multiple reflections within the sample can be ignored. Treating a slab as a *thick* sample imposes some limitations on the minimum sample thickness. If multiple reflections within the sample are taken into account, all higher order terms of the geometric series are considered in the calculation. In this case, the slab is called a *thin* sample. The terms *thick* and *thin* are used only for distinguishing between two type of measurement with regard to ignoring or considering multiple reflections. Since the combination of electrical length and loss tangent define the type of sample, these terms do not imply physically thin and thick slabs.

3.7 Free-wave calibration

In free-wave techniques, calibration is slightly different from conventional methods used in coaxial and waveguide measurements. The propagation of waves in free-wave paths between the antennas and the sample introduces some new error terms. A detailed discussion of the free-wave calibration procedure is presented in chapter 4. Here, only a brief account of the calibration process is presented.

In the calibration process, a highly conducting surface and a sheet of radiation absorbing material (RAM) are used to implement a short circuit and a matched load. The location of the front surface of the short circuit defines the reference plane in the reflection coefficient measurement. For implementing the '*thru*' standard, the transmission coefficient of the empty frame is measured.

3.8 Free-wave measurement

In transmission coefficient measurements, the ratio of the transmitted wave to the incident wave is measured. In the calibration process, the coupling between the antennas and the frequency response associated with the cables, waveguides and connectors are measured. These values are saved in the network analyser memories and used for normalising the

subsequent measurements. The transmission coefficient of the empty sample holder is measured and saved as the '*thru*' standard, and the effect of the slice of air which is deleted from the free-wave path after introducing the specimen into the apparatus should also be taken into account.

In the reflection coefficient measurement, the parameter of interest is the reflected wave from the sample surface. In calibrating the measurement system, a flat sheet of a highly conducting material is used as a standard short circuit. Then by placing the sample in the sample holder, the reflected wave from the sample at the desired polarisation is measured. In the reflection coefficient measurement, the location of the front surface of the sample and the standard short should be the same, and any variation may result in an error in the measured phase of the reflection coefficient. The error due to the mechanical repeatability of the sample holder increases with frequency. This error can be considerable, since displacement of only 12 microns causes an error of 1° in the measured phase of the reflection coefficient at 45° incident angle and 100 GHz.

3.9 Calculation

The complex permittivity and permeability of a sample are calculated from four independent measurements. Regarding the combination of the measured data and considering the multiple reflections within the sample, various methods for calculating the material properties are devised. In most of these techniques, the use of iterative numerical methods for calculating the sample properties from the measured parameters is inevitable (references [55] and [56]). The multi-valued nature of the transcendental equations and the fact that phase is measured modulus-2π introduce ambiguity to the calculated values. Therefore, a certain amount of a priori knowledge of the sample properties in finding the correct values is required.

4 Sources of error

4.1 Introduction

In all measurement systems, whether they are as simple as a power meter or as complicated as an automatic vector network analyser, the measured parameters are subject to error. In a measurement technique, a good knowledge of error mechanisms can be used to devise appropriate methods for improving the accuracy. In free-wave techniques the sample properties are calculated from the measured transmission and/or reflection coefficients, and any error in measuring these parameters results in error in the calculated permittivity and permeability. The aim of this chapter is to present a detailed account of the error mechanisms taking part in free-wave measurements. Different sources of error in free-wave measurements are reviewed, and techniques for removing their impact from the measurement results are presented and discussed. First the error terms associated with the waveguide and coaxial measurements are presented, then the sources of error due to the propagation of the wave in free space paths are discussed.

4.2 Error in S-parameter measurement

In this part, the general sources of error in measuring scattering parameters are presented. Since a *Hewlett Packard* automatic vector network analyser (HP-8510B) is employed for the measurement throughout this project, HP terminologies are used for explaining the error terms and calibration techniques. The detailed definition of the error terms and error correction techniques can be found in reference [57]. In this part, a brief account of the error mechanisms in measuring the scattering parameters, and the appropriate techniques for removing their impact, are briefly reviewed.

The error sources associated with S-parameter measurements can be divided into two categories. The first class of error (*random errors*), are non-repeatable variations in the measured quantities. These variations are due to noise, temperature fluctuations, and the

non-repeatable physical changes in different parts of the measurement system. The second type of error sources (*systematic*), are repeatable variations in the measured parameters. In contrast with random errors, systematic errors are predictable and can be measured by appropriated calibration methods.

In free-wave measurements, the propagation of the wave in an unbounded area also introduces some error terms. These sources of error are complicated and cannot be modelled easily, therefore they can be treated as random errors in some cases. In most microwave measurements systematic errors are the most significant error terms, and the main effort is devoted to removing their impact. In the error analysis each error term is represented by a vector, and the total error is calculated by summing the error vectors. In the error correction and calibration procedures, the error vectors are measured and their effects on the measurement results are cancelled out mathematically.

4.3 Systematic errors

In network analysers, systematic errors are mainly due to leakages between the measurement ports, mismatches, finite directivity of the couplers, and the frequency responses of different parts. In estimating the maximum error or the achievable accuracy, only the magnitudes of error vectors are taken into account, since the phases of these vectors cannot be well defined. In other words, we assume that the vectors representing the error terms are either in phase or 180° out of phase with each other. This assumption simplifies the analysis and gives the error estimation for the worst case.

In the error correction process each source of error is modelled, then the elements of the model are calculated by measuring a set of standard components. The higher the required measurement accuracy, the greater the number of error terms that should be considered in the model. In the HP-8510B, each error model is devised to remove a specific set of error terms. In order to clarify the error correction process, the sources of error and their contribution to the total error are now explained. Then the different error models and their improvements in total accuracy are studied.

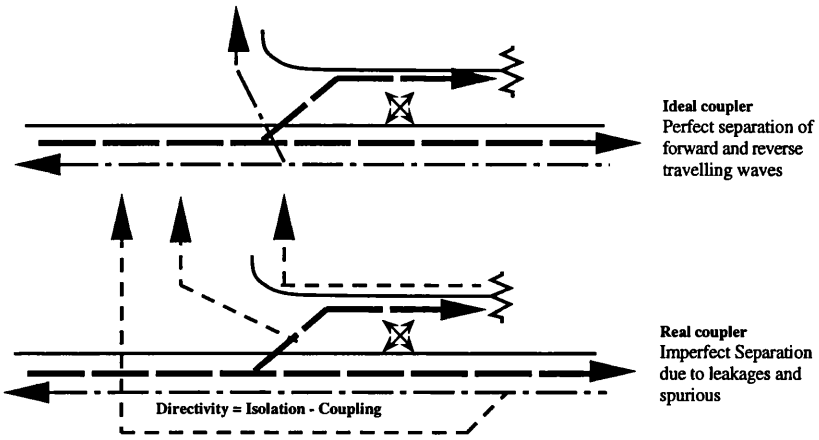

Figure 4.1 Systematic error in reflection coefficient measurements in an ideal coupler (upper) and in a real directional coupler (lower).

4.3.1 Reflection measurement

In reflection measurement, we are interested in the ratio of the reflected signal from the device under test to the incident signal. In order to separate the incident and reflected signals, a directional coupler is used. As directional couplers are not ideal, a part of the incident signal as well as the reflected signal appear at the measurement test port. Directivity is a figure of merit for how well a coupler separates the forward and reverse powers. By definition, directivity is the ratio of the power coupled into the coupled arm in the forward direction to the power that appears at the coupled arm in the reverse direction when the coupler is terminated by a matched load. A directivity of 40 dB means that the measured reflected power is 40 dB less for a matched load than that for a perfect short circuit. In reflection measurements, the frequency response, load and source mismatches also introduce some errors to the measured reflection.

The mismatches between the different parts of the measurement system also cause the wave to be reflected back and forth, and the multiple reflections generated in this way contain an infinite number of terms. In practice, the magnitudes of the higher order terms are much lower than the principal one. In modelling the error sources, multiple reflections between different components of a measurement system are ignored, and only the main term is taken into account.

4.3.1.1 Coupler directivity

As mentioned, a real directional coupler does not perfectly separate the forward and reverse signals and a small percentage of the incident signal appears at the coupled output. This signal is a combination of the leakage and the unwanted reflections (figure 4.1). The unwanted reflections are generated due to the imperfect termination in the coupled arm and the reflection from the coupler output connector. If the device under test needs an adaptor, the coupler directivity is further degraded because of the adaptor mismatches. The total directivity is a vector representing the sum of all leakage signals emerging from the system test input. This includes the signal which is generated due to inability of the coupler to separate the incident and reflected signals and the residual reflection. The residual reflection itself consists of the reflection from the test cables and adaptors between the test port and the signal separation device. The second part of the unwanted reflections is independent of the device characteristics.

In reflection measurement, the measured vector is the sum of the directivity and the actual reflection vector. In the worst case, the error in reflection measurement can be as large as the directivity. The most significant impact of directivity is in measuring small reflection coefficients. The maximum uncertainty in S_{11} measurement due to coupler directivity can be as much as $\pm D$, where D is the directivity of the coupler.

4.3.1.2 Source mismatch

The second most important source of error is that due to the source mismatch (figure 4.2). This error is generated due to inability of the source to maintain constant power at the test device input. If the source or the associated connectors and cables are not well matched, any reflected signal from the device is reflected back towards the device. The mismatches in the source means that all the reflected signal is not absorbed by the source and a part of the reflected signal is re-reflected towards the load. This signal has a magnitude of $\pm M_S S^2_{11}$, where M_S and S_{11} are the reflection coefficient of the source and the device under test respectively. The error due to the source mismatch can be significant for devices with high reflection coefficient.

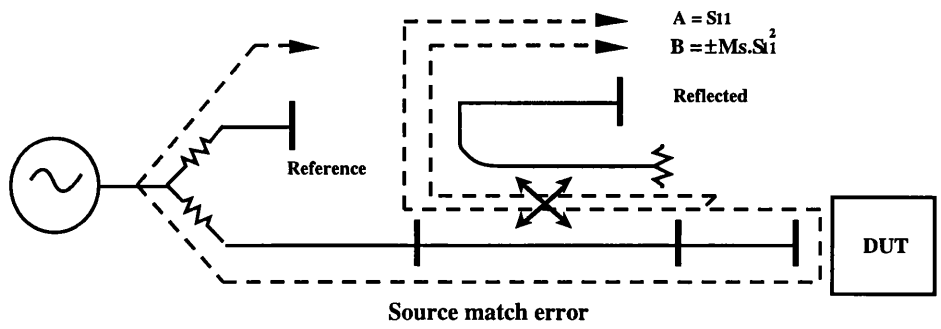

Figure 4.2 Source mismatch error in reflection coefficient measurements.

4.3.1.3 Frequency response

The system frequency response is a vector representing the variations in the magnitude and phase of the measurement system with frequency. The frequency response of all the components in the measurement setup including signal separation devices, test cables, adaptors and the variations in coupling ratio together constitute the total frequency response. The frequency response error vector also depends on the reflection coefficient of the device under test. This error vector has a magnitude $\pm T_R . S_{11}$, where S_{11} is the reflection coefficient of the device under test and T_R is the frequency response or tracking error. This error term can be measured in the calibration process and cancelled out mathematically.

4.3.1.4 Load mismatch error

In reflection coefficient measurement of multi-port devices, a load match error is added to the other systematic errors. Mismatches in test port 2 and other mismatches in the transmission signal path cause a portion of the transmitted signal to be reflected back (figure 4.3). The magnitude of the generated error depends on the load reflection coefficient and the transmission characteristics of the device under test. The maximum uncertainty due to this error is $\pm M_L . S_{12} . S_{21}$, where S_{21} and S_{12} are the forward and reverse transmission coefficients of the device under test respectively. The significance of this error is in

measuring bilateral devices. The effect of this error can be ignored for devices of 6 dB or greater insertion loss, since 12 dB isolation between two ports is adequate to reduce the impact of this error.

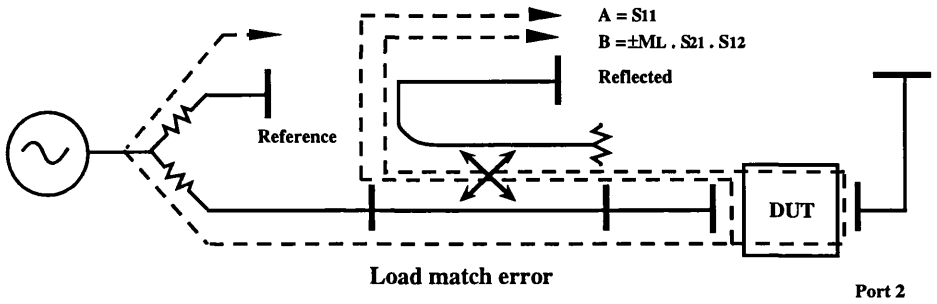

Figure 4.3 The load match error in reflection measurements.

4.3.2 Transmission Measurement

In transmission measurement, the ratio of transmitted power to incident power is measured. The error terms appearing in transmission measurements are similar to those explained in reflection measurements. In transmission measurements, the error terms can be categorized into three different types: transmission mismatch error, isolation or cross talk, and frequency response or tracking. As mentioned, the frequency response error term represents the amplitude and phase changes in the frequency responses of all the different parts of the transmission path.

4.3.2.1 Isolation and crosstalk error

Similar to the reflection measurement, leakage between reference and test channels causes an error in transmission measurements (figure 4.4). Although the main leakage is in the RF section of the test setup, leakage in the IF section could be significant as well. This error (X_c), is independent of the characteristics of the device under test and is more significant for devices of high insertion loss.

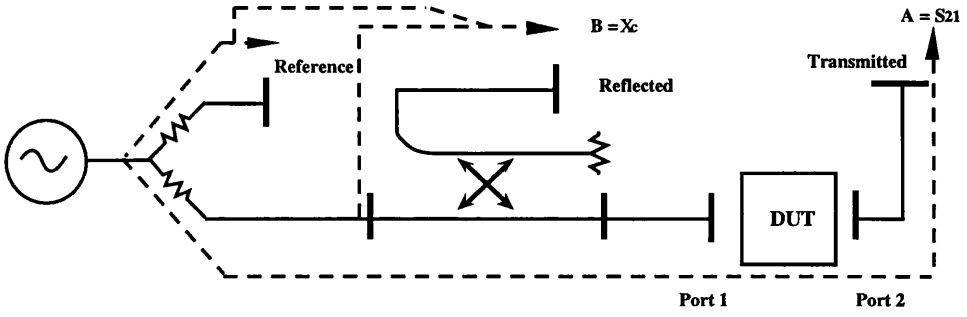

Figure 4.4 The isolation error in transmission measurement.

4.3.2.2 Transmission mismatch error

Transmission mismatch error is due to the mismatches between the measurement system test ports and the device ports, and can be significant in transmission measurements (figure 4.5). If the load mismatch is represented by M_L, the magnitude of the error term due to load mismatch can be expressed as a function of the device under test scattering parameters and the load mismatch, $S_{12}.S_{22}.M_L$.

Similarly, mismatch at the source (port 1) generates an error signal at port 2 of the measurement setup. This error term has an amplitude equal to $S_{21}S_{11}M_S$, where M_S is the source reflection coefficient. The contribution of this error heavily depends on the reflection and transmission coefficients of the device under test. This error becomes more serious when the insertion loss is less than about 6 dB.

4.3.2.3 Tracking error

The error due to transmission path frequency response has a magnitude equal to $T_T.S_{21}$, where T_T is the tracking error term and S_{21} is the transmission.

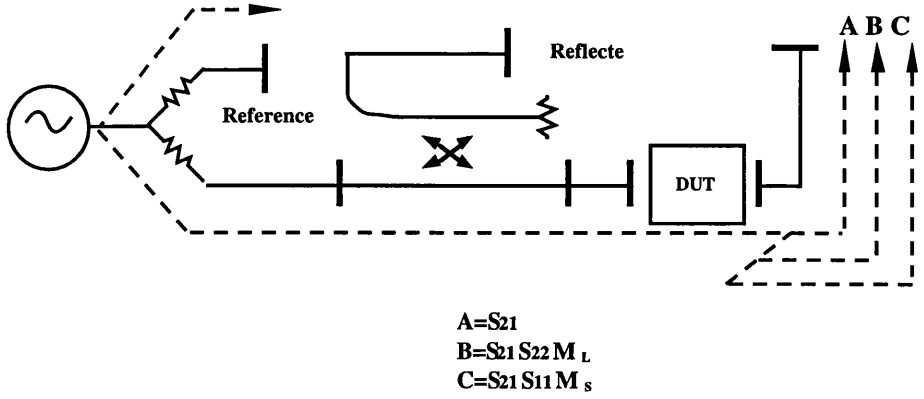

Figure 4.5 Load and source mismatch error in transmission measurements.

4.4 Random errors

Random errors are grouped into three different classes. Although these errors are non-repeatable and difficult to quantify, there are certain techniques for minimizing their effects on the measurement results. Different sources of random error and the techniques to reduce their impact are discussed in the next part.

4.4.1 Physical changes

The first type of random error is generated due to physical changes of the measurement setup. These changes can happen between two successive measurements or over a period of time. The only way to reduce this kind of error is to keep the physical configuration of the setup as unchanged as possible. The physical changes also include the pressure used for connecting the cables and connectors. This type of error can be reduced by periodically checking the repeatability of the mechanical switches. The changes in phase characteristics of the flexible cables is another source of error which can be reduced by avoiding extreme bends and minimizing the number of times the cable is flexed.

4.4.2 Temperature changes

The second type of random error is due to temperature changes. This class of error causes drift in the measurement results. As the internal temperature of the instrument changes after turning on, the measurement results can change as well. These changes are quite unpredictable and the system stabilizes only after its temperature is well stabilized. The drift can be due to changes in the frequency of the source and in the electrical lengths of the hardline cables in the test set with frequency. An ambient temperature change of 5 degrees Celsius can produce error of the order of 0.1 dB and 1 degree in the measurement results.

The impact of system warm up drift can be avoided by allowing the internal temperature of the instrument to stabilise. Although a full 2 hours warm up and a very stable ambient temperature are recommended for high accuracy measurements, a 45 minute warm up time can stabilize the instrument for most purposes. The control of ambient temperature can minimize the drift in the measurement results and a maximum change of ±2°C meets the required accuracy for most of the measurements.

4.4.3 Noise

Noise is the third type of random error. The HP-8510B has a tuned harmonic receiver with bandwidth of 10 kHz. At low frequencies, the noise floor of the front end (-100 dBm), outweighs the other sources of error, but the noise from the local oscillator in the phase-locked loop becomes the predominant factor at higher frequencies. This magnitude of noise error increases with frequency, since a higher harmonic mixing number is required to lock to the wanted signal. The impact of noise in the measurement can be reduced by increasing the signal to noise ratio at the test port.

For a test signal with 20 dB signal to noise ratio, an error of 1 dB in the magnitude of the signal is expected. Noise-related errors can be reduced by choosing an appropriate averaging factor. The use of the *trace smoothing* facility in the HP-8510 is an effective tool for averaging out noise in the measurements of broad band and flat response devices. As trace smoothing will distort the measurement results of devices that have rapid response variations with frequency, it is not recommended for them.

4.5 Calibration measurement

In all measurement systems, the isolation and directivity are finite and there is a crosstalk between different ports. The impedance mismatches and a varying frequency response are also two other imperfect characteristics of any network analyser. The role of error correction techniques is to remove the effect of these error terms from the measurement results. In the error correction process, each of the error terms is quantified by measuring a set of precision calibration standards, then the measured values are corrected mathematically. Figure 4.6 shows the flowgraph of a 1-port reflection measurement system. The contribution of directivity is independent of the test device. The mismatch in the source re-reflects the reflected power from the device and causes variations in the level of incident energy upon the device. The tracking error term scales the reflected signal from the device. The reflection coefficient of the device under test can be calculated as a function of measured reflection coefficient and the three associated error terms by using the non-touching loop rule, (references [58] and [59]).

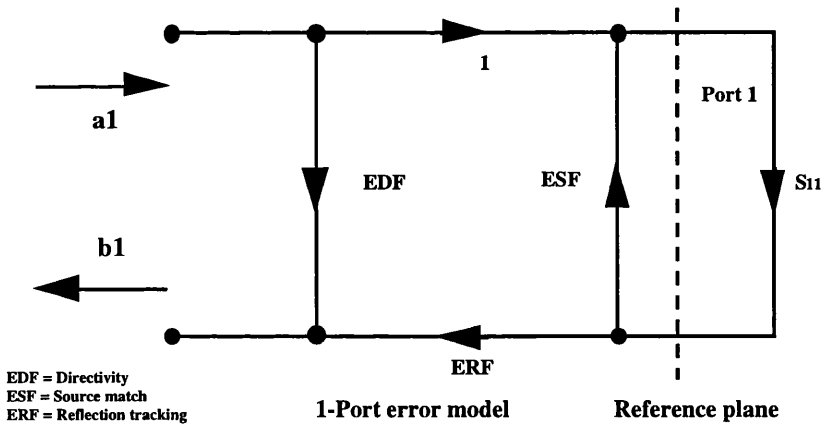

Figure 4.6 The reflection measurement flowgraph.

The role of the calibration process is to characterize each of the error terms at each frequency over the entire frequency range. The error vectors are measured as complex values, and they are used in accuracy enhancement equations to cancel out the systematic errors. The effectiveness of error correction is largely dependent on the quality of the standard impedances used in the calibration.

In reflection measurements, three independent standards are measured for characterizing the error terms. Although these standard impedances can have any value, the use of a short circuit, an open circuit and a matched load simplifies the calculations. These standard impedances can be well defined over a wide range of frequencies.

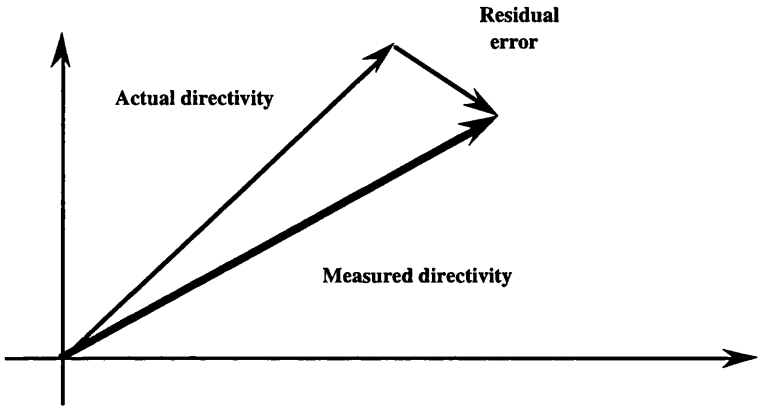

Figure 4.7 The directivity error correction vector diagram.

The directivity of the measurement system can be measured by connecting a perfect matched load to the test port. A perfect termination reflects no energy, thus the measured reflection coefficient is equal to the directivity. In practice, a perfect termination over a broad bandwidth of frequency is not achievable. Therefore, the measured directivity of the system is the sum of the actual directivity and the reflection coefficient of the load (figure 4.7). A method for cancelling out this error in directivity measurement is to use a moving load. In this technique, a matched load is connected to the test port. If the load is moved with respect to the reference plane, the angle of the vector representing the residual reflection of the load changes by 360° for each half a wavelength change in the location of load (figure 4.8).

The measurement of the reflection coefficient of the load at different positions of the sliding element provides the required information for finding the centre of the circle. In this method, the reflection coefficient must be measured at least at three different positions. The residual error in using an imperfect matched load for directivity measurement is the sum of the reflection from the load and the reflection of the connector and air line associated with the sliding load. The reflection of the air line cannot be cancelled out in this method.

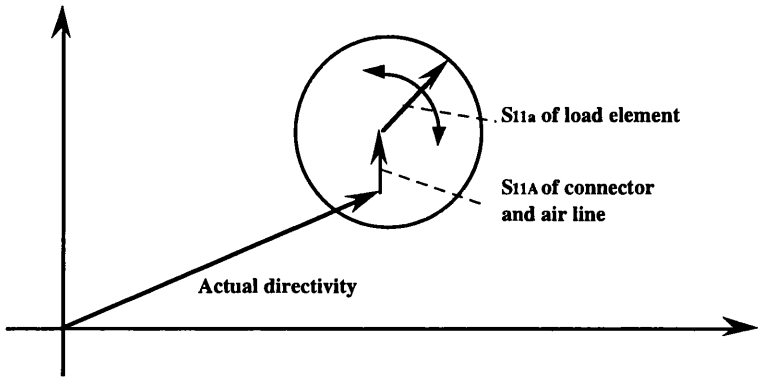

Figure 4.8 The use of a sliding load to cancel out the load mismatch.

Two remaining error terms can be determined by measuring two independent standards. A standard short circuit and a standard open circuit are used for these measurements. As we know, a short circuit has a reflection of $\Gamma = -1$ and the reflection coefficient of an open circuit is $\Gamma = 1$. In practice, an open circuit has a phase characteristic which varies with frequency. The phase variations in an open circuit standard can be modelled as a set of reactive elements. This modelling is equivalent to shifting the reference plane with frequency.

4.6 Accuracy enhancement

In 2-port measurements, there are four S-parameters associated with the device under test. Forward parameters are measured by exciting the input (a_1) and measuring the reflected signal (b_1), and transmitted signal (b_2). Similarly, the two reverse parameters are measured by exciting the output port.

The flowgraph for the error model associated with forward parameter measurements contains six error terms. The flowgraph for the reverse S-parameters is a mirror image of the forward S-parameter model. The accuracy enhancement computation requires all 12 error terms. All four S-parameters are characterized before solving the associated equations and calculating the actual values of the S-parameters (figure 4.9).

In error correction methods, error models with different degrees of complexity can be used. The required accuracy in the measurement defines the precision of the standard impedances and the type of error model. In the HP-8510B, five classes of calibration are available. Each of them is appropriate for a particular type of measurement and removes a specific set of error terms.

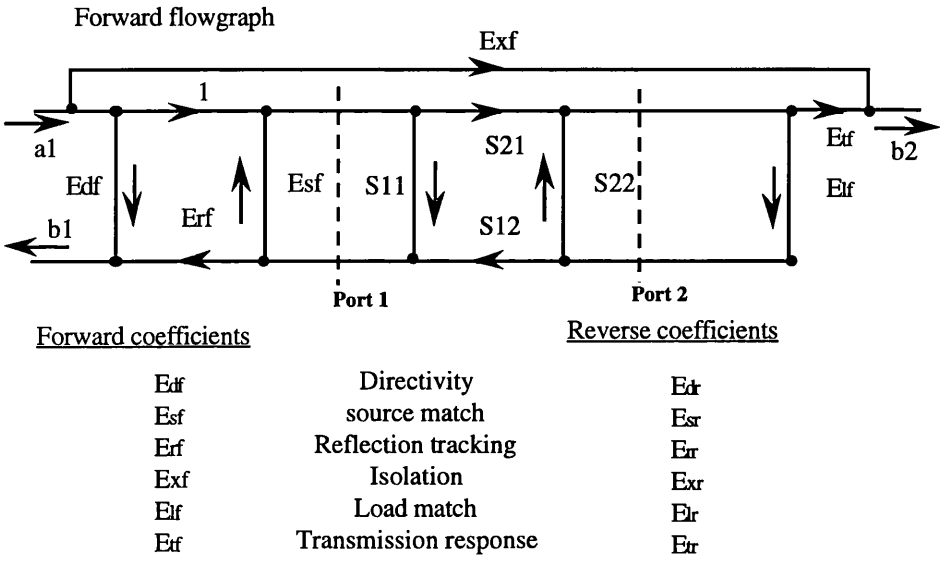

Figure 4.9 A two port measurement flowgraph.

4.6.1 Full 2-port calibration

Full 2-port accuracy enhancement removes all twelve error terms. The forward and reverse terms are measured individually by connecting precise standards to port 1 and port 2. This calibration needs the device under test automatically to be reversed and multiple measurements are made in order to measure all four S-parameters. In the HP-8510B automatic network analyser, this calibration method is not available at frequencies above 26.5 GHz. For measuring the reverse parameters, the device under test should be reversed. It is worth mentioning that the facility of measuring the reverse parameters is available in the new generation of network analysers.

4.6.2 TRL calibration

The TRL calibration procedure is similar to the full 2-port, but uses a different technique for characterizing the error terms. This calibration method is the most appropriate technique for free-wave measurements, since it has been devised for non-coaxial transmission lines (references [60] and [61]).

4.6.3 One-path 2-port calibration

In one-path 2-port calibration, the forward parameters are measured directly and the device under test is reversed for measuring the reverse parameters. The one-path 2-port calibration measures forward error coefficients and considers them for the reverse error coefficients. Although the device under test must be reversed manually to measure its reverse parameters, the measurement accuracy is nearly the same as for full 2-port calibration.

4.6.4 S11 / S22 one-port calibration

A class of calibration which can be used for one-port devices is S_{11} one-port or S_{22} one-port method. This calibration method considers a model for all three error terms and is the most accurate calibration for one-port measurements. A short circuit, an open circuit and a matched load are used for determining three error terms associated with the error model.

4.6.5 Response/Isolation calibration

The last error correction technique, which is more suitable for the devices with low reflection at the input and output ports, is *Response* calibration. In *Response* error correction, the errors due to tracking and isolation are removed. In forward parameter measurements a '*thru*' connector is used to characterize forward tracking and a short or an open circuit is used for determining reverse tracking. The isolation error can be quantified and cancelled out in this technique. The *Response/Isolation* correction model is more suitable for measurement of devices with low reflection coefficient and high insertion loss.

4.7 Millimetre wave calibration techniques

At frequencies above 26 GHz, four types of calibration method are available. The detailed calibration process can be found in reference [62]. In this part, a summary of these methods is presented. At mm-wave frequencies, the present arrangement for the HP-8510B ANA is such that only the forward parameters can be measured and the reverse parameters are measured by reversing the device under test. Table 4.1 gives the different error terms that can be corrected by the available calibration methods.

	Response	Resp./Isol. Refl.	Resp./Isol. Trans.	S11 1-port	1-path 2-port
Frequency Response	X	X	X	X	X
Directivity		X		X	X
Source Match				X	X
Load Match					X
Crosstalk			X		X

Table T4.1 The error terms corrected in the different calibration methods at mm-wave frequencies in the HP-8510B.

Frequency Response corrects the frequency response error. This calibration is appropriate for devices with a small reflection coefficient.

Response/Isolation calibration removes the error associated with both frequency response and isolation. In reflection measurements, both tracking and directivity are removed, while tracking and crosstalk error terms are corrected in transmission measurements. *Response/Isolation* is more suitable for the devices of high insertion loss with well-matched ports.

S_{11} 1-port calibration provides the best accuracy for one-port devices and removes the impact of all three error terms. For performing this calibration technique, three standards are required.

One path 2-port calibration is a combination of S_{11} 1-port calibration, transmission isolation, and transmission frequency response. This calibration method provides the best accuracy for two-port measurements and considers all twelve error terms in the error model, but the device under test must be reversed for measuring reverse parameters.

The relative accuracies of different calibration techniques are shown in figures 4.10 and 4.11. The uncertainty in S_{21} measurements for a well-matched device with insertion loss of -10 dB is better than 0.05 dB, while the accuracy of the measurement of similar device but poorly matched is about 0.2 dB. In one-pass free-wave measurements, the measured scattering parameter is S_{21}. At normal incident reflection measurement or double-pass measurement systems, the required parameters are acquired by measuring S_{11}. As shown in figure 4.10, the error in measuring the reflection coefficient of low loss devices is about twice the error in the measurement of a high loss device. It is also shown that the uncertainty in S_{21} increases sharply for devices with $S_{21} < -20$ dB.

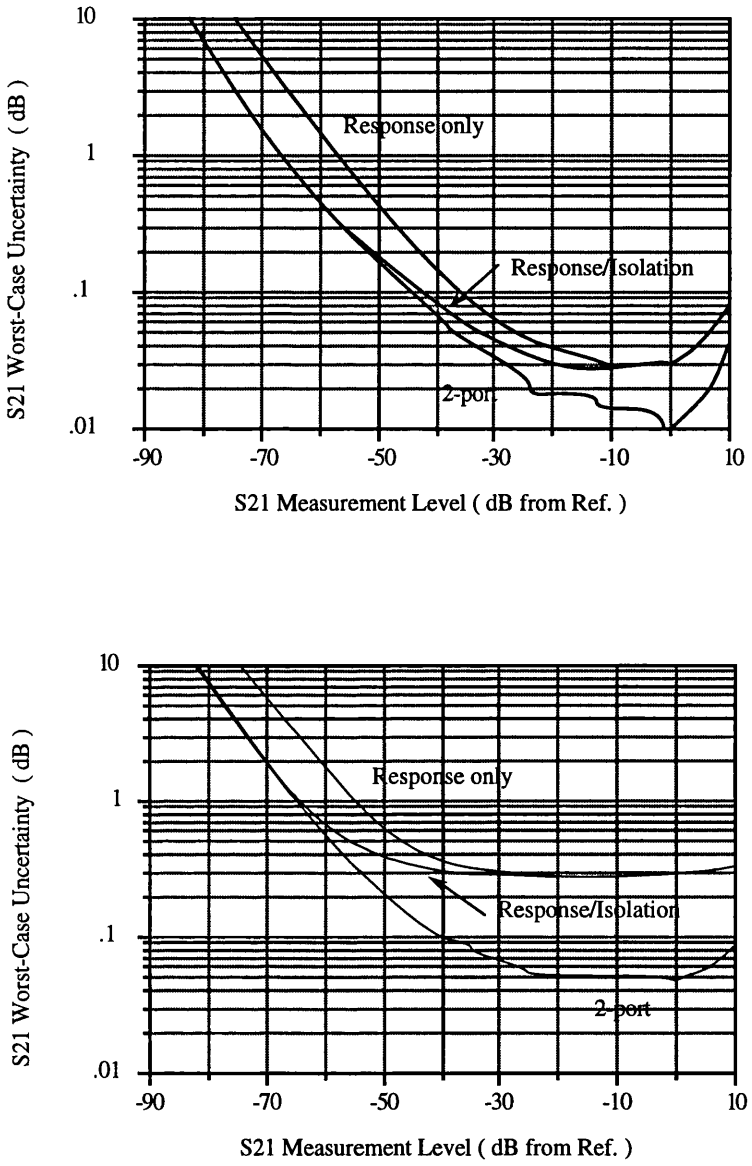

Figure 4.10 Transmission measurement accuracy for various calibration methods.

(a) Upper, S21 uncertainty for a well-matched device (S_{11}=S_{22}=0)

(b) Lower, S21 uncertainty for a poorly matched device (S_{11}=S_{22}=0.5)

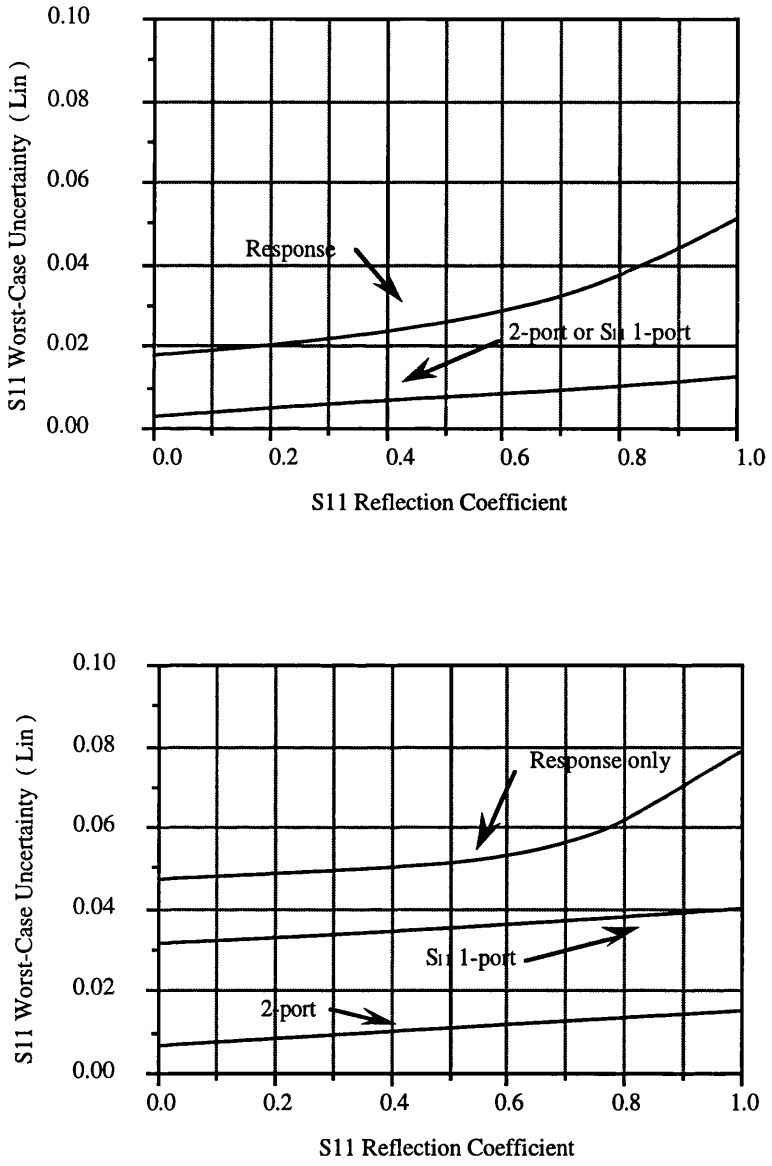

Figure 4.11 Reflection measurement accuracy for various calibration methods.

(a) Upper, S11 uncertainty for a high loss device ($S_{12}=S_{21}=0$)

(b) Lower, S11 uncertainty for a low loss device ($S_{12}=S_{21}=1$)

4.8 Error terms in free-wave measurement

The sources of error described so far are associated with coaxial and waveguide measurements. The propagation of the wave in an unbounded area introduces some other sources of error in free-wave techniques. The plane wave model simplifies the calculation of permittivity and permeability of a slab from the measured transmission and/or reflection coefficients, but the error due to the wavefront curvature and diffraction of the wave from the edges of the sample are not considered in this model. In the plane wave model, the measurement setup and the free-wave paths can be modelled as transmission lines with different characteristic impedances. Using the transmission line equivalent of a free-wave system simplifies the error analysis. A detailed analysis for calculating an equivalent transmission line of a free-wave system can be found in reference [63].

The sources of error associated with free-wave measurements can be divided into two different categories, systematic and random errors. The systematic errors are repeatable and can be modelled theoretically, however some of these error terms are quite complicated and cannot be modelled easily in practice. They are treated as random error, and their impact is reduced by the method used for random sources of error. The background reflections, multiple reflections between the sample surfaces and the antenna, time gating error and multiple reflections within the dielectric lens are the error terms associated with the free-space paths.

4.8.1 Unwanted reflections

Unwanted reflections denote the combination of unwanted signals generated by different mechanisms. The main difficulty in modelling unwanted reflections is their dependance on many parameters, including time. Although the plane wave assumption helps us to model and cancel out some of these error terms, such as multiple reflection within the sample, the propagated wave is not TEM in practice. As mentioned, they are treated as random error. The unwanted reflections themselves are generated by different mechanisms. The main sources contributing to the unwanted reflection are listed in this part.

4.8.1.1 Background reflection

The first type of unwanted reflection is generated by reflecting the wave from the metallic parts of the measurement system. Any changes in the free-space path between the antennas results in an error in the transmission and reflection coefficients. As the vibrations and small changes generated by the acoustic waves are random, this error term is considered as a random term. The quality of the absorbing materials (RAM) is an important parameter in reducing the impact of this error. If this class of unwanted reflections is treated as a systematic error term, such as leakage between two measurement ports, it can be reduced to some extent by using an appropriate calibration method. As explained, for removing any error term from the measurement result it should be characterized and remain unchanged during the calibration and the measurement processes. Averaging is the most effective technique to reduce the effect of this type of error.

4.9.1.2 Multiple reflections

The second class of the unwanted reflections is generated by multiple reflections between the antennas and sample surfaces. At oblique incidence, the reflected wave can be directed out of the measurement system and absorbed, but the use of time domain gating is the most effective technique to reduce the impact of this type of unwanted reflection. The use of radiation absorbing materials can also be considered as a solution for this problem. The radiated beam of an antenna can be focused on a sample by employing a dielectric lens. Multiple reflections within the lens also introduce error in the measurement results and degrade the focusing performance of the lens. The error due to multiple reflections within the lenses cannot be removed by time gating, therefore it is considered as random source of error. In practice, the magnitude of this term should be kept as small as possible by using matched lenses.

4.8.1.3 Sample holder repeatability

Imperfect repeatability of the sample holder is a source of error in reflection coefficient measurements. In free-wave techniques, a flat sheet of highly reflecting material is used as

a standard '*short*'. The location of the front surface of this sheet defines the reference plane. Any misalignment in placing the sample front surface at this plane results in a phase error in the measured reflection coefficient. This error can be reduced only by improving the repeatability and mechanical stability of the sample holder. A practical measurement at R-Band shows a typical error of ±0.05 dB and ±1.5° in the reflection coefficient measurement. At 30 GHz and 45° incident angle, this error corresponds to a displacement of 59 microns in the position of the sample.

4.8.1.4 Near-field measurement

The assumptions of illuminating the sample by a uniform plane wave and a large sample size are not true. In practical measurement systems, the sample surface is illuminated by a spectrum of plane waves travelling at different angles. The measurement in the near-field region introduces new sources of error. The calculation of this error term is extremely difficult, therefore it is treated as a random error term. In chapter 6, the measurement in the near-field region and the impact of the wavefront curvature in the measured transmission and reflection coefficient are discussed.

4.9 Free-wave calibration standards

In free-wave measurements, the matched load used for calibration is a flat sheet of absorbing material, and a flat sheet of highly conductive material is used as a short circuit. The offset short is realized by shifting the location of a short circuit in the direction of propagation. The sizes of the standards should be large enough to intercept the incident wave adequately.

TRL is the most appropriate calibration technique for free-wave measurements. This method is mainly devised for non-coaxial devices and corrects all twelve error terms. In this calibration method, three standards including '*Thru*', '*Reflect*', and '*Line*' are measured to characterize all the error terms. The '*Thru*' standard can be made by connecting two ports to each other, which is equivalent to direct transmission between transmitting and receiving antennas, sample out situation. The '*Reflect*' standard is made by placing a highly conductive sheet in the frame, and the '*line*' standard can be realized

by extending the free-wave path by a specific distance. Unfortunately, *TRL* is not available in the HP-8510B at frequencies above 26.5 GHz. Therefore we have to use the *Response* calibration method, which is the simplest technique of calibrating at frequencies above 26.5 GHz. It is worth noting that this technique removes only the tracking or frequency response error term.

4.10 Maximum error

As mentioned, quantifying the phases of the error terms is not practical, therefore the worst case error analysis is taken into account. In this case, the error vectors are either in phase or 180° out of phase with each other. In coaxial and waveguide measurements, the maximum expected systematic error is given by equations (1) and (2) for reflection and transmission measurements respectively. The source and load mismatches are represented by M_S and M_L. D, T_R, and X_C are directivity, tracking, and crosstalk errors respectively.

$$S11_{\text{Max Error}} = \text{Max.}[\pm D+(\pm T_R.S_{11})+(\pm M_S.S_{11}^2)] \quad \ldots(1)$$

$$S21_{\text{Max Error}} = \text{Max.}[\pm X_C+(\pm T_T.S_{21})+(\pm M_S.S_{21}.S_{11})+(\pm M_L.S_{21}.S_{22})] \quad \ldots(2)$$

In free-wave measurement, the maximum error in the reflection coefficient measurements is the sum of the maximum expected error in the coaxial and waveguide components and the error terms associated with the free-wave paths. The maximum expected errors in the reflection and transmission coefficient measurement are given by (3) and (4).

$$(\text{Reflection Method})_{Max\ Error} = Max.[\pm X_C \pm E_F \pm E_{wc} \pm E_N \pm E_{UR} + (\pm T_T.S_{21}) + (\pm M_S.S_{21}.S_{11}) + (\pm M_L.S_{21}.S_{22})] \quad \ldots(3)$$

$$(\text{Transmission Method})_{Max\ Error} = Max.[\pm X_C \pm E_{wc} \pm E_N \pm E_{UR} + (\pm T_T.S_{21}) + (\pm M_S.S_{21}.S_{11}) + (\pm M_L.S_{21}.S_{22})] \quad \ldots(4)$$

where E_F, E_{wc}, E_N, and E_{UR} are errors due to the frame repeatability, wavefront, noise,

and unwanted reflections respectively. If the measured reflection coefficient is greater than -20 dB, the error due to source mismatch and load mismatch can be ignored. T_T, the tracking error, can be measured in *Response* calibration and X_C, the crosstalk error, can be ignored for low sidelobe antennas. The error due to noise and vibration in the measurement setup can be decreased to a great extent by averaging the measured quantities. Therefore, the maximum expected error associated with the reflection and transmission coefficient measurements can be simplified to equations (5) and (6).

$$Maximum\ Error_{Ref.} = \pm E_F \pm E_{wc} \pm E_{UR} \pm E_R \quad ...(5)$$

$$Maximum\ Error_{Trans.} = \pm E_{wc} \pm E_{UR} \pm E_R \quad ...(6)$$

In practice, the error terms cannot be completely cancelled out in the calibration process and an error term representing the residual error must be taken into account. E_R in equations (5) and (6) represents the residual error after calibration which depends on the type of the calibration method employed.

The sample holder repeatability error (E_F) can be reduced by using rigid materials and taking specific precautions in its mechanical design. The unwanted reflections (E_{UR}), can also be reduced by using absorbing materials. The wavefront curvature error (E_{wc}) has not been studied yet and its significance is investigated in chapter 6.

In frequency range of 26.5 to 40 GHz and for measuring S-parameters greater than -20 dB, the error due to the coaxial and waveguide parts of the measurement system is about ±0.3 dB and ±0.04 dB for high and low reflection coefficients respectively (*Response calibration*, figure 4.5). If we ignore errors due to noise and wavefront curvature, and consider an error of ±0.05 dB and ±1.5° due to the frame repeatability, the maximum expected error in the measurement is ±0.35 dB, ±3.8° and ±0.09 dB, ±2.1° for a high reflection and a low reflection coefficient sample respectively. It is worth noting that the use of other calibration methods like *One-path 2-port* or *TRL* can reduce these quantities considerably.

4.11 Conclusion

In free-wave methods, the measurement accuracy depends mainly on the calibration method used. *Response* is the simplest and most practical calibration technique at oblique incidence, but it is recommended for low reflection coefficient materials. *One-path 2-port* and *TRL* calibration methods are the most accurate calibration techniques in free-wave measurements if they are available at the measured frequencies. It is worth mentioning that these calibration techniques need accurate mechanical positioners for realizing the offset short or reversing the device under test which is not practical in free-wave measurements.

The sources of error including the unwanted reflections from the frame, diffraction from the edges of the sample, wavefront curvature, frame repeatability, background reflections and multiple reflections between the sample surface and the antenna degrade the measurement accuracy. If the reflection coefficient is geater than -20 dB, the number of significant sources of error reduces to two and three for transmission and reflection measurements respectively. There are some techniques that can be used for improving the measurement accuracy, such as using time domain gating. The maximum expected error in the measurement is a combination of error generated by the coaxial and waveguides parts and the error due to the near-field measurement and repeatability.

A full 2 hours warm up and a very stable ambient temperature (23±2 °C) are recommended for high accuracy measurements. A maximum temperature change of ±2 degrees Centigrade can meet the required conditions. The error due to the sample holder repeatability is important in reflection measurement and can be reduced by designing a rigid sample holder.

5 Time gating

5.1 Introduction

In free-wave measurements the wave is propagated in an unbounded area, and the generated unwanted reflections introduce errors in the measured transmission and reflection coefficients. In compact measurement systems, where the sample is placed at a close distance from the antennas, the impact of the unwanted reflections become more significant. There are a number of techniques for reducing the impact of unwanted reflections, such as covering the reflective parts with radiation absorbing materials, directing the unwanted reflections to some other direction and employing the appropriate calibration method. These methods are effective to some extent, but residual error can still cause a significant error in the values for the sample properties.

The use of time domain gating is an effective technique to locate and remove the unwanted reflections. In modern network analysers, the time domain response can be computed from the measured frequency domain response. In the time domain, the unwanted reflections are identified and gated out, then the frequency domain response associated with the gated time domain response is calculated. Although time domain gating is a powerful tool for enhancing the measurement accuracy, it has some limitations and should be used cautiously.

In this chapter, time domain gating and its limitations are reviewed. The sources of error in measuring different types of sample are presented, and the gating error in measuring transmission and reflection coefficients for an ideal gate are calculated. The effect of imperfect gate characteristics are discussed, and the appropriate guidelines for setting the gate parameters are given. The minimum thickness for a sample to be treated as a *thick* slab and the minimum gate width for measuring *thin* samples are discussed. Finally, the error in a real gate for different sample types is simulated and compared with the calculated values for an ideal gate.

5.2 Time-domain reflectometry

In time domain reflectometry, the response of a device to a short pulse is measured in the time domain. If the pulse is adequately short, reflections from different parts of the device under test can be measured individually. In the response generated by the TDR the wanted reflections can be identified and measured. In spite of the ability of TDRs in showing the time domain response of a device, there are a number of intrinsic limitations associated with this technique. As shown in figure 5.1, the reflection from the discontinuity masks the reflected wave from the subsequent mismatches, (masking effect). As the number of discontinuities in the device under test increases, multiple reflections between them make interpretation of the response more difficult. In the time domain response, the magnitude and the phase of the reflections cannot be specified at a given frequency which limits the direct application of TDRs in free-wave techniques. In measuring dispersive devices, interpreting the time domain response also becomes more difficult

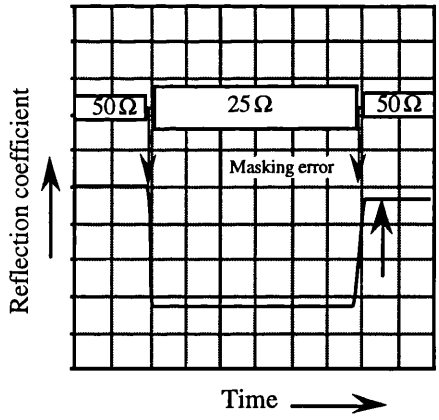

Figure 5.1 Masking effect in the time domain response.

In conventional time domain reflectometers, the response of the device under test to a short pulse is measured in the time domain. In synthetic time domain reflectometers the measurement is carried out in the frequency domain, and the time domain response is computed from the frequency domain measurement. Since the measurement is carried out in the frequency domain and in a relatively narrow frequency band, the calculated time domain benefits from the error correction facility and the high dynamic range of the

network analyser. In spite of the great flexibility synthetic time domain reflectometers, there are also some intrinsic limitations associated with them.

5.2.1 Conventional TDR

In conventional TDRs, the response of the device under test to a short pulse is measured in the time domain. Although the useful information can be deduced from the time domain response, it cannot be used directly in free-wave measurement. In the time domain, the ability to distinguish between two adjacent responses is a function of pulse width. For achieving a high resolution time domain response a short pulse should be applied to the device under test, and the required bandwidth for measuring the response of a device to a short pulse reduces the signal-to-noise ratio which results in a poor dynamic range.

5.2.2 Synthetic TDR

In synthetic time domain reflectometers, the time domain response is computed from frequency domain measurements. In the calculated time domain response, the unwanted reflections can be identified and cancelled out mathematically. Then, the frequency domain response can be computed from the gated time domain. Modern network analysers can carry out the whole process of calculating the time domain response from the measured frequency response, gating out the unwanted reflections and computing the gated frequency response in real time. Therefore, the gated frequency response can be measured easily. Since the measurement is carried out in a limited frequency span, the computed time domain response is different from those measured by conventional TDRs.

The Fourier transform describes the mathematical relationship between the time domain and frequency domain responses of a device. Either of these responses can be calculated if the other one is defined. The measurement in the frequency domain by automatic vector network analysers benefits from a wide dynamic range and error correction facilities. Therefore, the time domain response computed from the frequency response also benefits from the same advantages. Since a *Hewlett Packard* automatic network analyser (HP-8510B) is used in this project, *HP* terminology is used throughout this thesis to define the gating process.

The band pass nature of the components used in free-wave measurement forces us to use the *Band Pass Impulse* mode of operation which calculates the response of the device under test to an impulse (very short pulse). As we know, the frequency spectrum associated with an impulse is spread over an infinite interval in the frequency domain, (figure 5.2). Therefore the frequency response of the device at all frequencies is required for reconstructing the impulse response of the device.

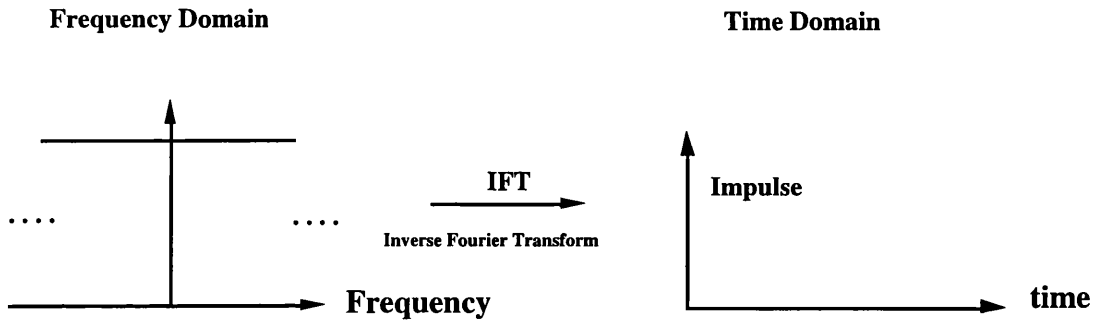

Figure 5.2 Frequency spectrum of an ideal impulse.

In practice, the network analyser measures the response of the device only at a limited number of frequencies. The measurement at discrete frequencies also causes the calculated response to be repeated in the time domain. The measurement in a limited frequency span causes the computed response to be equivalent to the response of the device to a short pulse, and the shape of this pulse is a function of frequency span over which the measurement is carried out. In order to clarify the process of calculating time response from the measurement in the frequency domain, we consider a device with a uniform frequency response such as a short circuit (figure 5.3). The time domain response of this device can be calculated by taking the Fourier transform of the response in the frequency domain. The Fourier transform of a rectangular function is a sinc function whose width is the inverse of the frequency span.

In practice, the measurement is carried out at discrete frequencies. Sampling in the frequency domain causes the time domain response to repeat itself at intervals of $1/\Delta f$ seconds, where Δf is the sampling frequency interval. The measurement in a limited

frequency span and at discrete frequencies introduces some restrictions to the time domain response which are discussed in the next section.

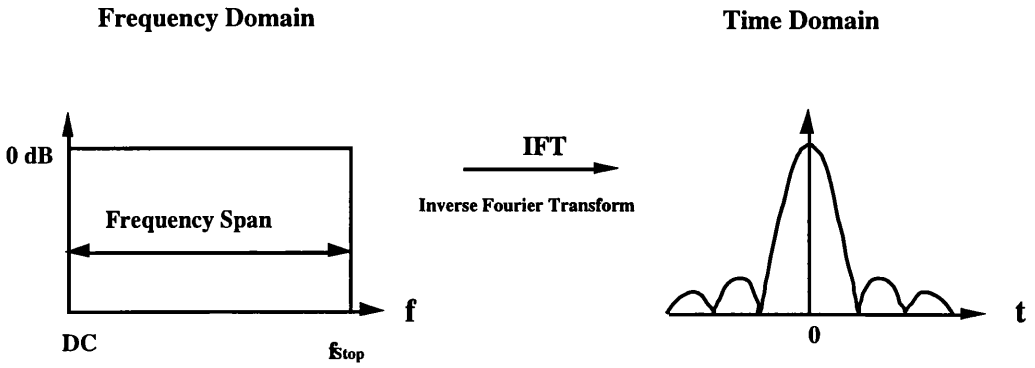

Figure 5.3 The time response associated with a rectangular function.

5.3 Time domain gating limitations

The time gating technique is based on identifying and cancelling out the unwanted reflections in the time domain response. Therefore, the frequency response calculated from the gated time domain response does not include the unwanted reflections. The use of time domain gating improves the measurement accuracy, if the gate parameters are set properly. In this part, the intrinsic limitations with the time gating technique and the associated sources of error are presented. First, the basic terms and definitions in this technique are explained. Then, the mechanisms involved error generation and the techniques to reduce their impact on the measurement results are presented.

5.3.1 The alias-free range

As mentioned, the measurement at discrete frequencies causes the calculated time response to be repeated in the time domain, (figure 5.4). In the time domain, the distance between two identical responses is defined as the alias-free range. In the time domain response, the location of each reflection can be measured in the alias-free range without any ambiguity. The alias-free range is equal to the inverse of the sampling frequency ($1/\Delta f$). This range is more important in characterising devices with a long electrical length such as delay lines. In practice, the alias-free range can be extended by increasing the number of measured

frequencies per sweep. The alias-free range does not cause any significant problem, since the free-space path between transmitting and receiving antennas is cancelled out in the calibration process.

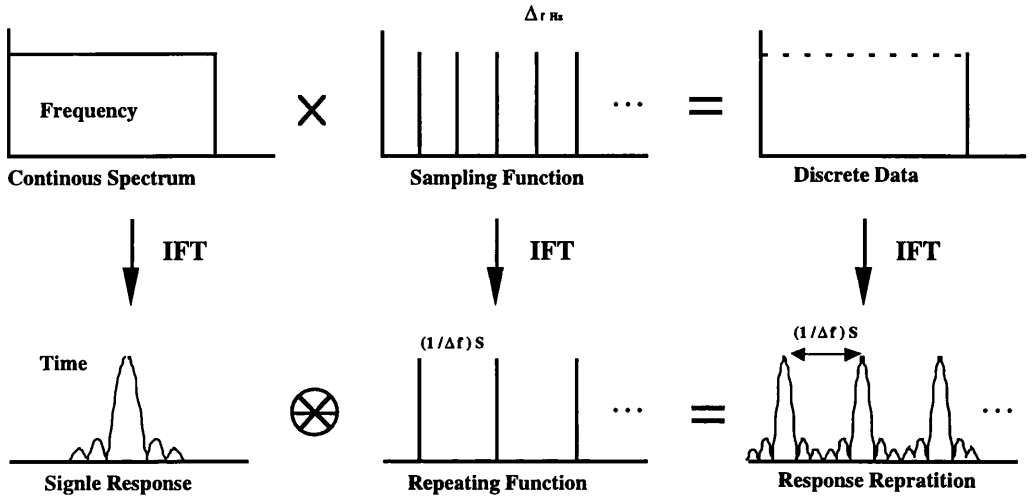

Figure 5.4 The effect of sampling on the calculated time domain.

5.3.2 Response resolution

The ability to resolve the responses of two closely spread objects in the time domain is defined as the response resolution. In the time domain response, distinguishing between the wanted and unwanted components depends on the response resolution and the spacing between them. As the unwanted reflections must be identified and gated out, the response resolution is a key parameter in time domain gating. The response resolution is inversely proportional to the frequency span. The achievable response resolution, which is equal to the width between two -6dB points in the time response, is $0.45/f_{span}$, $0.6/f_{span}$ and $1.2/f_{span}$ for *Narrow*, *Normal* and *Maximum* window types respectively. The response resolution is mainly limited by the frequency span over which the measurement is carried out. In mm-wave frequencies, the maximum frequency span is mainly limited by the maximum usable bandwidth of the waveguide. The maximum frequency span, and consequently the achievable resolution, increases at the upper end of mm-wave frequencies.

5.3.3 Windowing

As explained, the time response associated with a uniform frequency response is a sinc function. The sidelobes associated with a sinc function can mask small responses and reduce the dynamic range, (figure 5.5). In order to improve the sidelobe level and increase the measurement dynamic range, the measured quantities are weighted by a mathematical function before applying the Fourier transform. The weighting improves sidelobe level at the expense of increasing the main lobe width. In the HP-8510B, three functions with different weighting factor can be selected. Each of these windows is appropriate for a specific type of measurement.

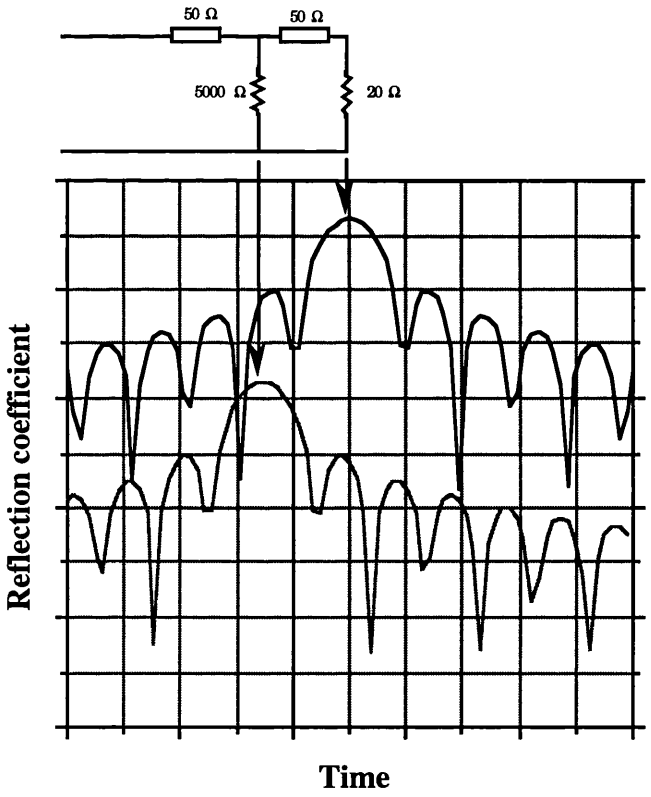

Figure 5.5 The small responses by the side lobes of a strong response.

The width of the main lobe defines the resolution in the time response (response resolution). In free-wave measurements, a high spatial resolution is required to distinguish the wanted responses from the unwanted reflections. In the time domain response, the resolution is limited by the frequency span and the type of window. Figure 5.6 shows the

effect of the three available windows in the HP-8510B on a uniform function. Each of these windows is appropriate for a specific type of device.

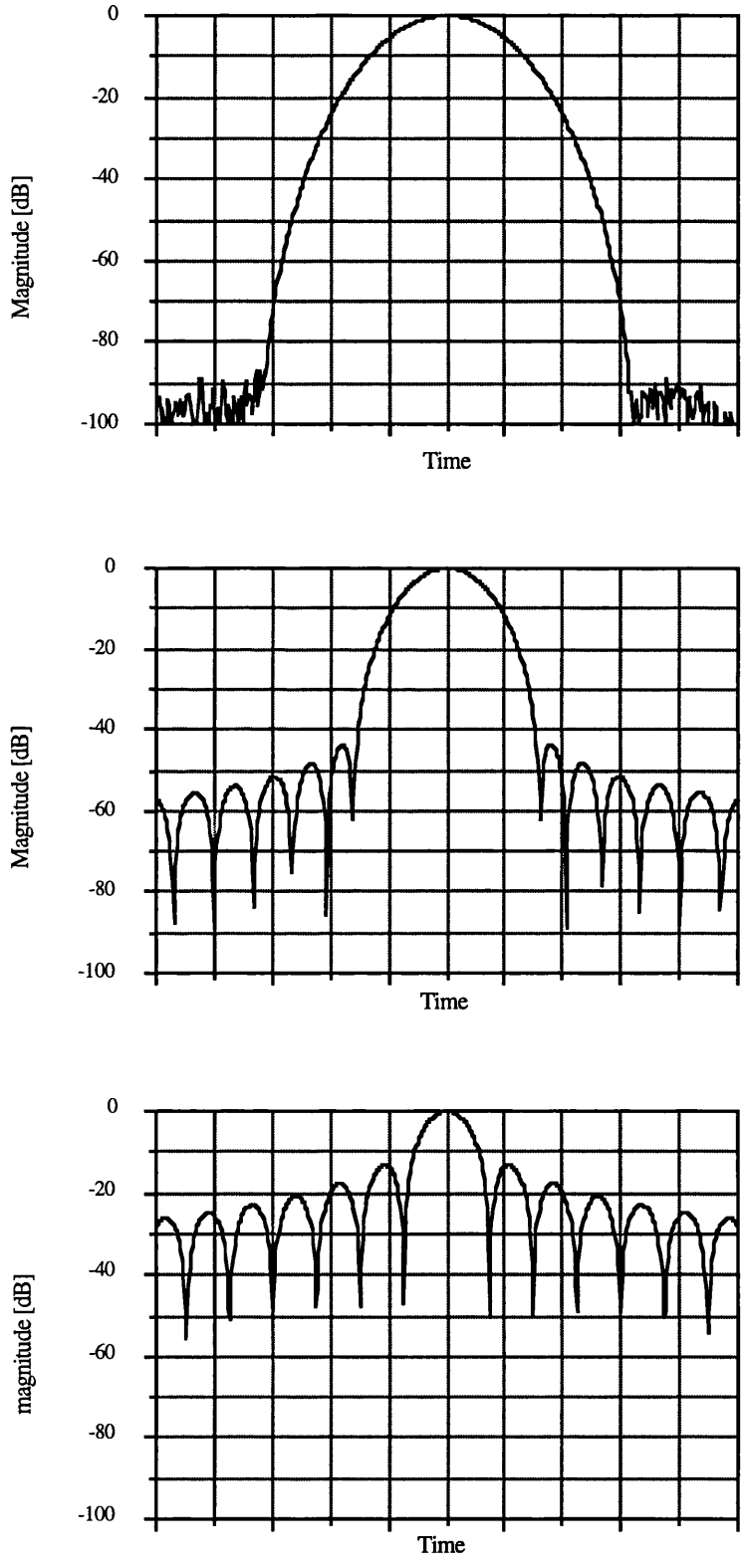

Figure 5.6 Different window types in the HP-8510B.

5.4 Time gating error

Time domain gating is a mathematical process and four different gate shapes can be selected in, the HP-8510B. Figure 5.7 shows the specifications associated with each gate shape. The pass band ripple and the cutoff rate make each of them appropriate for a specific type of measurement.

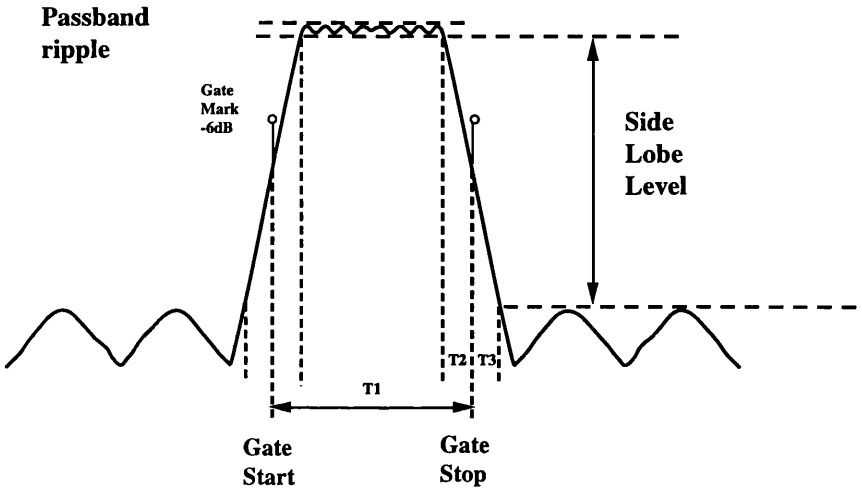

Gate Shape	Passband Ripple	Sidelobe Level	Cutoff Time T2=T3	Minimum Gate Span T2
Minimum	± 0.40 dB	-24 dB	0.6 / f_{Span}	1.2 / f_{Span}
Normal	± 0.04 dB	-45 dB	1.4 / f_{Span}	2.8/ f_{Span}
Wide	± 0.02 dB	-52 dB	4.0 / f_{Span}	8.0 / f_{Span}
Maximum	± 0.01 dB	-80 dB	11.2 / f_{Span}	22.4 / f_{Span}

Figure 5.7 Specifications of each gate shape in the HP-8510B.

Although the use of time gating can remove the effect of unwanted reflections, it introduces some errors in the measured transmission and reflection coefficients. The imperfect characteristics of the gate and the measurement at discrete frequencies result in some constraints in the time gating technique. Discarding a part of the wanted data in the time domain also introduces error in the gated response. As we know, a limited function in the frequency domain has an unlimited duration in the time domain. Therefore, the time domain

response calculated from the measurement in a limited band of frequencies is spread over an infinite interval in the time domain. Regarding the limited width of the gate, a part of the measured data is discarded in the gating process. This causes error in the measured parameter which is more serious in devices with long electrical length.

Multiple reflections within a slab can be represented by a geometric series of infinite terms. If the multiple reflections are taken into account in calculating the complex permittivity and permeability, all terms of this series should be considered in the measurement. In free-wave techniques, the gating is mainly used for removing the effect of the unwanted reflections from the measured parameters. In the time domain response, the multiple reflections between the sample surfaces and the antennas constitutes the nearest unwanted reflection to the wanted response. The location of this reflection depends on the geometry of the measurement system, and the time gate should be narrow enough to exclude it. Therefore, the higher order terms of the multiple reflections located outside the gate are discarded in the gating process.

If the higher order terms of the multiple reflections are not taken into account and the sample treated as a *thick* slab, the gate width should be narrow enough to exclude all the higher terms of multiple reflections. As mentioned, the minimum gate span is dictated by the frequency span over which the measurement is carried out. If the electrical length of the sample is not sufficiently great, the higher order terms cannot be eliminated by the gating technique. In *thick* sample measurements, failure to eliminate the higher order terms of the multiple reflections is the main source of error.

5.5 Time gating error analysis

The error mechanisms taking part in the time domain gating are quite complicated and cannot be modelled easily, but the error can be calculated for an ideal gate. In a real time domain gate, the specifications of the gate and the response of the device should be well defined. In calculating the error for a real gate, the use of Fourier transform and the other time consuming computations is inevitable. A practical method for estimating the gating error is to use the available facilities in the network analyser to simulate different gate parameters on the measured response.

In order to simulate the gating error in the HP-8510B, the transmission and reflection coefficients of a slab with given properties are calculated and saved in the network analyser memories. The network analyser calculates the time domain response from these data, then time gates with different parameters are applied. As the original response is well defined and saved in the computer memories, the changes between two responses can be found by comparing them.

The systematic error due to the gating can be categorized into two classes. The first type includes the error caused by discarding the higher order terms of the multiple reflections within the slab. For an ideal gate, this error can be calculated. This error term is mainly considered in the *thin* sample measurements. The inability of the gate to separate two close reflections in the time domain and imperfect gate characteristics like pass band ripple and finite sidelobe level constitute the second type of error. This error term cannot be calculated easily, since it is quite complicated and all the parameters associated with sample and gate take part in constituting this error term. This type of error is mainly taken into account in the *thick* sample measurement, where the higher order terms of the multiple reflections within the sample should be removed by the time gating technique.

5.6 Time gating error simulation

The available facilities in the HP-8510B can be used for simulating the gating error. In the time gating process, the measured data in the frequency domain are saved in the network analyser memories, then they are used to compute the corresponding time domain response. A computer program modelling scattering parameters of electrical circuits is used for calculating transmission and reflection coefficients associated with a slab. This computer program has the capability of transferring data through the HP-IB to the network analyser. For simulating the gating error, a free-wave measurement system is modelled by a number of transmission lines. Then, the transmission and reflection coefficients associated with the sample are calculated by this program (Circuit Modelling Program) and saved in the allocated memories in the network analyser. The calculated data are considered as measured data, and all the required mathematical operations associated with applying different gate parameters are carried out.

5.7 Transmission line model

Figure 5.8 shows the model associated with a free-wave measurement system. In this model, the mismatches in the antennas and the diffraction of the wave from the edges of the sample are ignored. In order to simplify the modelling, the propagated wave is also assumed to be a uniform plane wave, (plane wave model). For calculating the transmission and reflection coefficients of a slab by the Circuit Modelling Program, the mathematical relationship between the transmission line parameters and the slab properties should be defined. In the Circuit Modelling Program, a transmission line is defined by its length, characteristic impedance, shunt and series impedances per unit length. The detailed calculations and the required derivations can be found in appendix 1.

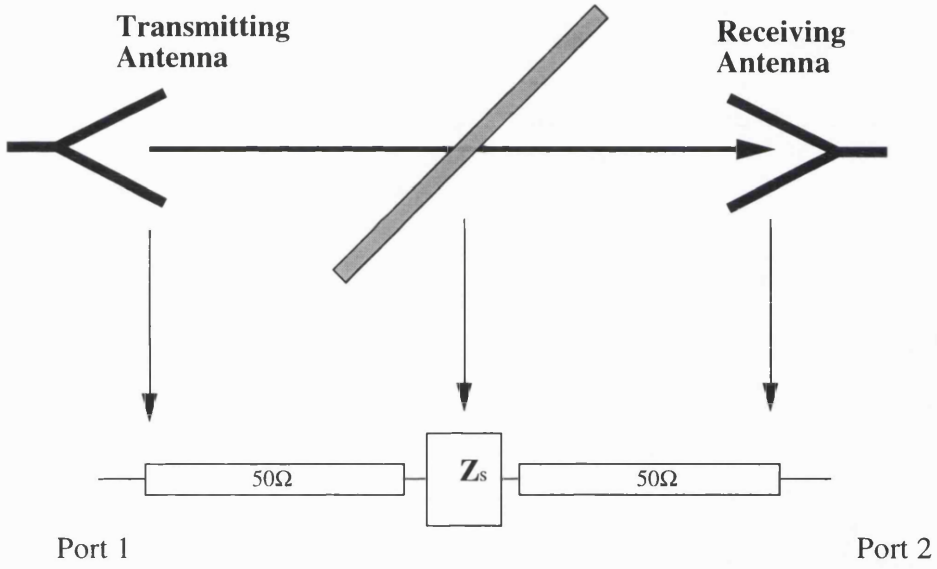

Figure 5.8 Free-wave measurement system transmission line model.

In the transmission line model, the magnetic loss is simulated by a series resistance and the dielectric loss is represented by a shunt conductance. The transmission line model gives precise transmission and reflection coefficients associated with a slab only for lossless materials. Since this model does not accept variable parameters, modelling the lossy material is not accurate in this model. Therefore, some differences between the simulated loss by this model and actual loss associated with a slab are expected. These differences are not crucial for our purpose and can be ignored (appendix 1).

5.8 Thin slab time domain gating error

As explained, discarding the higher order terms of the multiple reflections within the sample introduces errors in the measured transmission and reflection coefficients. In this calculation, the imperfect characteristic of the gate is ignored and the unwanted reflections are not taken into account. The maximum gate width is limited by the distance between the sample surface and antenna (figure 5.9).

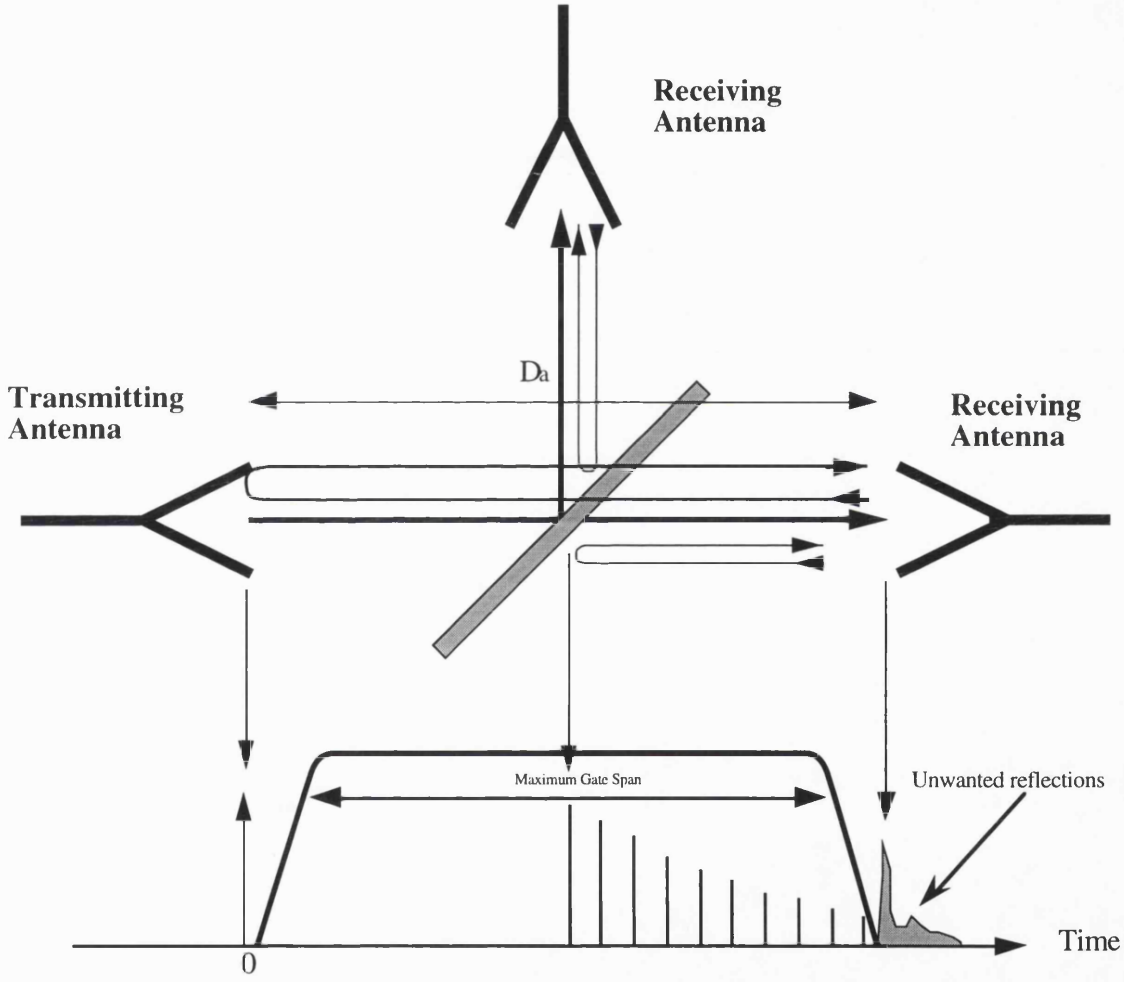

Figure 5.9 Unwanted reflections in the measurement system.

5.8.1 Thin slab transmission error

If the multiple reflections are taken into account, the total transmitted wave through the slab can be expressed by a geometric series. In the gating process, higher order terms of this

series are discarded. If only the first N components of the multiple reflections are included in the gating process, the discarded components introduce error in the measured transmission coefficient. Figure 5.10 shows the process of gating higher order components of the multiple reflection in transmission coefficient measurements. The detailed derivation of the error in transmission coefficient measurement for an ideal gate can be found in appendix 2.

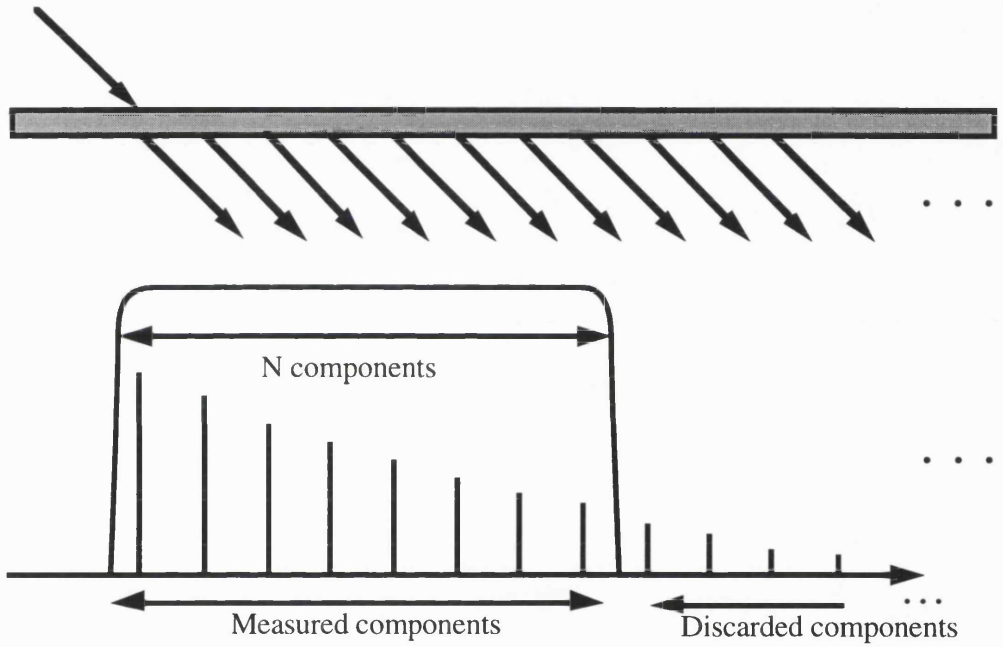

Figure 5.10 The higher order of multiple reflection within the sample in a transmission coefficient measurement.

5.8.2 Thin slab reflection error

As shown in figure 5.11, the total components of the reflected wave from a slab can also be shown by a geometric series. Discarding a number of higher order terms of the multiple reflections results in an error in the magnitude and the phase of the measured reflected wave. If the first N components are included in the gating process, the maximum expected error for a given sample and an ideal gate can be calculated, (appendix 3).

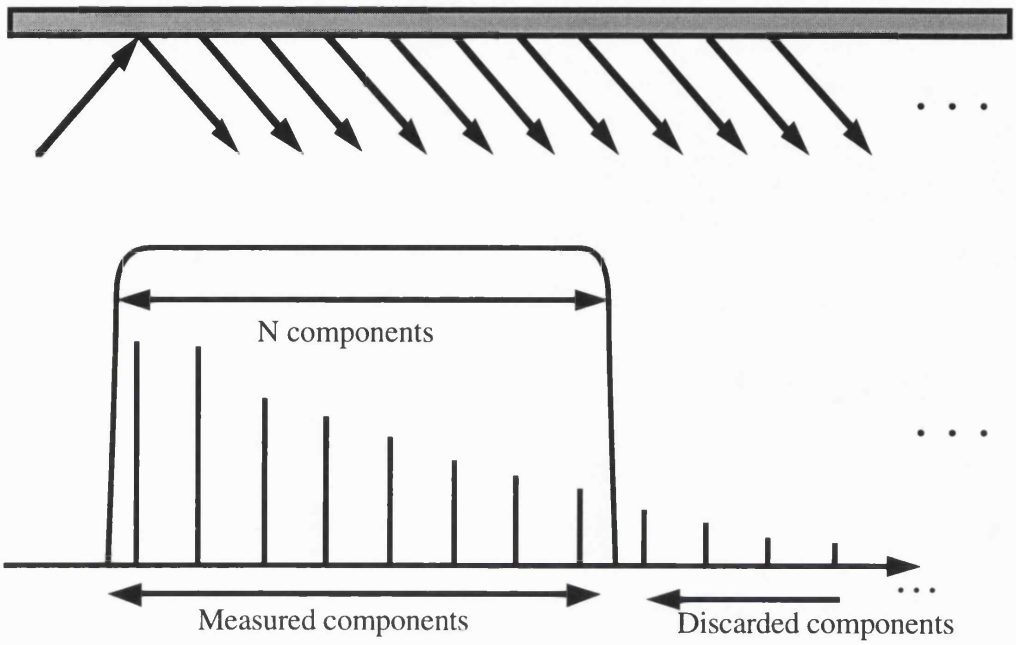

Figure 5.11 Discarding the higher order of multiple reflection within the sample in a reflection coefficient measurement.

5.9 Slab thickness

In *thin* sample measurements, the multiple reflections within the sample should be taken into account. In this case, the main restriction on the gate parameters is the maximum gate width, which results in discarding the higher order terms of the multiple reflections. If the combination of the sample thickness and the material properties is such that only the main term of the multiple reflections can be measured, (*thick* slab), the dependence of the measurement accuracy on the sample electrical length decreases considerably.

Thick sample measurements are based on measuring the main term of the multiple reflections. In *thick* slab measurement, the main limitation is the minimum gate width which is dictated by the frequency span. Although treating a sample as a *thick* slab is usually preferred, the measurement in a limited frequency band imposes a minimum sample thickness. In the next part, we define a set of simple criteria for setting the gate parameters with regard to the the sample thickness.

5.10 Thin slab time gating error simulation

As mentioned, the magnitude of the multiple reflections within the sample decreases as the wave is reflected from the sample surfaces. The rate of decay depends on the loss properties of the sample and the sample thickness. In the plane wave model, the total transmitted or reflected wave is expressed by a geometric series. The elements of these series are spaced by twice the sample electrical length in the time domain, and the geometry of the measuring system defines the maximum gate width. In gating process, all the responses outside the time gate are discarded. In *thin* sample measurements, the gating error can be calculated from appendices 2 and 3 for an ideal gate.

If the magnitude of the error term is less than -50 dB with respect to the measured parameter, an error of 0.03 dB in magnitude and 0.2° in the phase of the measured parameters are expected. For achieving this accuracy, the gate should be wide enough to include the required number of the multiple reflections terms. In the prototype measurement system, transmitting and receiving antennas are located 30 centimetres apart. Therefore, the main unwanted reflection occurs as close as 1000 picoseconds from the main response. This reflection is generated by bouncing the wave between the sample surfaces and the antennas, therefore the gate width should be narrow enough to exclude this reflection.

If only the first 3 terms of the multiple reflections in a loss-less dielectric slab with permittivity of 9 are included in the gating process, the gating error is -36 dB lower than the measured parameter. This error vector results in an error of 0.13 dB and 0.9° in the magnitude and phase of the transmission coefficient. In this case the gate width is as wide as six times the slab electrical length, but the error is considerable.

If the first 4 terms of the multiple reflections are included in gating process, the expected error is 0.03 dB and 0.2° in the magnitude and phase of the measured transmission coefficient. In this case, the gate width should be as wide as eight times the sample electrical length. Regarding the maximum gate width (30 cm), the sample electrical length should be less than 125 and 166.6 picoseconds for gating the first four and three terms of the multiple reflections respectively.

The above calculations are based on an ideal situation. In order to evaluate the validity of

this calculation for a real gate, the gating error in the HP-8510B can be simulated, (appendix 5).

In the first example, the gating error in a lossless dielectric slab ($\varepsilon_r = 2.6$) with thickness of 10 mm is simulated. The intrinsic limitations of the time domain gating cause the error to increase rapidly at the two ends of the measured frequency band. The simulation results show that a gate width of 500 picoseconds is wide enough for measuring the transmission and reflection coefficients with acceptable accuracy. It is worth noting that the discrepancies between the calculated and simulated gating error are due to the finite frequency span.

If the sample electrical length is such that a gate width of wider than 1000 picoseconds is needed, the unwanted reflections cannot be attenuated sufficiently. In the second example, the gating error in a lossless dielectric with long electrical length ($\varepsilon_r = 10.4$), and thickness of 10 mm is simulated. The detailed simulation results can be found in appendix 5. The comparison of the results obtained from the calculation and simulation show a good agreement. It can be concluded that the electrical length of this sample is not small enough to be treated as a *thin* slab.

If the decay rate of the multiple reflections within the sample is sufficiently high, the multiple reflections can be ignored. In the third example, the gating error in a lossy ferrite sample is simulated. Sample 3 is a ferrite ($\varepsilon_r = 7.5 - j0.50$, $\mu_r = 0.8 - j0.15$) with thickness of 10 millimetres, corresponding to an electrical length of 24.49 mm. The detailed simulation of the gating error in sample 3 can be found in appendix 5. The results obtained from the simulation agree with the maximum calculated error for an ideal gate. The loss properties of this sample causes the multiple reflections to decay rapidly, therefore a narrower gate can be used. In this sample, a gate with 500 picosecond width is sufficiently wide to include all the significant terms of multiple reflections.

Simulating the gating error in these samples shows that the gate width should be at least six times wider than the sample electrical length in measuring low-loss materials. In lossy materials, multiple reflections can be ignored if the propagation coefficient (P) is less than -15 dB.

5.12 Thick slab time gating error simulation

If the propagation coefficient (*P*) is less than -15 dB, multiple reflections within the sample can be ignored. In this case (*thick* sample), the calculation of permittivity and permeability becomes simpler and the dependence of total accuracy on sample electrical length decreases. As mentioned, the minimum gate width is dictated by the frequency span and the gate shape. In *thick* sample measurement, the gate should be narrow enough to separate two adjacent terms of the multiple reflections which are separated from each other by twice the sample electrical length. The maximum available frequency span in R-band is 13.5 GHz, therefore the minimum gate width is 88, 206, 592 and 1658 picoseconds for *Narrow*, *Normal*, *Wide* or *Maximum* gate shapes respectively. Simulating the gating error in *thick* sample measurement shows that slabs with minimum electrical length of 1.5~2 times the gate width can be treated as *thick* slabs.

5.13 Conclusion

Time domain gating error is mainly caused by either discarding the higher order terms of the multiple reflections within the sample or by the intrinsic imperfections of the time domain gate. The maximum gate span is dictated by the location of the most significant component of the unwanted reflections in the time domain response. This reflection generated by bouncing the wave between the sample surface and the antenna, and the location of this reflection is equal to the antenna distance in the time domain response. Regarding the geometry of the prototype measurement system, the maximum usable gate width is 1000 picoseconds corresponding to 30 cm.

The frequency span over which the measurement is carried out and the gate parameters dictate the minimum gate width. At R-band (26.5 to 40 GHz), the minimum gate width is about 26 mm. This gate width is calculated for 13.5 GHz frequency span and *narrow* gate shape. The edge effect in the time gating technique causes the error at two ends of the gated response to increase rapidly. For *Minimum* and *Normal* gates, the usable area in the gated response is the centre frequencies of the bandwidth, while this region extends to 60% and 80% of the full range for *wide* and *maximum* gate shapes (figure A5.2).

In measuring *thin* slabs, multiple reflections within the sample are taken into account in calculations and the gate width should be wide enough to include the most significant components of the multiple reflections. The number of terms of multiple reflections which should be included in the gating process is a function of the material properties and the acceptable tolerance in the measurements. For low-loss materials, at least the first three terms of multiple reflection should be included in the gating process to achieve an acceptable tolerance.

In measuring low-loss materials with high electrical length, a wide gate width is required. The measurement of lossy material requires a narrower gate width, since the multiple reflections decay rate is higher. If the required gate width for measuring a *thin* slab cannot be implemented, treating the sample as a *thick* slab is recommended. The maximum gate width for a *thin* slab and the maximum thickness for a slab to be considered as a *thin* sample can be calculated for an ideal gate.

The gating error increases sharply in measuring reflection coefficients at frequencies where the sample electrical length is a multiple of 180°, and the measurement should be avoided at these frequencies. In the reflection coefficient measurement the multiple reflections start decaying from the second term, therefore a wider gate should be considered for measuring the reflected wave.

If the combination of sample thickness and material properties is such that only the first term of the multiple reflections within the sample can be measured, the calculations become simpler and the measurement accuracy becomes less frequency dependent. If time domain gating is used for separating the higher order terms of the multiple reflections, the gate width should be narrow enough to suppress the unwanted reflections adequately. The minimum thickness for a sample to be considered as a *thick* slab is a function of the gate shape and the frequency span over which the slab is measured. For 13.5 GHz frequency span and *Narrow* gate, the electrical length of a slab should be greater than 40 mm to be treated as a *thick* sample.

6 Angular spectrum model

6.1 Introduction

In free-wave techniques the relationship between the sample properties and the measured parameters is expressed by a mathematical model, and the achievable accuracy depends on how realistically this model relates the transmission and reflection coefficients to the material properties. In the plane wave model, the sample is assumed to be illuminated by a uniform plane wave and the diffraction of the wave from its edges is ignored. These assumptions simplify calculations, but the effect of the measurement in the near-field region is not taken into account. This error can be ignored if the sample is placed at a distance adequately far from the antenna. But in compact free-wave systems, where the measurement is carried out in the near-field region, the wavefront curvature error can be significant.

In this chapter, a new model for calculating the properties of a slab from the measured transmission and/or reflection coefficients in the near-field region is introduced. The improvement of the angular spectrum model in reducing the total error is shown, and the limitations in using this model are presented. The use of a lens antenna for reducing the diffraction of the wave from the edges of the sample is studied, and the associated sources of error in using a focused beam are discussed.

6.2 Antenna coupling

Diffracted waves from an aperture can be approximated by a uniform plane wave only at very far distances from the aperture plane. At the front of a radiating aperture, three distinct regions are defined. The first region, which starts from the aperture plane, is the reactive region in which the evanescent waves as well as propagating waves contribute to constituting the field. This region is few wavelengths wide. The next region is the Fresnel region where all the propagating waves in the angular spectrum contribute to constituting

the field. This region extends to many wavelengths beyond the radiating aperture. The Fresnel region eventually shades into the far-field region where the field is determined by a single plane wave. In practice, free-wave measurements are carried out in the Fresnel region, where all components of the angular spectrum contribute to constitute the transmitted and reflected waves.

If a slab is illuminated by a spectrum of plane waves the transmitted and reflected waves are distorted, and the location of transmitted and reflected waves also displaced from what geometric optics predicts. The lateral shift and deformation of the reflected beam are studied by many researchers (references [64] to [71]). But none of them gives an explicit formula for calculating transmission or reflection coefficients of a slab in the near-field region. The angular spectrum model calculates transmission and reflection coefficients of a slab illuminated by a spectrum of uniform plane waves.

In free-wave measurement systems the sample surface is illuminated by the transmitting antenna, and the reflected or transmitted wave is measured by the receiving antenna. For calibrating the measurement system, the reflection coefficient of a metal sheet or transmission coefficient of the empty sample holder is used. Then, the sample is placed in the sample holder and the coupling between receiving and transmitting antennas is measured. The coupling between two antennas while the wave is reflected from or transmitted through the sample is given by equation (1). $F_X^T(\alpha, \beta)$ and $F_X^R(\alpha, \beta)$ are the Fourier transform of the field distribution at the plane of transmitting and receiving antennas, δe is a complicated function expressing the interaction of the sample. The detailed derivation of transmission and reflection coefficients of a sample which is indeed the coupling between two antennas is presented in appendix 7.

$$C = \frac{\lambda_0}{2Z} \int_{\alpha,\beta=-\infty}^{+\infty} F_X^R(\alpha, \beta) F_X^T(\alpha, \beta) \delta e \exp\left(\frac{-j\, 2\pi D_a \gamma}{\lambda_0}\right) d\alpha\, d\beta \qquad \ldots(1)$$

The coupling between two antennas while the wave is reflected from or transmitted through a slab is a generalized form of the case investigated by Clarke and Brown [72]. For very long antenna distances, the coupling integral can be simplified by using the stationary phase method. But the use of numerical methods for calculating transmission and reflection coefficients of a slab in the near-field is inevitable in practice.

6.3 Angular spectrum model

The transmission and reflection coefficients of a slab in the Fresnel region can be calculated by determining the coupling integral, equation (1). In the general case, this integral cannot be expressed by a closed mathematical expression. The phase of the exponential term in the integrand varies rapidly with the spatial angle, and the rate of phase changes is proportional to the antenna distance (D_a). In order to have a tolerable error in the computation, the integrand should be calculated at an adequate number of points. In determining this integral, the Fourier transform of electric field at the plane of transmitting and receiving antennas should also be calculated, therefore the antenna excitation should be well defined.

For small antenna distances, the coupling integral can be computed accurately with a moderate number of points by numerical algorithms, but the computation error increases with increasing antenna distance. Therefore the number of points in computing the coupling integral should be increased by increasing the antenna distance. Failing to consider adequately small increments in computing the integral results in instability in the calculated values. This instability is caused by the oscillatory nature of the exponential term in the integrand and can be removed only by increasing the number of points. The limitations associated with determining the coupling integral and the angular spectrum model are discussed in appendix 9.

In the calibration process, transmission through the empty sample holder or the reflection from a flat metal sheet are measured. In the angular spectrum model, the contribution of all elements of the spectrum in constituting the transmitted and reflected waves are taken into account. A computer program evaluating the coupling integral is used for simulating the measured transmission and reflection coefficients of a sample in the near-field region.

The diffracted wave from the antenna can be focused on a small area on the sample surface by using dielectric lenses or microwave reflectors. Therefore, the diffraction from the edges of the sample can be reduced and a smaller sample can be used. In practice matching a dielectric lens in a wide frequency band is difficult, and the multiple reflections within the lens degrade the focusing performance of the antenna. If the multiple reflections within the lens and the mismatches of the lens are ignored, a lossless dielectric lens can be introduced to the angular spectrum model easily.

In order to study the effect of the aperture field distribution on the transmission and reflection coefficients, three different types of antennas are considered. In the first type (*diverging beam*), there is no lens at the front of the aperture and the wave starts propagating spherically from the antenna phase centre. If the phase of the propagated wave is compensated by a dielectric lens such that the wavefront is plane at the antenna aperture (*parallel beam*), the wave propagates in a more collimated fashion. In the third type (*converging beam*), the dielectric lens is such that the wave is focused on a focal point at the front of antenna. It is worth mentioning that the wave is focused to a point in theory, but the diffraction of the wave and the multiple reflection within the lens degrade the focusing quality and the wave is focused to a larger spot.

6.4 Near-field measurement error simulation

In this part, the wavefront curvature error in transmission and reflection coefficient measurements is studied. In appendix 9, the simulated error in two lossless dielectric slabs and a ferrite sample are presented. Figure 6.1 shows the wavefront curvature error in a dielectric sample ($\varepsilon_r=2.6$). As can be seen, the error approaches zero by increasing the antenna distance. In the near-field the error in magnitude of the permittivity is rather small, but the error in loss tangent is considerable.

The simulation results show that the values calculated by the angular spectrum model approaches the results given by the plane wave models by increasing the antenna distance. It can also be concluded that the use of focusing the beam increases the deviation between two models. This difference can be justified by considering that the angular spectrum corresponding to a focusing beam occupies a wider interval of spatial angles with respect to the same antenna without a lens.

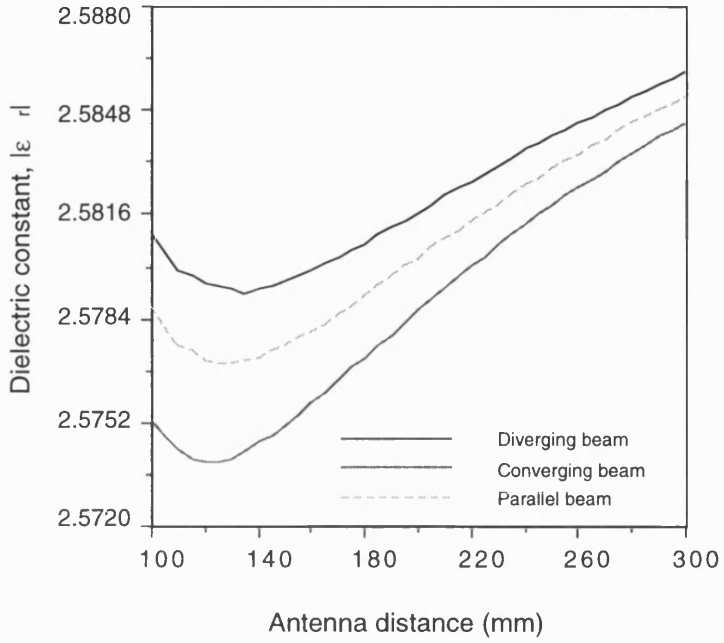

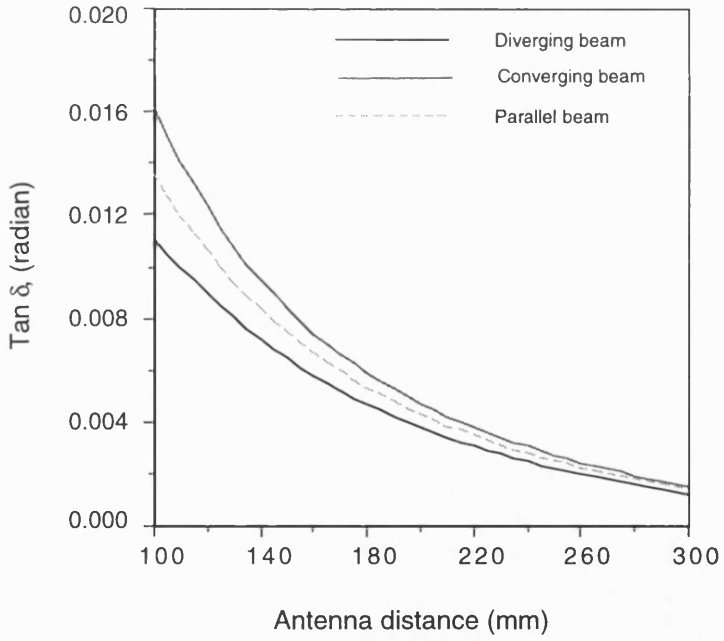

Figure 6.1 The simulation of wavefront curvature error in a lossless dielectric specimen (ε_r=2.6, d=10 mm).

Although transmission and reflection coefficients of a sample in the near-field region can be calculated by the angular spectrum model, determining the complex permittivity and permeability associated with a set of measured transmission and/or reflection coefficients needs a great computation time. In practice, the plane wave model can be used, if the sample is placed adequately far from the antenna. In order to simulate the error due to the wavefront curvature in permittivity and permeability, the transmission and reflection coefficients calculated in the angular spectrum model are used to determine the associated ε_r and μ_r by the plane wave model (appendix 10).

Results obtained from the simulation show that the error in permittivity and permeability increases sharply at frequencies where the sample thickness is a multiple of $\lambda/2$ in *thin* samples, while the error is rather independent of frequency for the samples treated as *thick* slabs. It is worth mentioning that the computation error in the angular spectrum model also increases at frequencies where the sample thickness is a multiple of $\lambda/2$. Therefore, the error at these frequencies is a combination of the computation error as well as the intrinsic error of free-wave techniques. There are various methods for calculating permittivity and permeability of a slab from the measured transmission and/or reflection coefficients. The total error in the calculated permittivity and permeability are functions of the error in the measured parameters and the method of calculation. If the material properties are calculated from the transmission coefficient at two orthogonal polarisations, the product of $\mu_r\varepsilon_r$ can be calculated more accurately than μ_r and ε_r individually. Therefore, the error in the product of $\mu_r\varepsilon_r$ can be considered as a criterion for comparing the difference between two models.

The angular spectrum model improves the measurement accuracy at the expense of a huge computation time. In most of the cases the wavefront curvature error is not the most significant error term, therefore the plane wave model can be employed confidently. Increasing the aperture size or reducing the antenna distance results in increasing the wavefront curvature error. In this case, the improvements made by the angular spectrum model outweighs its computation time. The Rayleigh distance can be considered as a key factor in choosing the best model for the calculations.

6.5 Sample size

In free-wave measurement, the diffraction of the wave from the edges of the sample causes error in the measured transmission and reflection coefficients. The attenuation of the fields at edges of the sample respect to the field strength at centre of the slab is a function of sample size, antenna distance, aperture excitation, frequency and the incident angle. The magnitude of the wave at a given distance from the aperture plane at the front of the antenna can be calculated by its angular spectrum. The contour mapping of the magnitude of the diffracted wave from a standard rectangular horn with different lenses are given in appendix 11. Regarding the small size of the aperture (25x35 mm), the propagated beam cannot be focused on a small area on the sample surface. In the prototype measurement system, the sample is placed at distance of 15 cm from the aperture plane. At this distance, -30 dB beam waist is 19, 19.3 and 26 cm for *converging*, *parallel* and *diverging* beams respectively. At oblique incidence, the footprint of the antenna on the sample increases and a larger sample surface is required. At 45° incident angle, the footprint of an antenna corresponding to -30 dB beam width is 26.8, 27.6 and 37.7 cm. The wave should be attenuated at least -40 dB at the edges of the sample to ignore the diffraction error term.

Multiple reflections within the lens and the lens mismatch are two important factors which cannot be considered in calculating the antenna radiation pattern. These factors degrade the focusing quality of the beam. Dielectric lenses should be well matched in a frequency band and the beam waist should be rather small at focal plane to allow small samples to be measured. In free-wave techniques the use of parabolic reflectors is preferable, since the multiple reflections can be kept at a tolerable value. Parabolic reflectors are less flexible than to lens antennas, and special care should be made in making the reflector surface.

6.6 Conclusion

The angular spectrum model calculates the transmission and reflection coefficient of a slab in the near-field, but it requires a great computation time. This model considers the wavefront curvature and the effect of the beam forming elements such as dielectric lenses. The difference between the angular spectrum and plane wave models decreases by increasing the antenna distance and approaches zero for measurement in the far-field.

In order to decrease the diffraction of the wave from the edges of the sample, the wave should be attenuated adequately (-40 dB or less) at the sample edges. The use of dielectric lenses or parabolic reflectors can reduce this error, but focusing the beam causes the associated angular spectrum to be spread over a wider interval of spatial angles. Therefore, the difference between the two models increases if a focused beam antenna is used. As the multiple reflections within the dielectric lens and the lens mismatch cannot be taken into account in the angular spectrum model, these error terms should be kept as low as possible.

The presented simulation is based on the actual specifications in the prototype measurement system which is made on the basis of the available components. The aperture size employed is quite small, therefore the propagated wave cannot be focused on a small area on the sample surface. In practice, in order to ignore the diffraction of the wave from the edges of the sample a larger aperture size is required. The angular spectrum model improves the accuracy of the measurements with respect to the plane wave model, but a great computation time is required. For a given aperture size and frequency, the wavefront curvature error increases as the antenna distance decreases. In most of the cases the wavefront curvature is not the most significant source of error, therefore the wavefront curvature error can be ignored and the plane wave model can be used confidently. However, the use of larger aperture size and/or carrying out the measurement in relatively close distance from the antenna increase the improvement can be achieved by the angular spectrum model.

The Rayleigh distance can be considered as a criterion in the design and choice of the appropriate model. The Rayleigh distance gives the minimum distance from the aperture for a given error in the wavefront curvature. For a simple case and 22.5° phase error, the minimum distance can be calculated by $2D^2_{max}/\lambda$, where λ and D_{max} are the wavelength and the maximum size of the aperture. If the ratio of the antenna distance to the Rayleigh distance is greater than 2, the plane wave model can be used confidently. If this ratio is less than 1, the use of the angular spectrum model is suggested. The required accuracy and the properties of the sample are also important in choosing the appropriate model. In the error analysis, it is shown that the product of permittivity and permeability can be measured more accurately than μ_r and ε_r individually. The wavefront curvature error mainly affects the measured loss properties of the sample, therefore the degree of improvement in accuracy is less considerable for lossy materials.

7 Error analysis

7.1 Introduction

In principle the complex permittivity and permeability of a slab can be calculated from four independent measurements, but the multi-valued nature of the equations and inaccuracy in measuring transmission and reflection coefficients introduce ambiguities and error in the calculated values. The aim of this chapter is to study free-wave error mechanisms and to estimate the achievable accuracy in free-wave techniques. It is also shown that the product of $\mu_r\varepsilon_r$ and the ratio of ε_r/μ_r can be calculated more accurately than ε_r and μ_r individually in certain methods. The error in $\varepsilon_r\mu_r$ and ε_r/μ_r for given samples are simulated, and the optimum method for using the measured data is recommended. The effect of the sample electrical length on total accuracy is discussed, and the improvement that can be achieved by treating the sample as a *thick* slab is demonstrated.

7.2 Error sensitivity

In the free-wave technique, sample properties cannot usually be expressed by a closed mathematical expression. For small errors in the measured parameters ($\Gamma_\parallel$, $\Gamma_\perp$, $T_\parallel$, $T_\perp$, θ, λ_o and d), the partial differentials of the sample properties ($\delta\varepsilon_r$ and $\delta\mu_r$) can be calculated. If the error in the measured parameters is sufficiently small, the total error in ε_r and μ_r can be approximated by $\delta\varepsilon_r$ and $\delta\mu_r$. This method delivers the required accuracy for estimating the total error in the material properties for small errors in the measured parameters. A detailed analysis of this technique can be found in appendix 12. In order to calculate the total error in ε_r and μ_r for large errors in the measured parameters, $\delta\varepsilon_r$ and $\delta\mu_r$ are integrated over the required range. A computer program calculating $\delta\varepsilon_r$ and $\delta\mu_r$ for a given set of errors in the measured parameters is employed to simulate the total error (appendix 13). In the error analysis, we assume that the sample is illuminated by a uniform plane wave and that diffraction of the wave from the edges of the sample is ignored.

If the multiple reflections within the slab are taken into account, the reflected wave is minimum and the transmitted wave is maximum at frequencies such that the electrical length of the sample is a multiple of 180°. At these frequencies and for a lossless slab, regardless of the material properties and the plane of polarisation, there is no reflection and the whole incident wave is transmitted through the sample, ($|T_{\parallel}|=|T_{\perp}|=1$ and $|\Gamma_{\parallel}|=|\Gamma_{\perp}|=0$). Therefore, the measurement of transmission coefficients at two orthogonal polarisations does not provide the required data for calculating ε_r and μ_r individually at these frequencies. A similar argument is applicable for justifying the increase of error in lossy materials, and the reflected wave does not give the required information for calculating ε_r and μ_r. If multiple reflections within the sample are ignored, the error analysis becomes simpler and the dependence of the measurement accuracy on the sample electrical length decreases considerably.

7.3 Total error in thick slabs

The reflection coefficient associated with a semi-infinite slab at parallel and perpendicular polarisations are given by (1) and (2). Multiple reflections can be ignored if the propagation coefficient is sufficiently small (P < -15 dB). At oblique incidence, the transmission and reflection coefficients of a slab are also functions of the incident angle. In order to simplify the analysis, normal incidence is considered.

At normal incidence, the reflection coefficient of a semi-infinite sample is only a function of the wave impedance, $(\mu_r/\varepsilon_r)^{1/2}$. In this case, the magnitude and phase of the reflection coefficient mainly depend on μ'/ε' and ($tan\ \delta m$-$tan\ \delta e$) respectively. Therefore, the ratio of μ_r/ε_r and the difference of the loss tangents can be calculated more accurately than these parameters individually from the reflection coefficient measurement.

If multiple reflections within the sample can be ignored (*thick* slab), the reflection coefficient is a function of μ_r/ε_r. In reflection coefficient measurement, the front surface of the sample should be placed at the reference plane defined by the location of the metallic sheet in the calibration process. In practice, this alignment cannot be performed with the required accuracy and an error in the measured phase of the reflection coefficient is experienced. The error in the reflection coefficient phase results in an error in the difference

of loss tangents, (*tan δm-tan δe*). In *thick* sample measurements, the ratio of μ_r/ε_r is independent of the incident angle.

At oblique incidence, the transmission coefficient associated with a *thick* slab is given by (3) and (4) at parallel and perpendicular polarisation respectively. *P* is the complex propagation coefficient given by (5). As can be inferred from equations (4) and (5), the transmission coefficient mainly depends on the propagation coefficient (*P*). The propagation coefficient itself is mainly a function of $\mu_r\varepsilon_r$, therefore the product $\mu_r\varepsilon_r$ can be calculated from the transmission coefficient more accurately than μ_r and ε_r values individually.

$$\Gamma_{\parallel} = \frac{\sqrt{\varepsilon_r\mu_r - \sin^2(\theta)} - \varepsilon_r\cos(\theta)}{\sqrt{\varepsilon_r\mu_r - \sin^2(\theta)} + \varepsilon_r\cos(\theta)} \qquad ...(1)$$

$$\Gamma_{\perp} = \frac{\mu_r\cos(\theta) - \sqrt{\varepsilon_r\mu_r - \sin^2(\theta)}}{\mu_r\cos(\theta) + \sqrt{\varepsilon_r\mu_r - \sin^2(\theta)}} \qquad ...(2)$$

$$T_{t\parallel} = (1-\Gamma_{\parallel}^2)P \qquad ...(3)$$

$$T_{t\perp} = (1-\Gamma_{\perp}^2)P \qquad ...(4)$$

$$P = e\left(\frac{-j2\pi d}{\lambda_o}\sqrt{\varepsilon_r\mu_r - \sin^2\theta}\right) \qquad ...(5)$$

Figure 7.1 shows the total error in sample 1 (ε_r=*2.6, d=10 mm*) treated as a *thick* slab for 0.5 dB error in the magnitude of the parallel transmission coefficient. As can be seen, there is no rapid change in the error at frequencies such that the sample electrical length is a multiple of 180°.

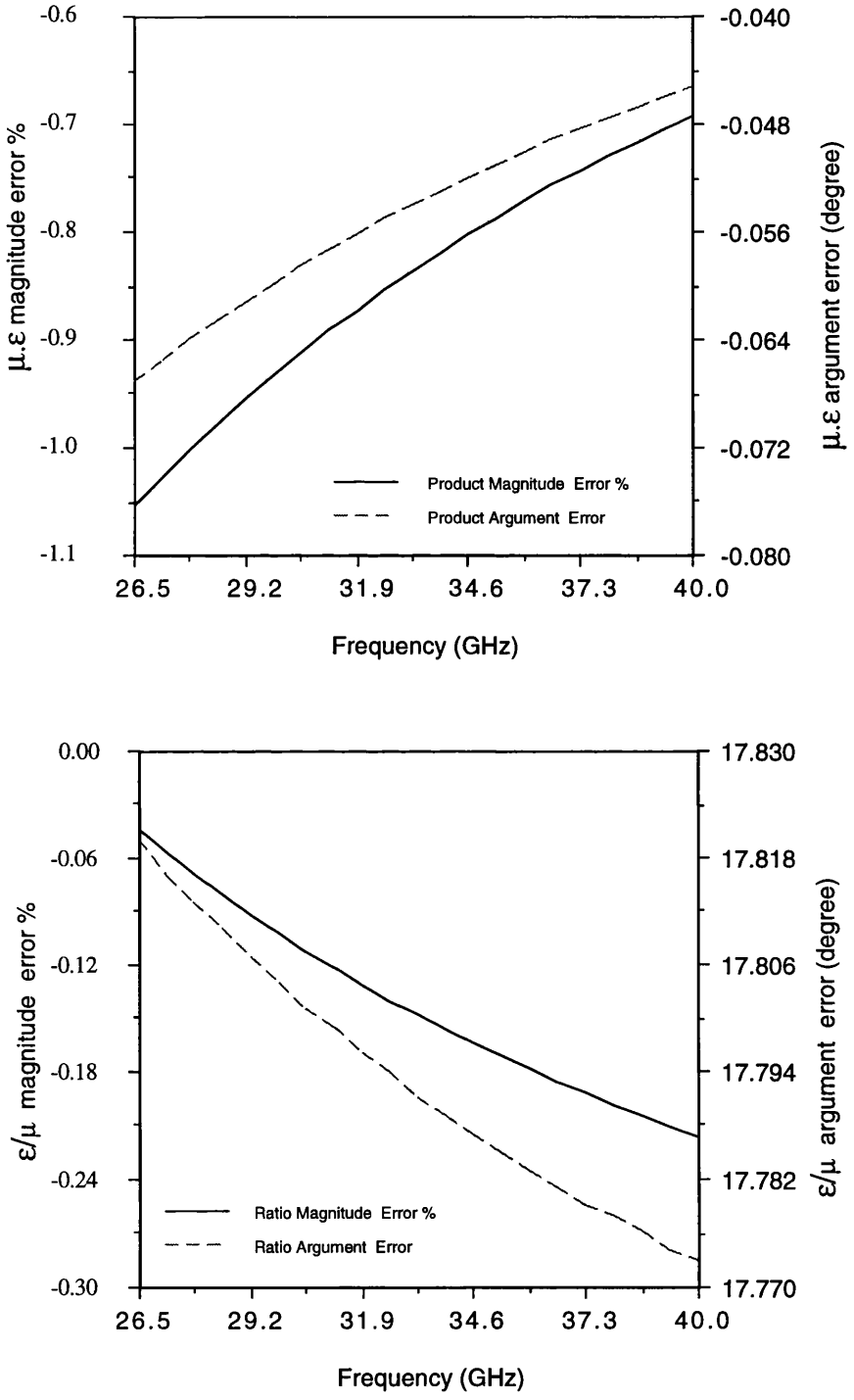

Figure 7.1 Simulated total error in sample 1 treated as a thick slab against the transmission coefficient magnitude (transmission method).

7.4 Total error in thin slabs

If multiple reflections within the sample cannot be ignored (*thin* slab), the transmission and reflection coefficients are given by equations (6) to (9). In this case, both the reflection and transmission coefficients are functions of the sample electrical length (P). As mentioned, the reflection coefficient is minimum and the transmission coefficient is maximum at the frequencies such that the slab electrical length is a multiple of 180°. Figure 7.2 shows the total error in sample 1 (ε_r=*2.6, d=10 mm*) treated as a *thin* slab for 0.5 dB error in the magnitude of transmission coefficient. In this figure, the rapid increase of the total error at frequencies such that the sample thickness is a multiple of $\lambda/2$ is shown. At these frequencies, most of the incident wave is transmitted through the slab. In this case, the transmission coefficient does not provide enough data for determining μ_r and ε_r individually, but it can still be used to calculate the product $\mu_r\varepsilon_r$.

$$T_{t\parallel} = \frac{P(1-\Gamma_{\parallel}^2)}{(1-P^2\Gamma_{\parallel}^2)} \qquad ...(6)$$

$$T_{t\perp} = \frac{P(1-\Gamma_{\perp}^2)}{(1-P^2\Gamma_{\perp}^2)} \qquad ...(7)$$

$$\Gamma_{t\parallel} = \frac{\Gamma_{\parallel}(1-P^2)}{(1-P^2\Gamma_{\parallel}^2)} \qquad ...(8)$$

$$\Gamma_{t\perp} = \frac{\Gamma_{\perp}(1-P^2)}{(1-P^2\Gamma_{\perp}^2)} \qquad ...(9)$$

The dependence of transmission coefficient on $\mu_r\varepsilon_r$ is stronger at frequencies such that the sample thickness is multiple of $\lambda/2$, since the transmission coefficient mainly depends on the propagation coefficient (P). At other frequencies, the transmission coefficient is a function of P and Γ. As mentioned, P is mainly a function of $\varepsilon_r\mu_r$, and Γ mainly depends on the ratio μ_r/ε_r.

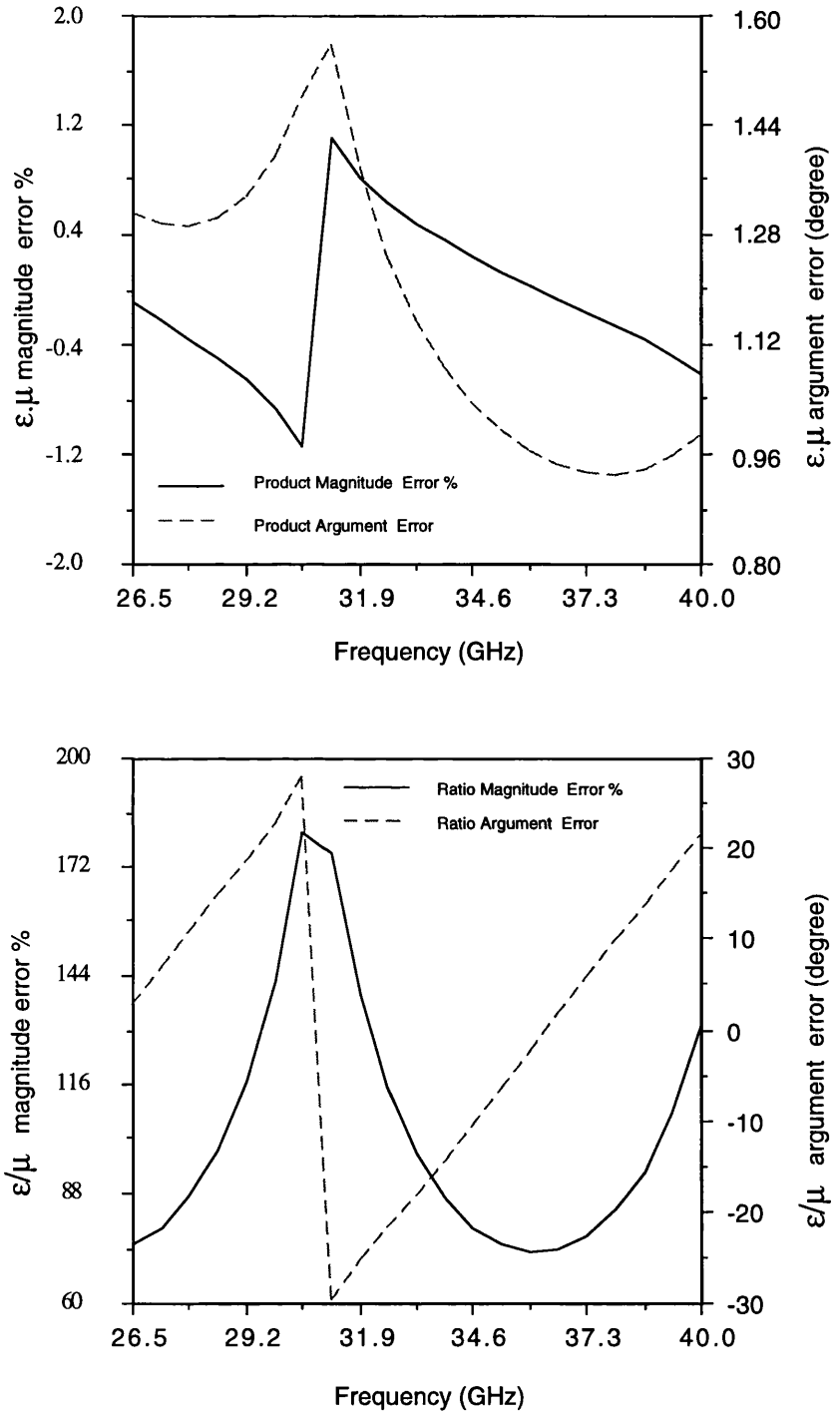

Figure 7.2 Simulated total error in sample 1 treated as a thin slab against the transmission coefficient magnitude (transmission method).

7.5 Total error simulation

A computer program calculating the total error in a slab for a given set of errors in the measured parameters is employed for simulating the error in different free-wave techniques, (appendix 13). The total error in ε_r and μ_r for a given set of errors in each of the measured parameter ($\Gamma_{\parallel}$, $\Gamma_{\perp}$, $T_{\parallel}$, $T_{\perp}$, θ, λ_o and d) can be simulated by this program.

Various methods can be devised for calculating the material properties from a combination of independent measurements. In the error analysis, only four fundamental methods which are based on calculating the material properties from the measured $T_{\parallel}\&T_{\perp}$, $\Gamma_{\parallel}\&\Gamma_{\perp}$, $T_{\parallel}\&\Gamma_{\parallel}$ and $T_{\perp}\&\Gamma_{\perp}$ are taken into account. In the error assessment, these four methods are considered for simulating total error in two samples. Sample 1 is a lossless dielectric (ε_r=*2.6*) of thickness 10 mm, and sample 2 is a 10 mm slab of a lossy ferrite (ε_r=*7.5-j0.5* μ_r=*0.8-j0.15*) representing a typical material made from ferrite powder. The simulation is carried out at 45° incident angle and 30 GHz (appendix 14).

In the simulation, the transmission method (*method 1*) denotes the case where the material properties are calculated from the measured transmission coefficients at two orthogonal polarisations. The material properties of a slab can also be calculated from the measured reflection coefficients at two polarisations, (reflection method or *method 2*). The measurement of transmission and reflection coefficients at one polarisation can also provide the required data for determining the material properties. *Method 3* and *method 4* denote the cases where the transmission and reflection coefficients at parallel polarisation or perpendicular polarisation respectively, are used to calculate ε_r and μ_r.

As the product $\mu_r\varepsilon_r$ or the ratio ε_r/μ_r can be calculated more accurately than ε_r and μ_r individually in certain methods, the total error in ε_r/μ_r and $\varepsilon_r\mu_r$ are considered as a criterion for comparing the error sensitivity in different methods. Figures 7.3 and 7.4 show the total error in ε_r/μ_r and $\varepsilon_r\mu_r$ in sample 1 treated as a *thick* and *thin* slab respectively. As shown, the total error in $\varepsilon_r\mu_r$ of sample 1 considerably decreases if it is treated as a *thick* slab. In order to simplify the comparison of different techniques, the average error rates are shown as a number of tables (appendix 14).

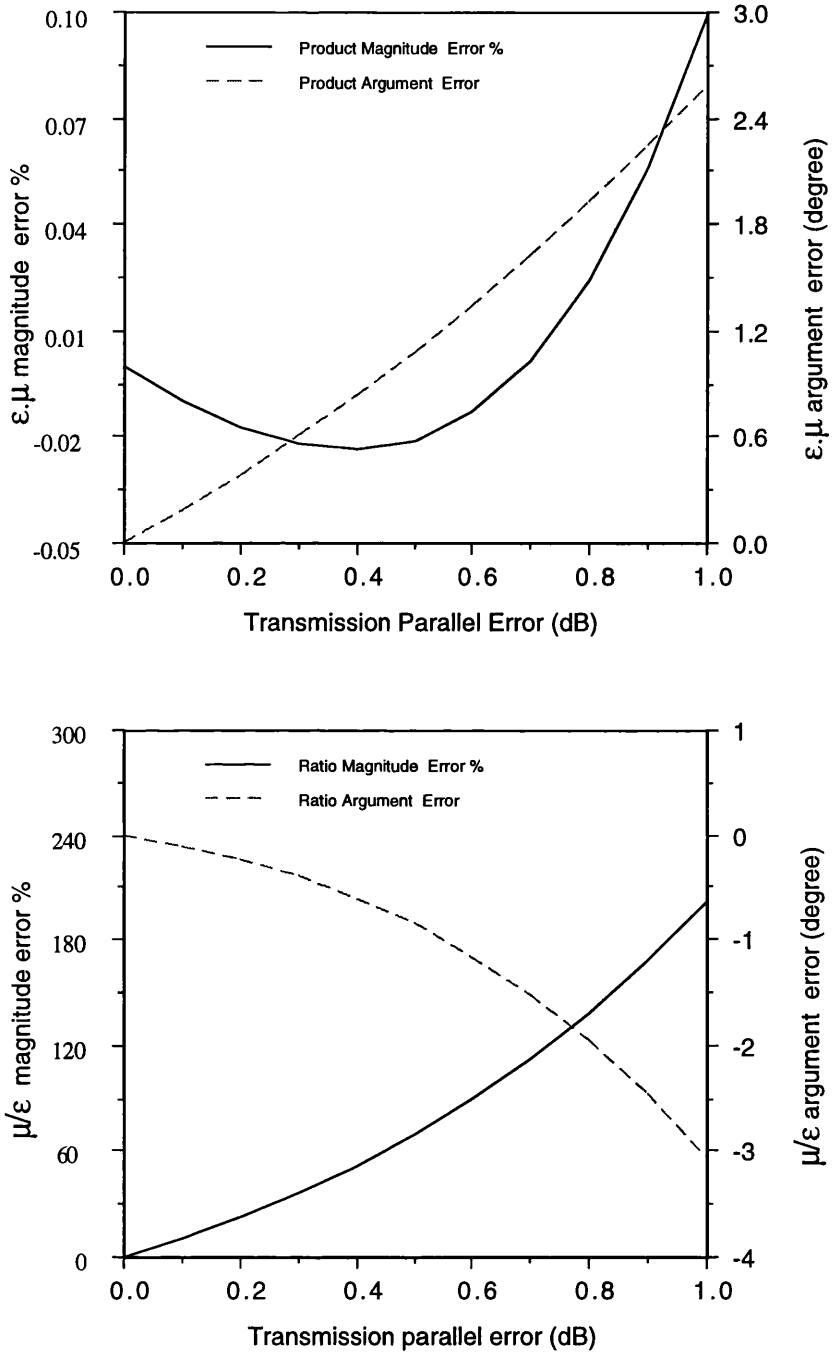

Figure 7.3 Simulated total error in sample 1 treated as a thick slab (transmission method, f=30 GHz and θ=45°).

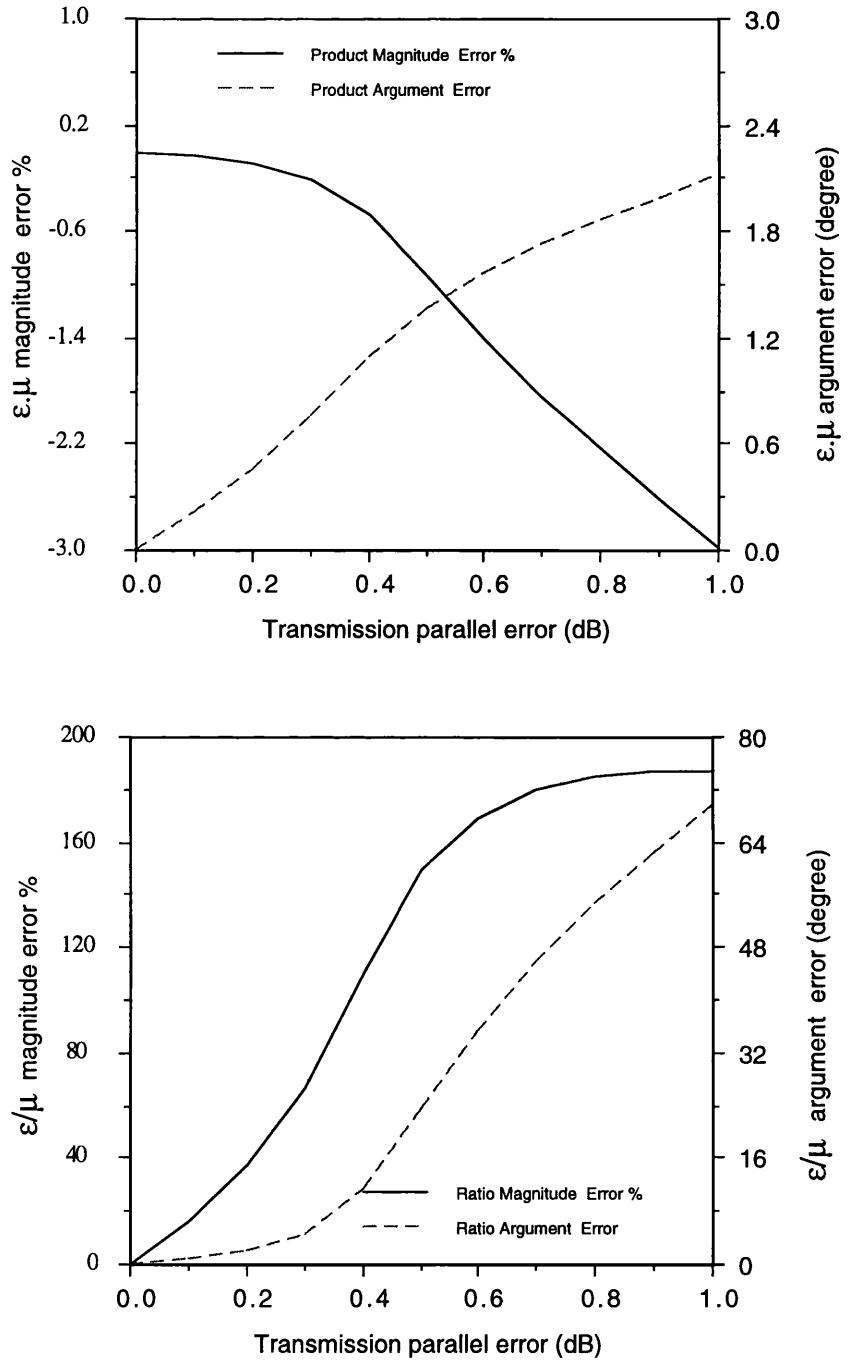

Figure 7.4 Simulated total error in sample 1 treated as a thin slab (transmission method, f=30 GHz and θ=45°).

In free-wave techniques, the magnitude and phase of the transmission and/or reflection coefficients at two orthogonal polarisations are measured in *dB* and *degree*. Therefore, we show the total error in ε_r and μ_r for changes in the magnitude per *dB* and the changes in the phase per *degree*. The results obtained from simulating the total error for the *thick* slab show that the transmission method delivers a better accuracy in determining $\varepsilon_r\mu_r$ than ε_r/μ_r, ε_r or μ_r. Error in the magnitude of transmission coefficient affects the imaginary part of $\varepsilon_r\mu_r$, while error in the phase of the transmission coefficient results in an error in the real part of $\varepsilon_r\mu_r$.

As discussed, the reflection method is more appropriate for calculating μ_r/ε_r than $\varepsilon_r\mu_r$, ε_r or μ_r. In the reflection method, errors in magnitude and phase of the reflection coefficient introduce error in the real and imaginary parts of the ratio μ_r/ε_r respectively. Decreasing the incident angle and/or increasing the product of $\varepsilon_r\mu_r$ increases this dependency. In other words, the accuracy in measuring μ_r/ε_r with respect to measurement of $\mu_r\varepsilon_r$ increases for materials with high values of $\varepsilon_r\mu_r$. The same conclusion can be made by examining the results obtained from simulating the total error for samples 1 and 2. It is worth noting that the phase of the reflected wave cannot be measured accurately. Therefore, the error in difference of the loss tangents ($tan\ \delta_m$-$tan\ \delta_e$) can be considerable in practice.

If the transmission and reflection coefficients are used to calculate the material properties, the total error is minimised in most cases. The simulation results show that the product $\mu_r\varepsilon_r$ can be calculated more reliably with respect to determining μ_r or ε_r individually in most of the cases. The simulation results do not show any distinction in using the measured transmission and reflection coefficients at parallel or perpendicular polarisation.

In the error analysis, only the error in the measured electrical quantities ($\Gamma_{\parallel}$, $\Gamma_{\perp}$, $T_{\parallel}$, $T_{\perp}$) are taken into account. But uncertainty in measuring the frequency, thickness and incident angle can also cause error in ε_r and μ_r. In the reflection method, if the sample is treated as a thick slab, the material properties are independent of the incident angle, thickness and frequency. Any uncertainty in the phase of the reflected wave causes an error in the imaginary parts of μ_r/ε_r. Since the phase of the reflected wave cannot be measured accurately, this technique does not deliver high accuracy in practice. If multiple reflections within the slab are taken into account (*thin* slab), the total error is a complicated function of

the electrical length of the sample. At frequencies such that the sample thickness is a multiple of 180°, the reflected wave from a *thin* slab is minimum and the total error increases rapidly. At these frequencies, reflection coefficient measurement does not provide the required data for calculation of permittivity and permeability. In the general case, measurement at frequencies such that the sample thickness is an odd multiple of 90° is recommended.

7.6 Conclusion

In free-wave techniques, treating the sample as a *thick* slab is preferred. The total error in μ_r and ε_r and their variation with frequency are relatively less in *thick* samples. If the combination of the material properties and the sample thickness is such that the sample cannot be considered as a *thick* slab, the sample thickness should be an odd multiple of 90°. Transmission coefficient measurement gives the product of $\mu_r\varepsilon_r$ more accurately than μ_r and ε_r individually, while the error in the ratio of μ_r/ε_r is minimised if the reflection coefficient at two polarisations are used. It is worth noting that the phase of the reflection coefficient cannot be measured accurately, which leads to an error in μ_r/ε_r. In the general case, the use of transmission and reflection coefficients at one polarisation delivers a higher accuracy and greater reliability with respect to the transmission and reflection methods.

The measurement of eight data, transmission and reflection coefficients at two polarisations, delivers relatively satisfactory results for lossy materials. This method is based on calculating μ_r/ε_r and $\mu_r\varepsilon_r$ from reflection and transmission coefficients respectively (Lynch et al [51]). In this method, the reliability of the measured parameters is also taken into account. This method is recommended for lossy materials, but fails to converge in calculating the properties of low-loss samples. This technique (*eight data optimization method*) is explained in chapter 8.

In free-wave measurements, the frequency, incident angle and the sample thickness can be measured relatively accurately. Therefore, inaccuracy in transmission and reflection coefficients are considered as the main sources of error. The error in μ_r and ε_r is a complicated function of the error in the measured parameters, the material properties and the method used for calculations. In the general case, it is difficult to estimate the accuracy

in free-wave techniques. For an error of 0.1 dB and 1° in transmission and/or reflection coefficients, an accuracy of 1% and 0.5° in $\mu_r\varepsilon_r$ and 2% and 2° in μ_r/ε_r are expected. As the phase of μ_r/ε_r cannot be measured accurately, free-wave techniques are not appropriate for measuring the properties of low-loss materials, ($tan\delta_m+tan\delta_e< 50$ milliradians).

Inaccuracy in measuring ($tan\delta_m-tan\delta_e$) has been verified by the simulation results. The results obtained from simulating the total error also show that the magnitude of μ_r and ε_r and the sum of the losses ($tan\delta_m+tan\delta_e$) can be measured accurately. The uncertainty in measuring ($tan\delta_m-tan\delta_e$) is more significant in measuring low-loss materials. Therefore, some information about the material loss properties should be used to separate the magnetic and dielectric losses. The measurement of the sample at other frequencies and considering the trend of the changes in the loss properties of the sample with frequencies can be used as a priori knowledge for this purpose.

8 Prototype measurement system

8.1 Introduction

A prototype single-pass free-wave system using a *Hewlett Packard* automatic vector network analyser (HP8510B) for measuring the complex permittivity and permeability of materials was designed and built. This was designed as a multi-function system, and measures ε_r and μ_r in the frequency range of 26.5 to 40 GHz. In this system, the plane of polarisation can be changed easily and maximum repeatability in the design of the sample holder has been considered. In transmission coefficient measurement, the incident angle can be set accurately to the desired value, but the reflection coefficient measurement can be carried out only at 45°. The use of rigid waveguide has provided maximum repeatability and stability in the measurement. The aim of this chapter is to present the single-pass free-wave prototype system, and discuss the design considerations. The required specifications for a free-wave measurement systems are discussed, and the measurement procedure is reviewed. At the end, the weak points of this prototype are discussed and a number of modifications are recommended.

8.2 Design considerations

A prototype single-pass free-wave system (figure 8.1), is designed and built as a test bed for studying various techniques and practical difficulties in free-wave measurements. It is worth mentioning that this system is designed on the basis of the available components. As the first single-pass prototype this system cannot be claimed to be perfect and the need for making a number of modifications is quite obvious. In practice, the results obtained from the measurement of dielectric and ferrite samples show that the reliability and accuracy of this system are sufficient for our purposes. The design of this system is such that both circular and rectangular horns can be used. In this part, the design considerations and the limitations of the system are presented.

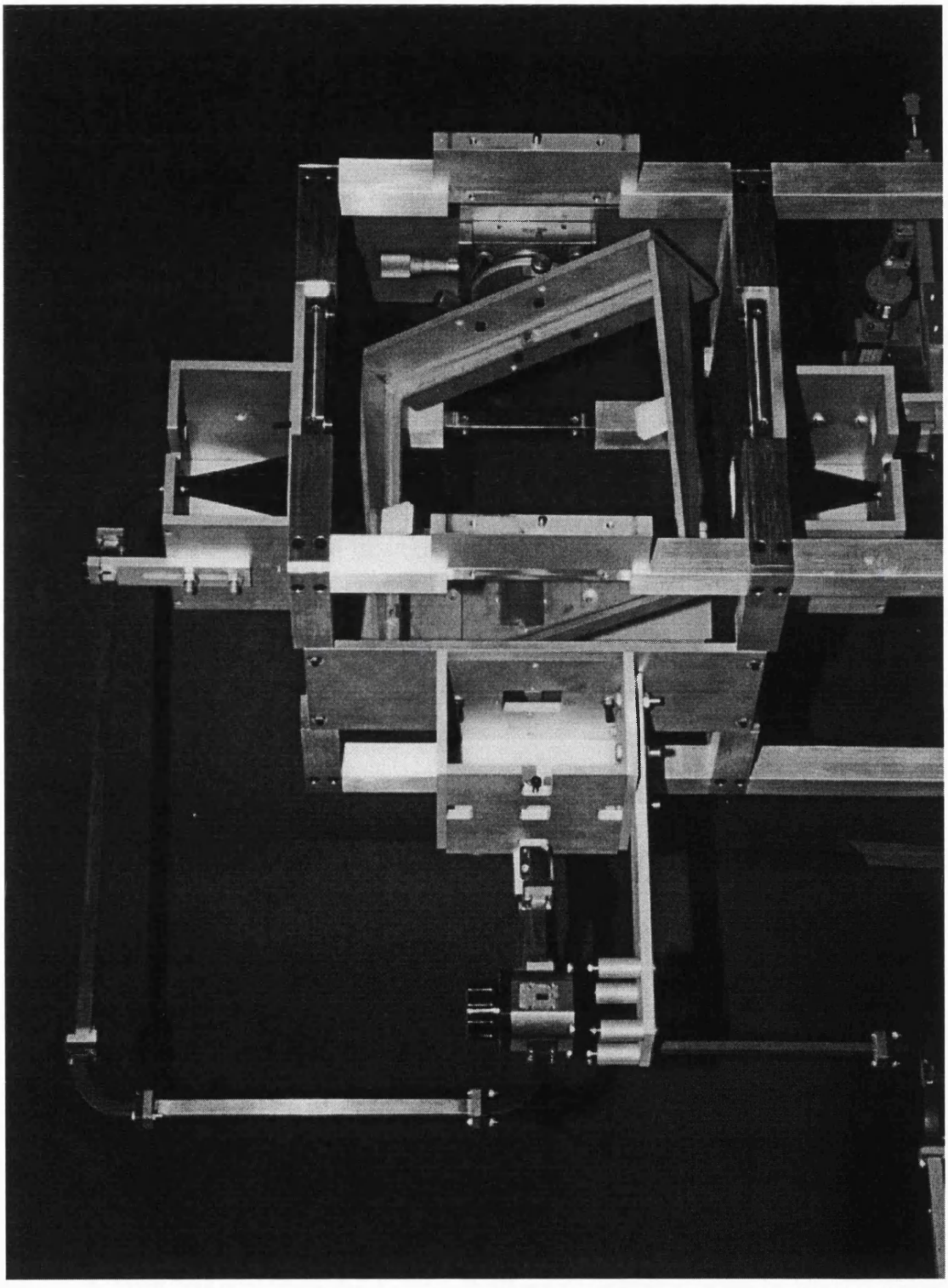

Figure 8.1 Single-path free-wave measurement system.

8.2.1 Sample size

In free-wave measurement, diffraction of the wave from the edges of the sample causes error in the measured transmission and reflection coefficients. The sample size should be large enough to intercept the incident wave adequately. The minimum sample size depends on the antenna radiation pattern and the distance between the aperture plane and the sample surface. Although a large sample size is preferred, technical constraints in making ferrite specimens limit the maximum diameter of the samples to approximately 20 cm. Regarding the ferrite and dielectric samples provided, two sample holders are designed. The circular sample holder is made for round slabs of 170 mm diameter, and the rectangular one is designed for square samples of 230x230 mm. As discussed in appendix 11, the error due to diffraction of the wave from the edges of the sample is a complicated function of sample size, antenna radiation pattern and the distance between antenna and the sample surface. Therefore, these three parameters are considered in designing a free-wave system.

8.2.2 Sample holder repeatability

In reflection coefficient measurement, the reference plane is defined by the front surface of the metal sheet used for calibration. Any displacement of the sample front surface from the reference plane causes error in the measured reflection coefficient. In our design, the sample sits on three small ball bearings which are mounted at the rim of the frame. This design provides good mechanical repeatability for the sample. It is worth noting that the rigidity of the sample and the sample holder are two important factors in the repeatability obtained. One of the main sources of error in reflection coefficient measurement is caused by physical changes in the sample holder. The sample holder can be bent under the weight of the sample or the calibrating metal sheet. Therefore, the metallic sheet used for calibration should have the same weight as the sample to minimize this type of error.

8.2.3 Antenna distance

Although the use of the plane wave model simplifies calculations, it does not consider measurement in the near-field region. In practice, wavefront curvature and diffraction of the

wave from the edges of the sample are considered as random error terms, since it is difficult to model them. The wavefront curvature error decreases with increasing antenna distance and approaches zero in the far-field region, but the minimum sample size increases with increasing antenna distance. Therefore, the optimum antenna distance is calculated with regard to the sample size and the radiation pattern of the antennas.

In the prototype system, the distance between the antennas is 30 cm. At 30 GHz, the distance between the antenna and the sample surface is only 15λ. The Rayleigh criterion ($\frac{2D_{max}^2}{\lambda}$) can be considered as a measure for estimating the wavefront curvature error. For the used antenna (square aperture of 25x35 mm), the Rayleigh distance is 24.5 cm. As discussed before the antenna distance should be twice the Rayleigh distance to ignore the wavefront curvature error, therefore the required distance is about 50 cm. In practice, the maximum size of the sample limits the antenna distance to 30 cm which is less than that required.

8.2.4 Focused beam

In order to minimise the error due to diffraction of the wave from the edges of the sample, either the sample should be adequately large or the propagated wave should be focused on a small area of the sample surface. Dielectric lens or microwave reflectors can be employed for focusing the beam on the sample surface. In practice dielectric lenses are compact, but multiple reflections within the lens and lens mismatches degrade their focusing performance. The reflected wave from the lens also degrades the accuracy in measuring transmission and reflection coefficients, therefore the lens antenna should be well matched. In practice, matching dielectric lenses over a broad frequency band is difficult. The implications associated with microwave reflectors are much less, but they are relatively large and need accurate alignment. The antennas used in the prototype are well matched over the frequency range of 26.5 to 40 GHz, but using the available dielectric lenses degrades their return loss considerably. The error terms associated with reflection from the antenna or the dielectric lens are complicated and their impact cannot be removed easily. Therefore, the use of a well matched antenna over the whole measured frequency band is a key parameter in improving the accuracy.

8.2.5 Aperture Size

The plane wave model calculates the transmission and reflection coefficients of a slab in the far-field region. In practice, the aperture size should be enough large to generate a narrow beam, but increasing the aperture size causes the near-field region to be extended as well. The antenna used in the prototype is a standard pyramidal horn (25x35 mm). As discussed in appendix 11, in order to focus the beam on the sample surface and ignore the diffraction error, a larger aperture is required. Therefore, we should not expect a good focusing beam from the present arrangement.

8.2.6 Plane of polarisation

In free-wave techniques, the sample transmission and reflection coefficients are measured at two orthogonal polarisations. The plane of polarisation should be altered without causing any changes in the other parameters of the measurement system, such as the lengths of the free-wave paths. For changing the plane of polarisation, only the position of the sample holder is changed in the transmission coefficient measurement. In reflection coefficient measurements, the position of the sample and the location of the receiving antenna should also be changed. In the prototype system, the appropriate antenna configuration with respect to the measured parameters can be selected by a set of waveguide switches. It is worth mentioning that only one waveguide switch is used in our prototype, and changing the plane of the polarisation needs a small alteration in the waveguide configuration. This problem can be removed if two waveguide switches are used. In this case, changing the plane of polarisation is as simple as setting the switches and the position of the sample holder.

8.2.7 Waveguide connections

In a free-wave measurement system, reflections in the waveguide and coaxial components cause error in the measurement. In practice, the physical length and consequently the electrical length of a piece of waveguide changes with temperature. The magnitude of these changes are proportional to the length of the waveguide, therefore the waveguide

connections should be designed for the shortest possible length. The ambient temperature should also be controlled to minimize this type of error. The number of waveguide junctions used in the measurement system should also be minimized, since each waveguide twist or bend contribute to the total unwanted reflection.

8.2.8 Single-pass free-wave calibration

The use of improved calibration techniques such as *Full Two Port*, *TRL* or *TRM* can remove the most significant error terms from the measurement results, but performing these calibration techniques requires accurate mechanical instruments in free-wave measurements. At mm-wave frequencies, these calibration methods are not available in the HP-8510B. The use of the available calibration technique (*Response*) can deliver the required accuracy, if the total reflections are small. This calibration method normalises the measured responses with respect to the measured standards, but the residual error can still be large for the samples of high reflection coefficient. The mismatches in the waveguide and coaxial junctions degrade the total measurement accuracy, therefore reflection from the waveguide junctions, specifically from the antenna, should be kept small.

8.3 Measurement procedure

The measurement procedure is divided into three stages. In the first step, the measurement system is warmed up and calibrated. Then the transmission and reflection coefficients of the sample are measured and stored in the computer memories. In the final stage, the complex permittivity and permeability of the sample are calculated from the measured values. These stages are carried out in a semi-automated fashion, but can be fully automated. A computer program written in HP-BASIC automates the measurement in the double-pass apparatus. This program can be adapted for the single-pass measurement system. In this part, the different stages of the measurement procedure in single-pass measurement system are presented.

8.3.1 Warming up

Although a 2 hour warming up time is recommended for the HP-8510B, the network analyser can be ready for measurement after 30 minutes in most cases. The ambient temperature should also be stable during the calibration and measurement processes, (23±1°C). Failing to control the ambient temperature can result in an error in the phase measurement. Since the measurement system is made from a metallic structure, its temperature should be stabilized as well. Changes in the waveguide lengths and the free-wave paths should be minimized by controlling the ambient temperature. Observing the changes in the phase of transmission coefficient can be used as a measure for checking the temperature stability. It is also recommended to leave the sample and the metallic sheet used for calibration in the measurement environment, to avoid any temperature gradients during the calibration or measurement procedure.

8.3.2 Calibration

A specific calibration kit has been devised for the single-pass free-wave measurement system. This calibration kit is based on the *Response* calibration method, and the calibration procedure is carried out by measuring the reflection coefficient of a short circuit and the transmission coefficient of the empty sample holder. In transmission coefficient measurements, the coupling between the transmitting and receiving antennas is measured and normalised with respect to the measured antenna coupling for the empty sample holder. Although changing the plane of polarisation should not affect the free-space paths of the measurement system, it is recommended to perform a separate calibration measurement at each polarisation. This technique minimizes the error due to possible physical displacement of the measurement system after changing the plane of polarisation. The calibrations at parallel and perpendicular polarisations are saved in two sets of computer memories considered for this purpose.

In the reflection coefficient measurement, the reflected wave from a metallic sheet is measured and saved as a reference for normalising the successive measurements. Similarly, the calibration measurement should be repeated at each polarisation. In order to minimize the error due to temperature and physical changes of the system, it is recommended to

perform the calibration measurement just before carrying out the sample measurement. It is worth noting that the sample or the metallic sheet used as short circuit in the calibration process should be placed carefully in the frame to minimize the phase error in the reflection coefficient measurement.

8.3.3 Measurement

In the measurement procedure the sample is placed in the sample holder, then the transmission and reflection coefficients at two orthogonal polarisations (four complex numbers) are measured. In order to minimize the error due to the temperature and mechanical changes, each of these parameters are measured just after carrying out the associated calibration measurement. The measured values are saved in the network analyser memories as a set of *Raw Data*. It is worth mentioning that *raw data* denotes the measured scattering parameters before applying error correction and time domain gating. Having completed the measurement process, the stored data can be used for calculating the sample properties. At this stage, time gating and calibration are applied to the stored *raw data* data. The corrected and gated transmission and reflection coefficients can be saved on a floppy disk or transferred to a desktop computer for further processing.

8.3.5 Gate parameter setting

The gate centre and gate width should be set correctly for different samples. In *thick* sample measurement, the gate width is set at twice the sample electrical length. In the reflection coefficient measurement the gate centre is set at zero, but it should be set at the effective sample electrical length in the transmission coefficient measurement. The effective sample electrical length is defined as the difference between the sample electrical length and the slice of air which is deleted from the free-space path because of placing the sample in the frame.

As mentioned, the minimum gate is limited by the frequency span over which the measurement is carried out. The measurement over a finite frequency span limits the minimum thickness for *thick* slabs. In practice, the gate width is set at its minimum for measuring *thick* samples. In *thin* samples, the gate should be wide enough to include the

most significant terms of the multiple reflections within the sample. The maximum gate width is dictated by the geometry of the measurement system and the location of the unwanted reflection in the time domain. The gate width can be as wide as the antenna distance in *thin* sample measurements. The gate centre should also be set with regard to the effective electrical length of the sample. If the sample electrical length is not defined, the gate width can set by observing the time domain response. Once the material properties are calculated, the measurement can be repeated for the corrected gate parameters.

8.3.6 Transferring data

The gated transmission and reflection coefficients saved in the network analyser memories or in a floppy disk are transferred to a desk top computer to calculate the complex permittivity and permeability. The data are transferred through the HP-IB port in the network analyser. In practice, any desk top computer with the capability of sending and receiving data via the GP-IB port can be used for this purpose. In the prototype system, a Macintosh computer is employed.

8.3.7 Calculation

In principle, complex permittivity and permeability of a slab can be calculated from any four independent measurements of transmission and/or reflection coefficients at different polarisations, thickness or incident angles. As shown, the total error in the calculated permittivity and permeability is a complicated function of the error in the measured data and the method used for determining the sample properties. In the general case, a priori knowledge of the material properties is required and the use of iterative numerical methods is inevitable.

9 Measurement results

9.1 Introduction

In previous chapters, different free-wave techniques and methods of calculating the sample properties from the measured transmission and/or reflection coefficients have been discussed. It has also been shown that the calculation becomes less complicated and the dependence of the measurement accuracy on sample thickness decreases if multiple reflections within the sample can be ignored. In this chapter, some results obtained from the measurement of ferrite and dielectric samples are presented and discussed.

The major difficulty for evaluating the accuracy in free-wave methods is the lack of any other reliable technique for measuring lossy materials at mm-wave frequencies. Although the properties of low-loss materials can be measured by other techniques at millimetre wavelengths, free-wave techniques are not suitable for measuring low-loss materials. Regarding the difficulties in providing large size ferrite slabs, the properties of the available samples are considered for comparison.

In order to estimate the accuracy of free-wave techniques, the properties of a polystyrene slab as a known dielectric are measured. The ferrite samples are made by mixing ferrite powder and a resin, so the sample properties can be controlled by varying the percentage of loading. The ferrite samples were made by DRA(Holton Heath) and their properties are measured by the waveguide technique.

9.2 Magnetic materials

In the general case, the sample is assumed to be magnetic ($\mu_r \neq 1$), therefore four independent measured data are required for calculating the complex permittivity and permeability. In this part the specimens are considered as magnetic materials, and three samples treated as both thick and thin slabs are measured. In practice, free-wave methods

are appropriate for measuring the product $\varepsilon_r\mu_r$ and the sum of loss tangents ($\tan\delta_m+\tan\delta_e$). The difference of loss tangents ($\tan\delta_m-\tan\delta_e$) cannot be measured accurately. Therefore, the accuracy in measuring $\varepsilon_r\mu_r$ is used as a measure of comparing different techniques.

9.2.1 Thick magnetic samples

If multiple reflections within the sample can be ignored, the complexity of the calculation decreases and the total measurement accuracy increases. For ignoring the multiple reflections, either the propagation coefficient (P) should be sufficiently small or the sample should be sufficiently thick such that the multiple reflections can be removed by the time gating technique. In this part, the measured properties of samples considered as *thick* slabs are presented. It is worth noting that the material properties are calculated from the measured transmission and reflection coefficient at perpendicular polarisation.

Table T9.1 shows the properties of a low-loss ferrite sample (*B2, d=13.03 mm*) measured by the waveguide method at 40 GHz. The measurement was repeated three times.

Sample	ε'	ε''	μ'	μ''
B2	5.67	-0.14	0.97	+0.05
B2	5.82	-0.01	0.99	+0.02
B2	6.03	-0.27	1.00	+0.02
Average	5.84	+0.14	0.986	-0.03

Table T9.1 The properties of sample B2 (d=13.03 mm) measured by the waveguide method at 40 GHz.

The complex permittivity and permeability of sample *B2* measured by the new free-wave method are shown in figure 9.1. The properties of this sample are rather constant over the measured frequency band, and the rapid changes at two ends of the band are due to the intrinsic time gating error. In this measurement a *Narrow* gate shape is used, therefore measurements at centre frequencies which are less subject to the gating error should be

considered (centre frequencies). At these frequencies, the complex permittivity and permeability of sample *B2* are ε_r=*5.95-j0.04* and μ_r=*0.96-j0.01*. Comparing these values with the results obtained from the waveguide method (ε_r=*5.84+j0.14* and μ_r=*0.986-j0.03*), the free-wave technique gives more accurate values for the imaginary parts of the permittivity and permeability. In the waveguide method, the error in the imaginary part of the permittivity is quite considerable (ε'' >0). The difference between the real parts of ε_r and μ_r is also less than 2%.

Figure 9.2 shows the electric and magnetic properties of a lossy ferrite slab (*D3, d=10.47 mm*). The properties of this sample varies with frequency and its average permittivity and permeability measured by waveguide method are given in table T9.2. The measurement is carried out between 26.5 and 40 GHz and the linear variation of the values between two limits is shown by '~'. In this sample, the results obtained by the free-wave measurement are in a very good agreement with the values measured by the other technique. It is worth noting that the results obtained from the waveguide method are also subject to error, and the repeatability of the technique is poor at these frequencies. Considering the repeatability and accuracy of the results obtained from the waveguide technique, it can be concluded that free-wave method delivers more reliable and more accurate values.

Sample	ε'	ε''	μ'	μ''
D3	6.91~7.02	0.55~0.6	0.85±0.02	0.29~0.07
D3	6.82±0.03	0.45±0.03	0.80±0.02	0.36~0.12
D3	7.09~7.32	0.66~1.10	0.87~0.81	0.32~0.07

Table T9.2 The properties of sample D3 (d=10.47mm) measured by the waveguide method in the frequency range of 26.5 to 40 GHz.

The measured properties of a polystyrene slab (*d=21.4 mm*) are shown in figure 9.3. Polystyrene is a low-loss dielectric and its complex permittivity can be measured accurately by an open resonator (ε_r=*2.545-j0.001* and μ_r=*1*, Yu [24]). If the measurement at two ends of the band (which is subject to gating error) are excluded, the average properties of

polystyrene measured by our technique are (ε_r=*2.545+j0.15* and μ_r=*1.017-j0.052*). It can be concluded that the accuracy in the real parts of the permittivity and permeability are better than 1%. As free-wave techniques are appropriate for materials with high loss tangents, the error in imaginary parts of the permittivity and permeability is considerable. However, the error in the sum of the losses is small, (better than 50 milliradians).

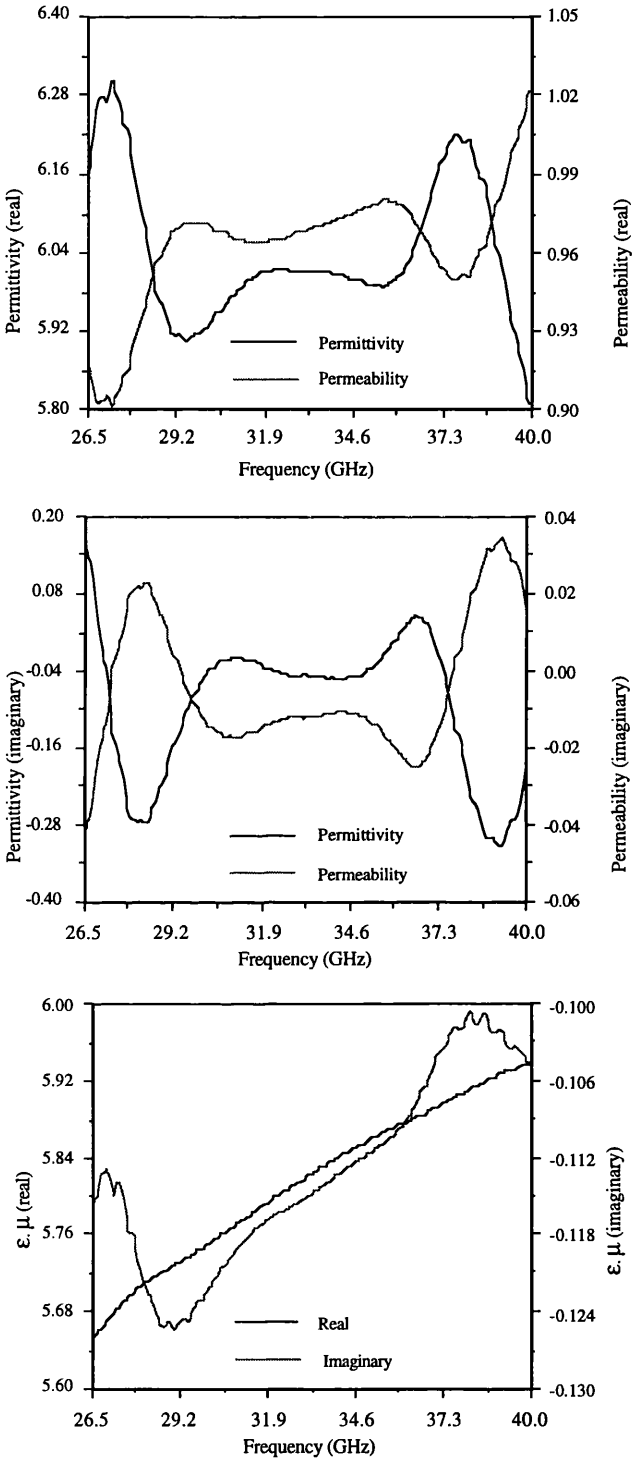

Figure 9.1 Complex permittivity and permeability of a low-loss ferrite sample (sample B2, thickness=13.03 mm) measured as a thick slab.

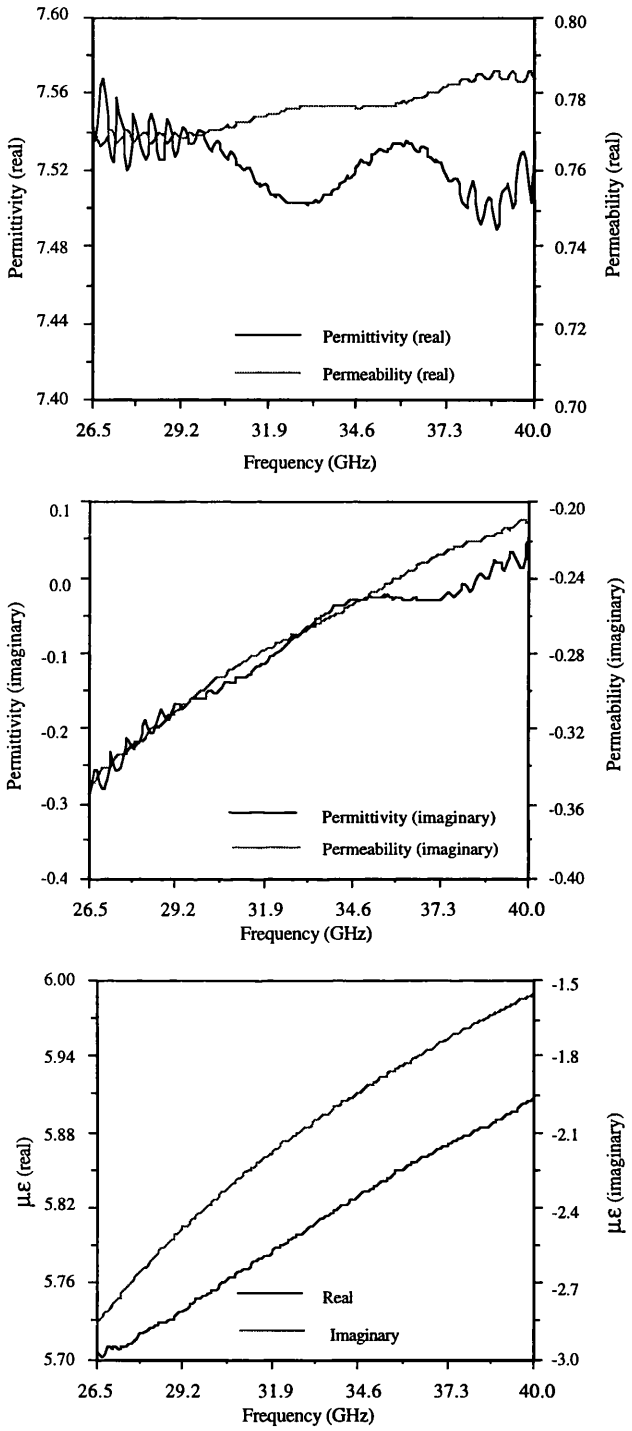

Figure 9.2 Complex permittivity and permeability of a lossy ferrite sample (sample D3, thickness=10.47 mm) measured as a thick slab.

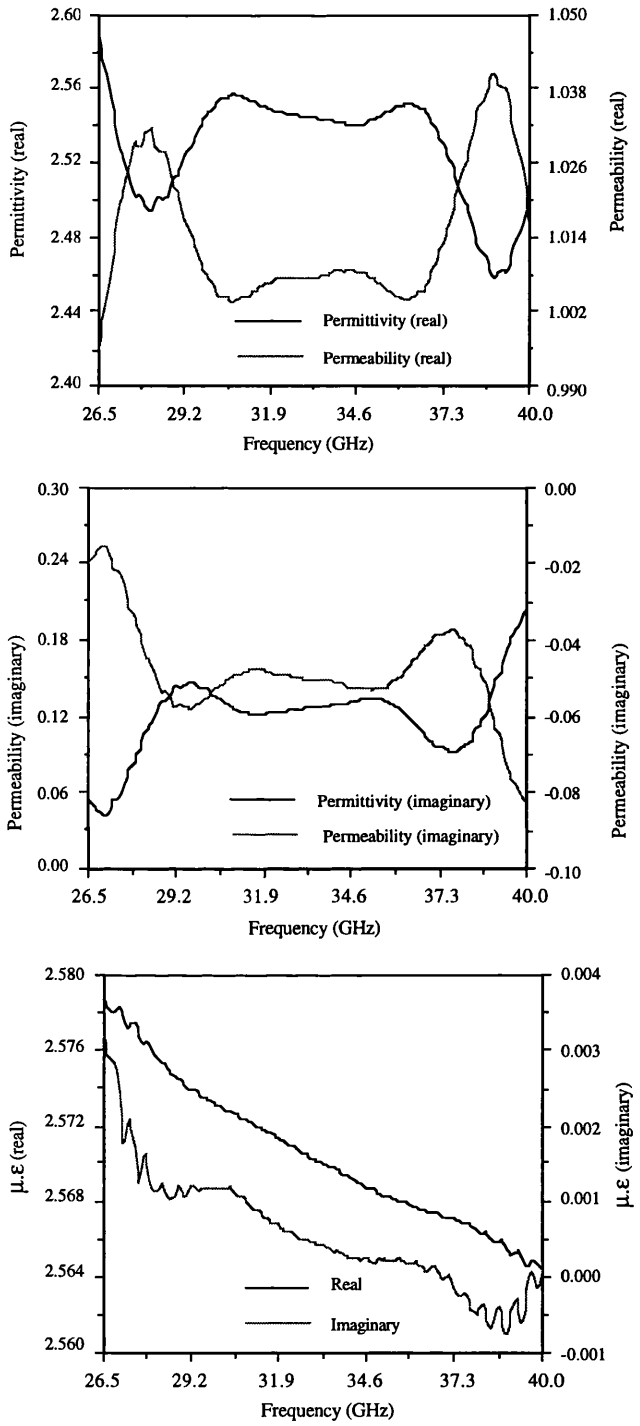

Figure 9.3 Complex permittivity and permeability of a polystyrene sample (ε_r=2.545-j0.001, thickness=21.4 mm) measured as a thick slab.

9.2.2 Thin magnetic samples

In thin slab measurements, the time domain gate is wide enough to include the most significant terms of the multiple reflections within the sample. As explained in previous chapters, the total accuracy decreases at frequencies such that the electrical length of the sample is a multiple of 180°, and measurement at these frequencies should be avoided. Therefore samples with thickness of less than $\lambda/2$ or an odd multiple of $\lambda/4$ are preferred.

Figure 9.4 shows the measured properties of the low-loss ferrite sample (*B2*) treated as a thin slab. The sample properties are calculated from the measured transmission and reflection coefficients at perpendicular polarisation. The complex permittivity and permeability of this sample are $\varepsilon_r=6+j0.2$ and $\mu_r=0.92-j0.06$. As can be seen, the multiple reflections cause the total error to vary with frequency. The error in the real parts of ε_r and μ_r are about 2.5% and 6% respectively, but the error in the electric and magnetic losses are more considerable. Although the total error increases at frequencies such that the sample electrical length is a multiple of 180°, the error in $\varepsilon_r\mu_r$ is relatively low.

The properties of the lossy ferrite (sample D3) treated as a thin slab are shown in figure 9.5. As the propagation coefficient (P) is sufficiently small in this sample, multiple reflections can be ignored. Therefore the use of time domain gating does not improve the results.

The electric and magnetic properties of the polystyrene slab ($d=21.4$ *mm*) treated as a *thin* sample are shown in figure 9.6. As we expect, the measurement error increases rapidly at frequencies such that the sample thickness is a multiple of $\lambda/2$. At optimum frequencies, the properties of this sample are $\varepsilon_r=2.4+0.j0.25$ and $\mu_r=1.1-j0.11$. It can also be seen that the error in $\varepsilon_r\mu_r$ ($\varepsilon_r\mu_r=2.57-j0.004$) is much less than the error in ε_r and μ_r.

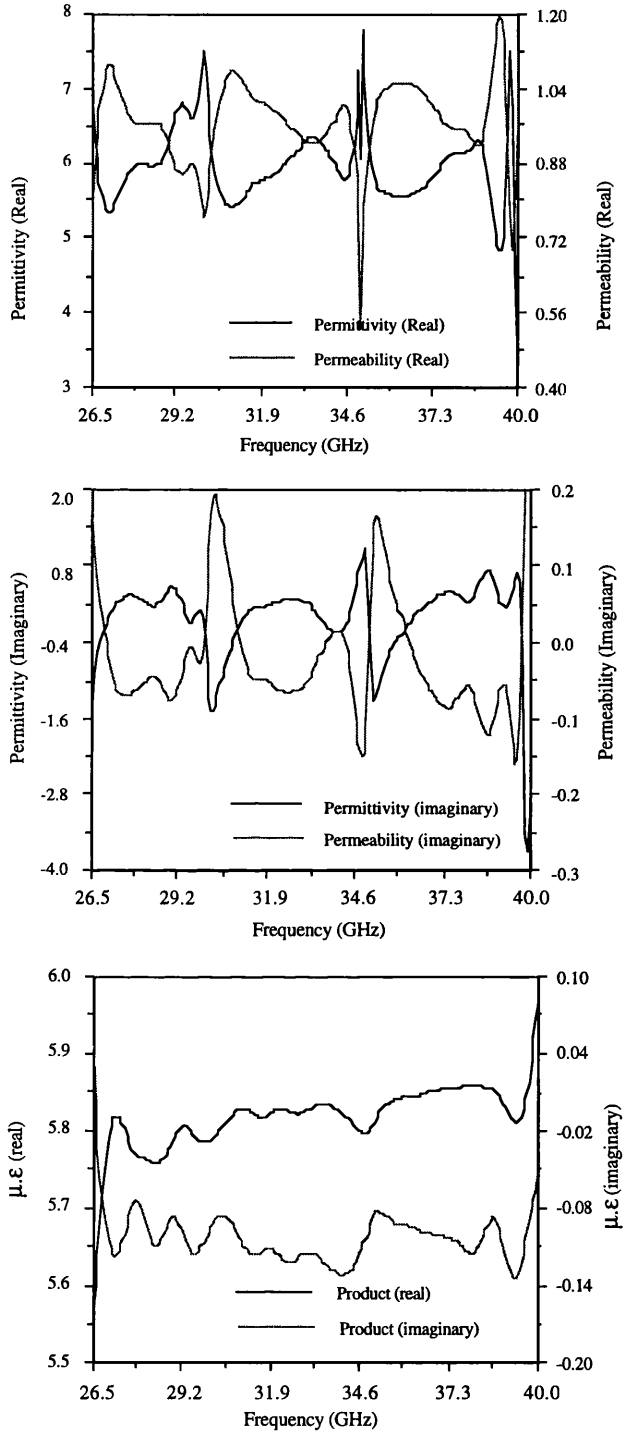

Figure 9.4 Complex permittivity and permeability of a low-loss ferrite (sample B2, thickness=13.03 mm) measured as a thin slab.

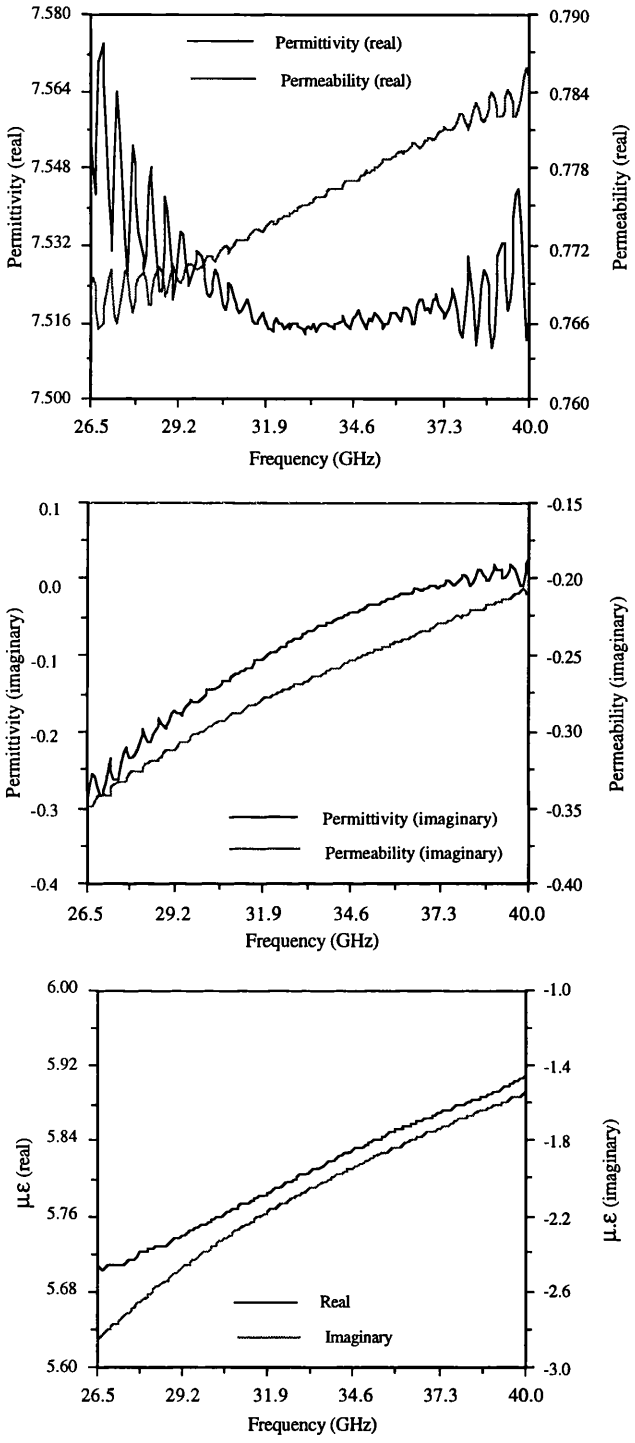

Figure 9.5 Complex permittivity and permeability of a lossy ferrite (sample D3, thickness=10.47 mm) measured as a thin slab.

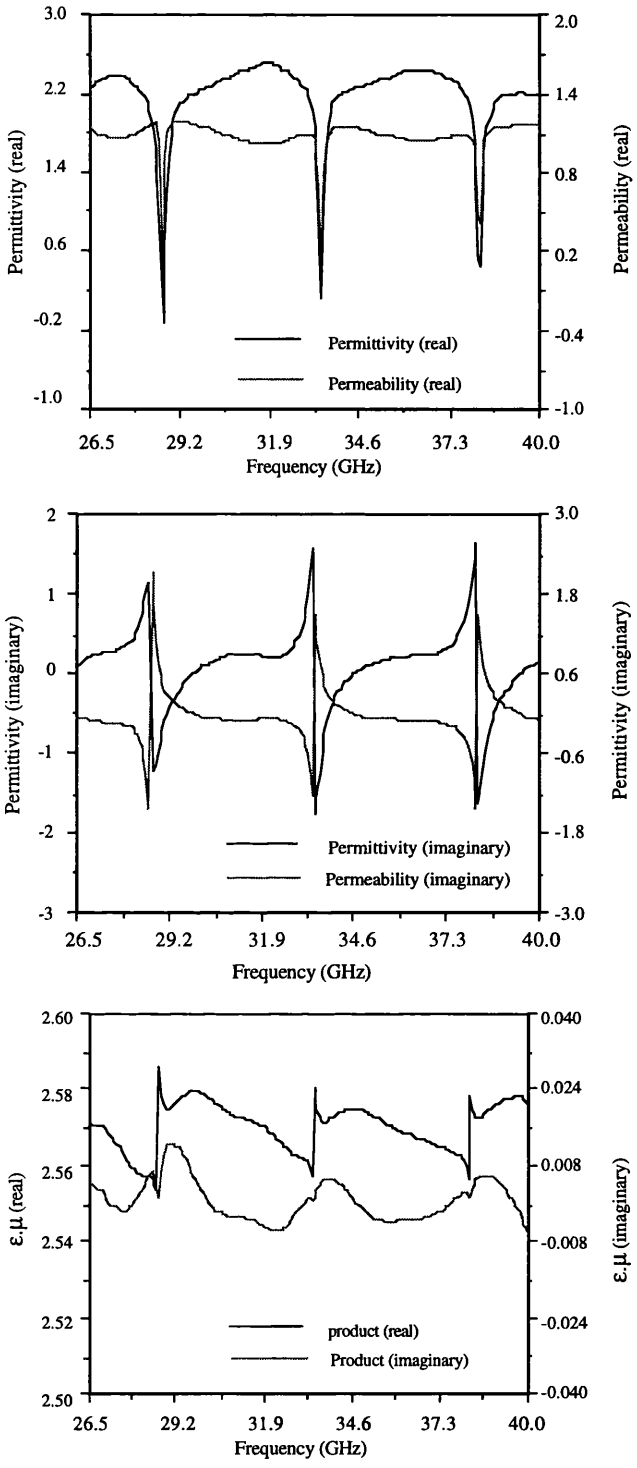

Figure 9.6 Complex permittivity and permeability of a polystyrene slab (ε_r=2.545-j0.001, thickness=21.4 mm) measured as a thin slab.

9.3 Minimum thickness

To remove the effect of multiple reflections by time domain gating, the electrical length of sample should be longer than twice the gate width. For lossy materials the sample can be thinner, since the multiple reflections decay relatively faster. In free-wave techniques *thick* slab measurement is preferred, but the condition for minimum sample thickness cannot be met in some cases. Failing to remove the effect of higher order terms of the multiple reflections causes error in the measured parameter. In this part, the gating error due to leakage of the higher order terms of the multiple reflections in the *thick* slab measurement is demonstrated.

Figure 9.7 shows the properties of a low-loss sample similar to sample *B2*, but thinner (*d=7.5 mm*). The properties of this sample measured by the waveguide method are shown in table T9.3.

Sample	ε'	ε"	μ'	μ"
B3	5.58	-0.01	0.95	+0.00
B3	5.58	-0.09	0.96	+0.01
B3	5.62	-0.10	0.98	+0.02
Average	5.593	-0.063	0.963	+0.01

Table T9.3 The properties of sample B3 (d=6.371mm) measured by the waveguide method at 40 GHz.

For 13.5 GHz frequency span, the minimum gate width in the HP-8510B is 88 nanoseconds which corresponds to 29.6 mm. Therefore the minimum sample thickness to qualify as a *thick* slab is about 40 mm. The electrical length of sample B3 is 15.6 mm, therefore leakage of the higher order terms of the multiple reflections results in error in the sample properties.

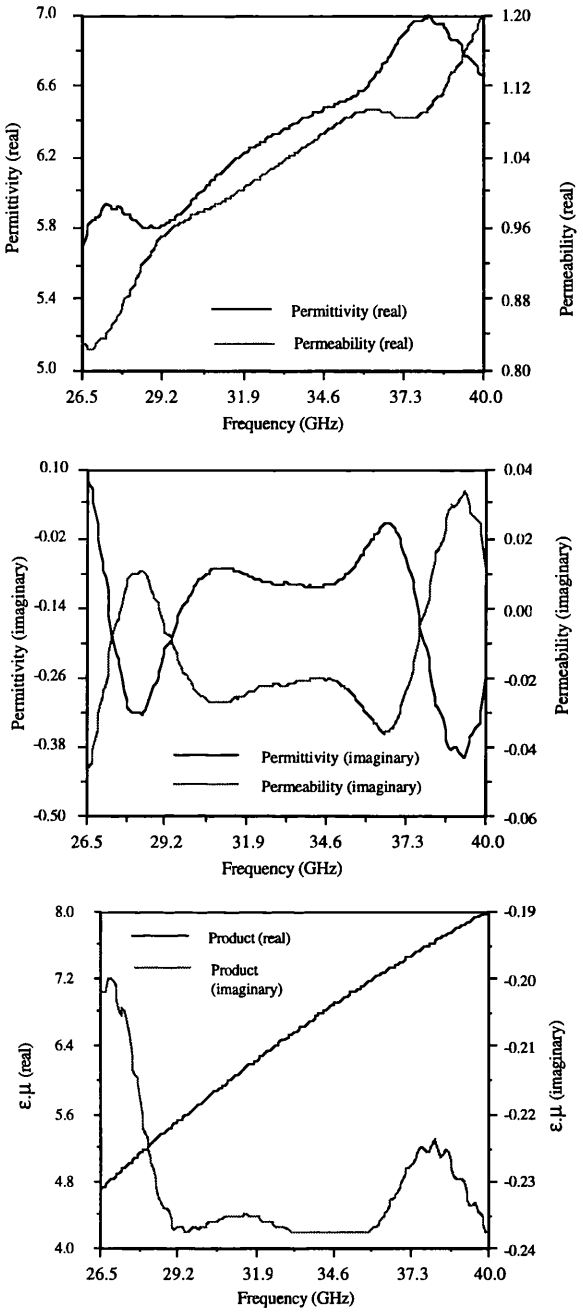

Figure 9.7 Complex permittivity and permeability of a low-loss ferrite (Sample B3, thickness=14.8 millimetres) measured as a thin slab.

The measured properties of a lossy ferrite (*D2*) similar to sample *D3*, but thinner (*d= 48.7 mm*) are shown in figure 9.8. The electrical length of sample *D2* is 11.6 mm and its properties measured by the waveguide method are given in table T9.4. As can be seen, the gating error is increased. The propagation coefficient (*P*) is relatively small in this sample, therefore multiple reflections decay faster and the gating error is relatively lower.

Sample	ε'	ε''	μ'	μ''
D2	6.89±0.01	0.35±0.02	0.78±0.02	0.38~0.15
D2	6.95~7.21	0.65~0.95	0.87~0.80	0.34±0.08

Table T9.4 The properties of sample D2 (d=4.78 mm) measured by the waveguide method in frequency range of 26.5 to 40 GHz.

Figure 8.9 show the measured permittivity and permeability of a polythene sample with thickness of 14.8 mm. Regarding the dielectric constant of polythene ($\varepsilon_r=2.3$), the electrical length of this sample is 19.8 mm. Therefore this sample cannot be measured as a *thick* slab, and a considerable gating error is examined.

The results of the measurement on the above samples show that samples with electrical length down to the gate span can be measured as a *thick* slab. If a sample with electrical length less than the gate width is considered as a *thick* slab, the gating error increases considerably. It should be noted that the above discussion is applicable to cases in which time gating is used to remove the multiple reflections within the sample. Samples with small propagation coefficient (P<-15 dB) can be measured as *thick* slabs confidently.

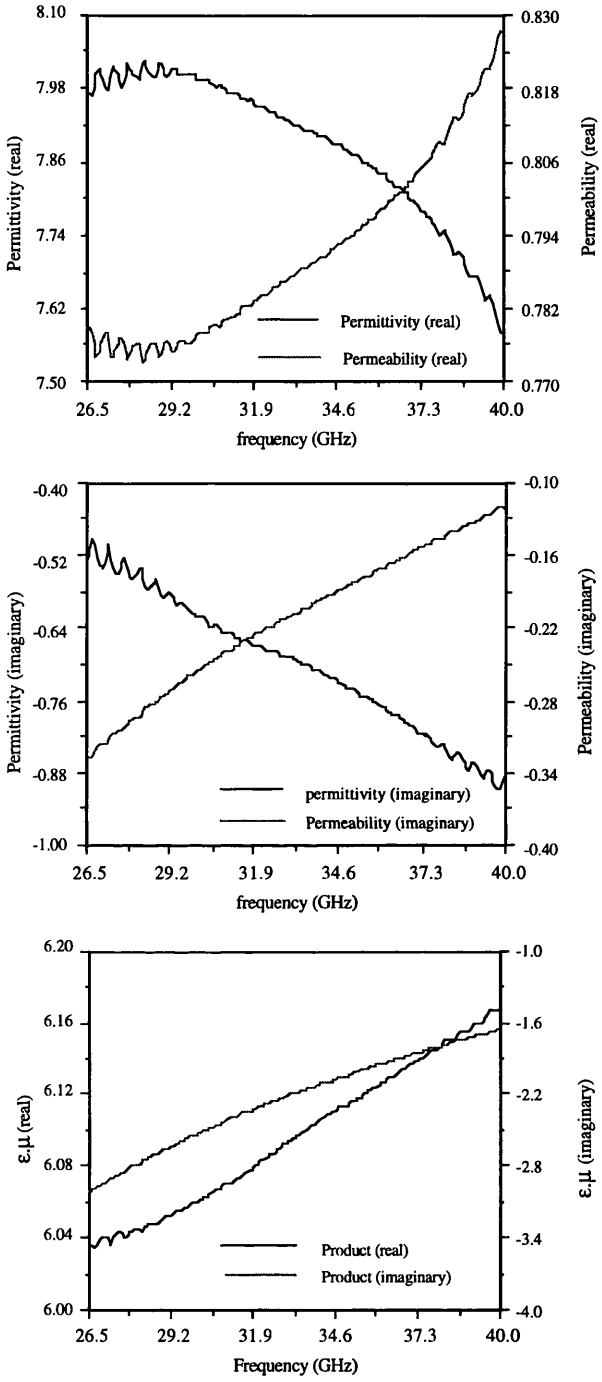

Figure 9.8 Complex permittivity and permeability of a lossy ferrite (sample, D2 thickness=4.87 millimetres) measured as a thin slab.

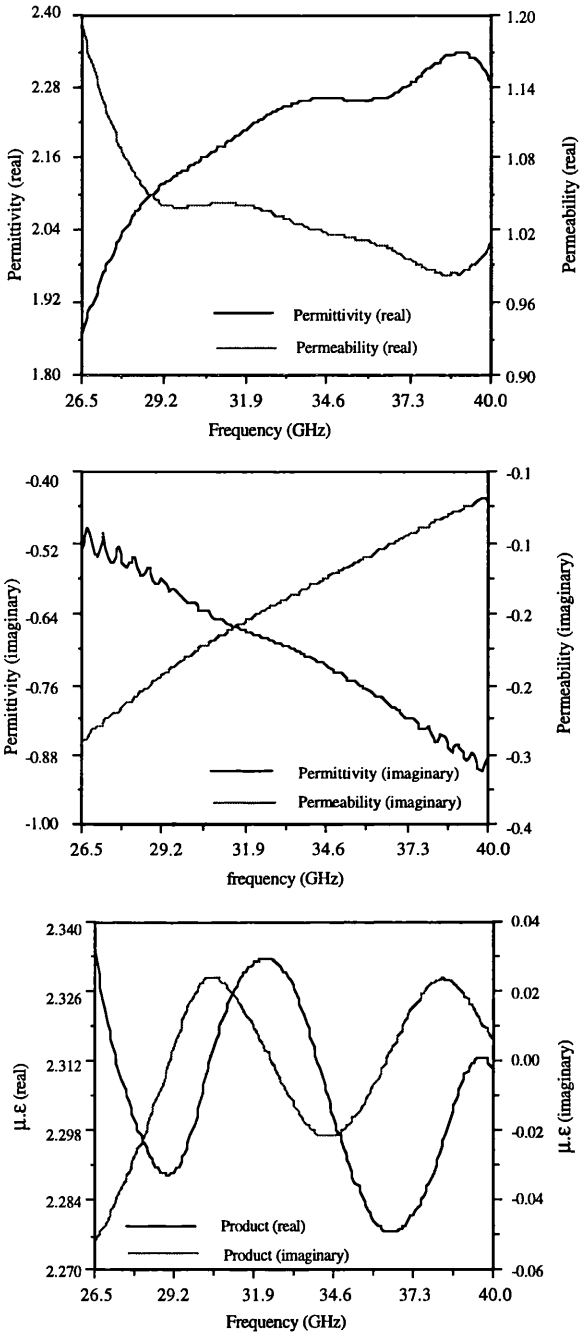

Figure 9.9 Complex permittivity and permeability of a polythene (ε_r=2.3, thickness=14.8 millimetres) measured as a thin slab.

9.4 Non-magnetic materials

In non-magnetic materials ($\mu_r=1$), the dielectric properties can be calculated from two independent measurements. In the error analysis, it is shown that the error in the product of $\mu_r.\varepsilon_r$ is much less than the error in ε_r and μ_r. In non-magnetic materials the assumption of $\mu_r=1$ can improve the accuracy, if four data are used in the calculation. In this case, the total error is a function of the method used for calculating the material properties. The idea of measuring the product of $\mu_r\varepsilon_r$ is based on the conclusion obtained in the error analysis and can be considered as a more generalized form of the method suggested by Baker-Jarvis et al [44]. In our approach, the sample properties can be calculated from any combination of transmission and/or reflection coefficients. The measurement can also be carried out at oblique or normal incidence. In free-wave techniques, the transmission coefficient is measured relatively accurately, but the error in measuring the phase of the reflected wave is considerable. The accuracy in calculating μ_r and ε_r of a slab from the measured transmission coefficient at two orthogonal polarisations is not reasonable, but the product of $\mu_r\varepsilon_r$ can be calculated relatively accurately. For non-magnetic materials, the complex permittivity can be found from the product of $\mu_r\varepsilon_r$.

The properties of polystyrene calculated from the measured transmission coefficient at two polarisations are shown in figure 9.10. The accuracy in measuring the properties of a sample increases if it is treated as a non-magnetic material ($\varepsilon_r=2.54-j0.01$). If this sample is measured as a thick slab, the measured properties are more accurate ($\varepsilon_r=2.544-j0.008$).

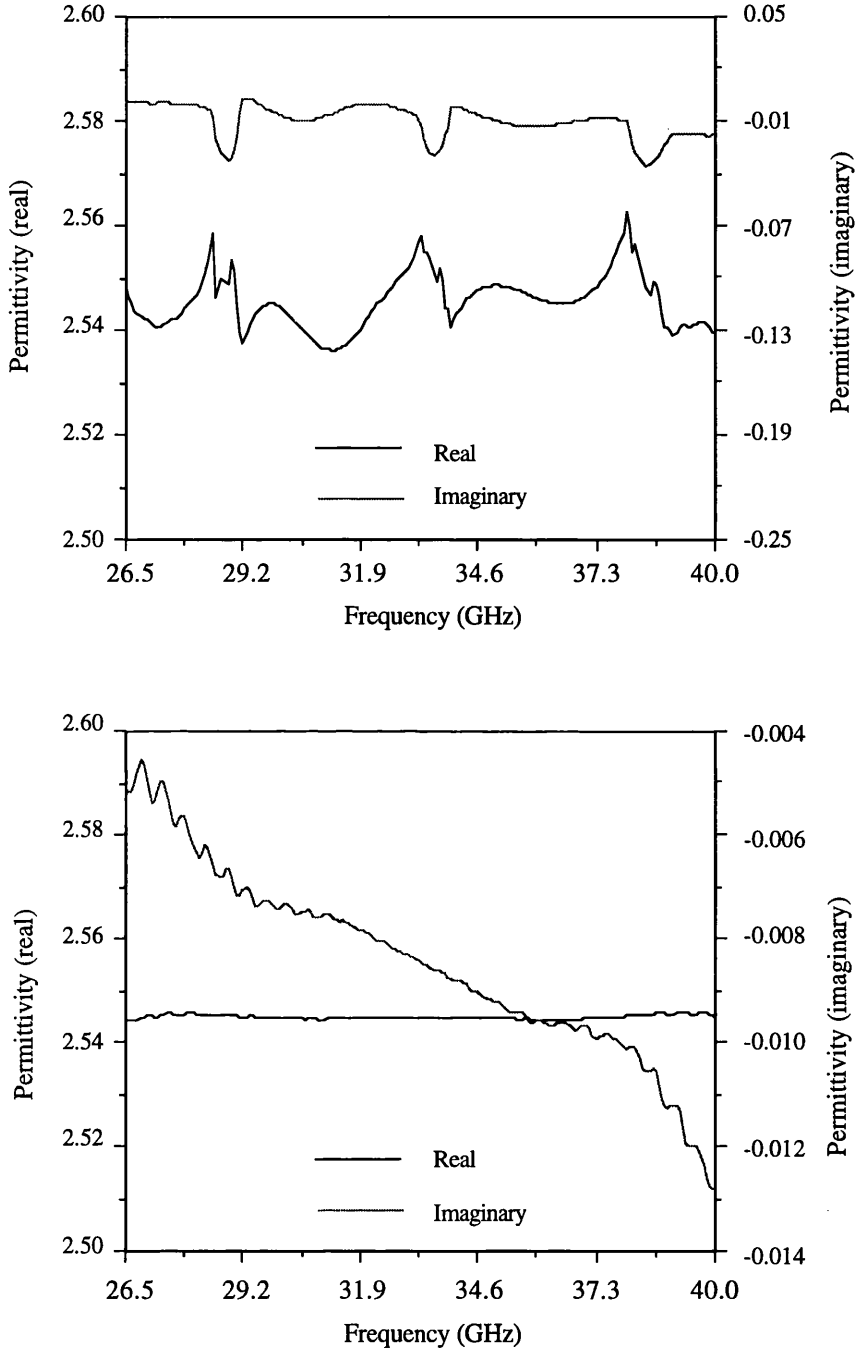

Figure 9.10 Complex permittivity polystyrene sample (thickness=21.84 millimetres) measured as a thin (upper) and thick (lower) slabs.

9.5 Eight data optimisation method

As mentioned, the properties of a slab can be calculated from eight measured data, (transmission and reflection coefficients at two polarisations). This method is appropriate for lossy ferrites, but fails to converge in measuring low-loss materials. In this method, the product and ratio of permittivity and permeability are calculated from the transmission and reflection coefficients respectively.

Figure 9.11 shows the results obtained from the measurement of sample D1 treated as a *thick* slab. The properties of this sample measured by the waveguide method are given by table T9.5. Although the properties of this sample are similar to those of sample *D2*, the lower thickness of this sample means that multiple reflections cannot be ignored. In measuring sample D1, this method fails to converge for frequencies above 34 GHz. Therefore the sample properties are shown up to this frequency. Figure 9.12 shows the measurement of sample D1 treated as a *thin* slab. As can be seen, the magnitude of variation increases. It is shown that the degree of dependence of transmission and reflection coefficients of a slab on $\varepsilon_r\mu_r$ and μ_r/ε_r increases, if the multiple reflections within the sample are ignored.

Sample	ε'	ε''	μ'	μ''
D1	6.60~6.47	0.09~0.10	0.70±0.02	0.43~0.21
D1	7.09±0.04	0.42±0.03	0.82~0.79	0.37~0.14

Table T9.5 The properties of sample D1(d=6.98mm) measured by the waveguide method in the frequency range of 26.5 to 40 GHz.

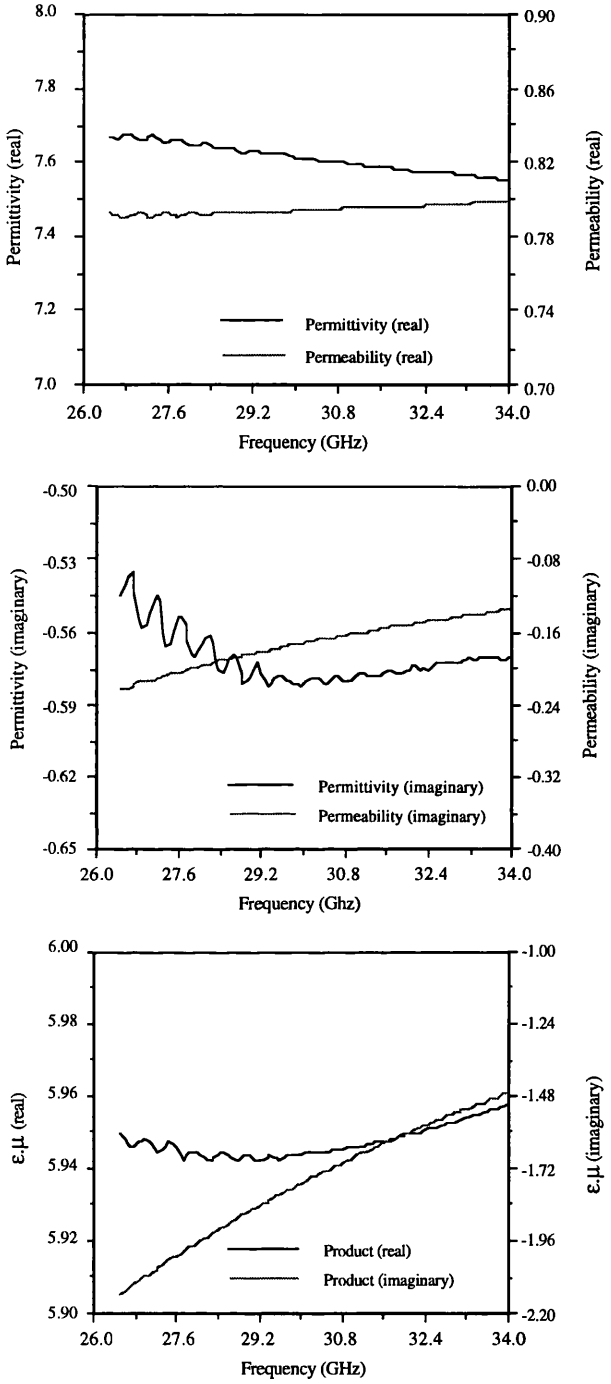

Figure 9.11 Complex permittivity sample D1 measured as a thick slab by the eight data optimisation method.

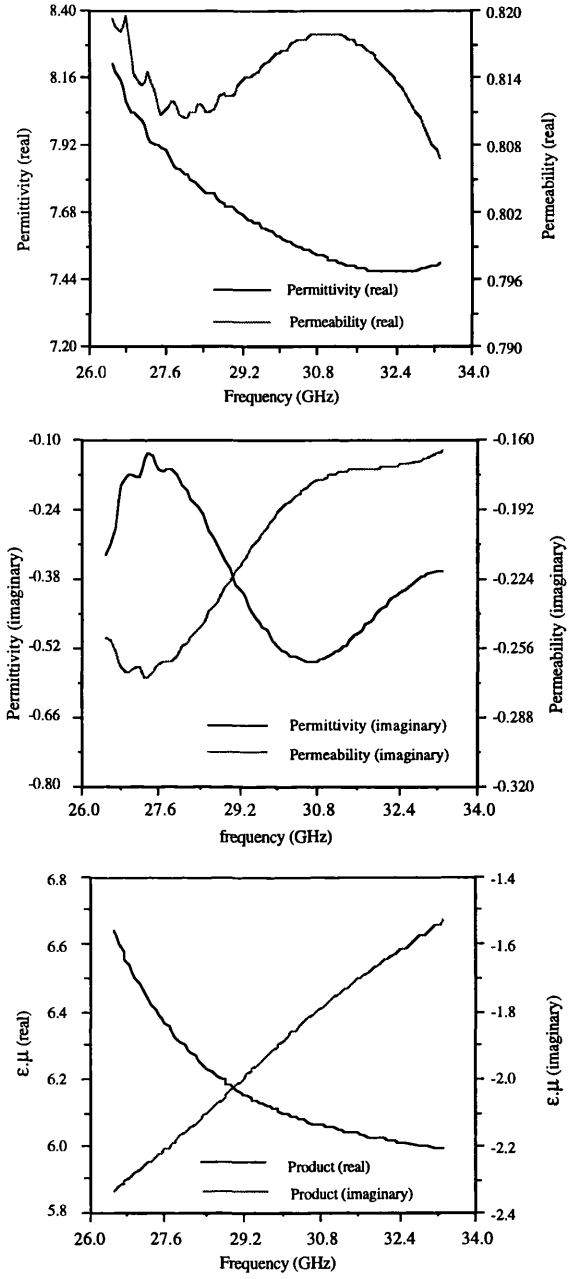

Figure 9.12 Complex permittivity sample D1 measured as a thin slab by the eight data optimisation method.

9.6 Optimum measurement technique

In this part, the optimum method for measuring the electric and magnetic properties of a sample is recommended. It is worth noting that free-wave techniques are at their best for measuring the properties of lossy materials. In free-wave measurements, a *thick* slab is basically preferred if the combination of the propagation coefficient (P) and the minimum gate width allows us to ignore multiple reflections. In the general case, simultaneous use of transmission and reflection coefficients at one polarisation delivers the most reliable results, and there are no significant differences for measuring either polarisation. The use of eight data and employing optimization techniques for calculating ε_r and μ_r delivers reliable values only for lossy materials. This method fails to converge for low-loss materials.

In free-wave measurements, choosing the appropriate thickness is one of the key parameters in minimizing the total error. In *thick* sample measurements the sample should be thick enough that the effect of the multiple reflections can be removed by time domain gating, but the error due to the wavefront curvature and the ambiguity increase by increasing the thickness. In practice, samples with electrical length longer than the gate width can be treated as *thick* slabs. Although increasing the thickness above this value decreases the time gating error, the total accuracy may not be improved due to increasing the magnitude of the other error terms. It is also worth noting that the sample properties are assumed to be somewhat constant over the measured frequency band in *thick* slabs. If the material properties change rapidly with frequency, the slab should not be treated as *thick*. If multiple reflections cannot be ignored, the sample should be considered as a *thin* slab. In this case, measurement at frequencies such that the sample thickness is a multiple of $\lambda/2$ should be avoided.

10 Summary and discussion

10.1 Introduction

This chapter is devoted to a review of the associated difficulties with free-wave methods and the achievements in devising a reliable technique for measuring complex permittivity and permeability of materials at millimetre wavelengths. In this chapter, the sources of error and the various techniques for removing their impact on the measurement results are briefly recalled, and the achievable accuracy in free-wave techniques is discussed. The use of time domain gating as a new method for removing the effect of multiple reflections is evaluated. The angular spectrum model and its improvement in removing the wavefront curvature error are reviewed, and the optimum technique for using the measured data is recommended. At the end of this chapter, the achievable accuracy is discussed and further research for improving free-wave techniques is suggested.

10.2 Sources of error in free-wave measurements

In free-wave measurements, the sources of error can be divided into two different classes. The first category includes the error terms generated in the coaxial and waveguide parts of the measurement system, and the second category consists of error sources associated with free-wave paths. The conventional calibration and error correction techniques can be used for reducing or removing the impact of the first type, but the error mechanisms associated with free space paths cannot be modelled and cancelled out by conventional techniques. Although some of the error sources in free-wave paths can be modelled and their effects removed from the measurement in theory, they are complicated and treated as random error terms in practice. Diffraction of the wave from the edges of the sample, unwanted reflections and the measurement in the near-field region are three major sources of error associated with the propagation of the wave in free space paths. The systematic and random error terms in the network analyser also contribute to the total the error in the free-wave measurement. Although the error terms associated with the waveguide and coaxial paths

can be removed by conventional error correction techniques, measurement at mm-wave frequencies introduces new sources of error and degrades the total accuracy. The dynamic range of the network analyser also decreases at mm-wave frequencies. This reduction in dynamic range, which is due to the frequency multiplier, degrades the accuracy in measuring small transmission and reflection coefficients (less than -20 dB). The use of special calibration techniques (e.g. *TRL* or *TRM*) which are devised for dispersive transmission lines or free-space improves the accuracy.

10.2.1 Total error

In free-wave techniques, inaccuracy in measuring transmission and reflection coefficients are considered as the main error terms. Inaccuracy in specifying the frequency, sample thickness and the incident angle are not taken into account, though the error in each of these parameter causes error in the sample properties. The total error in ε_r and μ_r is a complicated function of the error in the transmission and/or reflection coefficients and the sample properties. If multiple reflections within the sample are taken into account, the reflected wave is minimum and the transmission coefficient is maximum at frequencies such that the sample electrical length is a multiple of $\lambda/2$. At these frequencies, the reflection coefficient has the minimum interaction with the material properties and the total error in μ_r and ε_r increases rapidly. Measurement at these frequencies should be avoided, though the product $\mu_r\varepsilon_r$ can still be calculated rather accurately. If measurement at these frequencies is excluded, the product of $\mu_r\varepsilon_r$ can be calculated more accurately than μ_r and ε_r individually from the transmission coefficient. In most cases, the ratio μ_r/ε_r is less subject to error than μ_r and ε_r, if the measured reflection coefficients at two orthogonal polarisations are used for calculations. The dependence of $\mu_r\varepsilon_r$ and μ_r/ε_r on the transmission and reflection coefficients is a function of the sample electrical length, and the degree of this dependence changes with frequency in *thin* samples.

If multiple reflections within the sample are ignored (*thick* slabs), the ratio μ_r/ε_r can be calculated more accurately than μ_r and ε_r from the reflection coefficient measurements. In this case, the material properties are not dependent on the incident angle, thickness and frequency. The use of the transmission coefficient at two orthogonal polarisations is the most reliable technique for calculating the product $\mu_r\varepsilon_r$.

10.2.2 Angular spectrum model

The angular spectrum model gives a complete solution for transmission and reflection coefficients of a slab in the near-field region. In this model, the computation time is the main difficulty. This model improves the accuracy, but the degree of improvement is a function of the antenna distance and the aperture excitation. In the general case, the antenna coupling integral can be determined only by numerical methods. Regarding the implications of using the angular spectrum model, it is preferable to use an adequate antenna distance such that the wavefront curvature can be ignored. The angular spectrum model becomes more significant whenever the wavefront curvature error outweighs other error terms in the measurement system. This occurs in compact measurement systems where the sample is placed in the near-field region. In order to ignore wavefront curvature, the antennas should be separated by at least twice the Rayleigh distance.

10.2.3 Time gating error

In free-wave techniques, the unwanted reflections constitute one of the main error term. The unwanted reflections become more significant in compact measurement systems where different parts of the apparatus are placed close to each other. Time gating technique can be used to remove the effect of the unwanted reflections from the results. In the time domain response, the multiple reflections within the sample are represented as a set of reflections separated by twice the sample electrical length. If the multiple reflections are taken into account (*thin* slab), the time gate should be wide enough to include the most significant terms of this series. In practice, the main unwanted reflection is generated by bouncing the waves between the antennas and the sample surface which appears as distant as the antenna distance from the origin in the time domain response. In order to remove this unwanted reflection, the gate should be narrower than the antenna distance. As the multiple reflections within the sample are spread over a very wide interval in the time domain, the higher order terms of the multiple reflections within the sample are discarded in the gating process which cause error in the measured parameter. The gating error becomes more significant in measuring samples with long electrical length. In *thin* sample measurement, the gating error is a function of the sample electrical length, propagation coefficient (P) and the gate width. In practice, the maximum thickness of a low-loss sample treated as a *thin* slab

should be less than 1/8 the antenna distance. For lossy materials, the multiple reflections within the sample decay faster and the sample can be as thick as 1/6 the antenna distance.

If the sample is treated as a *thick* slab, the minimum gate width is the limiting factor. The minimum gate width is inversely proportional to the frequency span. In the time domain response, different terms of the multiple reflections are separated by twice the electrical length of the sample. In order to remove the higher order terms of the multiple reflections by time gating, the gate width should be adequately narrow. In practice, samples as thick as the minimum gate width can be treated as *thick* slabs. The minimum sample thickness is also a function of the propagation coefficient (P). For lossy samples ($P<-15$ dB), the multiple reflections can be ignored without the use of time gating.

10.3 Measurement accuracy and optimum method

In free-wave techniques, the total accuracy is a complicated function of the error in the measured parameters, the material properties and the method used for the calculation, therefore it is very difficult to specify the total accuracy. These techniques are basically appropriate for measuring lossy material, since they deliver poor accuracies in measuring loss properties. The lack of any other technique for measuring lossy materials makes free-wave methods attractive at mm-wave frequencies, but it makes the comparison difficult.

If the multiple reflections within the sample are taken into account, the accuracy decreases at frequencies such that the sample thickness is a multiple of $\lambda/2$, and measurement at these frequencies should be avoided. In practice, the phase of the reflected wave cannot be measured accurately, and this inaccuracy mainly affects the imaginary parts of the permittivity and permeability. In the general case, $|\mu_r\varepsilon_r|$ and the sum of loss tangents ($\tan\delta_m+\tan\delta_e$) are calculated more accurately with respect to the difference of loss tangents ($\tan\delta_m-\tan\delta_e$) and $|\mu_r/\varepsilon_r|$.

If multiple reflections within the sample can be ignored, the total error and the dependence of the measurement accuracy on the sample thickness decrease considerably. In *thick* sample measurements, the minimum thickness decreases with increasing frequency span over which the measurement is carried out. Since the maximum available bandwidth

increases at the higher end of millimetre wavelengths, the minimum sample thickness decreases. The gating error can be considerable, if a thin sample is treated as a *thick* slab. In measuring *thin* slabs the gating error can dominate the other sources of error, if the sample electrical length is higher than the maximum values.

In each measurement technique, the achievable accuracy is one of the main factors. The accuracy in *thick* slab measurements is relatively higher, and calculating the sample properties from the measured transmission and reflection coefficients usually delivers more reliable results. In measuring the properties of polystyrene (*thin* slab), the accuracy in measuring $|\mu_r\varepsilon_r|$ is better than 2%, and the error in the sum of loss tangents ($\tan\delta_m+\tan\delta_e$) is less than 10 milliradians. The accuracy in measuring the ratio μ_r/ε_r mainly depends on the error in measuring the phase of the reflection coefficient. The total accuracy in measuring material properties increases considerably if the multiple reflections are ignored. In measuring the complex permittivity of non-magnetic materials, either transmission and reflection coefficients at one polarisation or transmission coefficient at two polarisations can be employed. The accuracy of better than 0.1% in the real part and 10 milliradians in $\tan\delta_e$ of polystyrene are achieved by this technique. In measuring the properties of lossy materials, an accuracy of better than 5% in $|\mu_r\varepsilon_r|$ and 50 milliradians in the sum of loss tangents ($tan\delta_m+tan\delta_e$) are expected. It is worth noting that the instrumentation is an important factor in defining total accuracy in free-wave techniques. As a good example, the accuracy improvement obtained in the similar measurements carried out at DRA(Holton Heath) can be referenced.

10.4 Discussion

Design of the prototype measurement system is based on the available components, and better results are expected after making some modifications to this system. The restrictions in providing the required components and samples also forced us to use the comparison method to show the effectiveness of some of the devised techniques. Although the accuracy can be improved by providing better instrumentation, the presented accuracy is better or comparable with the available techniques. Time domain gating improves the total accuracy and removes one of the limitations in free-wave techniques. The effectiveness of this method is shown by comparing the results obtained from treating the same samples as *thin* and *thick* slabs.

In all results reported by other researchers, the error due to wavefront curvature is ignored. The angular spectrum model introduced in this thesis increases the accuracy in compact measurement systems. The degree of improvement is shown by simulating the wavefront curvature error, and using this model in the measurement of glass samples has shown improvement in the overall accuracy. It is worth explaining that the measured properties of glass are not presented in the thesis, since there is no other reference with which to compare them. The other researchers have also used matched lens antennas and considered sufficient space between the antennas to reduce the impact of the error terms associated with free-space paths. The effect of focusing the wave on the sample surface by a dielectric lens is also studied, and it has been shown that the wavefront curvature error increases for a focused beam.

In some reported work by other researchers, special calibration methods are used. In this project we have not used any specific technique, except time domain gating. Therefore, better accuracy is expected if we can perform more sophisticated calibration technique. Regarding the achieved accuracy in measuring lossy samples, devising time domain gating, and the angular spectrum model, this research has made significant progress in free-wave techniques.

10.5 Further work

In spite of the improvements achieved in this research, free-wave methods are not fully exploited and further work is recommended to be carried out in the following areas. This work can be divided into two categories. The first area includes further developments in the available techniques for improving the accuracy and removing some of the associated implications. The second proposed field of research consists of devising new measurement techniques.

10.5.1 Automation computer program

The network analyser can be controlled remotely via its HP-IB port. A computer program written in HP-BASIC language automates different stages of the measurement in the

double-pass apparatus. This program is used by an HP-300 personal computer which performs the required computation for the double-pass system. In the *single-pass* apparatus, the computer programs calculating the sample properties from the measured parameters are mainly written in FORTRAN. Performing the required mathematical operations requires a fast CPU, although a Macintosh desktop computer was employed. Unfortunately, this computer is not fast enough, but the availability of the other programming languages and libraries forced us to use it. In the process of transferring data from the network analyser, calculating the sample properties and plotting the results a combination of different software are used.

A fast personal computer with the capability of communicating with the network analyser via HP-IB can automate the *single-pass* apparatus. The possibility of combining computer programs written in different languages and the use of *Windows* based software (e.g. *MathLab* or *LabView*) can create a powerful interface for performing the measurement, transferring data, calculating and plotting the results. Integrating all the measurement processes in an interactive computer program reduces the total measurement time and offers the required flexibility. This program can also be run on a notebook computer which brings more versatility to the measurement system.

10.5.2 Adaptive computer program

For calculating the sample properties from the measured transmission and reflection coefficients, the use of iterative numerical methods is inevitable. In the calculation, *a priori* knowledge of the material properties and/or the correct number of the wavelength in the sample are required. As the measurement is usually carried out over a frequency band, the correct number of wavelengths in the sample may change several times. A computer program with the capability of showing the rate of convergence and finding the correct wavelength number in the sample can help the operator to find the correct set of answers. The facility of switching from one calculation method to another is also a valuable tool in converging to the correct set of permittivity and permeability in the minimum time.

10.5.3 Calibrating and time gating facility

The time domain gating and error correction facilities are carried out in the HP-8510B, but they are not available in all network analysers. These techniques are based on a mathematical process which can be performed in a desktop computer. Although the HP-8510B is capable of performing these tasks in real time, the flexibility in free-wave measurement techniques can be improved by a custom designed computer program doing all the required operations. This computer program can transfer the measured data from the network analyser and carry out error correction and time domain gating in a personal computer. Such a computer program allows us to use a wider range of network analysers for free-wave measurements and to implement appropriate calibration methods such as *TRL* and *TRM*.

10.5.4 Automatic gate setting

The gate parameters should be set properly, otherwise there will be considerable error in the measured parameters. Although the operator can set the gate parameters by observing the time domain response, this method is not accurate. In general, the low resolution in the time domain response causes difficulty in setting the gate parameters properly. This error is more serious in measuring *thick* samples. A computer program calculating the gate parameters from the sample properties is a useful tool for speeding up the measurement time and increasing the accuracy.

10.5.5 Full implementation of the angular spectrum model

The angular spectrum model improves total accuracy, if the computation error is sufficiently small. The main difficulty in using this model is its great computation time, and the following suggestions improve the accuracy and reduce the computation time. In computing the coupling integral, a number of mathematical operations should be carried out at each frequency. One of the time consuming parts of this process is taking the FFT of the aperture excitation. For a given measurement setup, the FFT of the aperture can be calculated and saved in the computer memories at the required frequencies. The use of this data can reduce total computation time to a good extent.

In the angular spectrum model, the accuracy in computing the coupling integral should be more than the required accuracy in the numerical algorithms used for finding the zeros of the transcendental equations. Therefore, the coupling integral should be computed at sufficiently small intervals. In order to achieve the required accuracy in computing the coupling integral, the number of samples should be increased. If the coupling integral is computed by samples with non-uniform intervals, the computation time can be decreased. In this method, the samples should be more dense at the angles close to antenna axis.

10.5.6 Improving reflection coefficient measurement

In reflection coefficient measurement, the phase of the reflected wave cannot be measured accurately. It is possible to correct the phase error in the reflection measurement by performing extra measurements. The extra data can be acquired by measuring transmission and/or reflection coefficients at different incident angles.

10.5.7 Focused beam

An antenna with a focused beam reduces diffraction from the edges of the sample, and allows us to measure samples of small size. As we showed, focusing the beam causes angular spectrum spreads over a wider interval and an increase in the wavefront curvature error increases. Therefore, the improvement delivered by the angular spectrum model becomes more significant. Since this model is based on calculating the angular spectrum of the diffracted wave, the field in the aperture plane should be well defined. Therefore, the use of matched lens antennas with a well defined field distribution is recommended.

10.5.8 Fully automated measurement system

At mm-wave frequencies, waveguide and coaxial measurement techniques are well established and appropriate error correction methods for enhancing the accuracy are available. In free-wave measurements, the mechanical repeatability of the apparatus is one of the main sources of error. Therefore, we should try to avoid making any non-repeatable

changes in the system. If a number of antennas for measuring transmitted and reflected waves at two orthogonal polarisations are arranged, the required parameters can be measured by setting the associated waveguide switches connecting the antennas to the network analyser ports. In this design, the position of the sample and six antennas are fixed, and only two antennas are connected to the network analyser at a time. Waveguide switches are relatively repeatable and can be controlled electronically by the computer, therefore the measurement and calibration can be carried out in an automated fashion. Since non-repeatable changes are avoided in this technique, the total accuracy is likely to be increased.

References

[1] Afsar, M.N., Brich, J.R., Clarke, R.N. 'The Measurement of Properties of Materials'; Proc. IEEE, Vol. 74, No. 1, January 1986 pp. 183-199

[2] Birch, J.R., Clarke, R.N., 'Dielectric and optical measurements from 30 to 1000 GHz'; The Radio and Electronic Engineer, Vol. 52, No. 11/12. pp. 565-584, November/December 1982

[3] Clark, R.N., Rosenberg, C.B., 'Fabry-Perot open resonators at microwave and millimetre wave frequencies, 2-300 GHz'; J. Phys. E:Sci. Instrum., Vol. 15 1982 pp. 9-23

[4] Lynch, A.C., ' Precise Measurements on Dielectric and Magnetic Materials'; IEEE Trans., Vol. IM-23, No. 4, pp. 425 431, December 1974

[5] Von Hippel, A.R., 'Dielectric Materials and Applications'; John Wiley &Sons, New York, 1954

[6] Lynch, A.C., 'Measurement of the dielectric properties of low-loss materials'; Proc. IEE Vol. 112. No. 2 February 1965, pp 426-431

[7] Hartshorn, L., Ward, W.H., 'The measurement of permittivity and power factor of dielectric at frequencies from 10^4 to 10^8 c/s'; J. IEE, Vol. 79, pp. 567-609, 1936

[8] Lynch, A.C., 'Edge capacitance in the measurement of dielectric properties'; Proc. IEE Vol. 120, pp 934-938, 1973

[9] Lynch, A.C., 'Unbalanced bridge for the measurement of dielectric loss'; Proc. IEE, Vol. 124, No. 2, February 1977

[10] Pratt, G. J., Smith, M. J. A., ' A wide-band bridge for the measurement of the complex permittivity of polymeric solids and other materials'; J. Phys. Chem. Vol. 73, No. 3, March 1969, pp 927-933

[11] Ogawa, I., Kakimato, A., 'Improved circuit for impedance measurement at very high frequency and its application in testing dielectric properties of insulating materials'; Rev. Sci. Instrum., Vo. 49, No. 7, July 1978, pp 936-939

[12] Kakimot, A., Ogawa, I., Matsushita, T., ' Improvements on the measurements of dielectric constant and dissipation factor in a wide frequency range'; Rev. Sci. Instrum., Vol. 48, No. 12, December 1977, pp 1570-1575

[13] Kakimot, A., Ochi, M., Matsushita, T., 'Precise measurement of dielectric properties at very high frequencies'; Rev. Sci. Instrum., Vol. 46, No. 10, October 1975, pp 1338-1341

[14] Bukingham, K. A., Belling, J. W., 'Aspects of the development of dielectrics for the radio frequency submarine telephone cables'; IEE Proc., Vol. 128, Pt. A, No. 3, April 1981 pp 215-224

[15] Kaczkowaski, A., Mileweski, A., 'High-Accuracy Wide-Range Measurement Method for Dermination of Complex Permittivity in Reentrant Cavity'; IEEE Trans. Microwave Theory and Tech., Vol. MTT-28, No. 3, March 1980 pp 225-231

[16] Clarke, R. N. 'A re-entrant cavity method for the measurement of non-linear polarization in organic liquids'; High frequency dielectric measurement (Proc. of a Tutorial of a Conference on Measurement of High Frequency Dielectric Properties of Materials), 1972 IPC Science and Technology Press Ltd.

[17] Ciuffini, V., Sotgiu, A., 'Lumped parameters for re-entrant resonators'; J. Phys. D: Apl. Phys., 16 1983 pp 2083-2091

[18] Sugget, A., 'Time spectroscopic measurements'; High Frequency Dielectric Measurement, Conf. Proc., March 1972 J. Chamberlain and G. W. Guildford

U.K., IPC Science and Technology Press, 1973

[19] Cole, R. H. ' Evaluation of dielectric behaviour by time domain spectroscopy-I. Dielectric response by real time analysis'; J. Phys. Chem., Vol. 79, No. 14, pp 1459-1469; " II Complex permittivity", pp. 1459-1474, 1975

[20] Cole, R. H., 'Time-domain spectroscopy of dielectric materials'; IEEE Trans. Instrum. Meas., Vol. IM-25, No. 4 pp. 371-375, Dec. 1976

[21] Mopsik, F. I., 'Precision Time-domain dielectric spectrometer'; Rev. Sci. Instrum., Vol. 55, pp. 79-87, Jan. 1984

[22] Robert, S., Von Hippel, A. 'A new method for measuring dielectric constant and loss in the range of centimeter waves'; J. Appl. Phys., vol. 17, pp. 610-616, 1946

[23] Product Note 8510-3 Hewlett-Packard

[24] Yu, P. K., 'Dielectric measurement using an open resonator'; PhD thesis, University of London 1970

[25] Li, S., Akyel,C., and Bosisio,R.G. 'Precise calculations and measurements on the complex dielectric constant of lossy materials using TE_{010} cavity perturbation techniques'; IEEE Trans. Microwave Theory Tech., Vol. MTT-29, pp.1041-1048, 1981

[26] Cook, R. J., 'Microwave cavity methods'; High Frequency Dielectric Measurement, Conf. Proc. March 1972, J. Chamberlain, G. W. Chantry, Eds, Guilford, U.K.; IPC Science and Technology Press, 1973, pp. 12-27

[27] Culshaw, W. 'High resolution Fabry-Perotinterferometer'; IEEE Trans. Microwave Theory Tech., Vol. MTT-8, pp. 182-189, 1960

[28] Culshaw, W.' Resonators for millimeter and submillimeter wavelengths'; IEEE Trans. Microwave Theory Tech., Vol. MTT-9, pp. 135-144, 1961

[29] Culshaw, W., Anderson, M.V. 'Measurement of permittivity and dielectric loss with a millimeter-wave Fabry-Perot interferometer'; Proc. IEEE, Vol. 109B, supp., pp. 820-826, 1964

[30] Cullen, A.L., Nagenthiram, P. 'Microwave open-resonator'; IPC Science and Technology Press, pp. 73-77, 1973

[31] Jones, R.G. 'Millimeter-wave dielectric measurements using open resonator'; IPC Science and Technology Press, pp. 78-82, 1973

[32] Saxton, J.A., Lane, J.A. 'The anomalous dispersion of water at very high radio frequencies'; in Metrological Factors in Radio Wave Propagation, pp. 278-292, The Physical Society London, 1946

[33] Redheffer, R.M. 'Measurement of dielectric constants'; in Technique of Microwave Measurements, C.G.Montgomery, Ed. New York: MacGraw-Hill, 1947

[34] Talpey, T.E., 'Optical method for the measurement of complex dielectric and magnetic constants at centimetric and millimeter wavelengths'; IRE Trans. Microwave Theory and Tech., Vol. MTT-2 PP. 1-12, Sept. 1954

[35] Breeden, K.H., 'Error Analysis for Waveguide-Bridge dielectric-Constant Measurements at Millimeter Wavelengths'; IEEE Trans. Instrumentation and Measurement. Vol.IM-18, No. 3, pp. 203-208, September 1969

[36] Jeyaraj, M., Kumaraswamy, A., Sobhanadri, J. 'Numerical curve fitting technique for evaluating complex permittivity of liquids at millimetre and centimetre wavelengths' J. Phys. E: Sci. Instrum., Vol. 12, pp-1179-1182, 1979.

[37] Campbell, C.K., 'Free-Space Permittivity Measurements on Dielectric Materials at Millimeter Wavelengths'; IEEE Trans. Instrumentation and Measurement. Vol.IM-27, No. 1, pp. 54-58, March 1978

[38] Cook, R.J., Rosenberg, C.B., 'Measurement of the complex refractive index of isotropic and anisotropic materials at 35 GHs using a free space microwave bridge'; J.Phys. D:Appl. Phys., Vol. 12, 1979. pp.1643-1652

[39] Kadaba, P.K. 'Simultaneous Measurement of Complex Permittivity and Permeability in Millimeter Region by a Frequency-Domain Technique'; IEEE Trans. IM, Vol. IM-33. No. 4,December 1984

[40] Shimabukuro, F.I. et al, 'A quasi-optical Method for Measuring the Complex Permittivity of Materials'; IEEE Trans. Microwave Theory and Techniques, Vol. MTT-32, No. 7, July 1984

[41] Cullen, A.L., 'A new free-wave method for ferrite measurement at millimeter wavelengths'; Radio Science, Vol. 22, No. 7, pp. 1168-1170, December 1987

[42] Ghodgaonkar, D.K., Varadan,V.V., Varadan, V.K., 'A Free-Space Method of Measurement of Dielectric Constant and Loss Tangents at Microwave Frequencies" IEEE Trans. Instrumentation and Measurement. Vol. 37, No. 3, pp. 387-394, April 1990

[43] Ghodgaonkar, D.K., Varadan,V.V., Varadan, V.K., 'Free-Space Measurement of Complex Permittivity and Complex Permeability of Magnetic Materials at Microwave Frequencies'; IEEE Trans. Instrumentation and Measurement. Vol. 39, No. 2, pp. 789-793, June 1989

[44] Baker-Jarvis, J., Vanzura, E. J., Kissick, W. A.,'Improved Technique for determining Complex permittivity with Transmission/Reflection method'; IEEE Trans. Mircowave Theory and Technique. 38 Agust 1990, pp. 33-36

[45] Umari, M. H., Ghodgonkar, D. K., Varadan, V. V., Varadan, V, V. V., 'A Free-Space Bistatic Calibration Technique for thr Measurmrnt of Parallel and Perpendicular Reflection Coefficients of Planar Samples'; IEEE Trans.Inst. and Meas. Vol. 40 No. 1 February 1991, pp 19-24

[46] Musil, J., Zacek, F., 'Microwave Measurements of Complex Permittivity by Free space Methods and Their Applications'; Elsevier 1986

[47] Blackham, D. 'Free Space Characterization of Materials'; 15th Annual Metting and Symposium AMTA, pp. 789-793, October 1993

[48] Roland, G. N., Jurgen, P., Erwin, M. B., 'A Free Space Technique for Measuring the Complex Permittivity and Permeability in the Millimeter Wave Range'; IEEE MTTS-94 , pp 1465

[49] Griffith, H.D., Lynch, A.C., A.L., Khosrowbeygi, A., Cullen, Benjamin, R., 'Free-wave Measurement of Complex Permittivity and Permeability at Millimetre-wave Frequency'; International Microwave Conference/Brazil 1991 SBM091, pp 2-6

[50] Lynch, A.C., Griffith, H.D., Cullen, A.L., Khosrowbeygi, A., Quilliard, V., Benjamin, R., 'Measurement of Permittivity and Permeability of Ferrites by Oblique Reflection Transmission'; Electromagnetic Measurement Conference 1991, pp26/1

[51] Lynch, A.C., Griffith, H.D., Cullen, A.L., Khosrowbeygi, A., Benjamin, R., 'Developments in the Measurement of Permittivity and Permeability of Ferrites by Oblique Reflection Transmission'; Electromagnetic Measurement Conference 1993, pp 4/1-4/3

[52] Khosrowbeygi, A., Griffiths, H.D. and Cullen. A. L. , 'A new free-wave dielectric and magnetic properties measurement sytem at millimetre wavelengths'; IEEE MTTS-94, April 1994 San Diego

[53] Khosrowbeygi, A., Griffiths, H.D., Cullen. A. L. , 'Error Assessment in Near-field Free-wave Measurements'; 24th European Microwave Conference, september 1994 Cannes (to be published)

[54] Collin, R.E., 'Foundations of Microwave Engineering', MacGraw-Hill, pp.224-227, 1964

[55] Press,W.H., Flannery, B.P., Teukolsky, S.A., Wetterling, W.T., 'Numerical Recipes, The Art of Scientific Computing'; Cambridge University Press, 1987

[56] Phillips, Jen, 'The NAG Library: A Beginner's Guide'; Clarendon Press, Oxford, 1986

[57] Basic Network Measurements Using the HP-8510B Network Analyzer System, Student Kit, Customer Education

[58] Kerns, D.M., Beatty, R.W., 'Basic Theory of Waveguide Junctions and Introductory Microwave Network Analysis'; Pergamon Press, 1967

[59] Mason, S.J., 'Feedback Theory-Some Properties of Signal Flow Graphs'; Proc. IRE, September 1953, pp. 920-926

[60] Product Note 8510-8 network, 'Analysis Applying the HP-8510B TRL calibration for non-coaxial measurements'

[61] Engen, G.F., Hoer, C.A., 'Thru-Reflect-Line: An improved Technique for calibrating the dual six-port automatic network analyzer'; IEEE Trans. Microwave Theory and Techniques, Dec. 1979

[62] Product Note 8510-12 Millimeter-Wave Measurements Using the HP-8510B Network Analyzer

[63] Booker, H.G., 'The Elements of Wave Propagation Using the Impedance Concept'; IEE Journal, 1947, Vol. 94, Part III, pp. 171-202

[64] Arthur, L., Read, A., Wong, M., and Reesor, G.E., 'Displacement of an electromagnetic beam upon reflection from a dielectric slab'; J. Opt. Soc. Am., Vol. 68. No. 3, March 1978 pp. 319-322

[65] Arthur, L., Read, A., and Reesor, G.E., 'Displacement of an electromagnetic beam upon transmission through a dielectric slab'; Can. J. Phys. Vol. 57 1979, pp. 1409-1413

[66] Arthur, L., Read, A., Dagg, I. R., and Reesor, G.E., 'Microwave Phase Measurements Associated with the Goss-Hanchen Shift '; CAN. J. PHYS. , Vol. 50, 1972 pp. 52-56

[67] Wong, M., and Reesor, G.E., Arthur, L., and Read, A., 'Displacement of an electromagnetic beam upon external dielectric reflection'; CAN. J. PHYS., Vol. 55., 1977 pp. 1061-1065

[68] Kozaki, S.and Sakurai, H., 'Characteristics of a Gaussian beam at dielectric interface'; J. Opt. Soc. Am., Vol. 68, No. 4, April 1978 pp. 508-514

[69] McGurik, M.and Carniglia, C. K., 'An angular spectrum representation approach to Goss-Hanchen shift'; J. Opt. Soc. Am., Vol. 67, No. 1, January 1977 pp. 107-107

[70] Ooya, T., Tateiba, M. and Fukumitsu, O., 'Transmission and reflection of a gaussian beam at normal incidence on a dielectric slab'; Journal of the Optical Society of America, Vol. 65, No. 5 pp537-541

[71] Akylas, V., 'Measurement of the longitudinal shift of the radiation at total internal reflection by microwave techniques'; American Journal of Physics Vol. 44, No. 1, January 1976 pp-77-80

[72] Clarke and Brown, 'Diffraction Theory and Atennas'; 1980, Ellis Horwood Limited (John Wiley & Sons)

Appendix 1

Transmission line model

The aim of this appendix is to devise a transmission line model for the free-wave measurement system. A transmission line can be represented by its characteristic impedance, propagation velocity, shunt and series resistive elements. The complex amplitude of the electric field corresponding to a plane wave propagating through a homogeneous medium is given by (1). E_o is the magnitude of the electric field at some reference position ($z=0$), and γ is the complex propagation constant.

$$E = E_0 e^{-\gamma z} \qquad \ldots(1)$$

It is convenient to express the propagation constant in terms of the real and imaginary parts. Therefore the attenuation constant (α) expresses the rate of decay in the magnitude, and the rate of change in the phase is defined by β.

$$\gamma = \alpha + j\beta \qquad \ldots(2)$$

The propagation constant in a medium with given permittivity and permeability can be found from (3), where λ_o is the wavelength in free space.

$$\gamma = \frac{2\pi j}{\lambda_o}\sqrt{(\varepsilon_r' - j\varepsilon_r'')(\mu_r' - j\mu_r'')} \qquad \ldots(3)$$

If the propagation constant (γ) is expanded, the attenuation constant and phase velocity can be found from equations (4) and (5).

$$\alpha = \frac{2\pi}{\lambda_o}\sqrt{\frac{\varepsilon_r'\mu_r'}{2}}\cdot\sqrt{\sqrt{1+\left(\frac{\mu_r''}{\mu_r'}\right)^2}\cdot\sqrt{1+\left(\frac{\varepsilon_r''}{\varepsilon_r'}\right)^2}+\left(\frac{\varepsilon_r''\mu_r''}{\varepsilon_r'\mu_r'}-1\right)} \qquad \ldots(4)$$

$$\beta = \frac{2\pi}{\lambda_o}\sqrt{\frac{\varepsilon_r'\mu_r'}{2}}\cdot\sqrt{\sqrt{1+\left(\frac{\mu_r''}{\mu_r'}\right)^2}\cdot\sqrt{1+\left(\frac{\varepsilon_r''}{\varepsilon_r'}\right)^2}-\left(\frac{\varepsilon_r''\mu_r''}{\varepsilon_r'\mu_r'}-1\right)} \qquad ...(5)$$

If the magnetic and dielectric losses are small, equation (6) can be simplified by using the binomial theorem.

$$\gamma=\frac{2\pi j}{\lambda_o}\sqrt{\varepsilon_r'\mu_r'}\cdot\sqrt{(1-j\frac{\varepsilon_r''}{\varepsilon_r'})(1-j\frac{\mu_r''}{\mu_r'})} \qquad ...(6)$$

$$\gamma\approx\frac{2\pi j}{\lambda_o}\sqrt{\varepsilon_r'\mu_r'}\cdot\left(1-j\frac{\varepsilon_r''}{2\varepsilon_r'}\right)\cdot\left(1-j\frac{\mu_r''}{2\mu_r'}\right) \qquad ...(7)$$

$$\gamma\approx\frac{2\pi j}{\lambda_o}\sqrt{\varepsilon_r'\mu_r'}\cdot\left(1-j\frac{\varepsilon_r''}{2\varepsilon_r'}-j\frac{\mu_r''}{2\mu_r'}+\frac{\varepsilon_r''\mu_r''}{4\varepsilon_r'\mu_r'}\right) \qquad ...(8)$$

The last term in equation (8) is relatively small and can be ignored. The attenuation constant and phase velocity for a slab can found from (9) and (10).

$$\alpha\approx\frac{2\pi}{\lambda_o}\sqrt{\varepsilon_r'\mu_r'}\cdot\left(\frac{\varepsilon_r''}{2\varepsilon_r'}+\frac{\mu''}{2\mu'}\right) \qquad ...(9)$$

$$\beta\approx\frac{2\pi}{\lambda_o}\sqrt{\varepsilon_r'\mu_r'} \qquad ...(10)$$

$$(Attenuation)_{dB/unit\ length} = -20\log_{10} e^{\frac{2\pi}{\lambda_o}\left(\frac{\varepsilon_r''Z_s}{2}+\frac{\mu_r''}{2Z_s}\right)} \qquad ...(11)$$

$$(Attenuation)_{dB/unit\ lenght} = -\frac{27.2878}{\lambda_o}\left(\varepsilon_r''Z_s+\frac{\mu_r''}{Z_s}\right) \qquad ...(12)$$

Z_s is the wave impedance in the sample and defines the ratio of the electric field to the magnetic field associated with a wave travelling in the material, (13).

$$Z_s=\sqrt{\frac{\mu_r'}{\varepsilon_r'}} \qquad ...(13)$$

The total attenuation constant of a plane wave travelling in a slab can be calculated from equation (14). As can be seen, the total attenuation is frequency dependent and changes linearly in a logarithmic scale, with frequency. The total loss can be divided into magnetic and dielectric parts. These losses are represented by the first and the second terms of equation (14) respectively.

$$(Attenuation)_{dB/unit\ length} = -\frac{27.2878}{\lambda_o}\varepsilon_r'' Z_s - \frac{27.2878}{\lambda_o}\frac{\mu_r''}{Z_s} \qquad ...(14)$$

In a transmission line, the propagation constant is defined by equation (15). The equivalent circuit of a transmission line is shown in figure A1.1. The series resistance and shunt conductance are denoted by R and G respectively. The inductance and the capacitance per unit length are denoted by L and C. For small losses, the attenuation constant in a transmission line can be approximated by the same method used in the previous part.

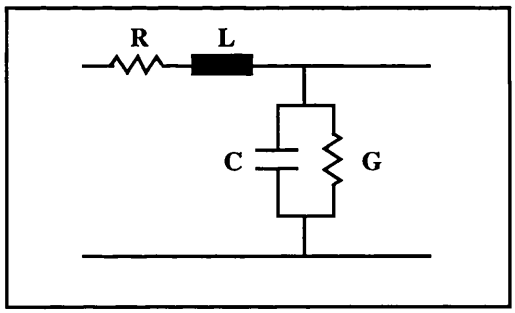

Figure A1.1 Transmission line equivalent circuit.

$$\gamma = \sqrt{(R + j\,\omega L)(G + j\,\omega C)} \qquad ...(15)$$

$$\gamma = j\,\omega\sqrt{LC}\sqrt{\left(1 - j\frac{R}{\omega L}\right)\left(1 - j\frac{G}{\omega C}\right)} \qquad ...(16)$$

For small losses, equation (16) can be approximated.

$$\alpha = \frac{\sqrt{LC}}{2}\left(\frac{R}{L} + \frac{G}{C}\right) \qquad ...(17)$$

$$\beta = \omega\sqrt{LC} \qquad ...(18)$$

$$(Attenuation)_{dB/unit\ length} = -4.343\left(GZ_c + \frac{R}{Z_c}\right) \quad ...(19)$$

Z_c is the characteristic impedance and is given by equation (20).

$$Z_c = \sqrt{\frac{L}{C}} \quad ...(20)$$

In the simple theory of the transmission line used in the *HP* model, the total loss in a length of transmission line is not a function of frequency. If the whole dielectric loss is represented by an equivalent conductivity, this equivalent conductivity should be a function of frequency. Since there is not such a possibility in the simulation program provided by HP, free-wave measurement systems can be approximated by transmission lines in this program.

The first term in (19) represents the effect of the shunt resistance, and the second term shows the contribution of the series resistance to the total loss. In the transmission line model, the magnetic and electrical losses are represented by series and shunt impedances. Therefore, the values of these impedances can be calculated from the specimen magnetic and electrical properties. It is worth noting that this model simulates a lossless transmission line accurately, but there is a frequency dependant difference between transmission and reflection coefficient associated with this model and a real slab. The equivalent transmission line of a slab is calculated at the centre frequency to minimize these differences. For a given wavelength, characteristic impedance, velocity factor, shunt and series resistance can be calculated from the electric and magnetic properties of the sample at a given frequency, equations (21) to (24).

$$Z_c = \sqrt{\frac{\mu_r'}{\varepsilon_r'}} \quad ...(21)$$

$$Velocity\ Factor = \frac{1}{\sqrt{\mu_r'\,\varepsilon_r'}} \quad ...(22)$$

$$R = -\frac{2\pi Z_c\,\mu_r''}{\lambda_o\,Z_s} \quad ...(23)$$

$$G = -\frac{2\pi Z_s\,\varepsilon_r''}{\lambda_o\,Z_c} \quad ...(24)$$

Appendix 2

Transmission gating error

The aim of this appendix is to calculate the gating error in measuring the transmission coefficient of a *thin* sample for an ideal gate. In this analysis, the magnetic and dielectric properties of the sample are assumed to be constant over the measured frequencies band.

In the time gating process, only a limited number of terms associated with the multiple reflections are included in the measurement, and the rest are discarded. The transmitted wave through a slab is represented by equation (1). Using the boundary conditions (equations 2 and 3), the total transmitted wave can be expressed as a geometric series, (equation 4). If only the first N components of the multiple reflection are included in the gating process, the discarded components can also be expressed by a geometric series, (equation 5). Equation (6) give the fractional error in transmission coefficient measurement. P is the propagation coefficient, and Γ is the reflection coefficient from the front surface of the slab.

$$T_{total} = T_{21}T_{32}P + T_{21}T_{32}\Gamma_2\Gamma_3P^3 + T_{21}T_{32}\Gamma_2^2\Gamma_3^2P^5 \qquad ...(1)$$

$$\Gamma_2 = -\Gamma \qquad \Gamma_3 = -\Gamma \qquad ...(2)$$

$$T_{21} = (1+\Gamma) \qquad T_{32} = (1-\Gamma) \qquad ...(3)$$

$$T_{total} = P(1-\Gamma^2)\sum_{n=0}^{\infty}(P\Gamma)^{2n} \qquad ...(4)$$

$$T_{discarded} = P(1-\Gamma^2)\sum_{n=N}^{\infty}(P\Gamma)^{2n} \qquad ...(5)$$

$$\frac{\delta T}{T} = (P\Gamma)^{2N} \quad \ldots(6)$$

The maximum expected error in the magnitude and phase of the transmitted wave can be calculated from (7) and (8). Figure A2.1 shows the vector representation of the error in the measured transmission coefficient. As can be seen, the error in the phase and magnitude of the transmission coefficient are in quadrature. The error in the phase is maximum when the error in the magnitude is minimum. The number of the terms of the multiple reflections which are included in the gating process (N) is proportional to the gate width and given by equation (4).

$$\textit{Maximum Magnitude Error} = \pm|P\Gamma|^{2N} \quad \ldots(7)$$

$$\textit{Maximum Phase Error} = \pm \tan^{-1}\left(|P\Gamma|^{2N}\right) \quad \ldots(8)$$

$$N = \frac{\textit{Gate width}}{2\,(\textit{Slab Electrical Length})} \quad \ldots(9)$$

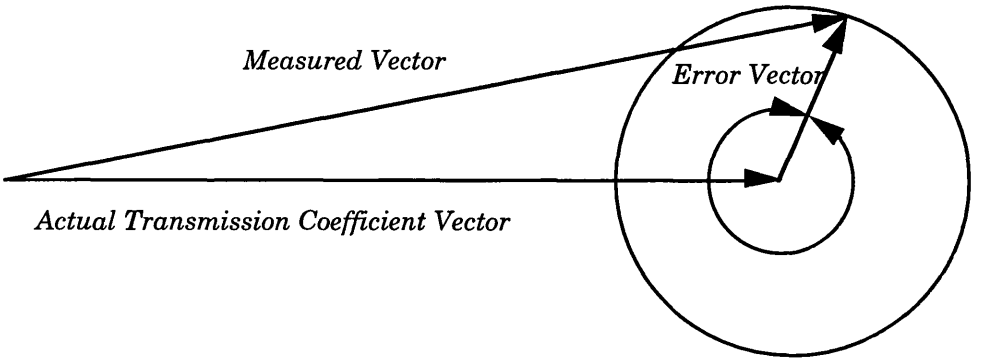

Phase Error = 0

Measured Vector = $1 + |P\,\Gamma|^{2N}$

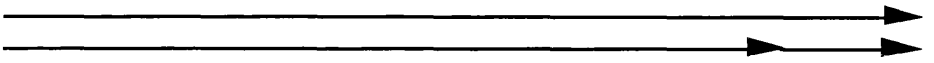

Actual Transmission Coefficient Vector = 1 Error Vector = $|P\,\Gamma|^{2N}$

Phase Error = 0

Measured Vector = $1 - |P\,\Gamma|^{2N}$ Error Vector = $|P\,\Gamma|^{2N}$

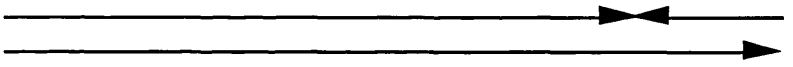

Actual Transmission Coefficient Vector = 1

Magnitude Error ≈

Maximum Phase Error = $\tan^{-1}(|P\,\Gamma|^{2N})$

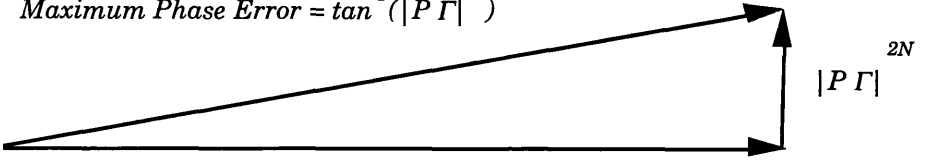

$|P\,\Gamma|^{2N}$

Actual Transmission Coefficient Vector = 1

Figure A2.1 Vector representation of the gating error in transmission coefficient measurement.

Appendix 3

Reflection gating error

In *thin* sample measurements, the multiple reflections within the sample are taken into account. Since the unwanted reflections should be gated out, a number of the higher order terms of the multiple reflections are discarded in the gating process. Discarding these terms causes error in the measured reflection coefficient. The aim of this appendix is to calculate the time gating error in reflection coefficient measurement for an ideal gate. In this appendix, the gating error for a real gate is simulated and compared with the calculated values for an ideal gate. In this analysis, the sample properties are assumed to be constant over the measured frequency band.

The total reflected wave from a slab is represented by equation (1). Substituting the boundary conditions (equations 3 and 4), the total reflected wave is expressed by a geometric series (4). In the gating process, the discarded terms of the multiple reflections also constitute a geometric series, (5). If only the first N terms of the multiple reflections are included in the gating process, the fractional error in the reflection coefficient is given by (6).

$$\Gamma_{total} = \Gamma + \Gamma_3 T_{21} T_{12} P^2 + \Gamma_3^2 \Gamma_2 T_{21} T_{12} P^4 + \ldots \qquad \ldots(1)$$

$$\Gamma_2 = -\Gamma \qquad \Gamma_3 = -\Gamma \qquad \ldots(2)$$

$$T_{21} = (1+\Gamma) \qquad T_{12} = (1-\Gamma) \qquad \ldots(3)$$

$$\Gamma_{total} = \Gamma - \Gamma P^2 (1 - \Gamma^2) \sum_{n=0}^{\infty} (P\Gamma)^{2n} \qquad \ldots(4)$$

$$\Gamma_{discarded} = -\Gamma P^2 (1 - \Gamma^2) \sum_{n=N-1}^{\infty} (P\Gamma)^{2n} \quad \ldots(5)$$

$$\frac{\delta\Gamma}{\Gamma} = \frac{-P^2 (1 - \Gamma^2)}{1 - P^2} (P\Gamma)^{2(N-1)} \quad \ldots(6)$$

In reflection coefficient measurement the magnitude of the first and second terms are comparable, and the multiple reflections start to decay from the third term. Therefore, a relatively wider gate is expected to be employed for a given error in the gating process. The gating error in reflection coefficient measurement (equation 5) is a function of $(PT)^{2(N-1)}$ while the error in transmission coefficient measurement decreases by a factor of $(PT)^{2(N)}$. The propagation coefficient (P) is a function of the material properties and the sample thickness. In lossless materials the wave is not attenuated by travelling within the sample ($|P|=1$), and reflection coefficient defines the decay rate of the multiple reflections. Therefore, the gating error is expected to be more with respect to the error in the lossy material with similar properties. In low-loss materials ($|P|\approx 1$), the same argument is applicable. In order to simplify the analysis, we consider a lossless sample which gives the extreme case.

In the vector representation, the propagation coefficient (P) is shown by a vector. This vector rotates 360° as the sample electrical length changes by λ_0. The denominator of equation (6) is minimum at frequencies such that the sample electrical length is a multiple of 180°. For a lossless sample the denominator becomes zero, and the error approaches infinity. In practice, the gating error increases rapidly at frequencies such that the sample thickness is a multiple of $\lambda/2$, and measurement at these frequencies should be avoided. It is worth noting that rapid increases of the error in the measured reflection coefficient discussed in this chapter is due to time gating which is quite distinct from the intrinsic error of free-wave techniques at these frequencies. As shown in figure A3.1, the magnitude and the phase of the propagation coefficient (P) vary with frequency, therefore the error analysis is difficult in the general case. For small error and thicknesses close to odd multiples of $\lambda/4$, the changes of error in the magnitude and the phase of the reflection coefficient can be assumed to be in quadrature.

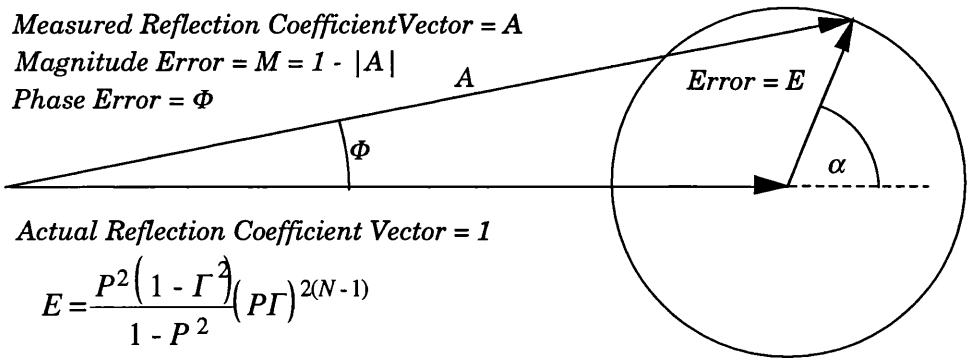

Figure A3.1 Vector representation of time gating error in reflection coefficient measurement of a slab.

If only the first term of the multiple reflections is included in the gating process (*N=1*), the changes in the magnitude and phase of the measured reflection coefficient can be estimated, (figure A.3.2). At frequencies such that the sample thickness is an odd multiple of $\lambda/4$ the error in the magnitude of the reflection coefficient is minimum, and the error vector is 180° out of phase with respect to the actual reflection coefficient, (figure A3.2a). By increasing the frequency the error in the magnitude approaches zero, then increases in the positive direction until it reaches its maximum, (figures A5.3.2b to A5.3.2e). The maximum magnitude error corresponds to a frequency such that the sample thickness is a multiple of $\lambda/2$. At frequencies such that the sample thickness is an odd multiple of $\lambda/4$, the phase error is zero and the magnitude error is maximum, (figure A3.2.a). By increasing the frequency, the magnitude error decreases while the phase error increases until the the magnitude error becomes zero, (figure A3.2.b). At higher frequencies, the error in the magnitude and phase increase.

Figures A3.3 and A3.4 show the error in the magnitude and phase against frequency, (*N=1*, *2* and *3*). In this simulation, the sample thickness is such that its electrical length increases by $\lambda/2$ by changing the frequency from 10 to 15 GHz. As can be seen, the number of minima in the magnitude error or the phase error is equal to *N*. By increasing the number of the multiple reflection terms which are included in the gating process, the rate of rotation in the error vector increases, and the error in the useable frequency band

decreases. $\delta\Gamma_{max}$ and Φ_{max} are defined as the maximum error in the magnitude and the phase of the measured reflection coefficient. The useable frequency band is defined by these parameters. As the gating error is a function of the propagation constant (P) and the reflection coefficient from the front surface (Γ), total error is calculated as a function of these parameters. For a lossless material, P is defined as a vector with magnitude of unity and angle of α. In this case, the angle of reflected wave from the front surface is independent of frequency, $\angle\Gamma = 0°$. The fractional gating error can be calculated from equation (8), where K is a constant given by (9).

$$P = 1 \angle \alpha \qquad \ldots(7)$$

$$\delta\Gamma = \frac{-P^{2N}}{1 - P^2} K \qquad \ldots(8)$$

$$K = (1 - \Gamma^2) \Gamma^{2(N-1)} \qquad \ldots(9)$$

In order to calculate the magnitude and phase of the error vector as a function of transmission constant, the denominator of equation (8) can be expanded, (10). Referring to figure A3.5 and for a lossless material, the numerator and denominator of equation (7) can be expressed as functions of α, (equations 11 to 13).

$$\delta\Gamma = \frac{-P^{2N}}{(1 - P)(1 + P)} \cdot K \qquad \ldots(10)$$

$$(1 + P) = \sqrt{2}\sqrt{(1 + \cos\alpha)} \angle \frac{\alpha}{2} \qquad \ldots(11)$$

$$(1 - P) = \sqrt{2}\sqrt{(1 - \cos\alpha)} \angle \left(\frac{\alpha}{2} - 90 \right) \qquad \ldots(12)$$

$$P^{2N} = 1 \angle 2N\alpha \qquad \ldots(13)$$

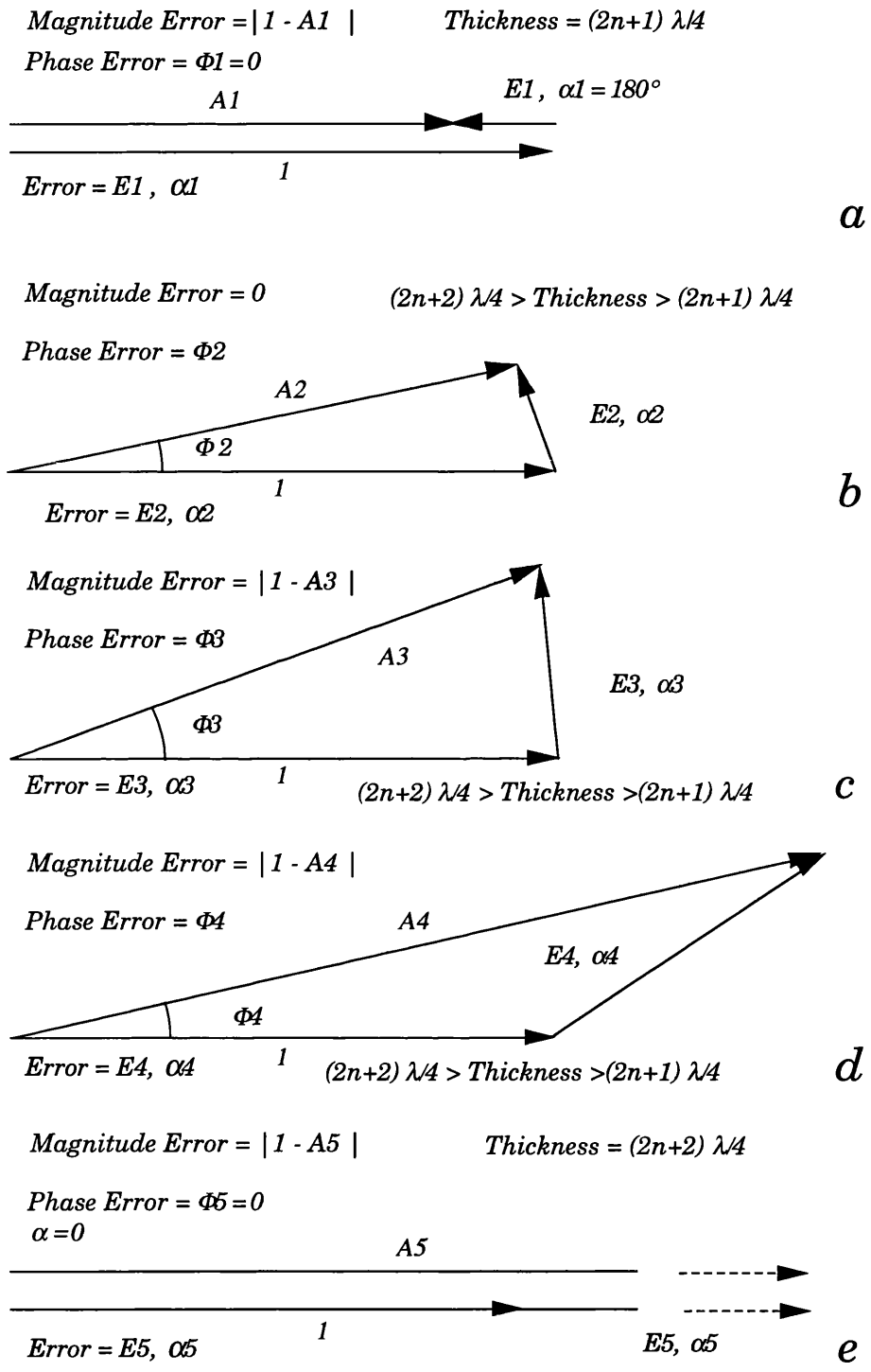

Figure A3.2 Vector diagram of the gating error in reflection coefficient measurement for the different thicknesses.

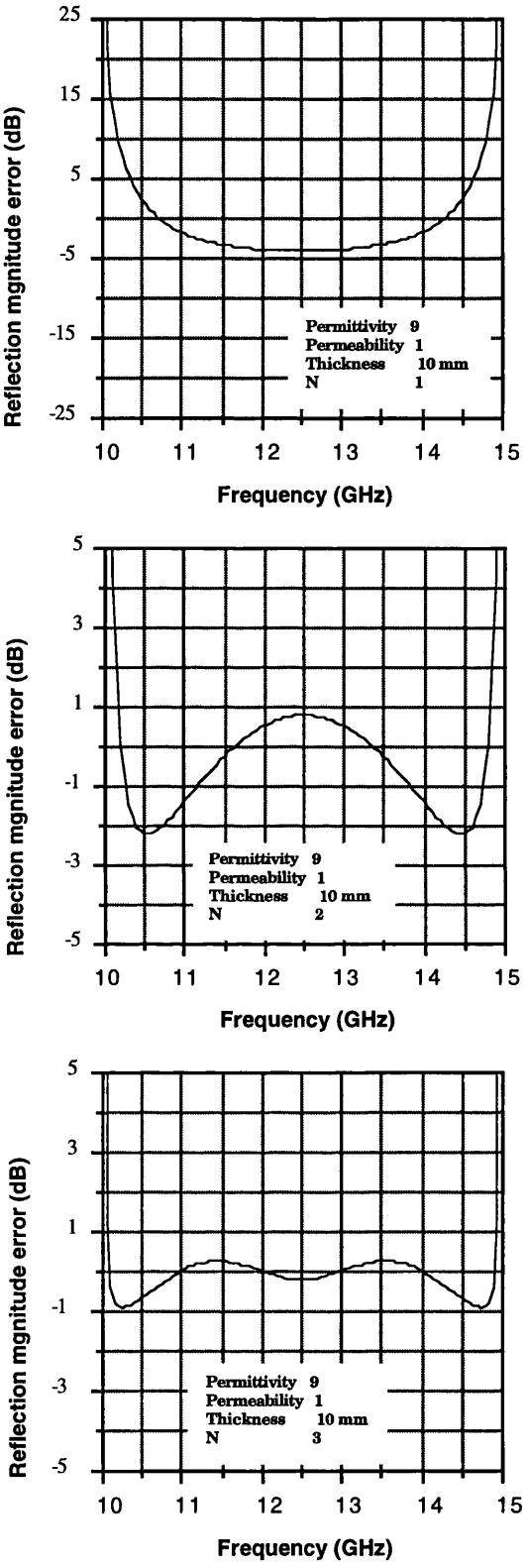

Figure A3.3 Changes of error in the magnitude of reflection coefficient with frequency for different values of N.

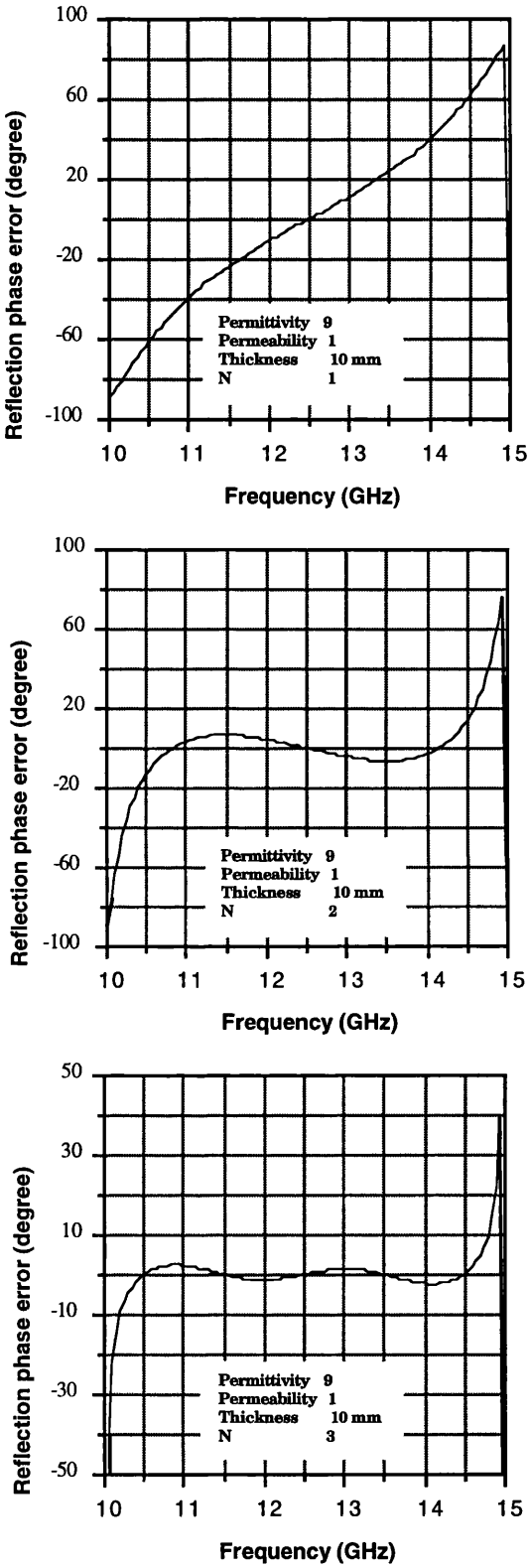

Figure A3.4 Changes of error in the phase of reflection coefficient with frequency for different values of N.

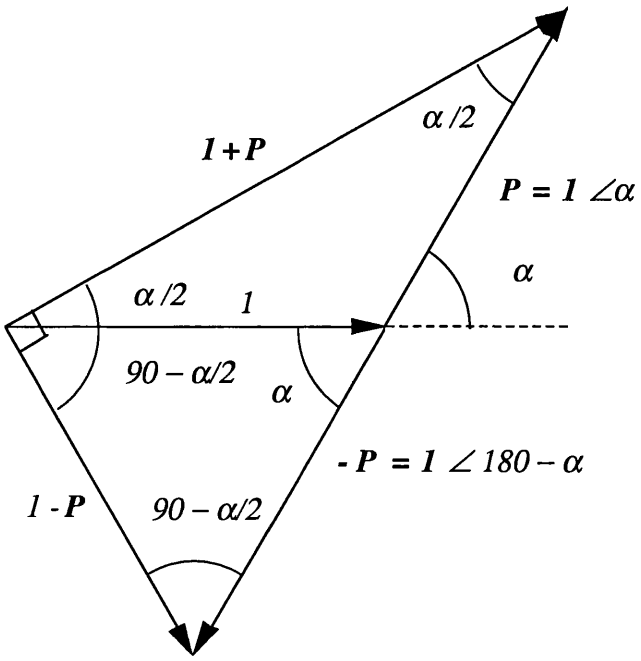

Figure A3.5 Vector diagram of the denominator in reflection coefficient measurement.

Figure A3.6 shows the vector diagram for zero error in the magnitude of reflection coefficient. For this case, the magnitude of the error vector can be expressed as a function of maximum phase error, (15). The maximum phase error which is associated with zero magnitude error (Φ_{max}), can be calculated.

$$\delta\Gamma = \frac{K}{2\sin\alpha} \angle\ ((2N - 1)\alpha - 90) \qquad ...(14)$$

$$|\delta\Gamma| = 2\sin(2N - 1)\alpha \qquad ...(15)$$

Using equations (11) and (12), the angle of α corresponding to the frequencies where the amplitude error is zero can be found from (13). The maximum phase error associated with these angles can be calculated from equation (14)

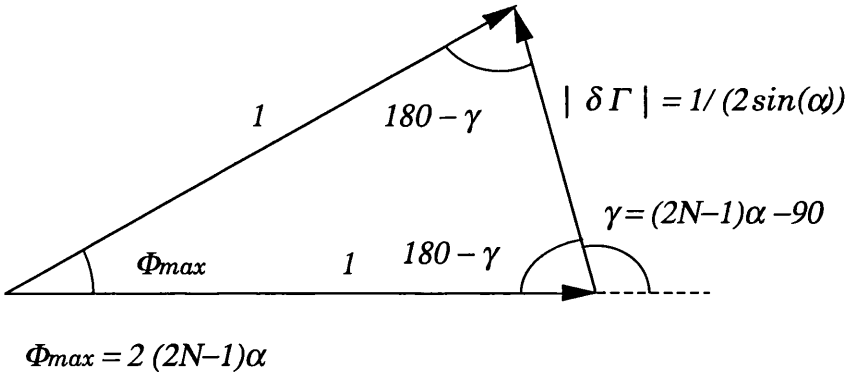

Figure A3.6 The vector diagram for zero magnitude error.

$$\frac{K}{4} = \sin(\alpha) \,.\, \sin(2N - 1)\alpha \quad . \qquad ..(16)$$

$$\Phi_{max} = 2\,(2N - 1)\alpha \qquad ...(17)$$

For $N=1$, equation (16) can be solved analytically, otherwise the maximum phase error should be found by numerical iterative methods. If $N> 1$, equation (16) has more than one solution for each correct multiple of $\lambda/4$ in the slab.

$$\Phi_{max} = 2\,(2N - 1)\,\sin^{-1}(\sqrt{K/4}) \qquad ...(18)$$

The maximum error in the magnitude of the reflection coefficient occurs at frequencies such that the error vector has 180° phase shift with the actual reflection coefficient. At these frequencies, the phase error is zero and the magnitude error (Γ_{max}) can be calculated from equation (19).

$$\Gamma_{max} = K/2 \qquad ...(19)$$

Appendix 4

Circuit modelling program

Circuit Modelling Program is a *Hewlett-Packard* computer program written in HP-PASCAL for simulating the scattering parameters of an electrical circuit. This program has the facility of sending the simulated values to the network analyser memories. Therefore, the calculated transmission and reflection coefficients can be treated in the same way as measured S-parameters, and the effect of gating can be simulated. As mentioned, a free-wave measurement system can be modelled by a number of transmission lines and the transmission line equivalent of a slab can be calculated, (appendix 1).

In *CMP*, a transmission line is defined by its characteristic impedance, length, phase velocity, series resistance, shunt resistance and the corner frequency. In order to simulate the changes in total loss of a slab by its equivalent transmission line model, the values of series and shunt resistances should be varied with frequency. Since *CMP* does not have such a capability, the equivalent transmission line of a slab is calculated at a single frequency. The calculated phase by *CMP* is as accurate as 0.1°, and this error is due to the small loss assumption that is made in the model used in the simulation. Since *CMP* is used for evaluating the gating error, the delivered degree of accuracy by *CMP* in modelling the slab specimens is quite acceptable.

In *CMP*, the input and output ports are assumed terminated by a matched load, therefore the equivalent transmission line of the sample should be calculated in a 50 Ω system. In order to simplify the modelling, normal incidence is considered and the material properties are assumed to be unchanged over the measured frequency band. In simulating the error in the measurement of *thin* samples, the ungated response calculated by *CMP* is saved in the network analysers memories and used as a reference for comparison with the gated response. The validity of calculating error in *thick* samples is also verified by comparing the simulated response with the calculated values. The simulation of lossless materials

shows good agreement with the calculated values, but there are small deviations from theory in simulating the lossy samples. These discrepancies are due to imperfect characteristics of the gate.

Figures A4.1 and A4.2 show the difference between the calculated and simulated transmission and reflection coefficients associated with a lossless dielectric sample. The accuracy in simulating a lossy ferrite slab (ε_r=*7.5-j0.5*, μ_r=*0.8-j0.15*) are shown in figures A4.3 and A4.4. It can also be concluded that the simulation of transmission and reflection coefficients of a slab by *CMP* is accurate enough for studying the gating error. The discrepancies between the calculated and simulated values can be justified by considering the approximation made in modelling the slab. It should be mentioned that the simulated error in figure A3.4 shows $|1-\delta\Gamma/\Gamma|$ in dB.

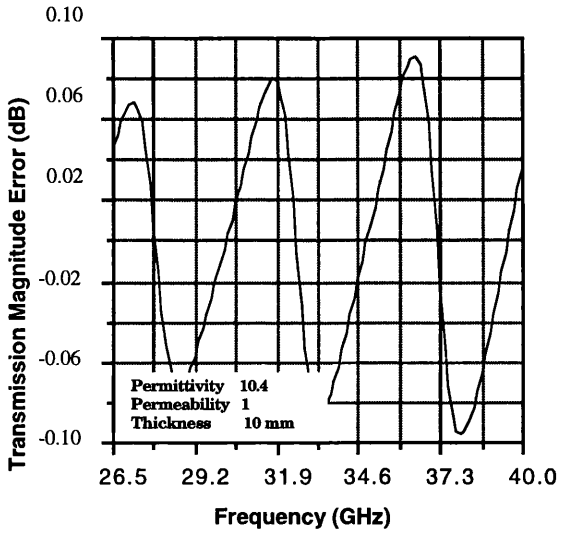

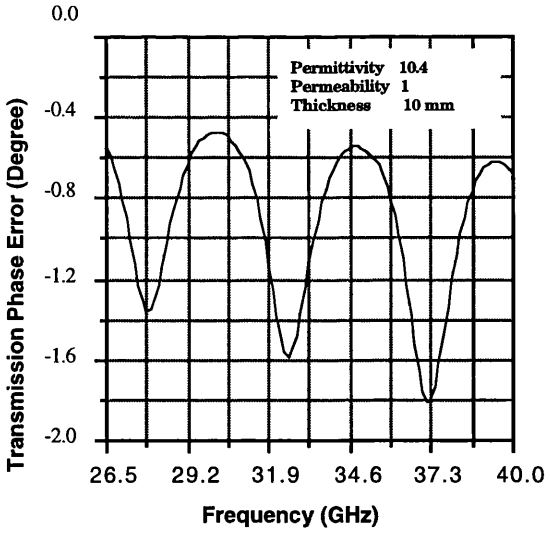

Figure A4.1 Difference between calculated and simulated transmission coefficient of a lossless dielectric (ε_r=10.4).

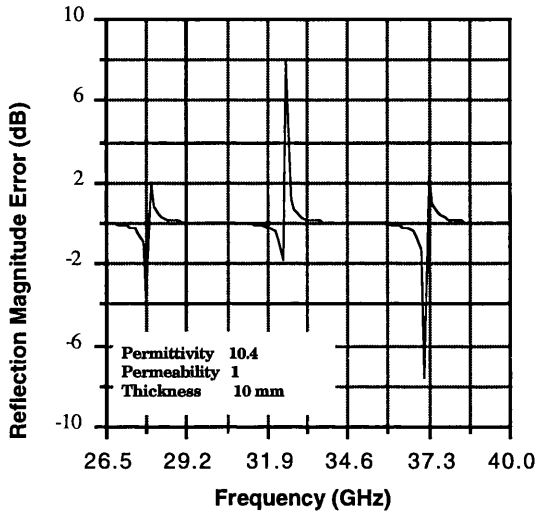

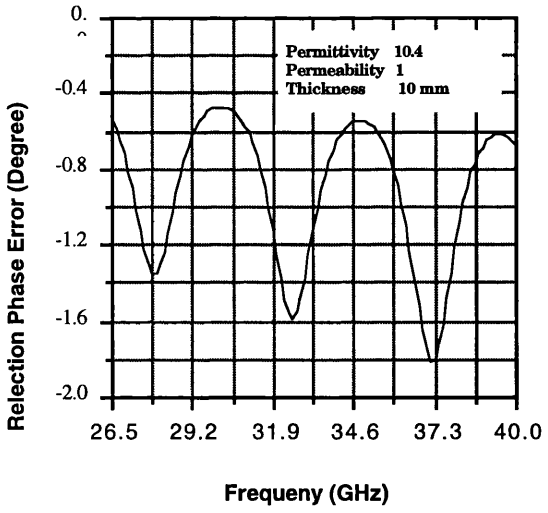

Figure A4.2 Difference between calculated and simulated reflection coefficient of a lossless dielectric (ε_r=10.4).

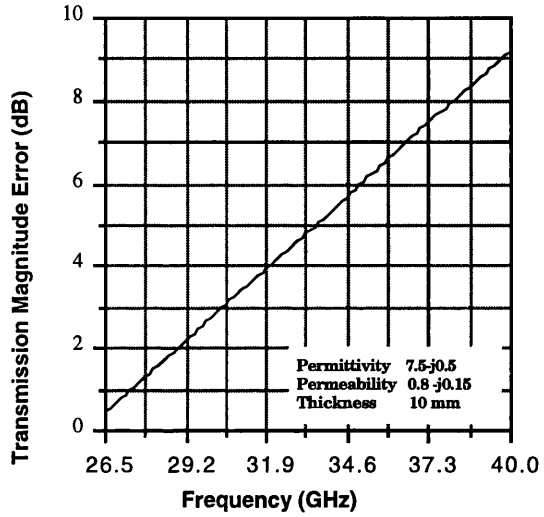

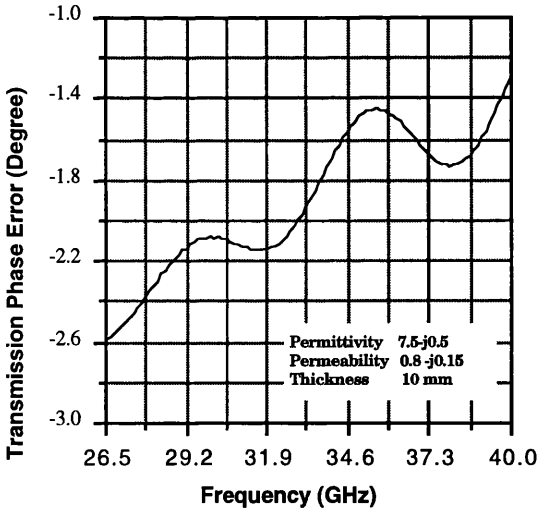

Figure A4.3 Difference between calculated and simulated transmission coefficient of a lossy ferrite (ε_r=7.5-j0.5, μ_r=0.8-j0.15).

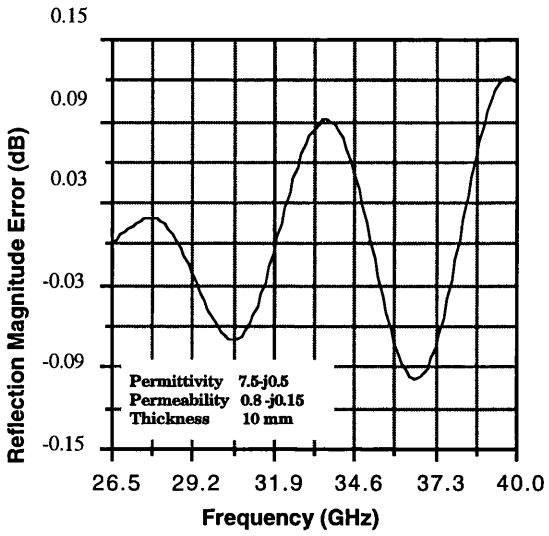

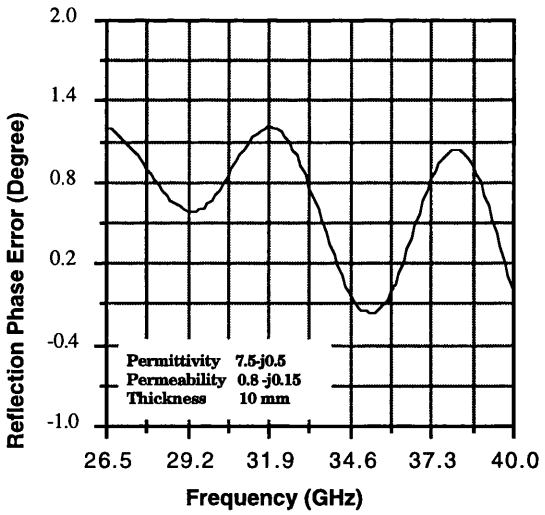

Figure A4.4 Difference between calculated and simulated reflection coefficient of a lossy ferrite(ε_r=7.5-j0.5, μ_r=0.8-j0.15).

Appendix 5

Gating error in thin samples

In appendices 2 and 3, the gating error for an ideal gate has been calculated. In that analysis, the effect of imperfect specifications of the gate such as pass band ripple and finite sidelobe level were ignored. In practice, the measurement over a limited frequency band introduces some restrictions in the measured parameters. The aim of this appendix is to investigate the validity of the formulae derived in appendix 4 in a practical case. The simulation method is explained in appendix 4, and the results of the simulation are presented and discussed.

In measuring *thin* samples, the main sources of error are the higher order terms of the multiple reflections discarded in the gating process. In this appendix, the error in transmission and reflection coefficients for different gate widths are simulated, and the results are compared with the calculated values. In order to show the effect of electrical length and the loss properties of the sample in the gating error, three samples are considered. Samples 1 and 2 are lossless dielectric slabs representing two classes of dielectric materials, and sample 3 is a lossy ferrite with a properties similar to the material can be made by mixing ferrite powder and a bonding resin.

A5.1 Sample 1

Sample 1 is a lossless dielectric ($\varepsilon_r=2.6$), with thickness of 10 mm. Regarding this dielectric constant, the electrical length of this slab is equal to 16.12 mm. Figures A5.1 to A5.4 show the simulated gating error in transmission and reflection coefficients for different gate widths. The calculated error for an ideal gate is shown by dashed lines. It is worth noting that the deviations between the simulated and calculated values show the effect of the imperfect gate specifications. The deviations decrease by increasing the

frequency span. The program listing used for simulating this sample in *CMP* is as follows:

$Z_c = 50\sqrt{1/2.6} = 31\ \Omega$

$V_c = \sqrt{1/2.6} = 0.62$

$R = 0\ \Omega$

$G = 0\ \Omega^{-1}$

```
10      PORT  1
20      TL    1 2 31.0 1 CM 0.62 0 0 0
30      PORT  2
40      FREQ  26.5 GHZ 40 GHZ 401 POINTS
50      OUTPUT S11/S21
```

The gating error corresponding to transmission and reflection coefficients of sample 1 can be calculated for the different gate widths. The widths of the time gate are a function of the number of the terms of the multiple reflections which are included in the gating process (N). For gating the first N terms of the multiple reflections, the gate width should be set to $(2N+3)$ times the sample electrical length. The gate centre should be set at zero for reflection measurement, while the gate centre is at a distance equal to the sample electrical length in transmission measurement.

$N=1$

$|P^2\Gamma^2|=0.0549$

$|1-\Gamma^2|=0.9450$

$M_{Tmax} = +0.46dB, -0.49\ dB$

$\Phi_{Tmax} = \pm 3.15°$

$M_{Rmax} = -5.55\ dB$

$\Phi_{Rmax} = \pm 58.16°$

$N=2$

$\Gamma=-0.2344$

$|P^4\Gamma^4|=0.00302$

$|(1-\Gamma^2)(P^2\Gamma^2)| =0.051939$

$\Phi_{Tmax} = \pm 0.026\ dB$

$\Phi_{Tmax} = \pm 0.173°$

$\Phi_{Rmax} = +0.22\ dB$

$\Phi_{Rmax} = \pm 1.74°$

$N=3$

$|P^6\Gamma^6|=0.000166$

$|(1-\Gamma^2)(P^4\Gamma^4)|=0.00285$

$M_{Tmax} = +0.46dB,\ -0.49\ dB$

$\Phi_{Tmax} = \pm 0.0095°$

$M_{Rmax} = -0.00124\ dB$

$\Phi_{Rmax} = 0.085°$

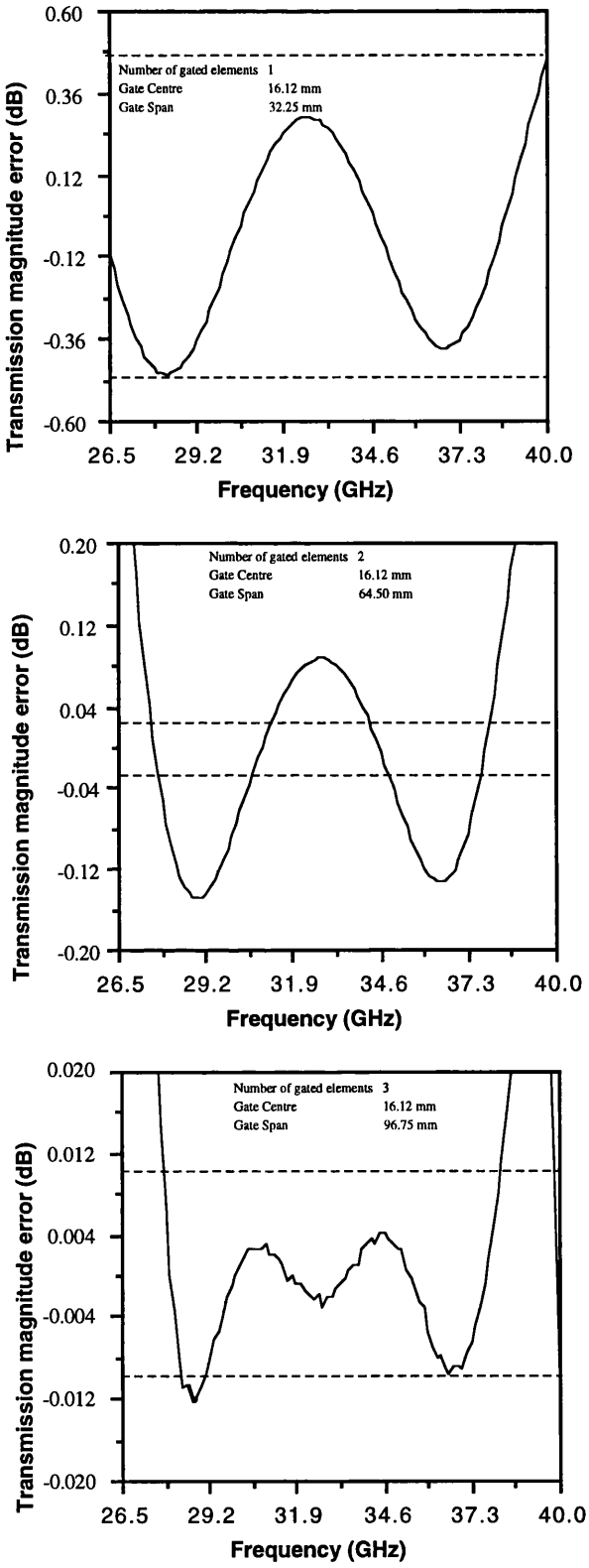

Figure A5.1 The simulated gating error in transmission coefficient magnitude of sample 1 (ε_r=2.6, μ_r=1).

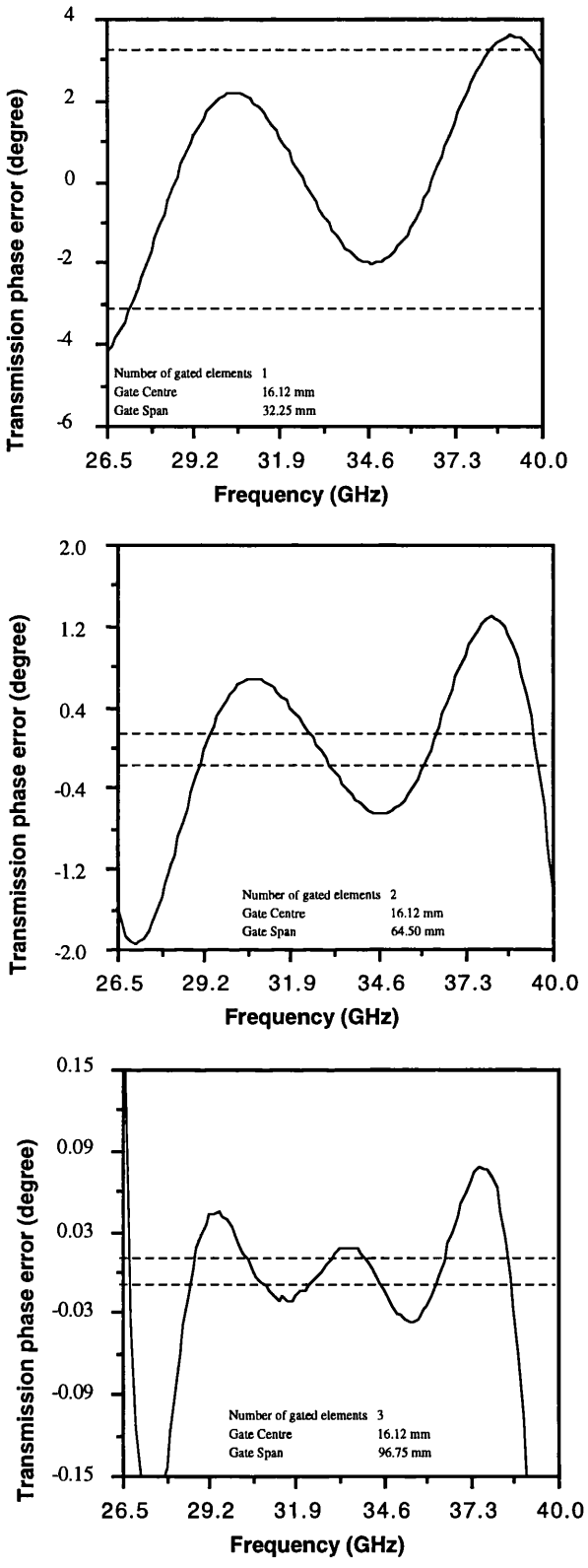

Figure A5.2 The simulated gating error in transmission coefficient phase of sample 1 (ε_r=2.6, μ_r =1).

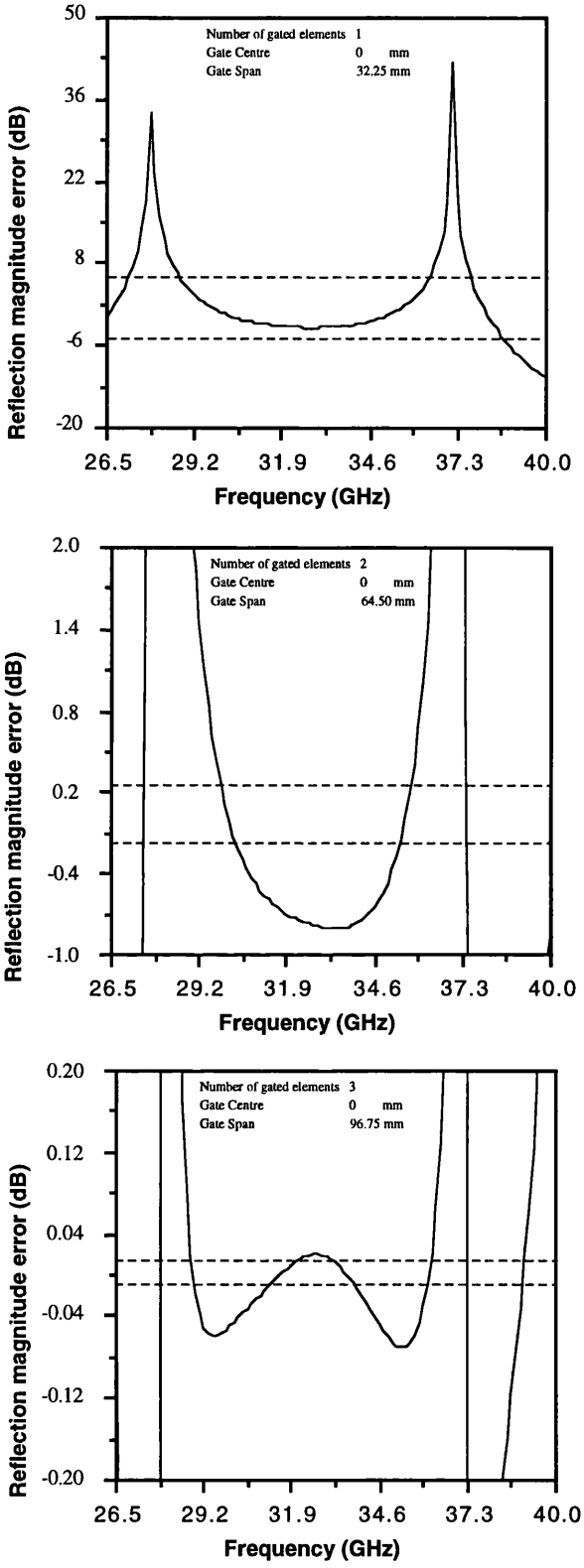

Figure A5.3 The simulated gating error in reflection coefficient magnitude of sample 1 (ε_r=2.6, μ_r =1).

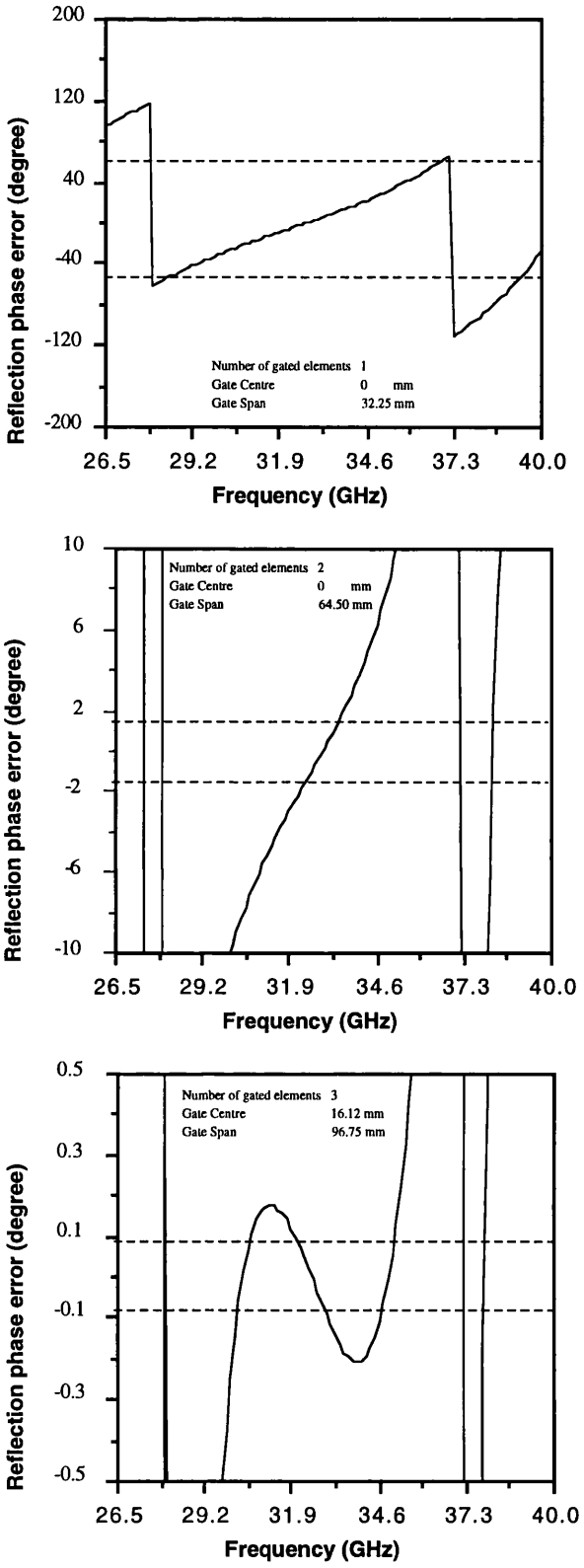

Figure A5.4 The simulated gating error in reflection coefficient phase of sample 1 (ε_r=2.6, μ_r=1).

A5.2 Sample 2

Sample 2 is also a lossless dielectric, $\varepsilon_r=10.4$ with thickness of 10 mm. The electrical length of this slab at normal incidence is twice the electrical length of sample 1, therefore a higher gating error is expected for this sample. Figures A5.6 to A5.9 show the error in transmission and reflection coefficients for different gate widths. The dashed lines show the calculated gating error for an ideal gate. The following calculations give the required program listing and the parameters for simulating sample 2 by *CMP*.

$Z_c = 50\sqrt{1/10.4} = 15.5\ \Omega$

$V_c = \sqrt{1/10.4} = 0.31$

$R = 0\ \Omega$

$G = 0\ \Omega^{-1}$

```
10      PORT  1
20      TL    1 2 16.5 1 CM 0.31 0 0 0
30      PORT  2
40      FREQ  26.5 GHZ 40 GHZ 401 POINTS
50      OUTPUT S11/S21
```

The gating error for different gate widths can be calculated. The gate centre and gate width are set on the basis of the number of required terms of the multiple reflection in the gating process.

$N=1$

$|P^2\Gamma^2|=0.2773$

$|1-\Gamma^2|=0.7226$

$M_{Tmax} = +2.13dB, -2.82\ dB$

$\Phi_{Tmax} = \pm 15.5°$

$M_{Rmax} = -3.89\ dB$

$\Phi_{Rmax} = \pm 50.3°$

$N=2$

$|P^4\Gamma^4|=0.00302$

$|(1-\Gamma^2)(P^2\Gamma^2)| =0.0200$

$M_{Tmax} = \pm 0.69dB$

$\Phi_{Tmax} = \pm 4.4°$

$M_{Rmax} = -0.92\ dB$

$\Phi_{Rmax} = \pm 6.72\ °$

$N=3$

$|P^6\Gamma^6|=0.02133$

$|(1-\Gamma^2)(P^4\Gamma^4)|=0.0556$

$M_{Tmax} = \pm 0.183$

$\Phi_{Tmax} = \pm 1.22°$

$M_{Rmax} = -0.24\ dB$

$\Phi_{Rmax} = \pm 2.73°$

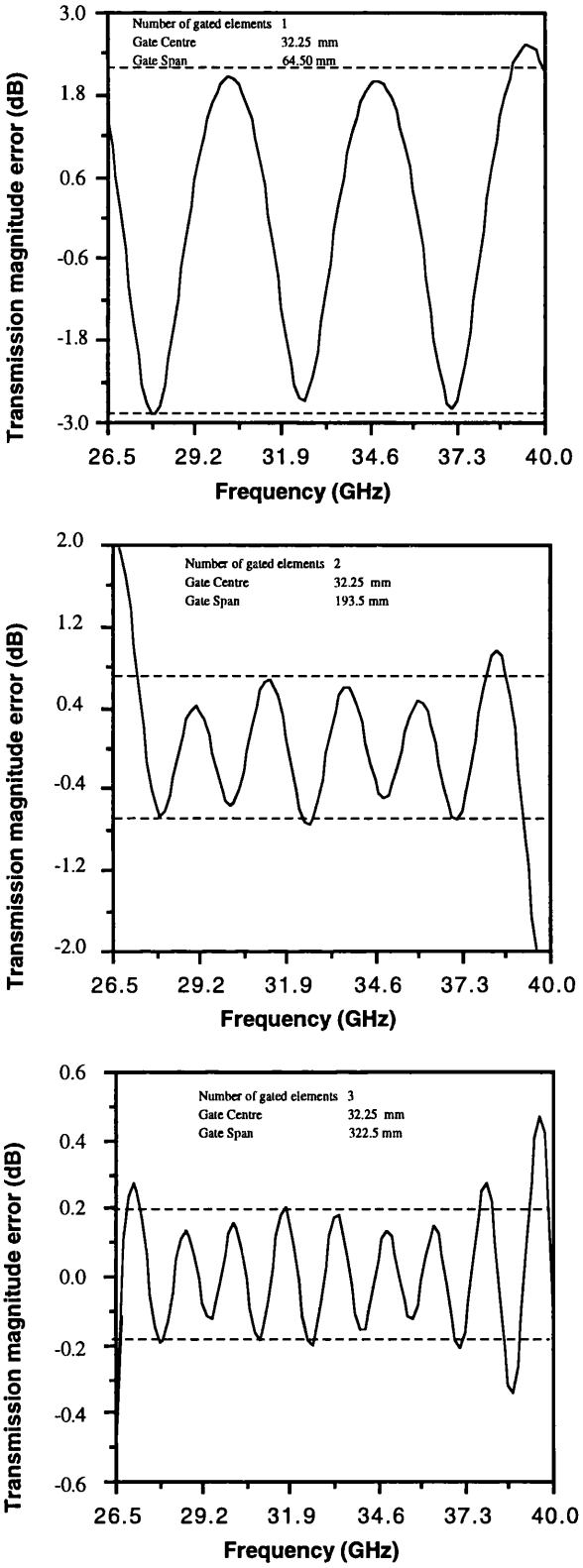

Figure A5.5 The simulated gating error in transmission coefficient magnitude of sample 2 (ε_r=10.4, μ_r=1).

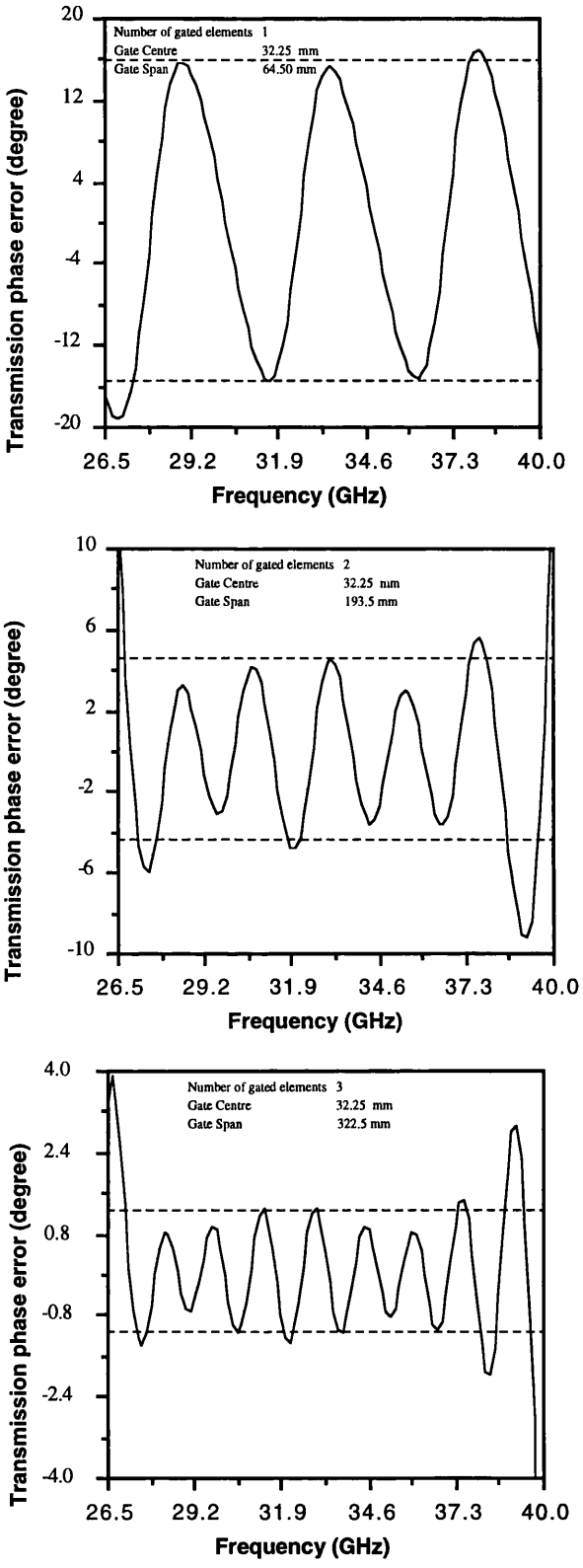

Figure A5.6 The simulated gating error in transmission coefficient phase of sample 2 (ε_r=10.4, μ_r=1).

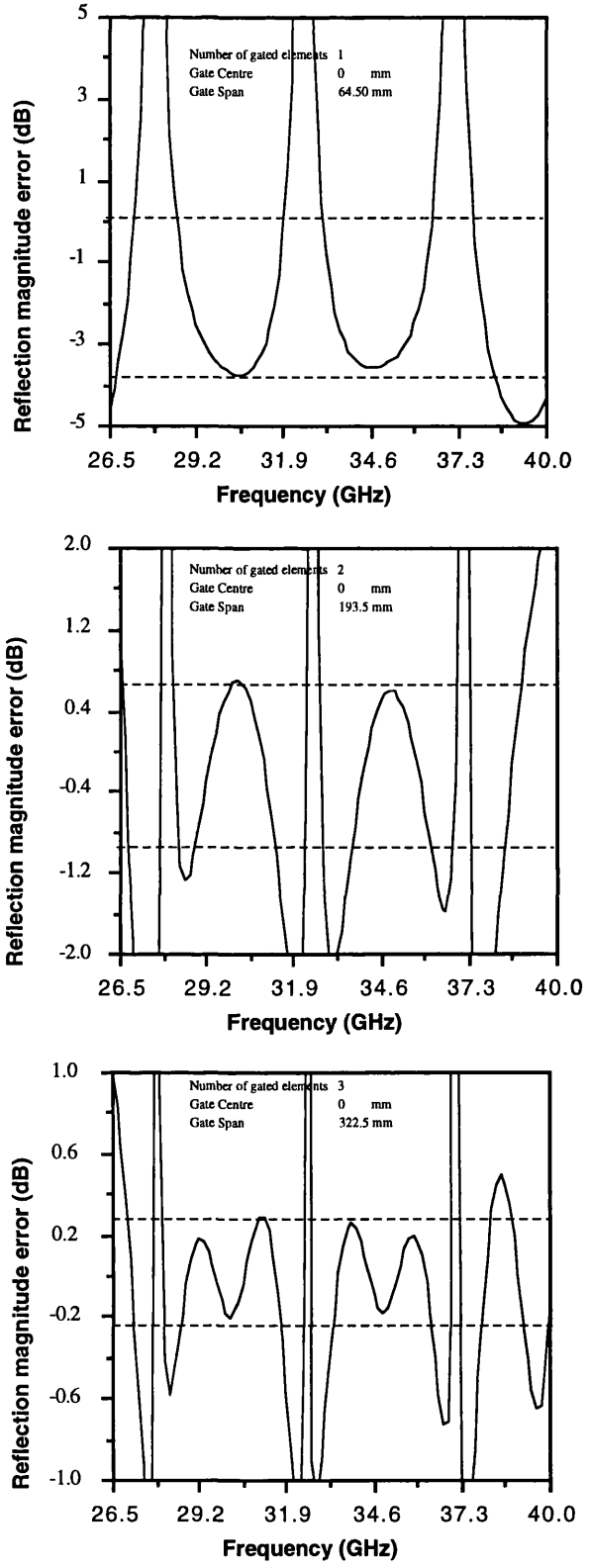

Figure A5.7 The simulated gating error in reflection coefficient magnitude of sample 2 (ε_r=10.4, μ_r=1).

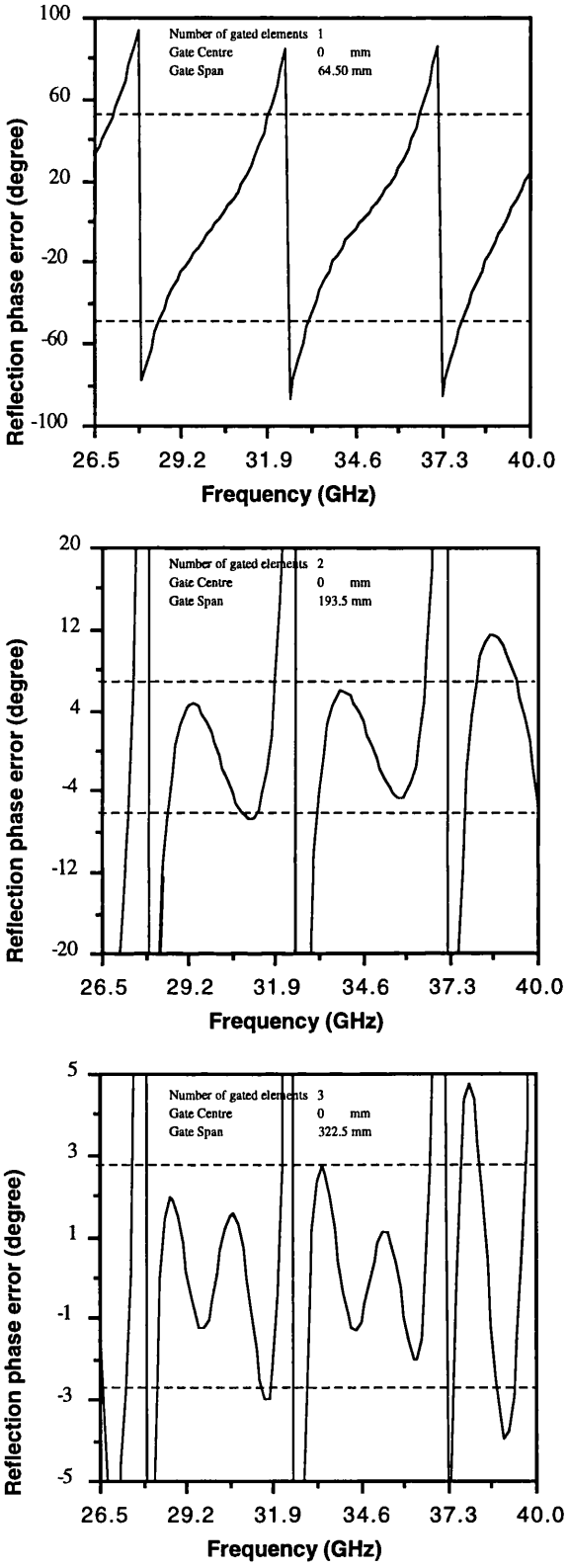

Figure A5.8 The simulated gating error in reflection coefficient phase of sample 2 (ε_r=10.4, μ_r=1).

A5.2 Sample 3

Sample 3 is a lossy ferrite representing the materials made by mixing resin with ferrite powder (ε_r=*7.5 -j0.5* μ_r =*0.8 -j0.15*). The thickness of this sample is 10 mm, which corresponds to an electrical length of 24.49 mm at normal incidence. The lossy properties of this sample cause the higher order terms of the multiple reflections to decay very fast. Figures A5.5.10 to A5.5.13 show the simulated gating error in transmission and reflection coefficients for different gate widths. The dashed lines show the calculated error for an ideal gate. In order to simulate the gating error in this sample, the following parameters and computer program are used.

$Z_c = 50\sqrt{0.8 / 7.5} = 16.3\ \Omega$

$V_c = \sqrt{1 / (7.5 \times 0.8)} = 0.408$

$R = 47.123\ \Omega$

$G = 0.06283\ \Omega^{-1}$

```
10      PORT  1
20      TL    1 2 16.3 1 CM 0.408 47.123 0 0.06283
30      PORT  2
40      FREQ  26.5 GHZ 40 GHZ 401 POINTS
50      OUTPUT S11/S21
```

The gating error for different gate widths can be calculated. N is the number of components which are included in gating.

N=1

$|P^2\Gamma^2| = 6.1 \times 10^{-3}$

$|P^2(1-\Gamma^2)|/|(1-P^2)| = 1.94 \times 10^{-2}$

$M_{Tmax} = \pm 0.053\ dB$

$\Phi_{Tmax} = \pm 0.35°$

$M_{Rmax} = \pm 0.16\ dB$

$\Phi_{Rmax} = \pm 1.1°$

$N=2$

$|P^4\Gamma^4|=3.7 \times 10^{-5}$

$|P^2(1-\Gamma^2)(P^2\Gamma^2)|\Lambda(1-P)| = 1.19 \times 10^{-4}$

$M_{Tmax} = \pm 3.2 \times 10^{-4}\ dB$

$\Phi_{Tmax} = \pm 2.1 \times 10^{-3}\ ^\circ$

$M_{Rmax} = \pm 1 \times 10^{-3} dB$

$\Phi_{Rmax} = \pm 6.8 \times 10^{-3}\ ^\circ$

$N=3$

$|P^6\Gamma^6|=2.3 \times 10^{-7}$

$|P^2(1-\Gamma^2)(P^4\Gamma^4)|\Lambda(1-P^2)| = 7.3 \times 10^{-7}$

$M_{Tmax} = \pm 2 \times 10^{-6}\ dB$

$\Phi_{Tmax} = \pm 1.3 \times 10^{-5}\ ^\circ$

$M_{Rmax} = -\ 6.3 \times 10^{-6}\ dB$

$\Phi_{Rmax} = \pm 4.2 \times 10^{-5}\ ^\circ$

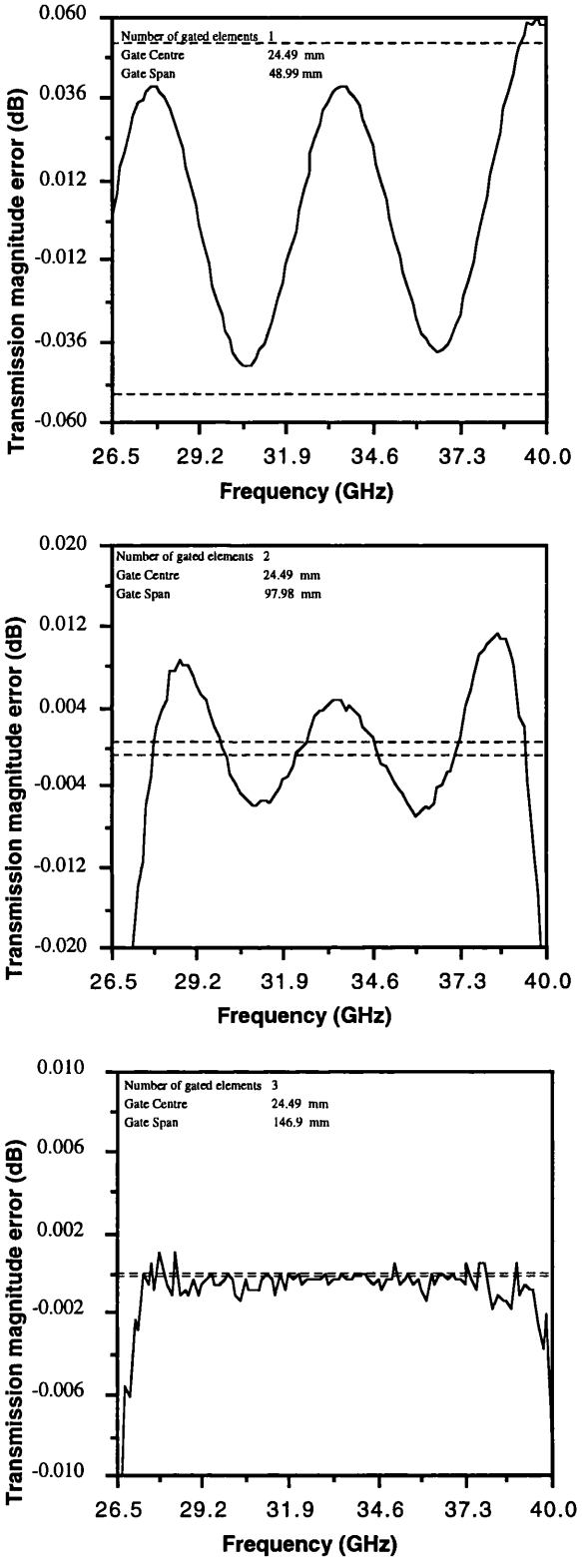

Figure A5.9 The simulated gating error in transmission coefficient magnitude of sample 3 (ε_r=7.5-j0.5, μ_r=0.8-j0.15).

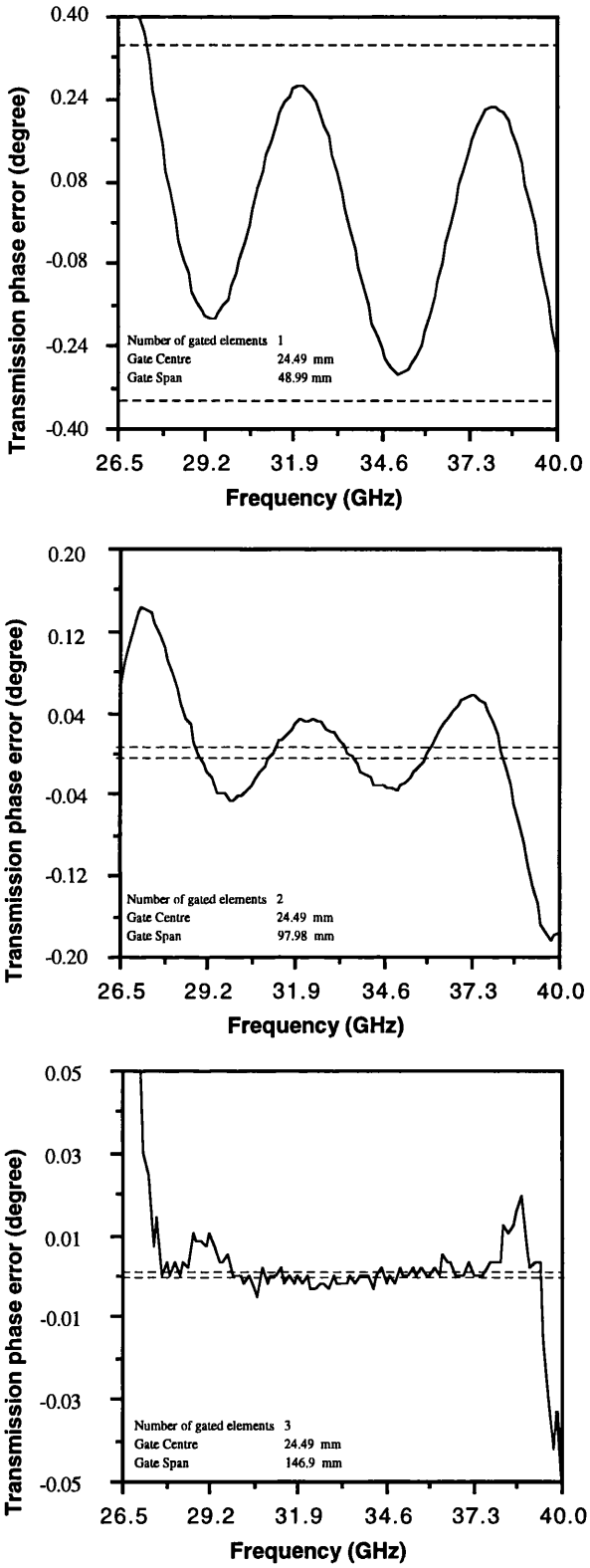

Figure A5.10 The simulated gating error in transmission coefficient phase of sample 3 (ε_r=7.5-j0.5, μ_r=0.8-j0.15).

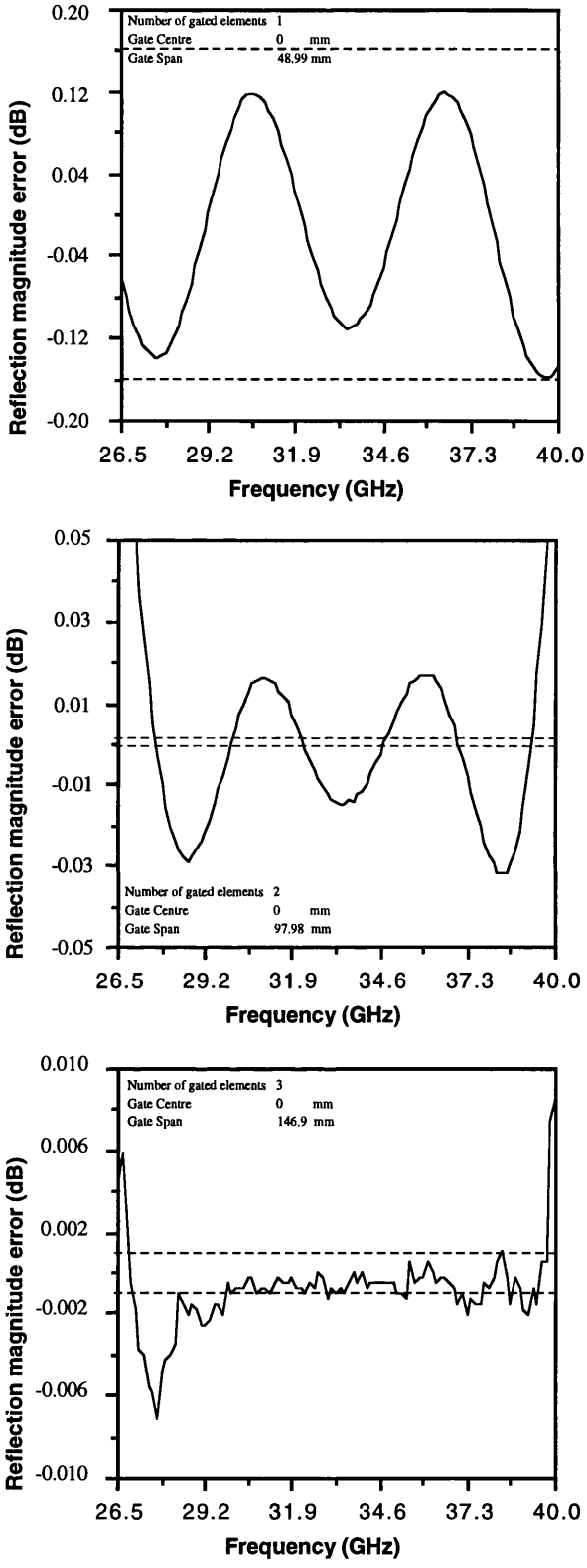

Figure A5.11 The simulated gating error in reflection coefficient magnitude of sample 3 (ε_r=7.5-j0.5, μ_r=0.8-j0.15).

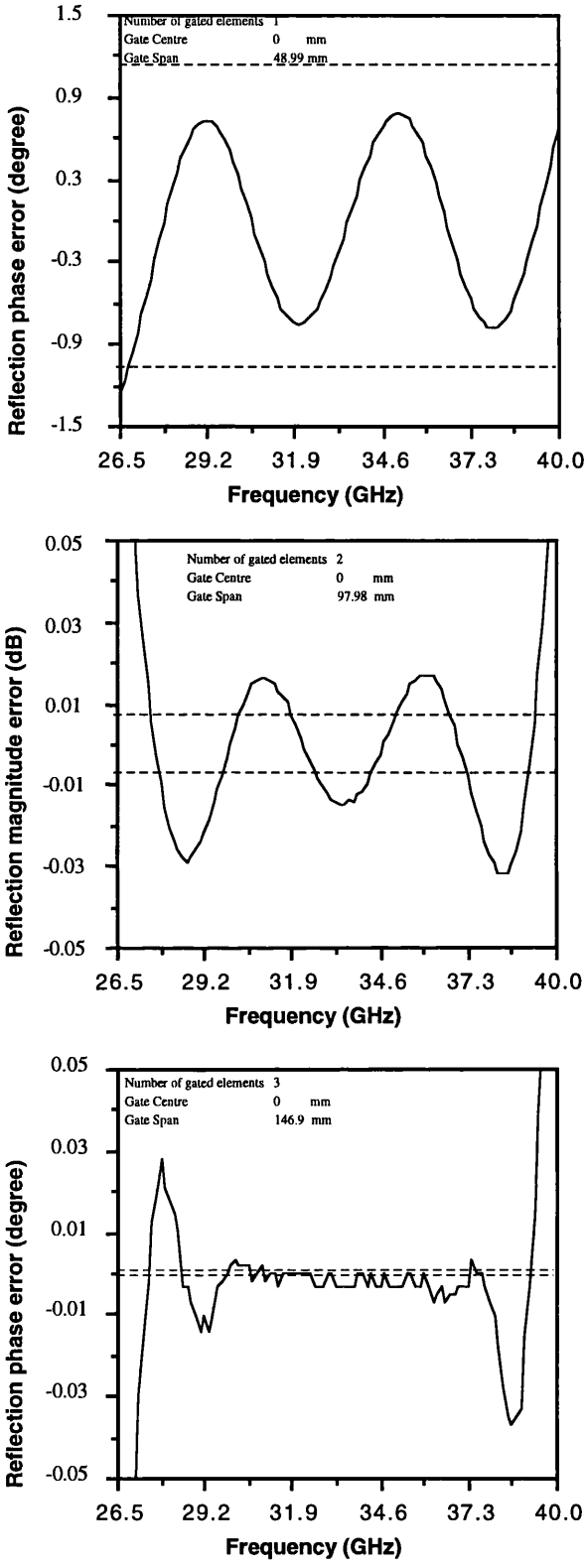

Figure A5.12 The simulated gating error in reflection coefficient phase of sample 3 (ε_r=7.5-j0.5, μ_r=0.8-j0.15).

Appendix 6

Gating error in thick Samples

If the electrical length of a sample is sufficiently high (*thick* slab), multiple reflections within the sample can be removed by time gating. In *thick* sample measurements, the gate should be narrow enough to exclude the higher order terms of the multiple reflections. In the time domain response, different terms of the multiple reflections are separated by twice the sample electrical length. In time gating, the minimum gate width is a function of the gate shape and the frequency span over which the measurement is carried out. In *thick* samples, leakages of the higher order terms of the multiple reflections and the gate pass band ripple introduce error in the measured transmission and reflection coefficients.

The aim of this appendix is to simulate the gating error in *thick* slabs in a real gate, and to estimate the minimum thickness of a *sample* slab for being treated as a *thick* slab. The gating error in *thick* samples cannot be modelled easily, since this analysis requires the detailed specifications of the gate and the sample properties. In our simulation, the *Hewlett Packard* computer modelling program (*CMP*) is used to estimate the minimum thickness of the sample.

Gate Shape	Passband Ripple	Sidelobe Level	Cutoff Time	Minimum Gate Span
Minimum	± 0.40 dB	-24 dB	0.6 / f_{Span}	1.2 / f_{Span}
Normal	± 0.04 dB	-45 dB	1.4 / f_{Span}	2.8/ f_{Span}
Wide	± 0.02 dB	-52 dB	4.0 / f_{Span}	8.0 / f_{Span}
Maximum	± 0.01 dB	-80 dB	11.2 / f_{Span}	22.4 / f_{Span}

Table TA6.1 Characteristic of different gate shapes in the HP8510B.

Table TA6.1 shows the specifications of the different gates shape in the HP-8510B. The use of the *Narrow* gate shape provides the maximum ability to separate two adjacent components, but high sidelobe level and pass band ripple degrade the measurement accuracy. In the gated frequency response, the accuracy of the measurement decreases rapidly at the two ends of the band. This phenomenon (*edge effect*), is due to the intrinsic limitations associated with the time gating. For different gate shapes, the useful parts of the trace are shown in A6.1.

The pass band ripple superimposes fluctuations on the gated frequency response, and the limited sidelobe level results in leakage of the unwanted reflections. If the electrical length of the slab is long enough, a wide gate width and *Maximum* gate shape is preferred. But maximum frequency span of 13.5 GHz (R-band), dictates the use of *Narrow* gate shape in most practical cases.

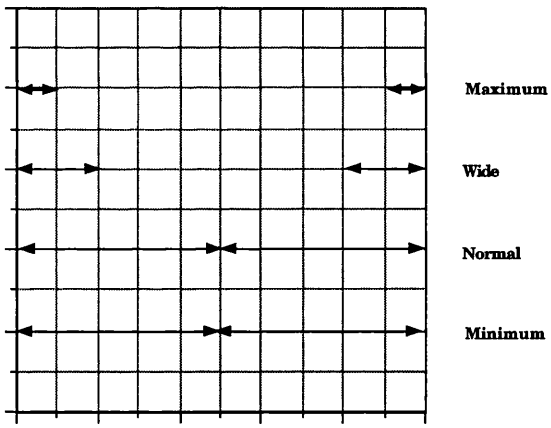

Figure A6.1 Edge effect for different gate shapes in HP-8510B.

In order to show the effect of gating in measuring *thick* slabs, the error in three different samples has been simulated. Figures A5.6.2 to A6.5 show the simulated error in a lossless dielectric (ε_r=2.6), for different thicknesses. Regarding the low dielectric constant of this sample, its electrical length is 1.61 times the slab thickness.

In the HP-8510B, the minimum gate width associated with 13.5 GHz frequency span is 26.4 mm. As can be seen, a thickness of 10 mm is not high enough to measure the

transmission and reflection coefficients with an acceptable accuracy. As mentioned, the error at the two ends of the measured frequency band increases rapidly because of edge effects, but the measurement at the centre frequencies is less subject to error.

By increasing the sample thickness, the error in the measured transmission and reflection coefficients decrease. If the electrical length of the sample is high enough, the error is mainly limited by the passband ripple in the gate. The simulation results show that this sample slab should be thicker than 20 millimetres in order to be considered as a *thick* slab.

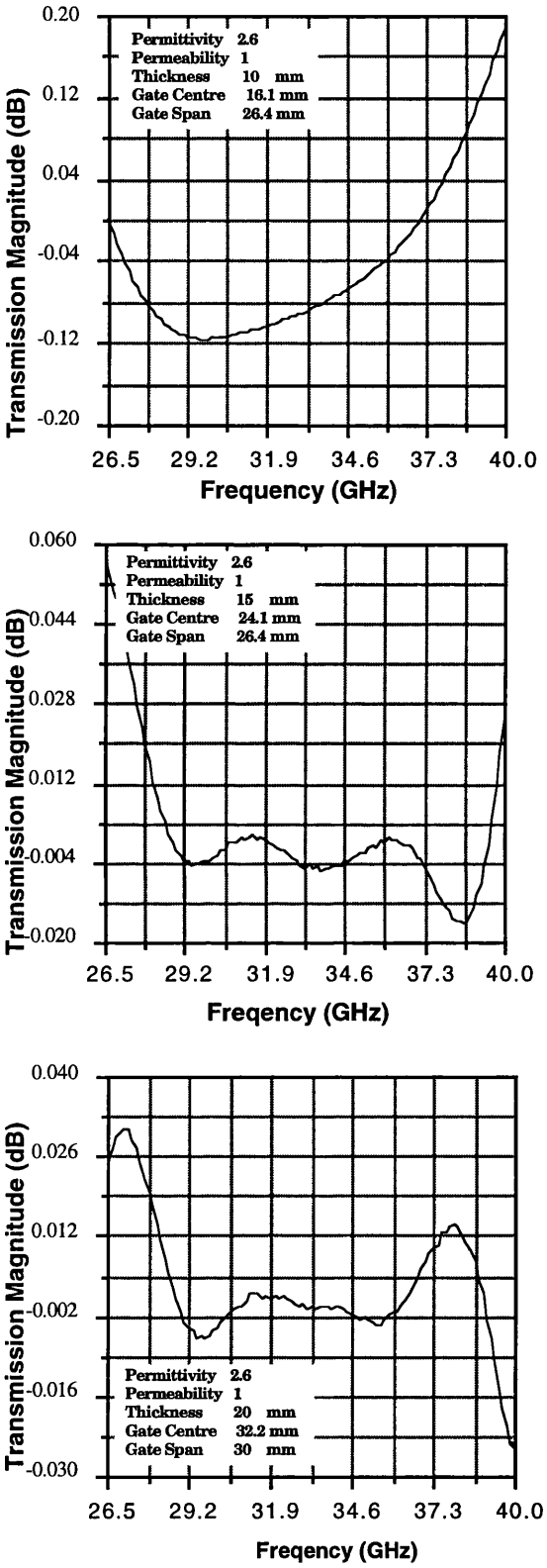

Figure A6.2 Transmission magnitude error in thick sample measurement for different thickness of slab 1 (ε_r=2.6, μ_r=1).

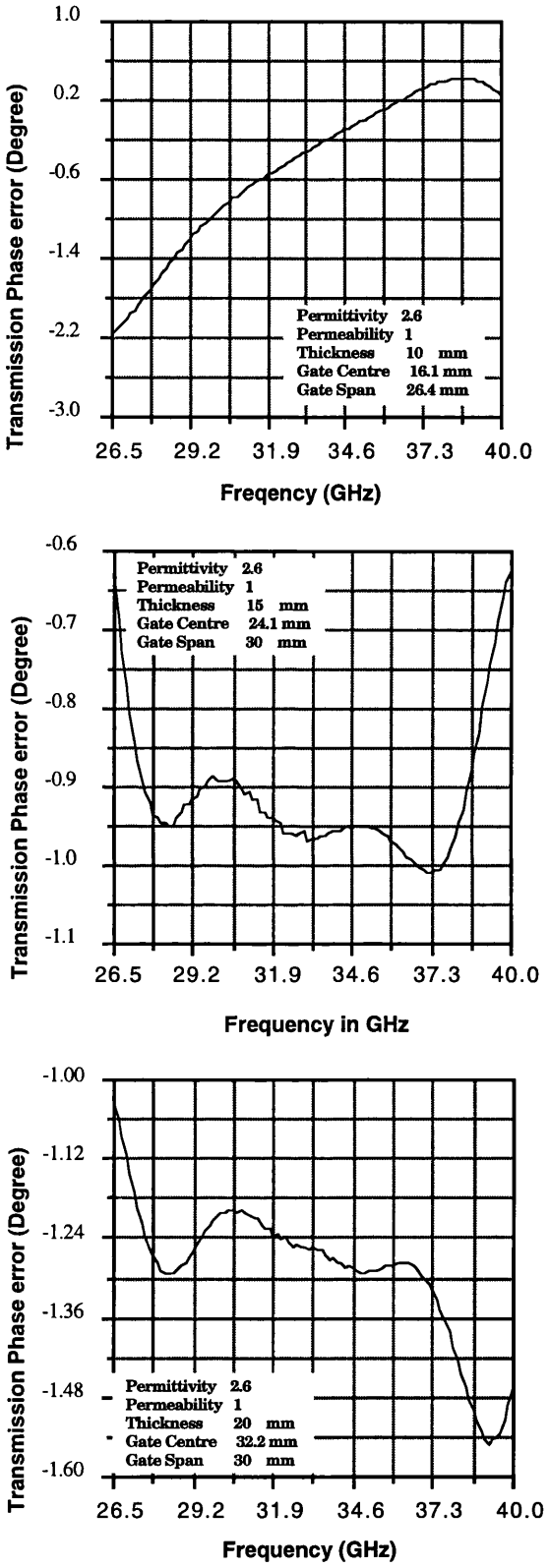

Figure A6.3 Transmission phase error in thick sample measurement for different thickness of slab 1 (ε_r=2.6, μ_r=1).

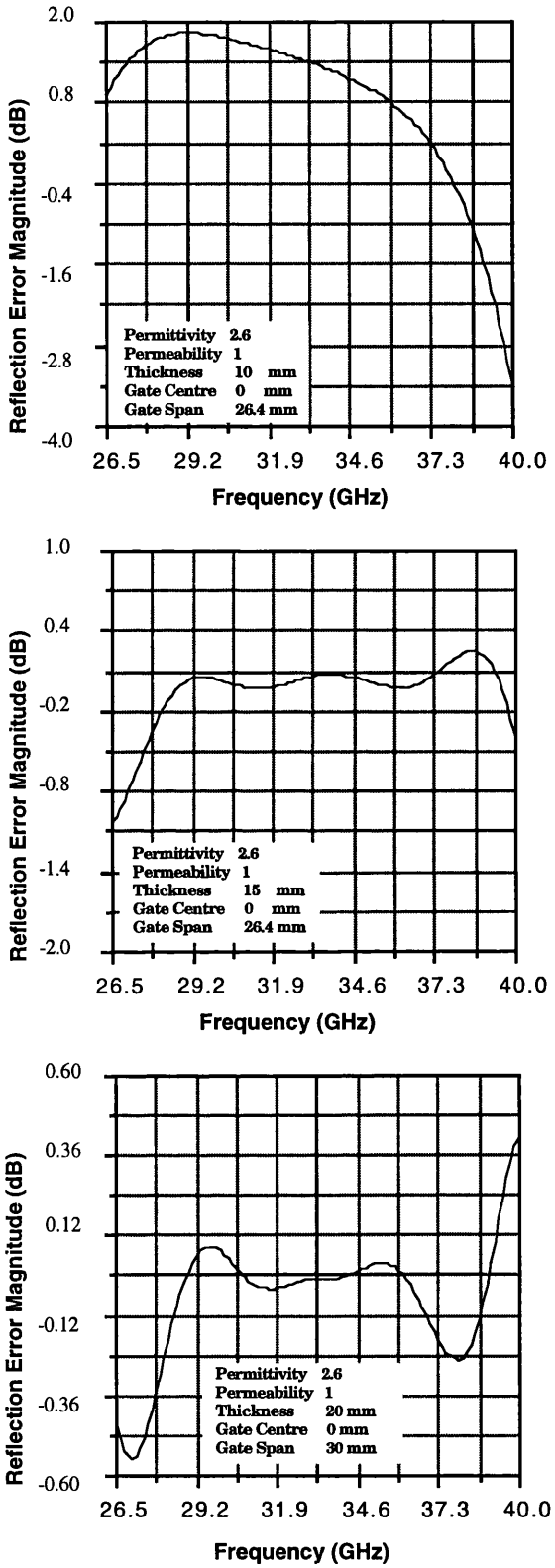

Figure A6.4 Reflection magnitude error in thick sample measurement for different thickness of slab 1 (ε_r=2.6, μ_r=1).

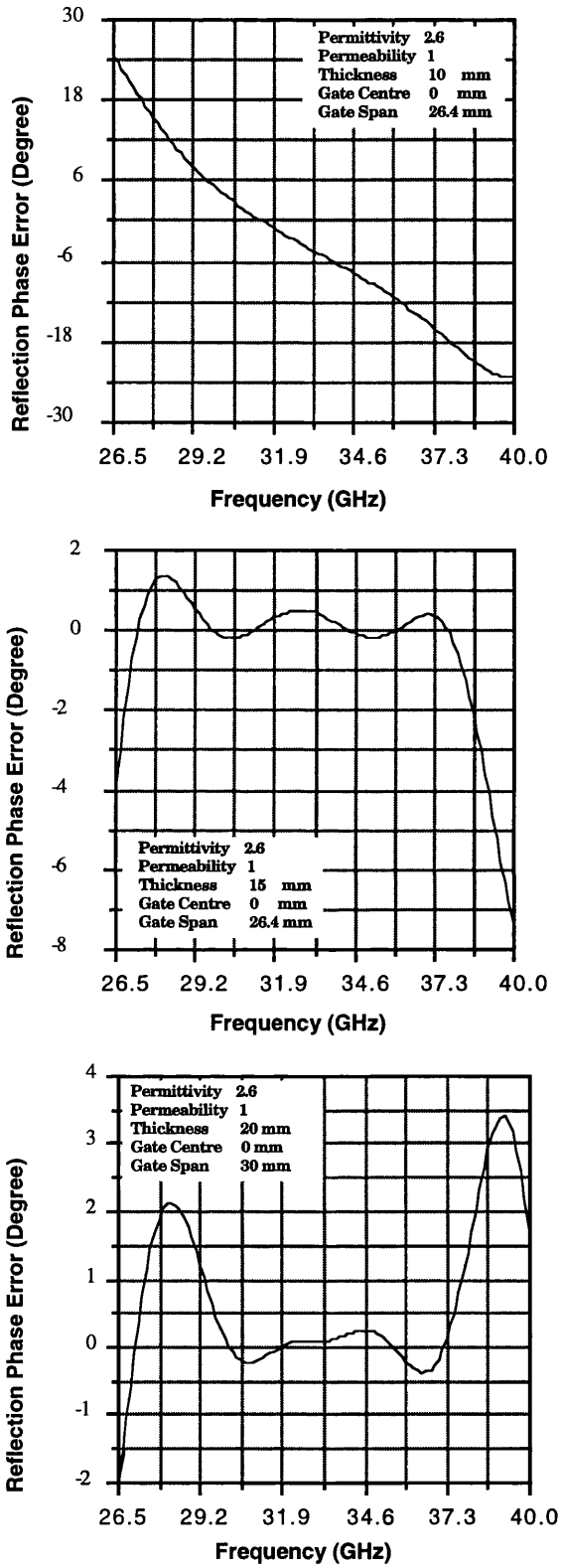

Figure A6.5 Reflection phase error in thick sample measurement for different thickness of slab 1 (ε_r=2.6, μ_r=1).

In R-band, the minimum thickness for treating a sample as a *thick* slab for materials with a high product of $\varepsilon_r \mu_r$ is quite practical. As an example, the simulation of the gating error in a lossless dielectric ($\varepsilon_r = 10.4$) is shown in figures A6.6 and A6.7. This sample has electrical length twice sample 1, therefore the main component of the transmitted or reflected waves can be measured with less error for a given gate width. The higher electrical length of this sample allows us to use a gate width of 0.1 nanoseconds, 30 mm, to exclude multiple reflections with only a small error in the measured parameters.

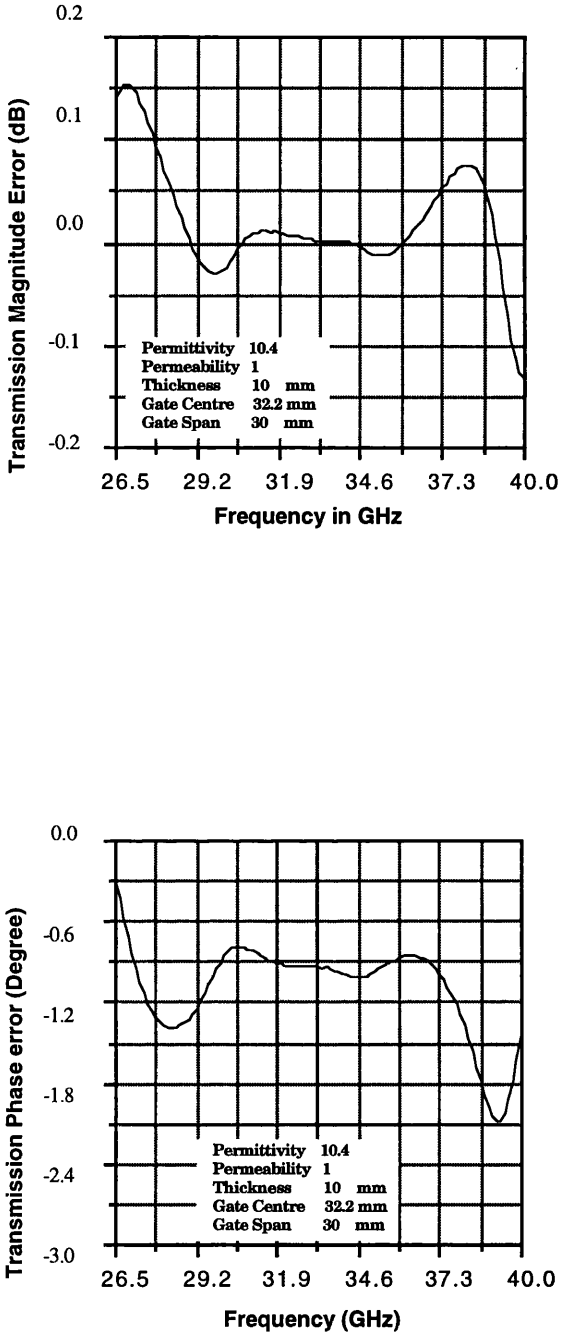

Figure A6.6 Transmission error in thick sample measurement slab 2 (ε_r=10.4, μ_r=1).

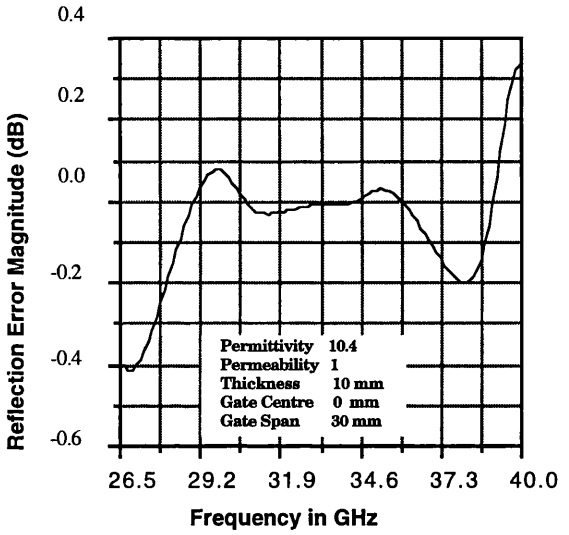

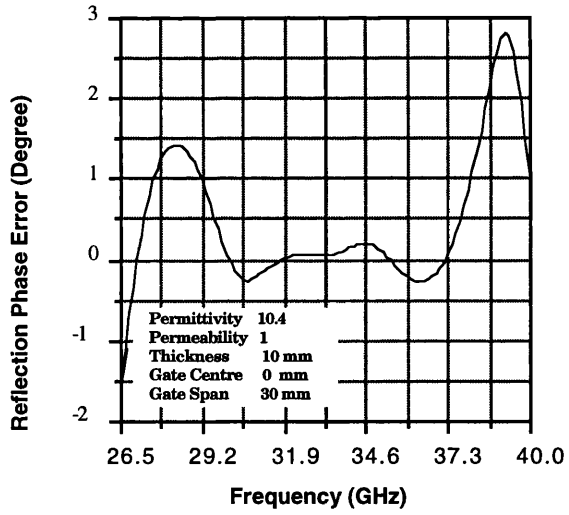

Figure A6.7 Reflection error in thick sample measurement slab 2 (ε_r=10.4, μ_r=1).

If the sample is lossy, the multiple reflections within the slab decay rapidly. The simulated gating error for a lossy ferrite (ε_r=*7.5 -j0.5,* μ_r=*0.8 -j0.15*) is shown in figures A6.8 and A6.9. In this sample, propagation coefficient is sufficiently small (*P=-16.99 dB*). Therefore, the multiple reflections within the slab do not contribute effectively in constituting total transmitted or reflected waves.

The simulation of these three samples shows that the reflection coefficient is more subject to error than the transmission coefficient for a given gate width. In reflection coefficient measurements, the second component of the multiple reflections is relatively strong and only attenuated by a factor of $P^2(1-\Gamma^2)$ with respect to the main component. For low-loss materials $|P^2(1-\Gamma^2)|\approx 1$, while the second component in transmission coefficient is attenuated by factor of $P^2\Gamma^2$. Since $(P^2\Gamma^2)/P^2(1-\Gamma^2)\approx\Gamma^2$, the leakage of the second component which results in error in the measured parameter is less in transmission measurements.

It can also be concluded that the maximum gate width is a function of loss properties and the electrical length of the slab. In practice, a sample can be considered as a *thick* slab if it is 1.5 to 2 times thicker than the gate width. For frequency span of 26.5 to 40 GHz, the minimum gate width is 26.4 millimetres. Therefore, the sample electrical length should be greater than 5.3 mm for low-loss and 4 mm for lossy materials. In the cases that the sample electrical length is sufficiently high, the use of a gate shape with lower sidelobes is preferred.

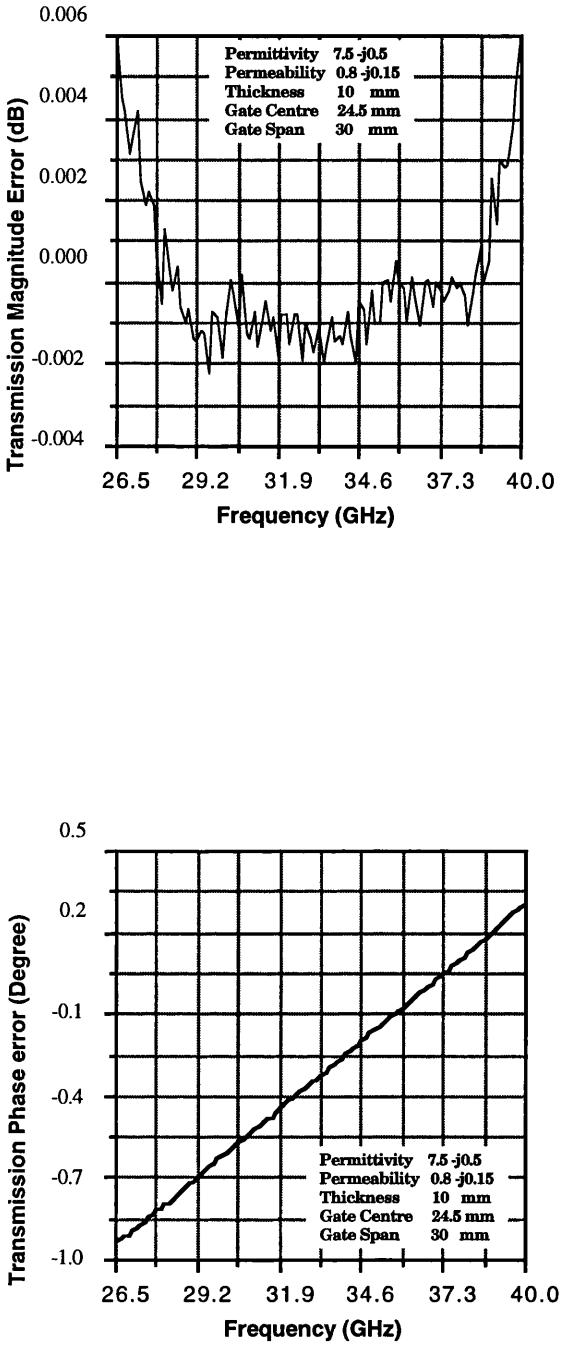

Figure A6.8 Transmission error in thick sample measurement slab 3 (ε_r=7.5 -j0.5, μ_r=0.8 -j0.15).

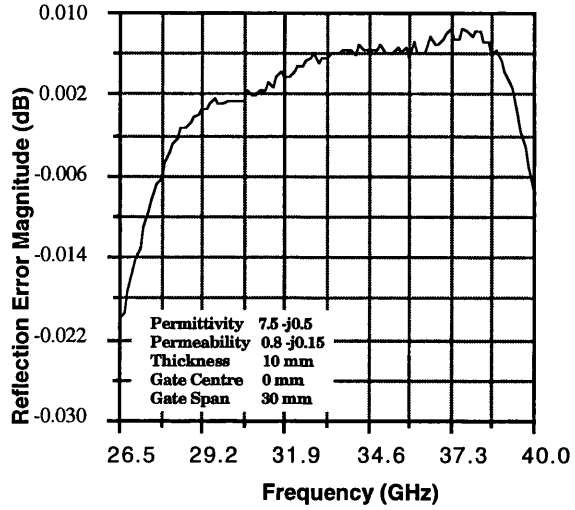

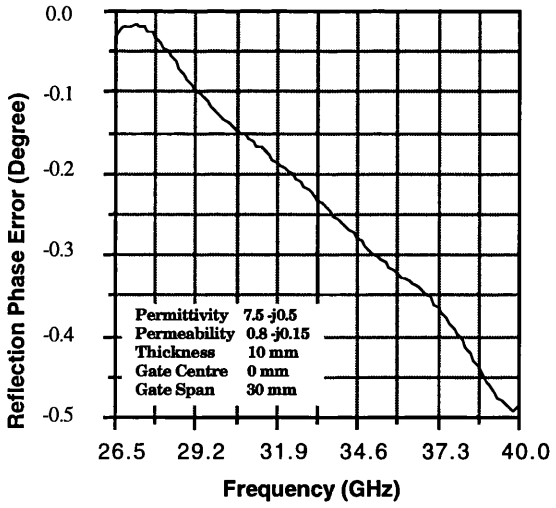

Figure A6.9 Reflection error in thick sample measurement slab 3 (ε_r=7.5 -j0.5, μ_r=0.8 -j0.15).

Appendix 7

Near-field antenna coupling

A7.1 Introduction

The aim of this appendix is to calculate the transmission and reflection coefficients of a slab in the near-field region. In free-wave techniques the coupling between two antennas while the wave is transmitted through or reflected from the sample is measured, and the sample properties are calculated from these measurements. In this analysis, we assume that the sample surfaces are flat, parallel and sufficiently large to intercept the wave adequately. The antenna mismatches and unwanted reflections are ignored, and the antennas are assumed to be aligned in the same plane of polarisation.

Although the arrangements of the measurement system for transmission and reflection coefficient measurements are different, the same analysis can be applied for both. First transmission measurement is considered, then the reflection coefficient of a slab in the near-field region is calculated. Regarding the practical size for a sample and the antenna, free-wave measurements are carried out in the Fresnel region. Therefore, contributions from all elements of the angular spectrum should be taken into account in calculating the transmission and reflection coefficients of a slab in this region.

A7.2 Transmission coefficient measurement

Figures A7.1 shows the configuration of a free-wave system for transmission coefficient measurement. In general cases, the diffracted wave can be resolved into components parallel with and perpendicular to the plane of polarisation. Since the reflection or transmission coefficient associated with each of these elements is a function of the incident angle and the plane of polarisation, the elemental plane wave vector is resolved into

components in the planes of parallel and perpendicular polarisation. The interaction of the sample with each component of the angular spectrum is calculated individually at each plane of polarisation.

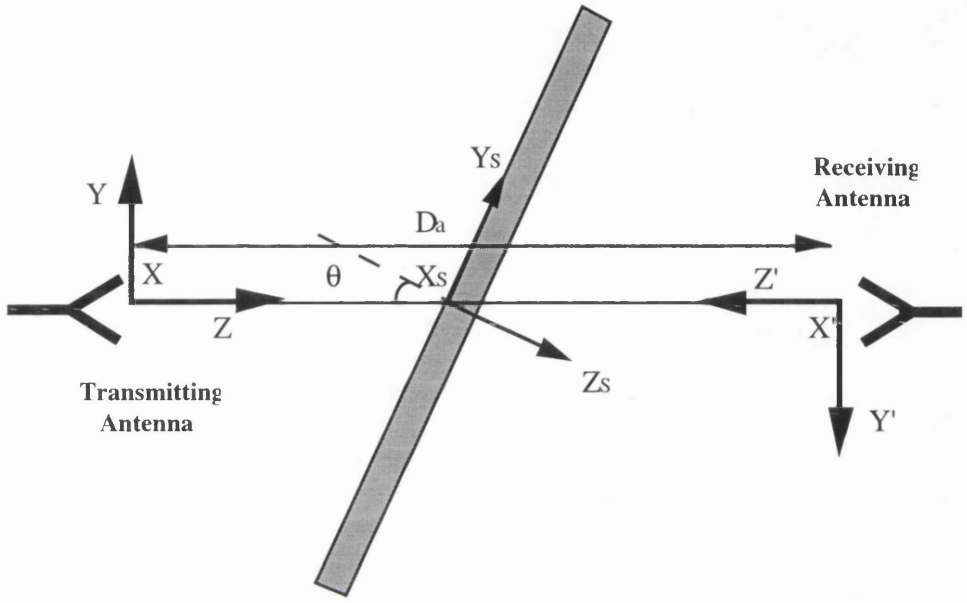

Figure A7.1 Transmission coefficient measurement arrangement.

The reflection coefficient corresponding to a semi-infinite slab illuminated by a uniform plane wave at parallel and perpendicular polarisations are given by equations (1) and (2). If multiple reflections within the sample are taken into account, equations (3) to (6) give the total transmission and reflection coefficients.

$$\Gamma_{\parallel} = \frac{\sqrt{\varepsilon_r\mu_r - \alpha_s^2 - \beta_s^2} - \varepsilon_r\sqrt{1 - \alpha_s^2 - \beta_s^2}}{\sqrt{\varepsilon_r\mu_r - \alpha_s^2 - \beta_s^2} + \varepsilon_r\sqrt{1 - \alpha_s^2 - \beta_s^2}} \qquad \ldots(1)$$

$$\Gamma_{\perp} = \frac{\mu_r\sqrt{1 - \alpha_s^2 - \beta_s^2} - \sqrt{\varepsilon_r\mu_r - \alpha_s^2 - \beta_s^2}}{\mu_r\sqrt{1 - \alpha_s^2 - \beta_s^2} + \sqrt{\varepsilon_r\mu_r - \alpha_s^2 - \beta_s^2}} \qquad \ldots(2)$$

$$T_{t\parallel} = \frac{P(1-\Gamma_{\parallel}^2)}{(1-P^2\Gamma_{\parallel}^2)} \qquad \ldots(3)$$

$$T_{t\perp} = \frac{P(1-\Gamma_{\perp}^2)}{(1-P^2\Gamma_{\perp}^2)} \quad ...(4)$$

$$\Gamma_{t\parallel} = \frac{\Gamma_{\parallel}(1-P^2)}{(1-P^2\Gamma_{\parallel}^2)} \quad ...(5)$$

$$\Gamma_{t\perp} = \frac{\Gamma_{\perp}(1-P^2)}{(1-P^2\Gamma_{\perp}^2)} \quad ...(6)$$

$$P = e\left(\frac{-j2\pi d}{\lambda_o}\sqrt{\varepsilon_r\mu_r - \alpha_s^2 - \beta_s^2}\right) \quad ...(7)$$

P is the propagation coefficient expressing the changes in the magnitude and phase of a uniform plane wave travelling within the slab for a distance of d, (equation 7). α_s and β_s are the components of a unit vector defining the direction of propagation in the sample system of coordinates (X_S-Y_S). The elemental vector representing the angular spectrum at a given angle can also be resolved into parallel and perpendicular polarisation components, (equations 8 and 9). In practice, the antennas are fixed and the direction of the sample surface defines the plane of polarisation. The unit vector normal to the sample surface $(\hat{n})$, is given by (11) and (12) for parallel and perpendicular polarisations respectively.

$$\hat{U}_{\parallel} = \hat{U}_{\perp} \times \hat{k} \quad ...(8)$$

$$\hat{U}_{\perp} = \frac{\hat{n} \times \hat{k}}{\left|\hat{n} \times \hat{k}\right|} \quad ...(9)$$

$\hat{k}$, $\hat{n}_{\parallel}$ and $\hat{n}_{\perp}$ are unit vectors defining the direction of propagation and the position of the sample surface at parallel and perpendicular polarisations, equations (10) to (12).

$$\hat{k} = \alpha\,\hat{U}x + \beta\,\hat{U}y + \delta\,\hat{U}z \quad ...(10)$$

$$\hat{n}_{\parallel} = -sin(\theta).\hat{U}_x + cos(\theta).\hat{U}z \quad ...(11)$$

$$\hat{n}_{\perp} = -sin(\theta).\hat{U}_y + cos(\theta).\hat{U}z \quad ...(12)$$

α, β, and γ are the X, Y, and Z components of an elemental plane wave travelling in the direction of $\hat{k}$. The incident angle (θ), and the unit polarisation vectors are also defined with respect to the normal to the sample surface and the direction of the main component of the electric field in the antenna aperture. It is worth mentioning that the plane of parallel and perpendicular polarisations are defined according to the direction of the electric field and the sample surface. At a given polarisation, each uniform plane wave in the angular spectrum has components in parallel and perpendicular planes.

Substituting (10) to (12) in (8) and (9), the elemental parallel and perpendicular vectors at two orthogonal polarisations for a uniform plane wave travelling in the direction of $\hat{k}$ can be found, (13) to (16).

$$\hat{U}_{\parallel\parallel}=\frac{1}{\sqrt{\beta^2+(\alpha.cos(\theta)+\gamma.sin(\theta))^2}}\times \left[\hat{U}_x(\alpha\gamma.cos(\theta)+sin(\theta)-\alpha^2 sin(\theta))+\hat{U}_y(\beta\gamma.cos(\theta)-\alpha\beta.sin(\theta))-\hat{U}z(cos(\theta)-\gamma^2 cos(\theta)+\alpha\gamma.sin(\theta))\right] \quad ...(13)$$

$$\hat{U}_{\perp\parallel}=\frac{-\hat{U}_x(\beta.cos(\theta))+\hat{U}_y(\alpha.cos(\theta)+\gamma.sin(\theta))-\hat{U}_z(\beta.sin(\theta))}{\sqrt{\beta^2+(\alpha.cos(\theta)+\gamma.sin(\theta))^2}} \quad ...(14)$$

$$\hat{U}_{\parallel\perp}=\frac{1}{\sqrt{\alpha^2+(\beta.cos(\theta)+\gamma.sin(\theta))^2}}\times \left[\hat{U}_x(\alpha\gamma.cos(\theta)+\alpha\beta.sin(\theta))+\hat{U}_y(sin(\theta)-\beta^2.sin(\theta)+\beta\gamma.cos(\theta))-\hat{U}_z(cos(\theta)-\gamma^2 cos(\theta)+\beta\gamma.sin(\theta))\right] \quad ...(15)$$

$$\hat{U}_{\perp\perp}=\frac{-\hat{U}_x(\beta.cos(\theta)+\gamma.sin(\theta))+\hat{U}_y(\alpha.cos(\theta))+\hat{U}_z(\alpha.sin(\theta))}{\sqrt{\alpha^2+(\beta.cos(\theta)+\gamma.sin(\theta))^2}} \quad ...(16)$$

The diffracted wave from an aperture can be expressed as a spectrum of uniform plane waves travelling at different angles, Clarke and Brown [72]. The parallel and perpendicular components associated with each element of the angular spectrum are given by (13) to (16).

According to the antenna reciprocity theorem, the induced complex voltage in an antenna illuminated by a plane wave whose electric field has the vector magnitude of ei is proportional to $ei.e(Ui)$, where $e(Ui)$ is the vector pattern function of the field in the direction of Ui when the antenna is used as a transmitter. The constant of proportionality is

$\lambda_o^2/j4pZP$, where P is the power and λ_o is the free-space wavelength. Therefore, the coupling between transmitting and receiving antennas can be found by integrating the induced voltage over all angles of the spectrum.

In the aperture plane ($Z=0$), the field is assumed to be wholly X-polarized. The Y-component of the field is zero over the entire aperture plane, therefore it is zero anywhere at the front of the aperture ($Z \geq 0$). If unit power delivered to the transmitting antenna the angular spectrum of the transmitted wave is $F_x^T(\alpha,\beta)$. The vector representing the electric field at a given angle can be be expressed by (17).

$$\hat{e} = F_x^T(\alpha,\beta)\left[\hat{U}_x - \hat{U}_z\frac{\alpha}{\gamma}\right] \quad ...(17)$$

In the general case, the electric field can be resolved into two orthogonal components in parallel with and perpendicular to the plane normal to the slab surface, (18). These two components of the electric field in the parallel polarisation measurement can be found from (19) and (20). Similarly, the components of the field at perpendicular polarisation measurement are given by (21) and (22).

$$\hat{e} = \hat{e}_{\parallel} + \hat{e}_{\perp} \quad ...(18)$$

$$\hat{e}_{\parallel\parallel} = \left|\hat{e}.\hat{U}_{\parallel\parallel}\right| . \hat{U}_{\parallel\parallel} \quad ...(19)$$

$$\hat{e}_{\perp\parallel} = \left|\hat{e}.\hat{U}_{\perp\parallel}\right| . \hat{U}_{\perp\parallel} \quad ...(20)$$

$$\hat{e}_{\parallel\perp} = \left|\hat{e}.\hat{U}_{\parallel\perp}\right| . \hat{U}_{\parallel\perp} \quad ...(21)$$

$$\hat{e}_{\perp\perp} = \left|\hat{e}.\hat{U}_{\perp\perp}\right| . \hat{U}_{\perp\perp} \quad ...(22)$$

Substituting the elemental vector electric field in (19) to (22), the components of the fields at each plane of polarisation can be found from (23) to (26).

$$\hat{e}_{\parallel\parallel} = \frac{\gamma.sin(\theta)+\alpha cos(\theta)}{\gamma.\left[\beta^2+(\alpha.cos(\theta)+\gamma.sin(\theta))^2\right]} \times F_x^T(\alpha,\beta) \times \left[\hat{U}_x(\alpha\gamma.cos(\theta)+sin(\theta)-\gamma^2 sin(\theta))+\hat{U}_y(\beta\gamma.cos(\theta)-\alpha\beta.sin(\theta))-\hat{U}_z(cos(\theta)-\gamma^2 cos(\theta)+\alpha\gamma.sin(\theta))\right] \quad ...(23)$$

$$\hat{e}_{\perp\parallel} = \frac{\alpha\beta.sin(\theta)-\beta\gamma.cos(\theta)}{\gamma.\left[\beta^2+(\alpha.cos(\theta)+\gamma.sin(\theta))^2\right]} \times F_x^T(\alpha,\beta) \times \left[-\hat{U}_x(\beta.cos(\theta))+\hat{U}_y(\alpha.cos(\theta)+\gamma.sin(\theta))-\hat{U}_z(\beta.sin(\theta))\right] \quad ...(24)$$

$$\hat{e}_{\parallel\perp} = \frac{\alpha cos(\theta)\ .\ F_x^T(\alpha,\beta)}{\gamma.\left[\alpha^2+(\beta.cos(\theta)+\gamma.sin(\theta))^2\right]} \times \left[\hat{U}_x(\alpha\gamma.cos(\theta)+\alpha\beta.sin(\theta))+\hat{U}_y(sin(\theta)-\beta^2 sin(\theta)+\beta\gamma.cos(\theta))-\hat{U}_y(cos(\theta)-\gamma^2 cos(\theta)+\beta\gamma.sin(\theta)\right] \quad ...(25)$$

$$\hat{e}_{\perp\perp} = -\frac{\beta\gamma.cos(\theta)+sin(\theta)-\beta^2 sin(\theta)}{\gamma.\left[\alpha^2+(\beta.cos(\theta)+\gamma.sin(\theta))^2\right]} \times F_x^T(\alpha,\beta) \times \left[-\hat{U}_x(\beta.cos(\theta)+\gamma.sin(\theta))+\hat{U}_y(\alpha.cos(\theta))+\hat{U}_z(\alpha.sin(\theta))\right] \quad ...(26)$$

If the sample is placed between the transmitting and receiving antennas, the field changes due to the interaction of the sample can be calculated by their effect on the transmission coefficient associated with each components of the angular spectrum, (equations 2 and 3). The transmitting and receiving antennas have the same plane of polarisation, and the vector pattern function of the field in the Fresnel region is given by (27).

$$\hat{e}(Ui) = J\ 2\pi F_x^R(\alpha',\beta')\left[\gamma\hat{U}_x - \alpha'\hat{U}_z\right] \quad ...(27)$$

The induced voltage at the receiving antenna due to the elemental spatial angle after transmission through the sample is expressed by (28). The total coupling between the transmitting and receiving antennas while the sample is placed between them can be found by integrating equation (28) for all angles of the spectrum.

$$\delta e_{ind.} = -\frac{\lambda^2}{2Z}F_x^R(\alpha',\beta')\left[\gamma\hat{U}_x - \alpha'\hat{U}_z\right].\hat{e}(\alpha,\beta) \quad ...(28)$$

If the system of coordinates is converted from the sample to the transmitting antennas, the coupling between two antennas can be expressed by (29).

$$C = \frac{\lambda_0}{2Z}\int_{\alpha,\beta=-\infty}^{+\infty} F_X^R(-\alpha,\beta)\,F_X^T(\alpha,\beta)\,\delta e\ exp\left(\frac{-j\ 2\pi D_a(\alpha\alpha_0+\beta\beta_0+\gamma\gamma_0)}{\lambda_0}\right)d\alpha\,d\beta \quad ...(29)$$

In the Fresnel region, the transmission and reflection coefficients of a slab with known properties can be calculated by (28). It should be noted that in deriving the general coupling formula, diffraction from the edges of the sample and mismatches in the antennas are ignored. Regarding the geometry of the measuring setup, the exponential term of the integrand can be simplified. Referring to the system of coordinates (figure A7.1), the value of α_o, β_o, and γ_o for the measurement setup can be found, (30) to (32).

$$\alpha_0 = 0 \qquad \ldots(30)$$

$$\beta_0 = 0 \qquad \ldots(31)$$

$$\gamma_0 = 1 \qquad \ldots(32)$$

$\hat{e}(\alpha,\beta)$ is the vector function representing the interaction of the sample for different components of the angular spectrum at two orthogonal polarisations, (33) and (34).

$$\delta e(\alpha,\beta)_{t\,\parallel} = \frac{1}{\gamma \cdot \left[\beta^2+(\gamma sin\,(\theta)-\alpha cos\,(\theta))^2\right]} \times \left(\left[(\gamma sin\,(\theta)-\alpha cos\,(\theta))^2\right] \cdot T_{t\parallel} + \left[(\beta\gamma cos\,(\theta)-\alpha\beta sin\,(\theta))^2\right] \cdot T_{t\perp}\right) \qquad \ldots(33)$$

$$\delta e(\alpha,\beta)_{t\,\perp} = \frac{1}{\gamma \cdot \left[\alpha^2+(\beta cos\,(\theta)-\gamma sin\,(\theta))^2\right]} \times \left(\left[(\alpha cos\,(\theta))^2\right] \cdot T_{t\parallel} + \left[(sin\,(\theta)-\beta^2 sin\,(\theta)-\gamma\beta cos\,(\theta))\right] \cdot T_{t\perp}\right) \qquad \ldots(34)$$

For converting the angles from the sample to the antenna coordinate system, (35) to (37) and (38) to (40) can be used for the measurement at parallel and perpendicular polarisations respectively.

$$\alpha_s = \alpha cos\,(\theta) - \gamma sin\,(\theta) \qquad \ldots(35)$$

$$\beta_s = \beta \qquad \ldots(36)$$

$$\gamma_s = \gamma cos\,(\theta) + \alpha sin\,(\theta) \qquad \ldots(37)$$

$$\alpha_s = \alpha \qquad \ldots(38)$$

$$\beta_s = \gamma \sin(\theta) - \beta \cos(\theta) \quad \ldots(39)$$

$$\gamma_s = \gamma \cos(\theta) + \beta \sin(\theta) \quad \ldots(40)$$

3.2 Reflection coefficient measurement

Figure A7.2 shows the configuration of the system for measuring reflection coefficient. In this arrangement, the measured parameter is the reflected wave from the sample surface. The same method employed in calculating transmission coefficient can be used to calculate the coupling between two antennas. The induced voltage at the receiving antennas at parallel and perpendicular polarisations are given by (41) and (42).

$$\delta e(\alpha,\beta)_{r\,\parallel} = \frac{1}{\gamma \cdot \left[\beta^2 + (\gamma \sin(\theta) - \alpha \cos(\theta))^2\right]} \times \left(\left[(\gamma \sin(\theta) - \alpha \cos(\theta))^2\right] \cdot \Gamma_{t\parallel} + \left[(\beta\gamma \cos(\theta) - \alpha\beta \sin(\theta))^2\right] \cdot \Gamma_{t\perp}\right) \quad \ldots(41)$$

$$\delta e(\alpha,\beta)_{r\,\perp} = \frac{1}{\gamma \cdot \left[\alpha^2 + (\beta \cos(\theta) - \gamma \sin(\theta))^2\right]} \times \left(\left[(\alpha \cos(\theta))^2\right] \cdot \Gamma_{t\parallel} + \left[(\sin(\theta) - \beta^2 \sin(\theta) - \gamma\beta \cos(\theta)^2)\right] \cdot \Gamma_{t\perp}\right) \quad \ldots(42)$$

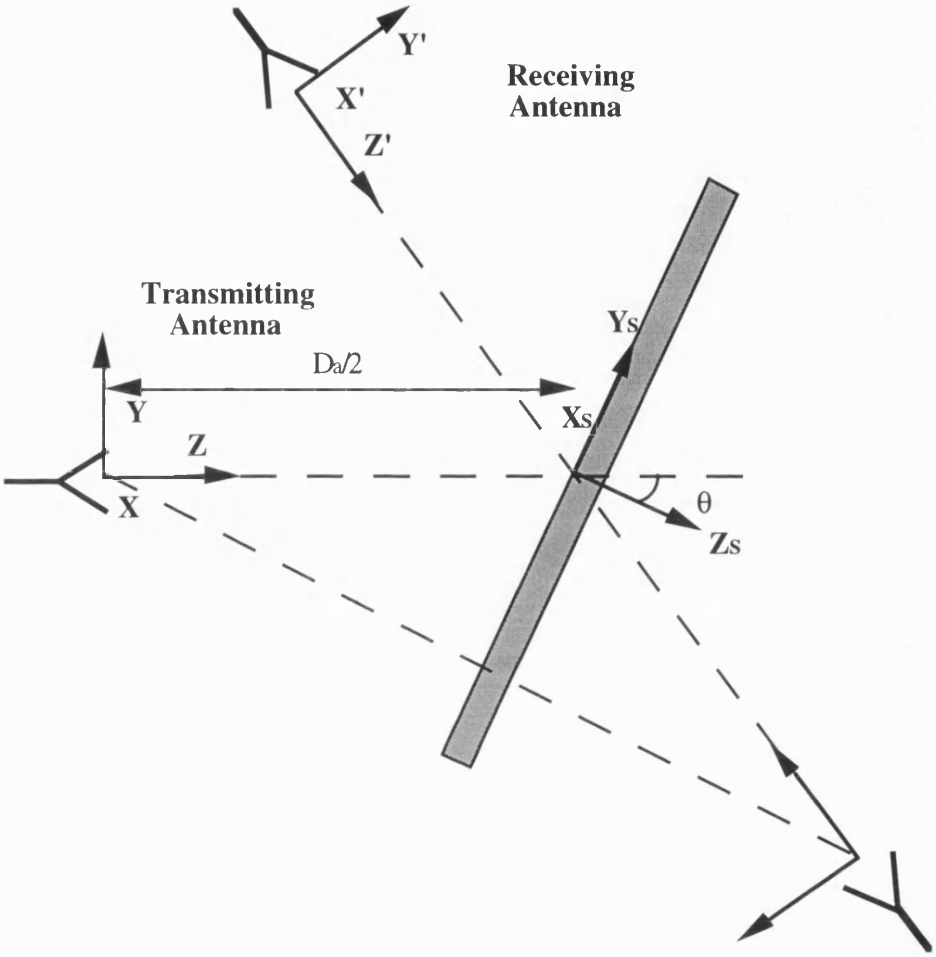

Figure A7.2 Reflection coefficient measurement arrangement.

$\Gamma_{t\parallel}$, and $\Gamma_{t\perp}$ are the reflection coefficients of a slab illuminated by a uniform plane wave, (5) and (6). For transferring the coordinate system, equations 35 to 40 are employed. In the general case, multiple reflections within the slab are taken into account. If the multiple reflection within the slab can be ignored, the calculations should be modified. In this case, equations 3 to 6 are replaced by (43) to (46) to consider the multiple reflections, (*thin* slabs).

$$T_{t\parallel} = P\,(1-\Gamma_{\parallel}^{2}) \qquad \ldots(43)$$

$T_{t\perp} = P\,(1-\Gamma_{\perp}^{2})$ ...(44)

$\Gamma_{t\parallel} = \Gamma_{\parallel}$ ...(45)

$\Gamma_{t\perp} = \Gamma_{\perp}$ ...(46)

Appendix 8

Angular spectrum model

In the near-field region, the transmission and reflection coefficients of a slab can be calculated from the general coupling integral, (appendix 7). In the free-wave technique, the complex permittivity and permeability of a slab are calculated from the measured transmission and/or reflection. The plane wave model describes the mathematical relationship between the material properties and the measured parameters in the far-field. Although this model can be used in most of cases, the accuracy is degraded if the measurement is carried out in the near-field region. In the general case, a closed mathematical expression for the coupling integral cannot be found, and the use of numerical methods for determining this integral is inevitable. The aim of this appendix is to study the wavefront curvature error and to discuss limitations in implementing the angular spectrum model.

In free-wave techniques, we measure the transmitted wave through and reflected wave from the sample surface, then these values are normalised with respect to the measured standard impedances. In simulating the transmission and reflection coefficients of a slab in the near-field region, different stages of the measurement process should be simulated by the angular spectrum model. Therefore, the reflected wave from a metal sheet and the transmitted wave associated with the empty sample holder should be calculated by the angular spectrum model. Then, the simulated transmitted and reflected waves associated with the sample are normalised with respect to the simulated calibrated measurement.

The coupling integral is determined only for the visible angles, ($-1<\alpha$ *and* $\beta<1$). The Fourier transform of the aperture excitation is usually calculated by the Fast Fourier Transform technique. The FFT calculates the Fourier transform of a function at a number of discrete points. As we determine the coupling integral for the visible angles, only a fraction of the samples delivered by the FFT are used. In FFT algorithms, the sampling rate

is a function of the aperture excitation, and increasing the number of samples in one domain does not change the intervals between the samples in the other domain. In order to increase the number of useful samples in the Fourier transform of the aperture excitation, we have to extend the aperture size by the padding technique. In this technique, a number of samples with zero magnitude are added to each side of the aperture. The error associated with FFT algorithms is a function of the number of samples, aperture excitation and aperture size. For the required accuracy in the FFT algorithms, a sufficient number of samples should be considered in the calculation. Regarding the fact that only a fraction of this number of samples are used, taking two dimensional Fourier transform requires a great computation time which increases very rapidly by increasing the number of samples. The coupling integral determined by numerical methods, and the numerous complex mathematical operations performed at each step causes computation of transmission and reflection coefficient by the angular spectrum model to become a time consuming process.

The integrand in the coupling integral includes an exponential term. The magnitude of this terms is unity, but its phase is a function of antenna distance and spatial angle. The rate of change in the phase of this term with changing α and β is proportional to the antenna distance. The coupling integral can be simplified by using a stationary phase technique for long antenna distances, but the use of a numerical method for determining transmission and reflection coefficients is inevitable in the near-field. In practice, the rate of variation of this term defines the required number of points in computing the coupling integral. For a given degree of accuracy in computing the coupling integral, the number of sampling points should be increased by increasing the antenna distance, otherwise the computation error increases considerably for large antenna distances. The computation error, which is mainly due to sampling the integrand function lower than the required rate, causes oscillation in the calculated values.

In the free-wave measurement technique, the complex permittivity or permeability of the sample cannot be expressed by a closed mathematical expression. The multi-valued nature of the transcendental equations linking the sample properties to the measured parameters causes the use of numerical iterative methods to be inevitable. For a given set of measured transmission and/or reflection coefficients, the best matched set of permittivity and permeability can be found by iterative numerical methods. In these techniques, the computation accuracy is an important factor in converging to the iterative numerical

method. The accuracy in calculating transmission and reflection coefficients should be much higher than the required total accuracy in permittivity and permeability, otherwise numerical algorithms fail to converge. If the angular spectrum model is used, a powerful computer and a long computation time are required. In general cases, the high computation time outweighs the accuracy improvement delivered by the angular spectrum model.

In most cases, the wavefront curvature is not the most significant sources of error, therefore employing the angular spectrum model does not improve the accuracy considerably. The antenna distance is a key factor in evaluating the effectiveness of this model in free-wave measurements. The Rayleigh distance is a simple measure for estimating the impact of the wavefront curvature. This criterion ($2D^2_{max}/\lambda_o$) gives the minimum distance from an aperture for 22.5° error in the wavefront curvature. λ_o is the free-space wavelength, and D_{max} is the maximum size of the aperture. If the ratio of the antenna distance to the Rayleigh distance is greater than 2, the angular spectrum model does not improve the accuracy considerably and the plane wave model can be used. For the compact measurement systems, where this ratio is less than 1, the wavefront curvature error becomes a significant error term. In this case, the angular spectrum model improvement may be worth employing.

Focusing the beam can reduce the diffraction of the wave from the edges of the sample. If multiple reflections within the lenses and mismatches at the interfaces of the air and the dielectric lenses are ignored, the dielectric lenses can be introduced to the angular spectrum model by an appropriate mathematical function modifying the aperture excitation. It is worth noting that the antenna distance is 300 mm and the aperture size is 25x35 mm in the prototype system. At 30 GHz the Rayleigh distance is 250 mm, and the minimum antenna distance for ignoring the wavefront curvature is 500 mm. Therefore, the antennas are not located sufficiently far from each other to ignore the wavefront curvature.

Appendix 9

Near-field measurement error

A.91 Introduction

The aim of this appendix is to show the impact of the wavefront curvature error in free-wave measurements. The differences between transmission and reflection coefficients calculated by the angular spectrum and the plane wave models are simulated for three samples. Sample 1 is loss-less dielectric ($\varepsilon_r=2.6$) representing a low-loss dielectric at millimetre wavelengths. Sample 2 is also lossless dielectric ($\varepsilon_r=10.4$) representing a typical high dielectric constant material, and the third sample is a lossy ferrite($\varepsilon_r=7.5\text{-}j0.5$, $\mu_r=0.8\text{-}j0.15$). The wavefront curvature error in these samples are simulated for both cases where the sample is treated as *thin* and *thick* slabs.

A9.2 Sample 1

Sample 1 is a lossless dielectric ($\varepsilon_r=2.6$), and the specifications of the measurement system can be found in chapter 9. The diverging beam is denoted to the antenna without a lens. The use of a lens to compensate the wavefront curvature at the antenna aperture plane is defined as a parallel beam, and a converging beam is denoted for the case where a lens is used to focus the wave at a focal distance in front of the antenna.

Figures A9.1 and A9.2 show the expected error in sample 1. As shown, the error approaches zero by increasing the antenna distance. It can also be concluded that focusing the beam on a small area on the sample surface increases the wavefront curvature error, since the associated angular spectrum with a lens antenna is spread over a wider interval of spatial angles with respect to the sample antenna without a lens.

A.9.3 Sample 2

Sample 2 is a lossless dielectric (ε_r=*10.4*) with thickness of 10 mm. The electrical length of this sample is twice the electrical length of sample 1. Figures A9.3 and A9.4 show the wavefront error for sample 2 treated as a thin and thick slab respectively.

A9.4 Sample 3

Sample 3 is a lossy ferrite representing a typical material made by mixing the ferrite powder and a bonding resin, (ε_r=*7.5-j0.5 and* μ_r=*0.8-j0.15*). Figures A9.5 and A9.6 show the error due to the wavefront curvature in this sample. The lossy properties of this sample mean that multiple reflections within the sample can be ignored. As can be seen, treating this sample as a thin or thick slab give similar results, since the multiple reflections do not contribute effectively in constituting transmission and reflection coefficients.

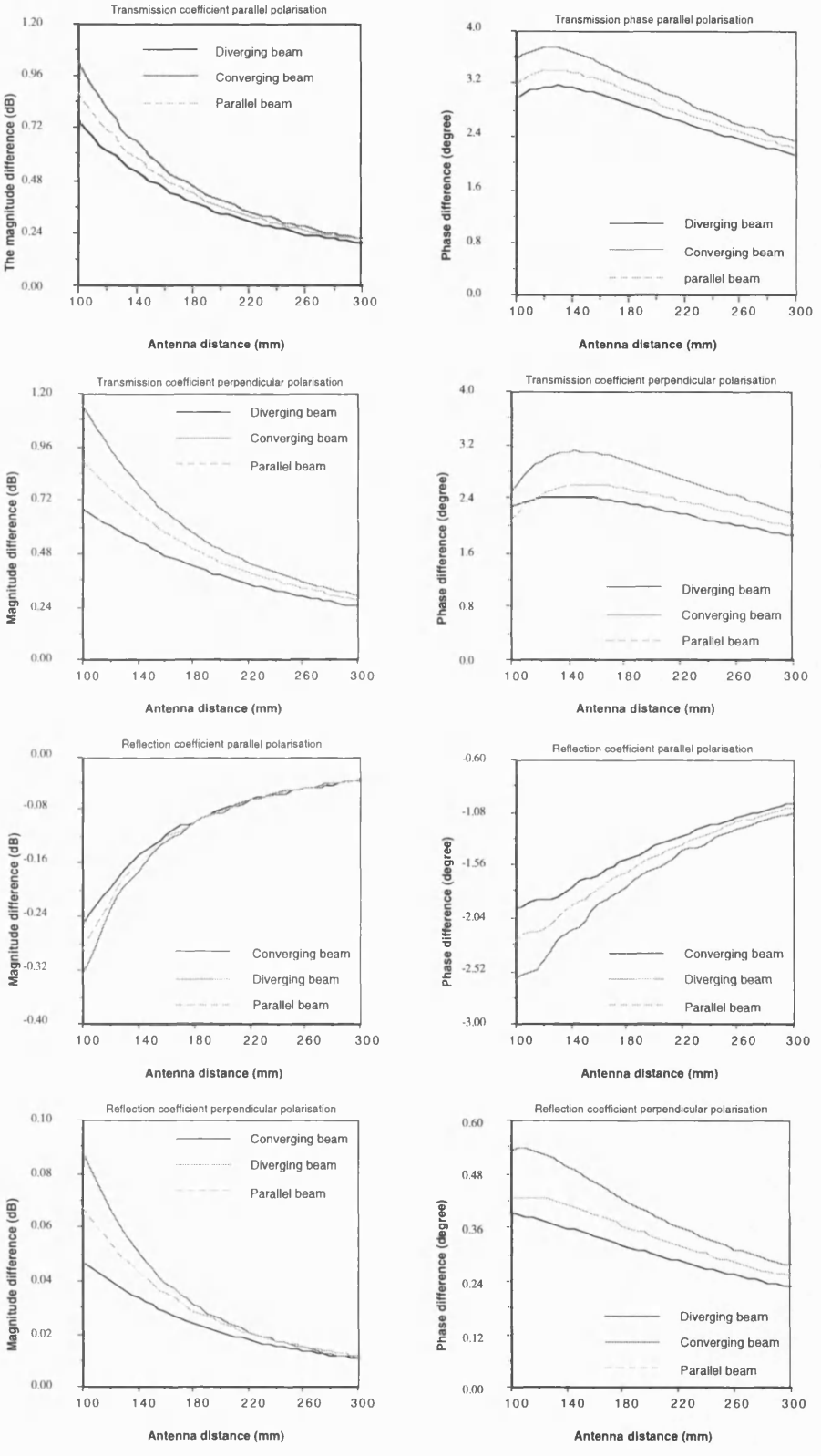

Figure A9.1 Wavefront curvature error in sample 1 (ε_r=2.6, 10 mm thickness) treated as a thin slab.

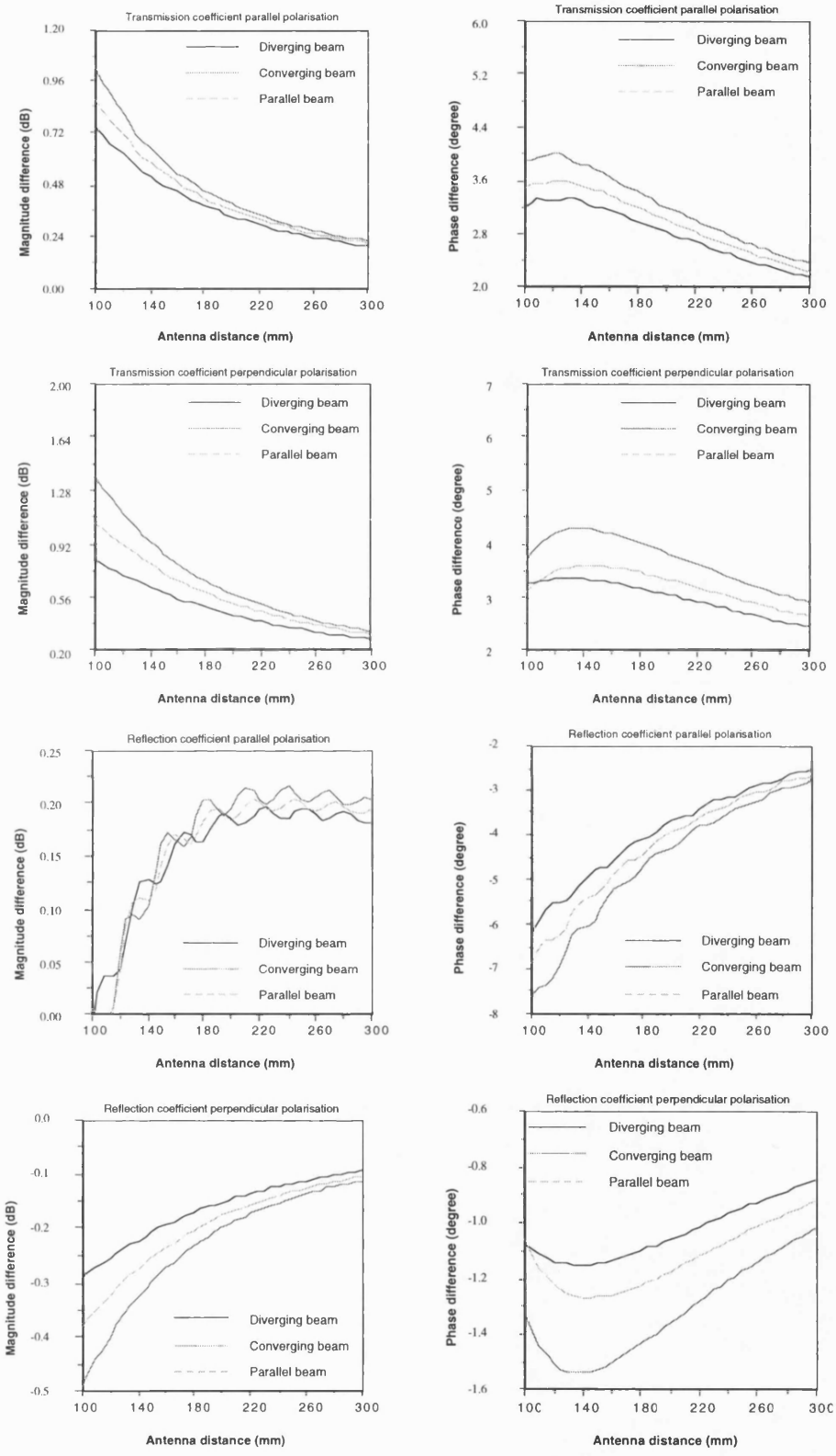

Figure A9.2 Wavefront curvature error in sample 1 (ε_r=2.6, 10 mm thickness) treated as a thick slab.

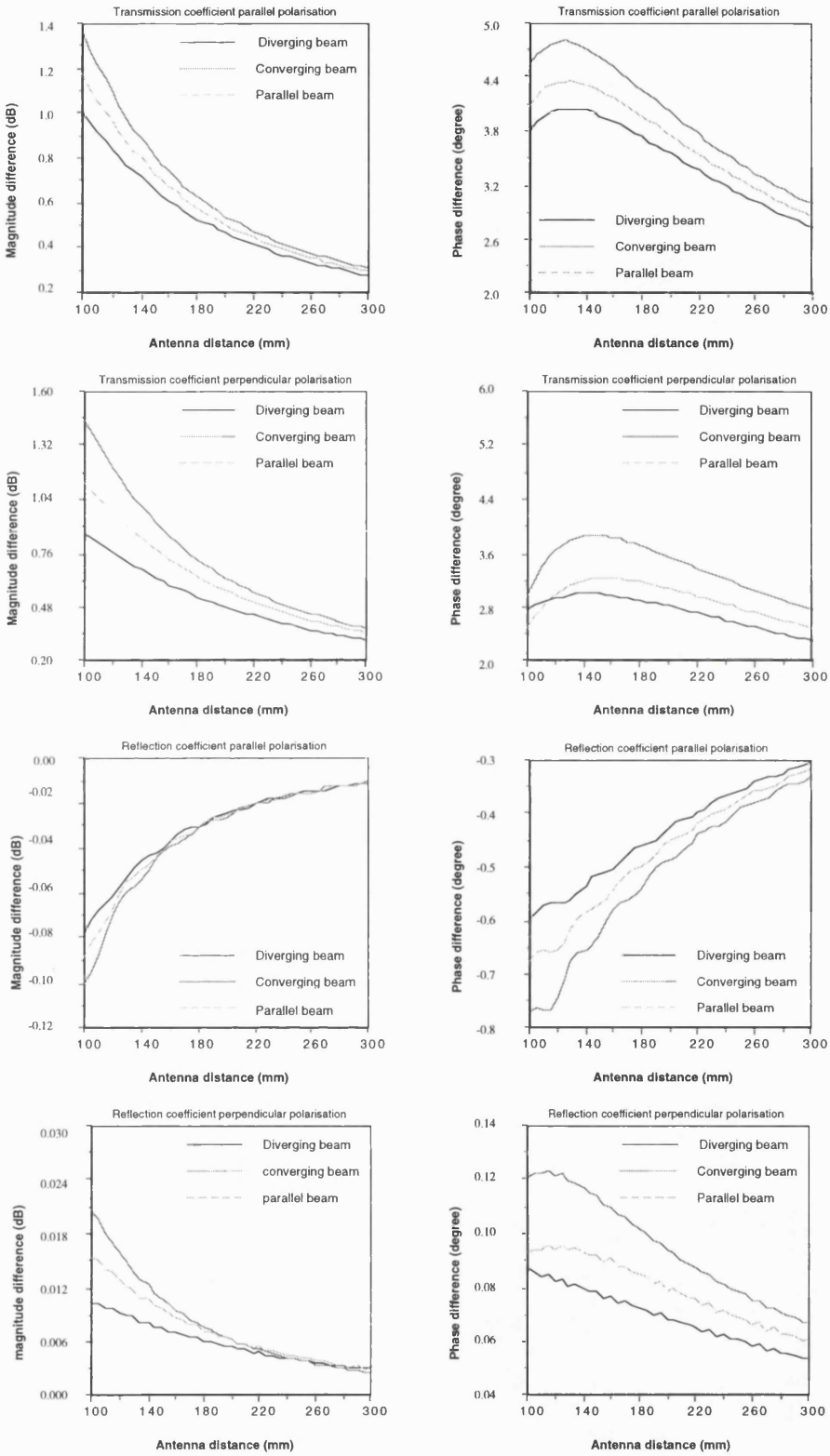

Figure A9.3 Wavefront curvature error in sample 2 (ε_r=10.4, 10 mm thickness) treated as a thin slab.

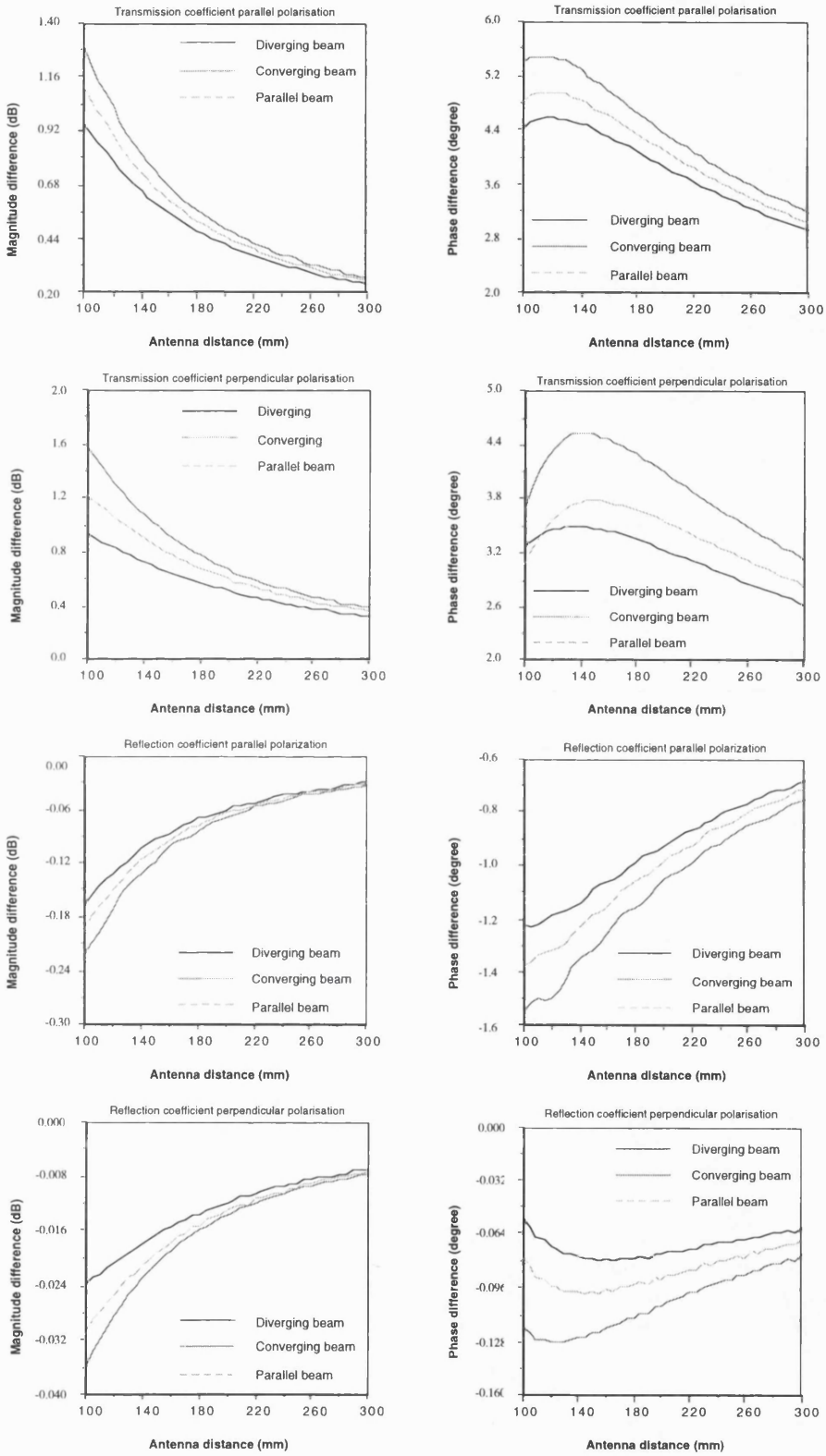

Figure A9.4 Wavefront curvature error in sample 2 (ε_r=10.4, 10 mm thickness) treated as a thick slab.

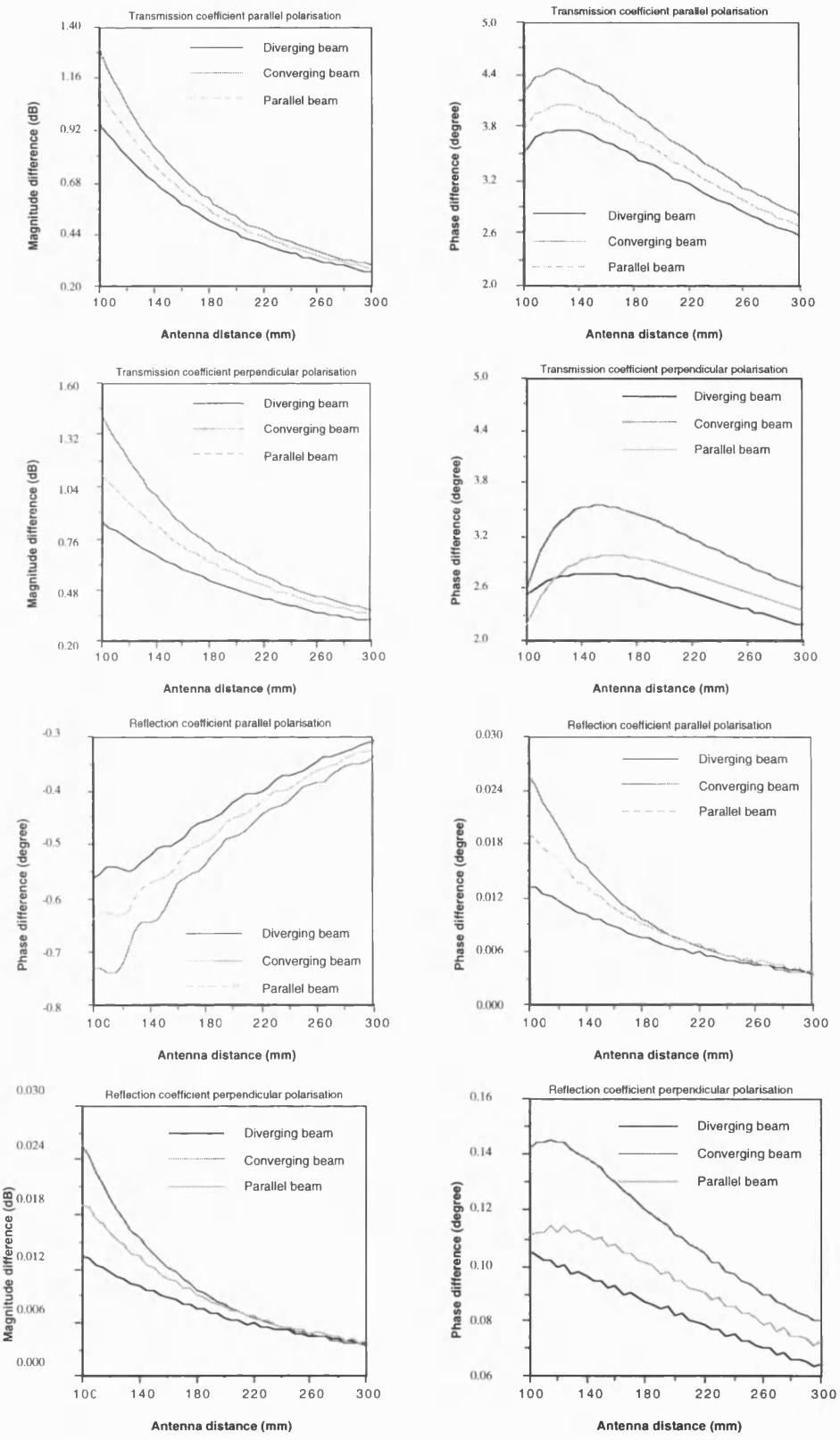

Figure A9.5 Wavefront curvature error in sample 3 treated as a thin slab, (ε_r=7.5-j0.5, μ_r=0.8-j0.15 and 10 mm thickness).

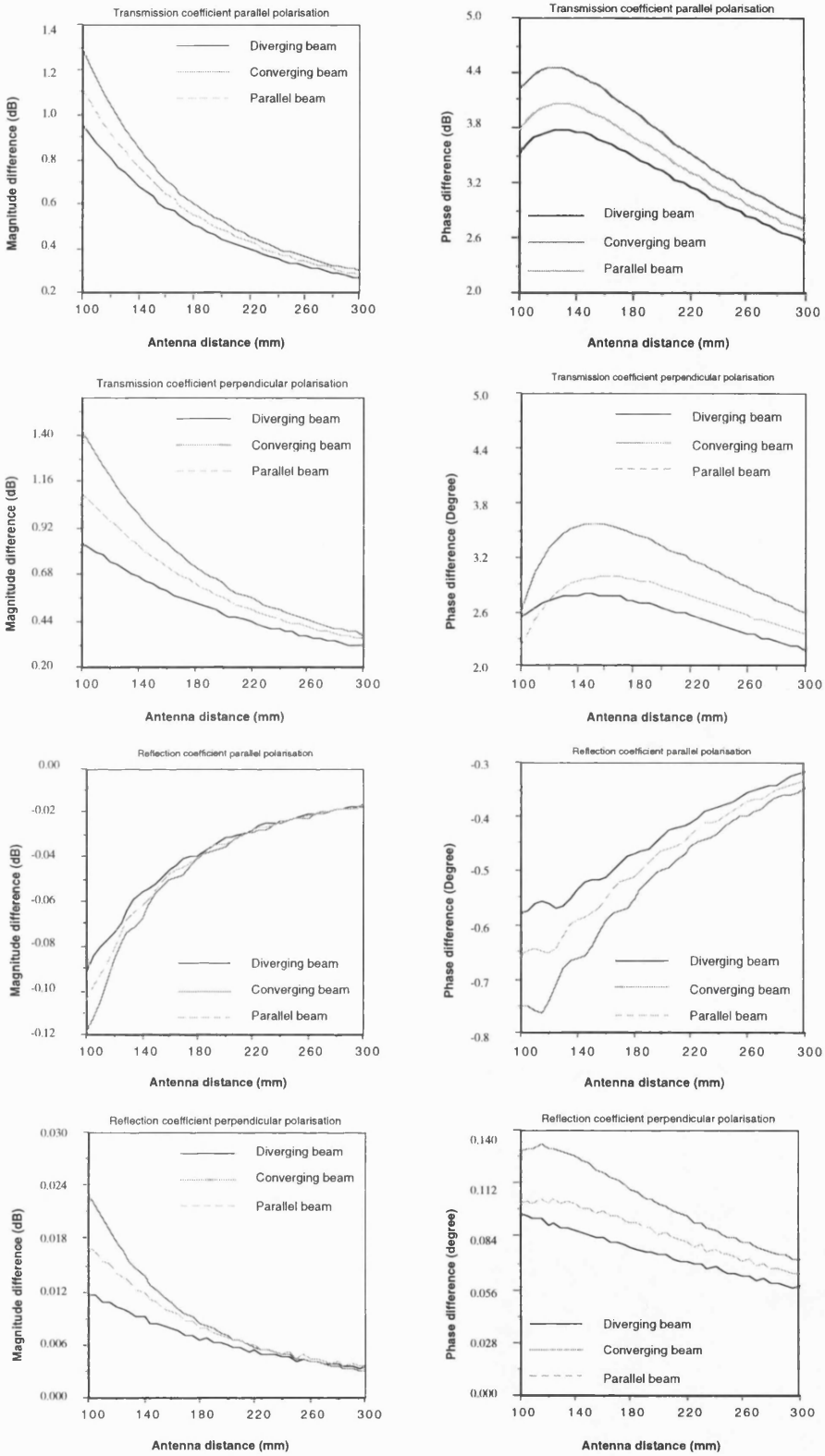

Figure A9.6 Wavefront curvature error in sample 3 treated as a thick slab, (ε_r=7.5-j0.5, μ_r=0.8-j0.15 and 10 mm thickness).

Appendix 10

Near-field measurement error simulation

In this appendix, the total error in permittivity and permeability due to the near-field measurement is demonstrated. In this simulation, a pair of square aperture antennas with dimension of 25x35 mm are used, and the diffracted wave is focused on the sample surface by using different dielectric lenses. The error in the measurement of the material properties in three samples are simulated. Sample 1 is a lossless dielectric ($\varepsilon_r=2.6$) representing low-loss dielectric materials at millimetre wavelengths. Sample 2 is lossless dielectric ($\varepsilon_r=10.4$) representing a typical high dielectric constant material, and the third sample is a lossy ferrite ($\varepsilon_r=7.5\text{-}j0.5$, $\mu_r=0.8\text{-}j0.15$). The error in permittivity and permeability of these samples while treated both as thin and thick slabs are simulated, figures A10.1 to A10.6.

In this simulation, the permittivity and permeability of the sample are calculated from the measured transmission coefficient at two orthogonal polarisations. In *thin* sample measurements, the total error in the measured magnetic and electric properties are functions of the electrical length of the slab. At frequencies such that the electrical length of the sample is a multiple of 180°, the reflection coefficient is minimum and the transmission coefficient is maximum. At these frequencies, the reflected wave does not provide useful information, while the transmission coefficient can still be used for calculating the product of permittivity and permeability of the sample.

The angular spectrum model gives the transmission and reflection coefficients associated with a slab illuminated by a spectrum of plane waves. This model can be used for calculating the magnetic and electric properties of a slab in the near-field region, but it needs a huge computation time. In order to show the effect of the wavefront curvature on the calculated permittivity and permeability, the simulated transmission and reflection coefficient of a slab with known properties in the angular spectrum model are used to calculate the sample properties by the plane wave model. As mentioned, the total error in

the measurement of the material properties depends on the calculations method, and each method is appropriate for calculating a certain group of parameters. As discussed, the transmission method delivers the product $\mu_r\varepsilon_r$ more accurately than μ_r and ε_r individually. Therefore, we consider $\delta(\mu_r\varepsilon_r)$ as a measure in estimating the wavefront curvature error.

As shown, the wavefront curvature error approaches zero by increasing the antenna distance. It is worth noting that the computation error can be ignored if a considerable number of points is considered in the numerical algorithms used for calculating the coupling integral. The computation error also increases by increasing the antenna distance and results in an oscillation superimposed on the actual values. As the main aim of this appendix is to demonstrate the effect of the wavefront curvature on the calculated permittivity and permeability, the computation error is ignored by extending the antenna distance to a limited distance. The use of FFT algorithms instead of the Fourier Transform also introduces some errors to the simulated values which are ignored.

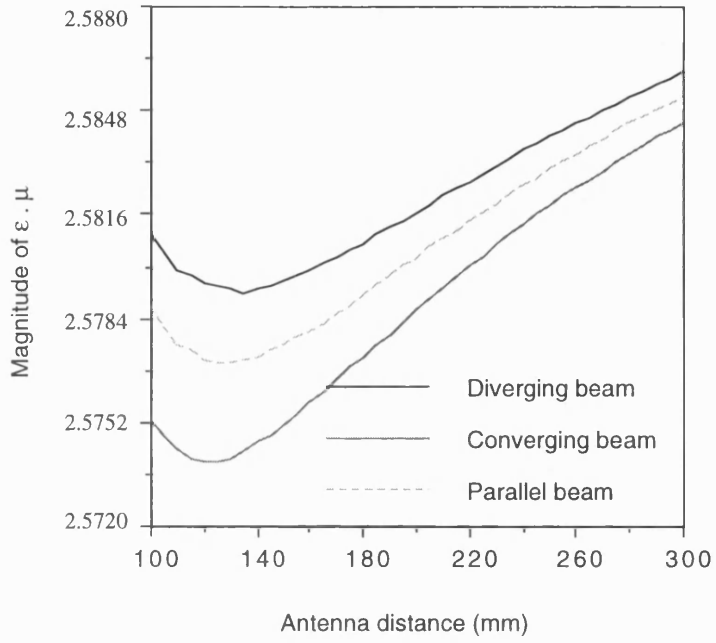

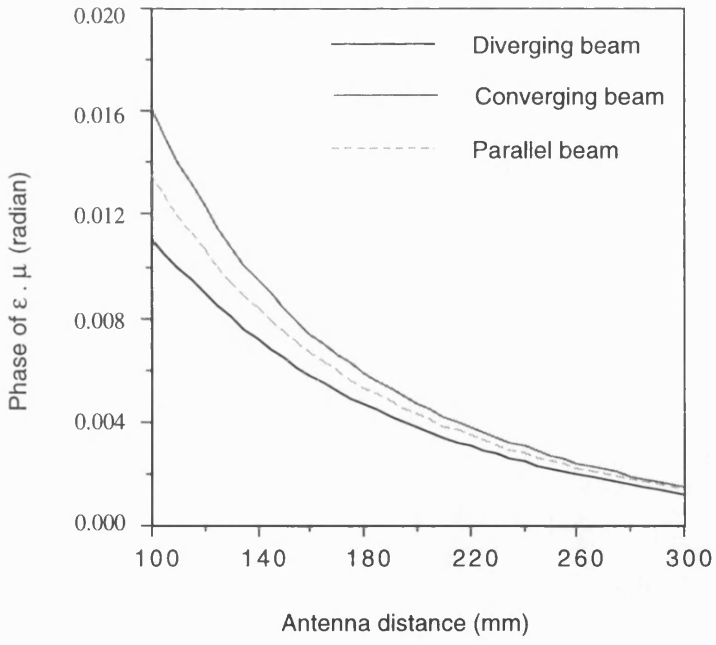

Figure A10.1 Wavefront curvature error in sample 1 ($\varepsilon_r\mu_r$ =2.6) treated as a thin slab for different antenna distances.

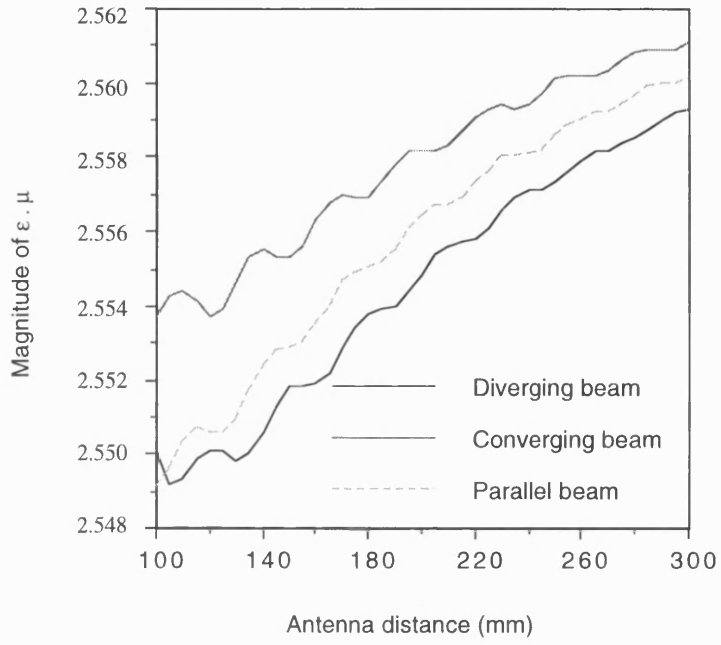

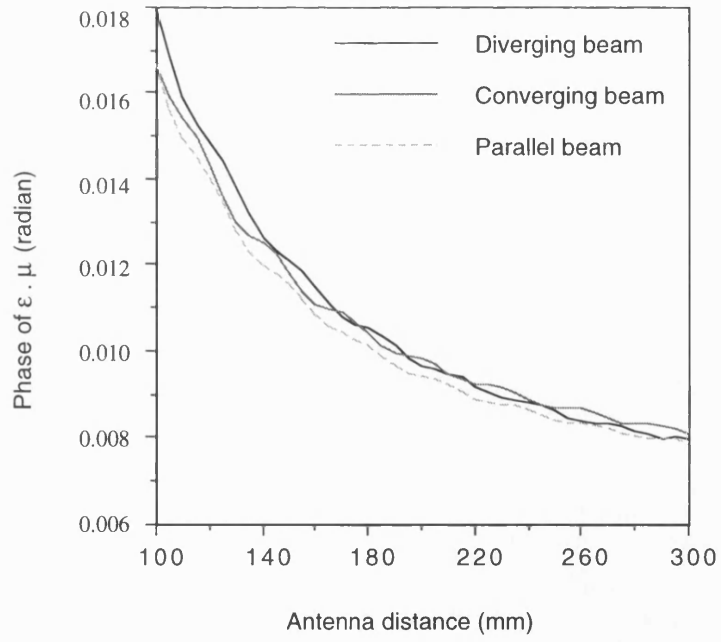

Figure A10.2 Wavefront curvature error in sample 1 ($\varepsilon_r.\mu_r$ =2.6) treated as a thick slab for different antenna distances.

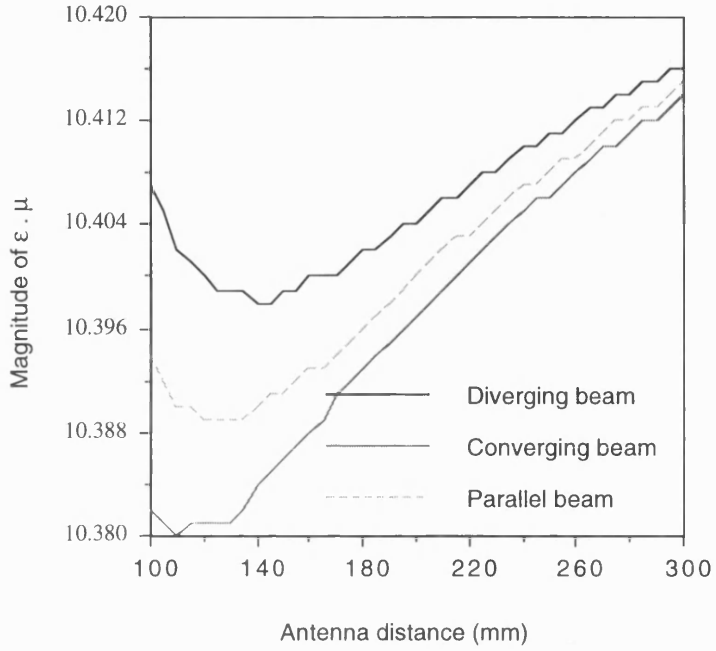

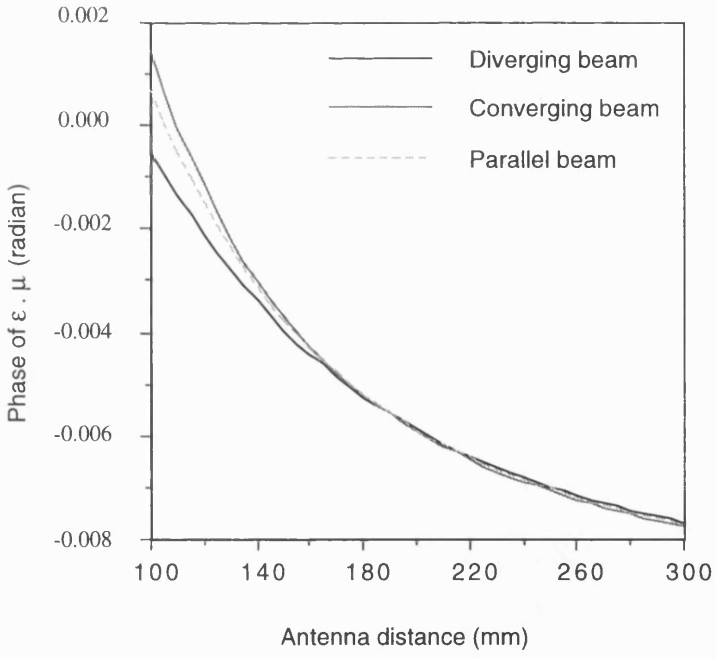

Figure A10.3 Wavefront curvature error in sample 2 ($\varepsilon_r\mu_r$ =10.4) treated as a thin slab for different antenna distances.

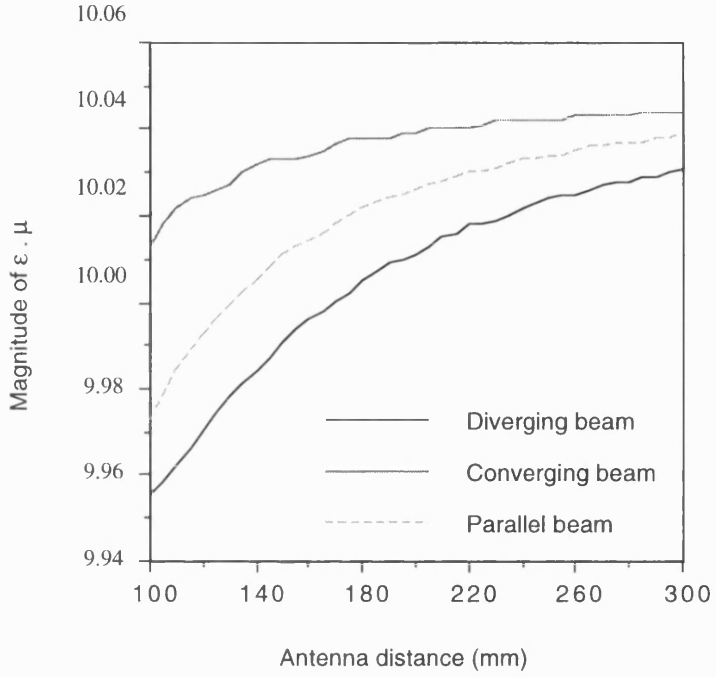

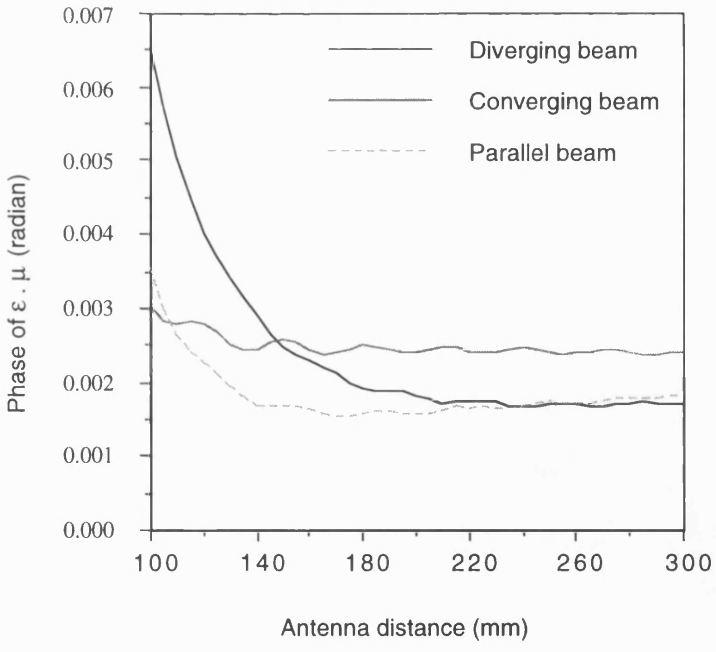

Figure A10.4 Wavefront curvature error in sample 2 ($\varepsilon_r\mu_r$ =10.4) treated as a thick slab for different antenna distances.

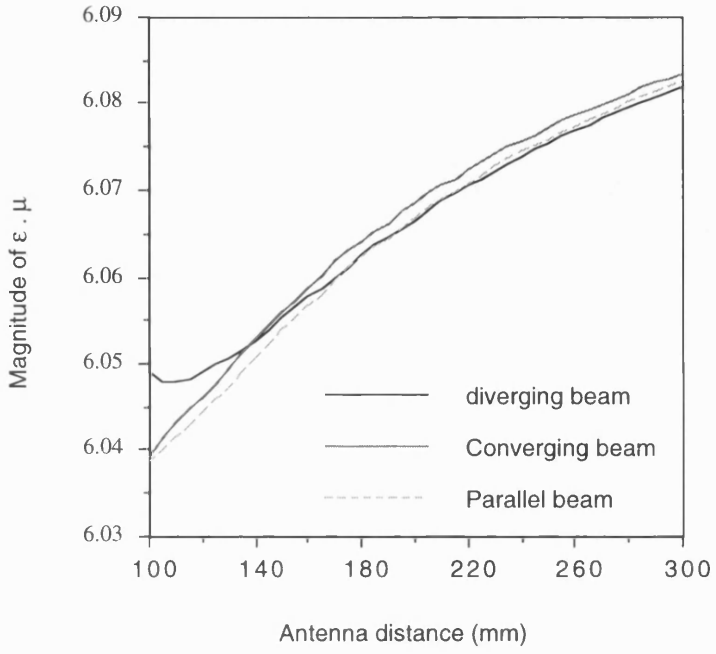

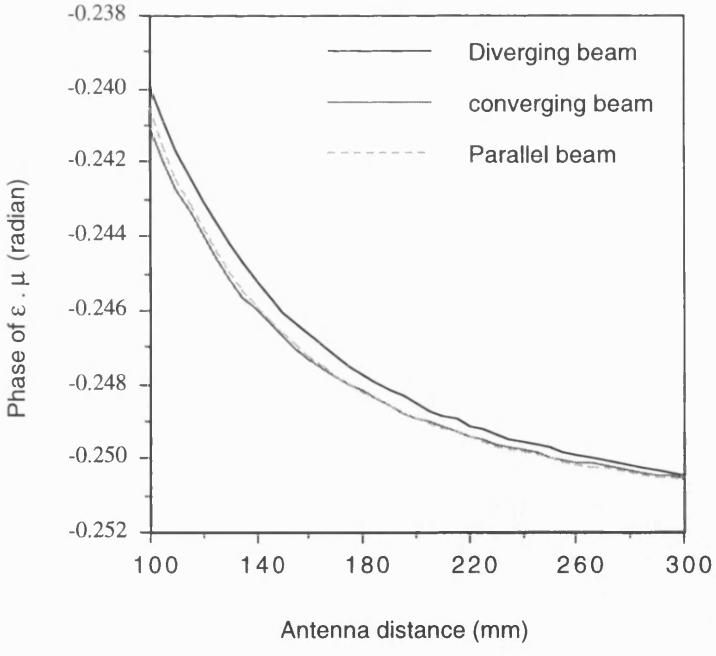

Figure A10.5 Wavefront curvature error in sample 3 ($\varepsilon_r\mu_r$ =6.12 -j0.251) treated as a thin slab for different antenna distances.

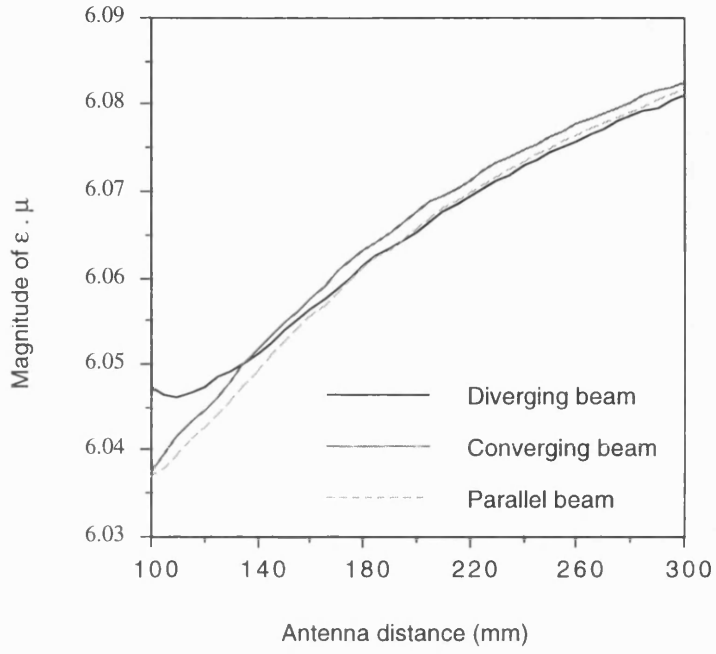

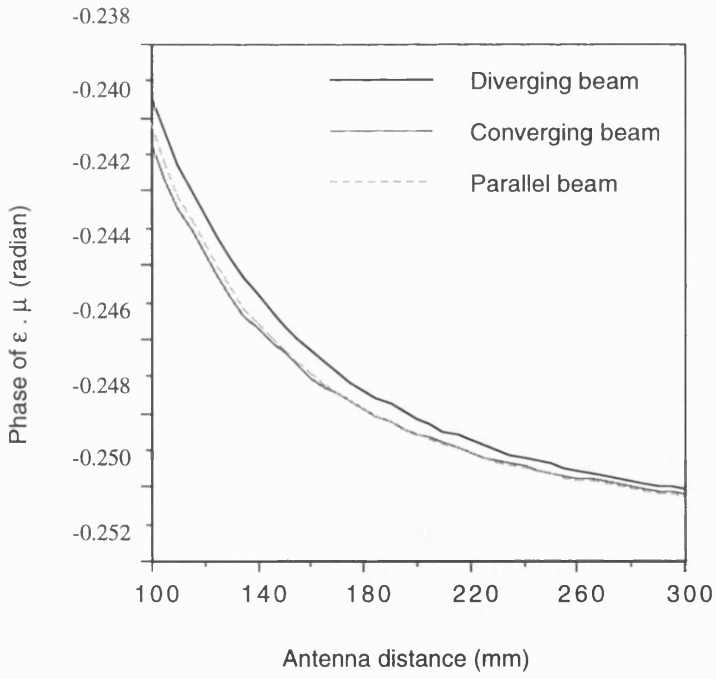

Figure A10.6 Wavefront curvature error in sample 3 ($\varepsilon_r\mu_r$ =6.12 -j0.251) treated as a thick slab for different antenna distances.

Appendix 11

Minimum sample size

In free-wave measurement, diffraction of the wave from the edges of the sample constitutes one of the sources of error. The propagated wave has its maximum magnitude at the antenna axis, and the field strength decreases by moving towards the sample edges. The field strength on the sample surface is a function of sample size, antenna distance, aperture excitation, frequency and the incident angle. A dielectric lens or a microwave reflector can be used to focus the wave on the sample surface. In this appendix, the minimum sample size and the effect of dielectric lenses for reducing the diffraction of the wave from the edges of the sample are discussed.

The angular spectrum expresses the diffracted wave from an aperture as a set of uniform plane waves travelling at different angles. For a given aperture, the angular spectrum can be calculated by taking the Fourier transform of the field distribution in the aperture plane. At a given distance in front of the aperture, the electric fields can be calculated from the angular spectrum. In this chapter, the magnitude of the electric field at the two orthogonal polarisations is calculated by a computer program.

In this simulation, the parameters associated with the prototype measurement system are considered, which can be found in chapter 9. The size of the antenna used is 25x35 mm, and its phase centre is located at 90 millimetres from the aperture plane. A dielectric lens can be used to form the diffracted wave and focus it on the sample surface. In this analysis, the electric field is assumed to be uniform in the E-plane (smaller dimension) and to have cosine variation in the H-plane (larger dimension).

If the antenna without any lens is used, the propagated wave expands spherically from the antenna phase centre (*diverging beam*). The use of a dielectric lens compensating the wavefront curvature generate a plane wavefront at the antenna aperture, (*parallel beam*).

The diffracted wave can be focused at the focal distance in front of the aperture, (*converging beam*). In this case, two identical lenses which are used for parallel beams are placed in front of a antenna. In this arrangement, the focal plane is equal to the antenna phase centre (90 mm). Figure A11.1 shows different arrangements of the antenna. It is worth mentioning that the dielectric lens used is designed on the basis of ray theory, and multiple reflection within the lens is ignored.

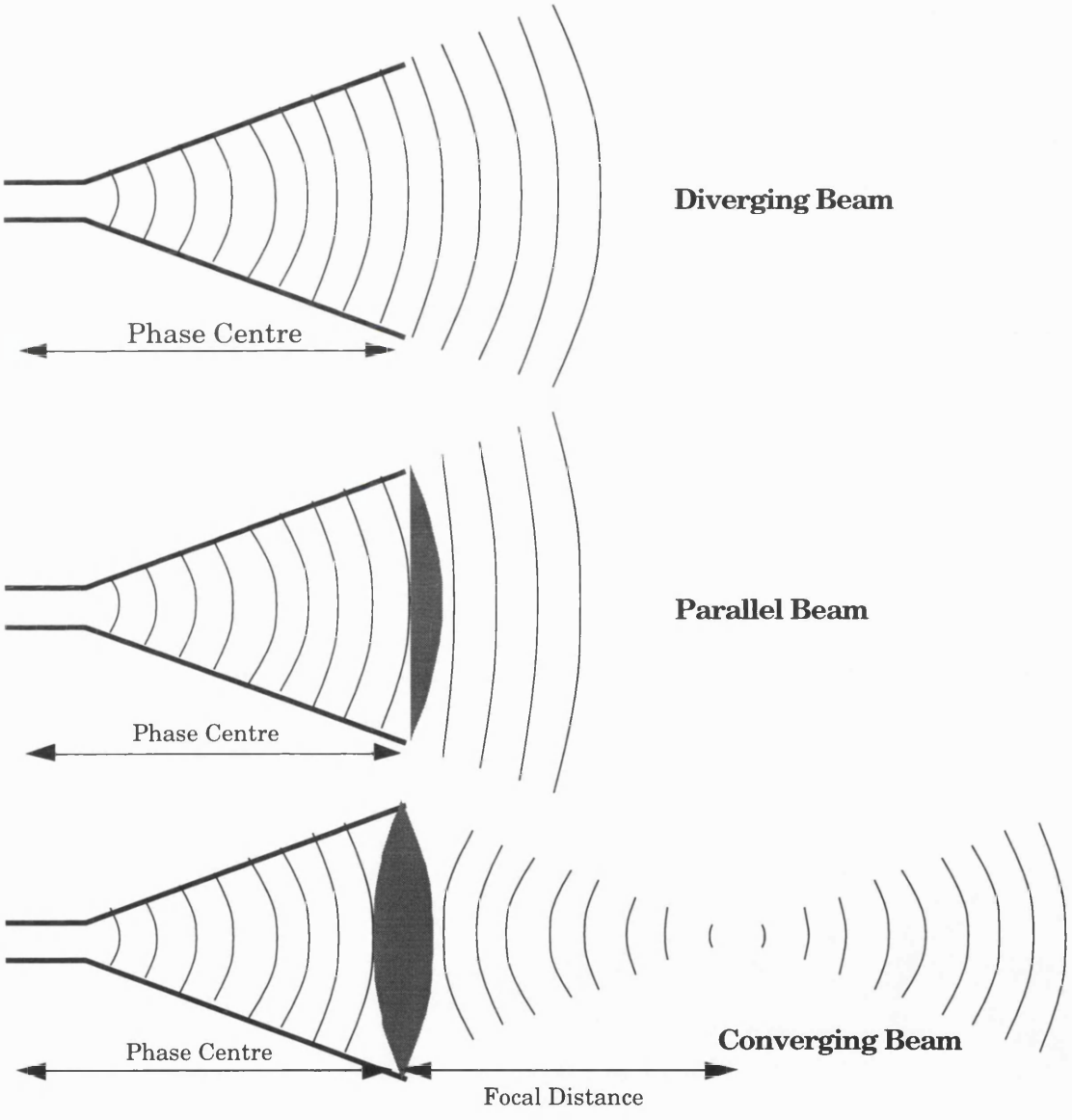

Figure A11.1 Focusing the diffracted wave by a dielectric lens.

Ray theory can give a realistic account of the behaviour of a lens, if the wavelength is much smaller than the aperture size. Multiple reflections within the lens and the lens mismatches also degrade the focusing effect of the lens.

The accuracy of the numerical methods used for calculating the electric field contour plots in front of an aperture is a function of the number of calculating points in the numerical algorithms used for this purpose. Regarding the limitations on the computer memories and the computation time, the curves associated with contours of -40 dB or less are not very accurate and should be treated cautiously.

Figures A11.2 to A11.4 show the contour mapping of the diffracted wave from a standard rectangular aperture with the different lenses at 30 GHz. Regarding the small size of the aperture ($3.5\lambda x2.5\lambda$), the wave at the front of the antenna is not well collimated and the beam waist is quite large. In the prototype measurement system, the sample is placed a distance of 15 cm from the aperture plane. At this distance and in the H-plane, the -30 dB beam waist is 40mm, 35mm and 35mm for converging, parallel and diverging beams respectively. The -30dB beam width in this axis is 53mm, 52mm and 50 mm for converging, parallel and diverging beams respectively. The quoted values are for normal incidence, and the footprint of the antenna on a slab at oblique incidence can be found by dividing them by the cosine of the incident angle.

From the simulated results, we can conclude that the use of dielectric lenses does not reduce the -30 dB beam width considerably, though it concentrates the beam more in the central area. Regarding the aperture shape and the tapering of the field only in one direction, the beam has different widths in the different plane of polarisations. At 45° incident angle, the minimum sample diameter for -30 dB and -40 dB attenuation of the field at its edges is 51 mm and 71 mm respectively.

The error in the reflection and transmission coefficient measurements is a function of the energy associated with diffraction of the wave from the edges of the sample. Although the attenuation of the wave at the edges of the sample can be considered as a measure for estimating the minimum sample size, the changes of the field strength and the concentration of the energy on the sample surface should also be taken into account. For the antenna used, the use of a lens for focusing the beam does not reduce the -30 dB or -40 dB beam

waists considerably, but the total error due to the diffraction of the wave from the edges of the sample is reduced by concentrating the wave in the antenna axis.

Increasing the aperture size improves the focusing capability of the dielectric lenses. Figure A11.5 and A11.7 show the electric field contour plots at 30 GHz in a larger apertures. If the aperture size increases by a factor of 4, the -20 dB beam waist is 2.5 mm and 5.1 mm at H-plane and E-plane respectively. Increasing the aperture size by a factor of 6 generate a smaller footprint of the antenna on the sample surface, and the -20 dB beam waist at normal incidence is 3.3 mm and 4.8 mm at H-plane and E-plane respectively.

Although the use of dielectric lenses causes the main portion of the energy to be concentrated in the antenna axis, the sidelobes could still cause a problem. In the general case, the mismatches of the lens surface and the multiple reflections within the lens degrade the antenna performance. Regarding the difficulties in making matched lenses working in a wide frequency band, the use of a microwave reflector is preferred whenever the restriction on the antenna size is not an important factor.

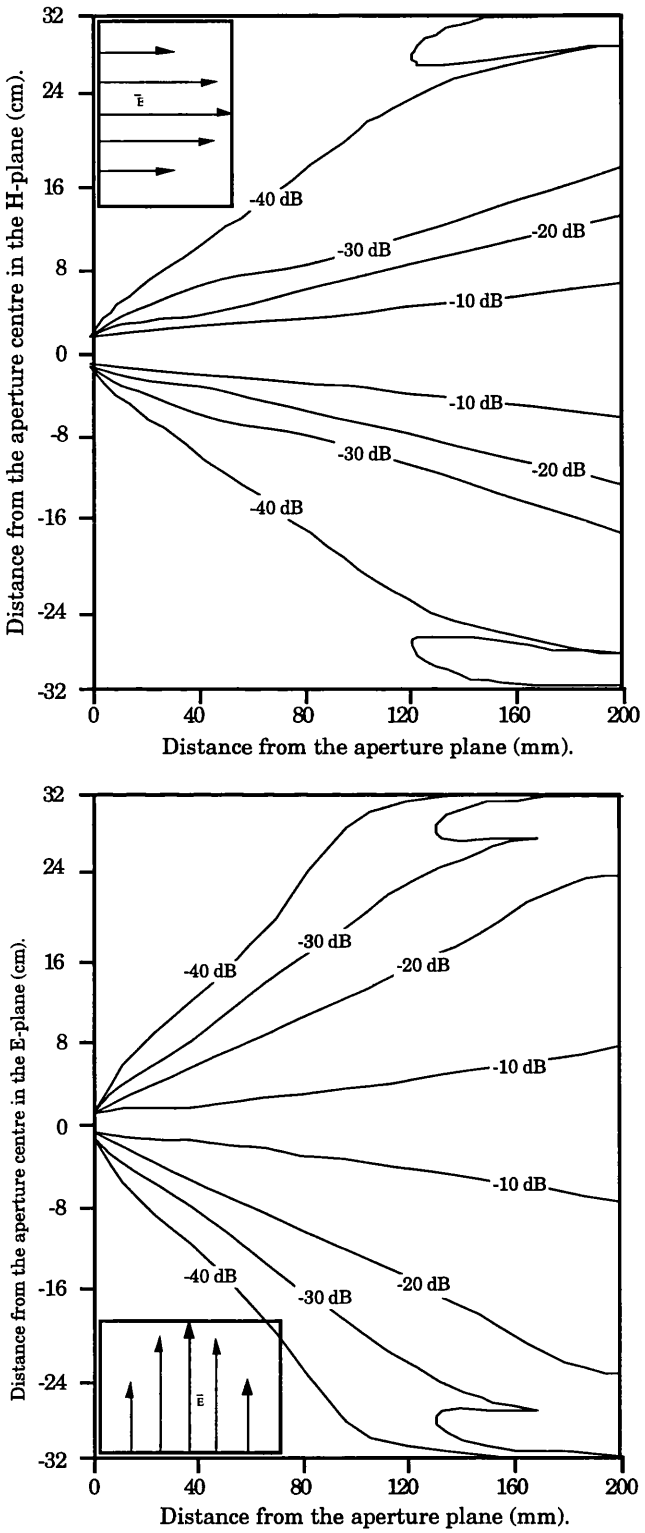

Figure A11.2 H-plane and E-plane contour mapping of the electric field for a square aperture (25x35 mm) at 30 GHz, diverging beam.

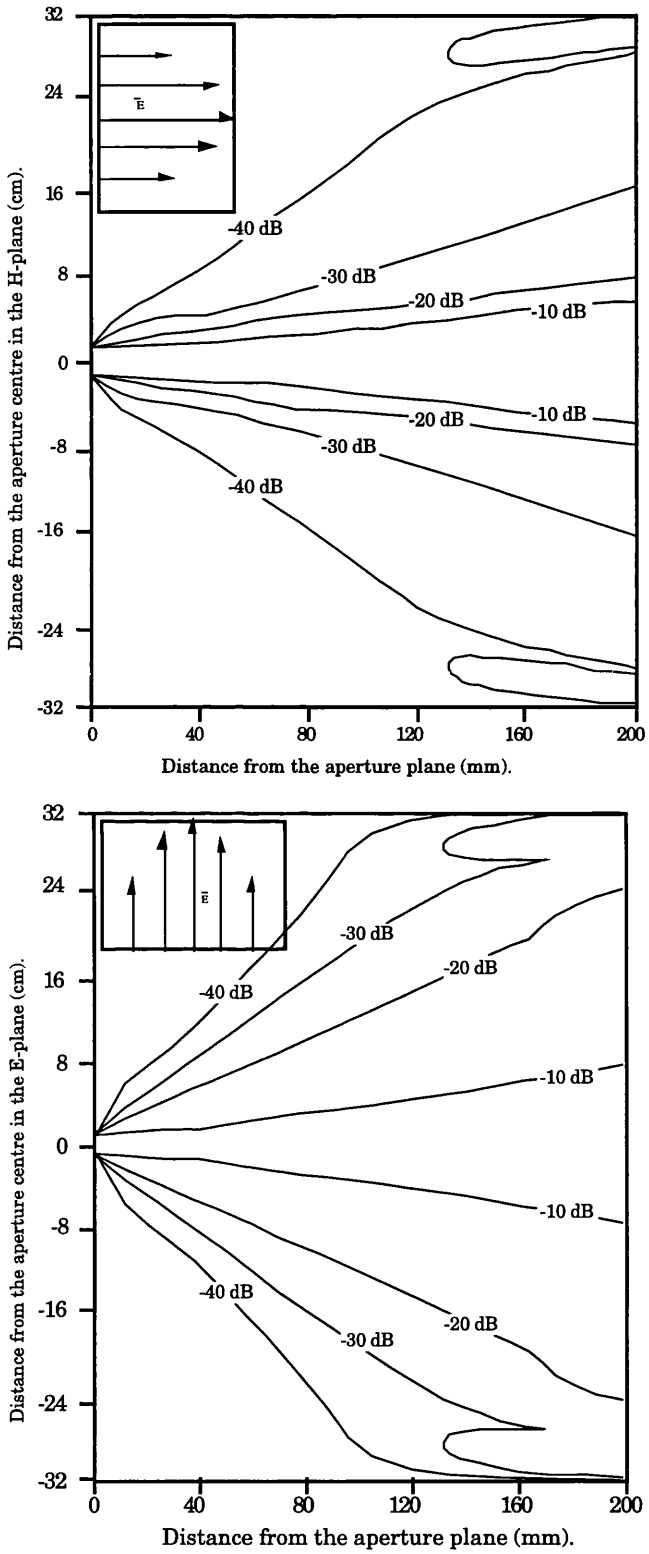

Figure A11.3 H-plane and E-plane contour mapping of the electric field for a square aperture (25x35 mm) at 30 GHz, parallel beam.

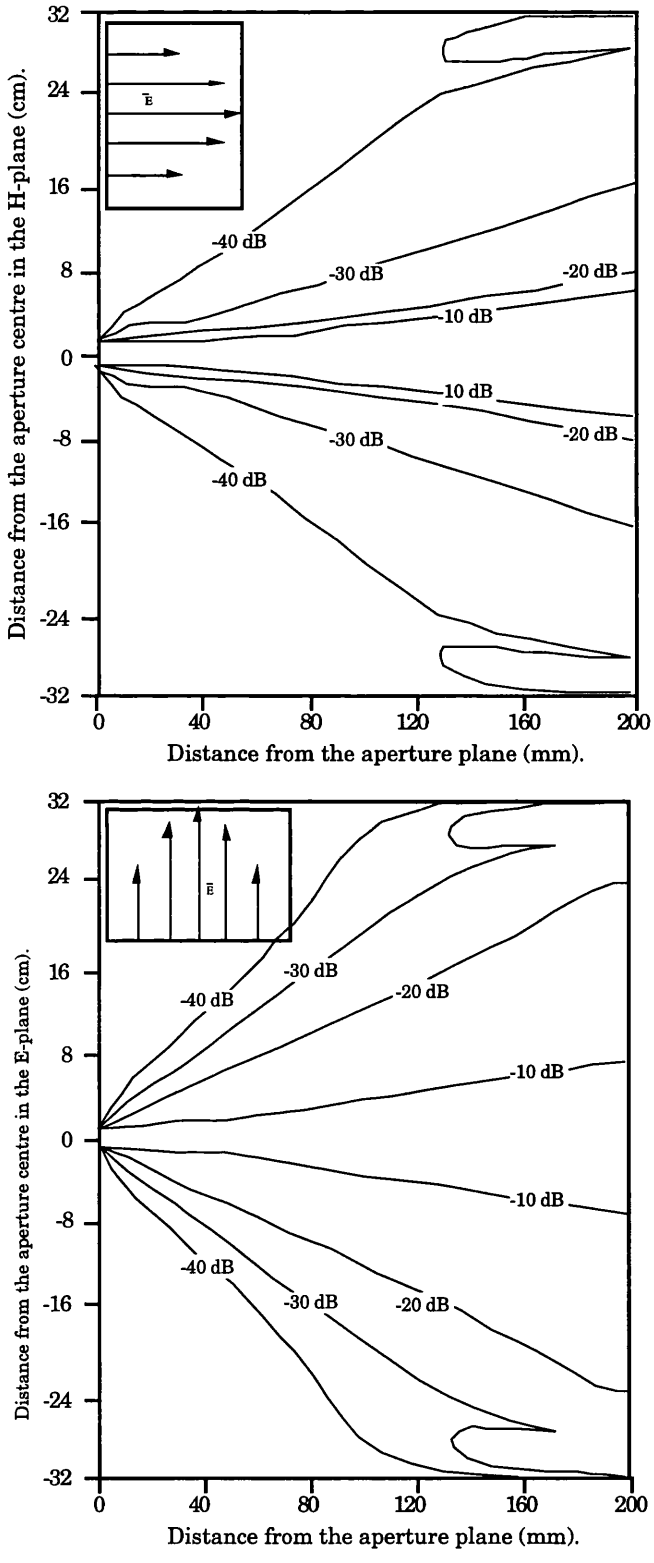

Figure A11.4 E-plane and H-plane contour mapping of the electric field for a square aperture (25x35 mm) at 30 GHz, converging beam.

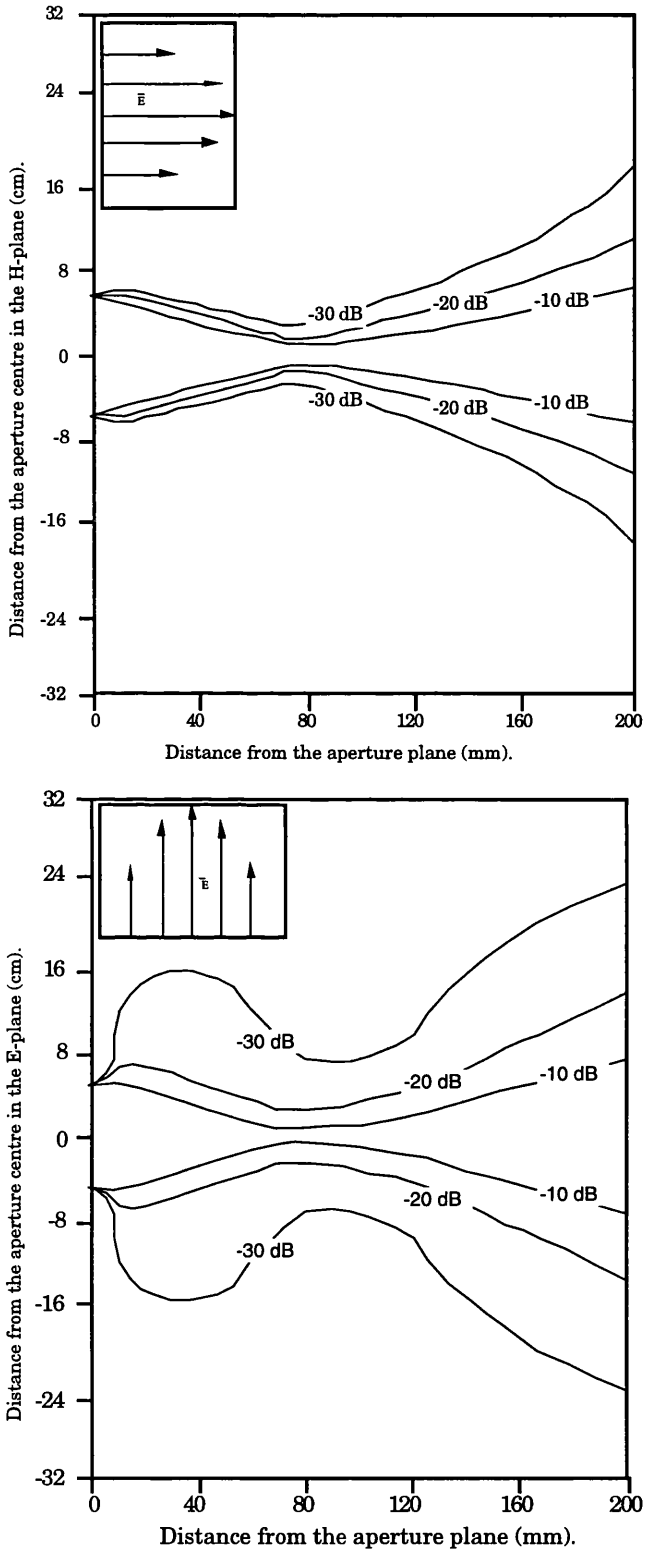

Figure A11.5 E-plane and H-plane contour mapping of the electric field for a square aperture (100x140 mm) at 30 GHz, converging beam.

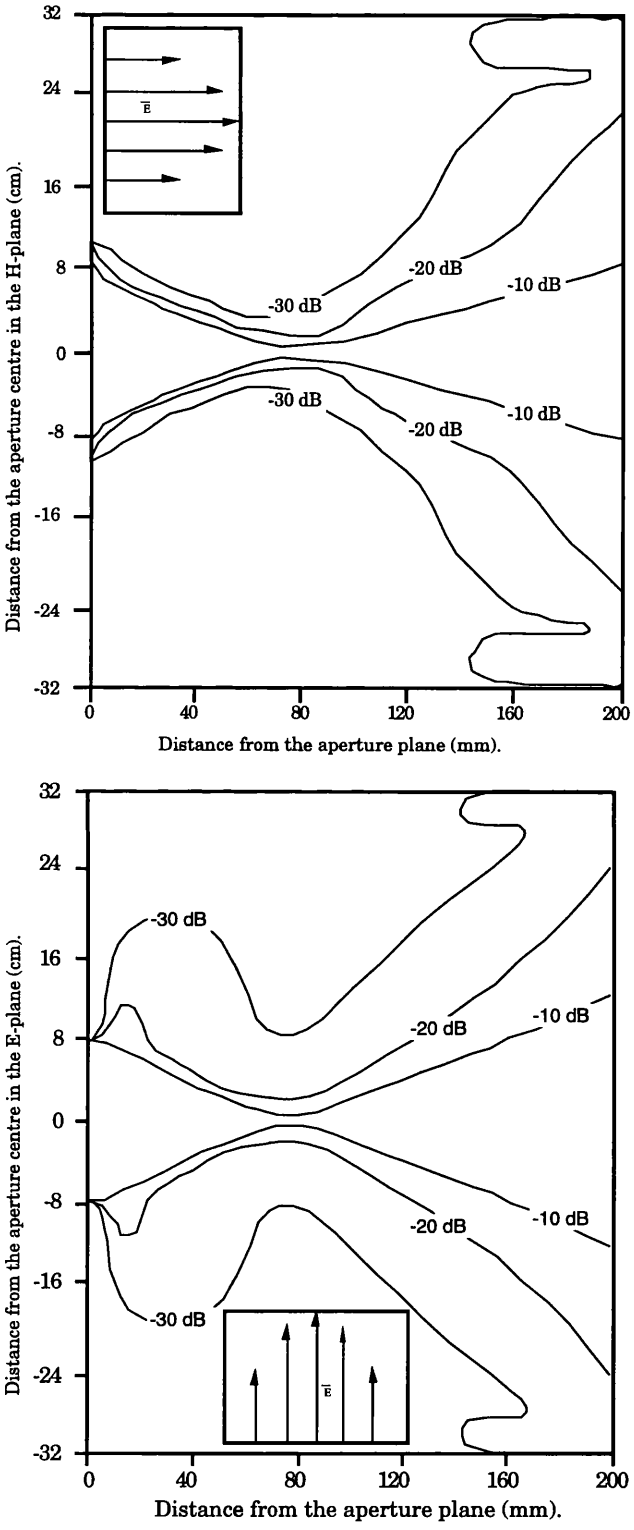

Figure A11.6 E-plane and H-plane contour mapping of the electric field for a square aperture (150x210 mm) at 30 GHz, converging beam.

Appendix 12

Partial differentials of ε_r and μ_r

A12.1 Introduction

In free-wave measurement, the complex permittivity and permeability of a slab can be calculated from four independent measurements. In the general case, ε_r and μ_r cannot be expressed by closed mathematical expressions. The error in ε_r and μ_r with respect to the error in the measured parameters are an important factor in evaluating the achievable accuracy and comparing the different free-wave methods. The aim of this appendix is to derive partial differentials of the material properties ($\delta\varepsilon_r$ and $\delta\mu_r$) with respect to the measured parameters, ($T_{t||}$, $T_{t\perp}$, $\Gamma_{t||}$, $\Gamma_{t\perp}$, θ, λ and d), which are used to calculate the total error in the measurement.

A12.2 Partial differentials of ε_r and μ_r

For a *thick* slab, the reflection and transmission coefficients at two orthogonal polarisations are given by equations (3) and (4). P is the propagation coefficient and is given by (5).

$$\Gamma_{||} = \frac{\sqrt{\varepsilon_r\mu_r - sin^2\theta} - \varepsilon_r cos\,\theta}{\sqrt{\varepsilon_r\mu_r - sin^2\theta} + \varepsilon_r cos\,\theta} \qquad ...(1)$$

$$\Gamma_{\perp} = \frac{\mu_r cos\,\theta - \sqrt{\varepsilon_r\mu_r - sin^2\theta}}{\mu_r cos\,\theta + \sqrt{\varepsilon_r\mu_r - sin^2\theta}} \qquad ...(2)$$

$$T_{f\parallel} = P\,(1-\Gamma_{\parallel}^2) \qquad \Gamma_{f\parallel} = \Gamma_{\parallel} \qquad \ldots(3)$$

$$T_{f\perp} = P\,(1-\Gamma_{\perp}^2) \qquad \Gamma_{f\perp} = \Gamma_{\perp} \qquad \ldots(4)$$

$$P = exp\left(\frac{-j\,2\pi d}{\lambda_O}\sqrt{\varepsilon_r\mu_r - sin^2\theta}\right) \qquad \ldots(5)$$

If multiple reflections within the slab are ignored (*thin* sample), the total transmission and reflection coefficients are given by equations (6) to (9).

$$T_{f\parallel} = \frac{P(1-\Gamma_{\parallel}^2)}{(1-P^2\Gamma_{\parallel}^2)} \qquad \ldots(6)$$

$$T_{f\perp} = \frac{P(1-\Gamma_{\perp}^2)}{(1-P^2\Gamma_{\perp}^2)} \qquad \ldots(7)$$

$$\Gamma_{f\parallel} = \frac{\Gamma_{\parallel}(1-P^2)}{(1-P^2\Gamma_{\parallel}^2)} \qquad \ldots(8)$$

$$\Gamma_{f\perp} = \frac{\Gamma_{\perp}(1-P^2)}{(1-P^2\Gamma_{\perp}^2)} \qquad \ldots(9)$$

A mathematical function can be expanded around a given point(a_1,a_2, ..., a_n) if all the higher order derivatives of the function are defined, (10). *Rn* is a function of the highest order of differentials with respect to x_1,x_2, ..., x_n. and can be ignored if (x_1-a_1), (x_2-a_2), ...and (x_n-a_n) are small.

$$f(x_1,x_2,\ldots,x_n) = f(a_1,a_2,\ldots,a_n)+(x_1-a_1)f_{x1}(a_1,a_2,\ldots,a_n)+(x_2-a_2)f_{x2}(a_1,a_2,\ldots,a_n) + \ldots+(x_n-a_n)f_{xn}(a_1,a_2,\ldots,a_n)+R_n \qquad \ldots(10)$$

For small changes in ε_r, μ_r, incident angle, thickness and frequency, the higher order differentials of transmission and reflection coefficients can be ignored. Therefore changes in transmission or reflection coefficient can be expressed as a function of the changes in the sample specifications, (11) and (14).

$$\delta T_{t\parallel} = \delta\varepsilon_r f_{1a}(\varepsilon_r, \mu_r, d, f, \theta) + \delta\mu_r f_{1b}(\varepsilon_r, \mu_r, d, f, \theta) + \delta d f_{1c}(\varepsilon_r, \mu_r, d, f, \theta) + \delta f f_{1c}(\varepsilon_r, \mu_r, d, f, \theta) + \delta\theta f_{1e}(\varepsilon_r, \mu_r, d, f, \theta) \quad ...(11)$$

$$\delta T_{t\perp} = \delta\varepsilon_r f_{2a}(\varepsilon_r, \mu_r, d, f, \theta) + \delta\mu_r f_{2b}(\varepsilon_r, \mu_r, d, f, \theta) + \delta d f_{2c}(\varepsilon_r, \mu_r, d, f, \theta) + \delta f f_{2d}(\varepsilon_r, \mu_r, d, f, \theta) + \delta\theta f_{2e}(\varepsilon_r, \mu_r, d, f, \theta) \quad ...(12)$$

$$\delta \Gamma_{t\parallel} = \delta\varepsilon_r f_{3a}(\varepsilon_r, \mu_r, d, f, \theta) + \delta\mu_r f_{3b}(\varepsilon_r, \mu_r, d, f, \theta) + \delta d f_{3c}(\varepsilon_r, \mu_r, d, f, \theta) + \delta f f_{3d}(\varepsilon_r, \mu_r, d, f, \theta) + \delta\theta f_{3e}(\varepsilon_r, \mu_r, d, f, \theta) \quad ...(13)$$

$$\delta \Gamma_{t\perp} = \delta\varepsilon_r f_{4a}(\varepsilon_r, \mu_r, d, f, \theta) + \delta\mu_r f_{4b}(\varepsilon_r, \mu_r, d, f, \theta) + \delta d f_{4c}(\varepsilon_r, \mu_r, d, f, \theta) + \delta f f_{4c}(\varepsilon_r, \mu_r, d, f, \theta) + \delta\theta f_{4e}(\varepsilon_r, \mu_r, d, f, \theta) \quad ...(14)$$

Regarding the combination of the parameters measured, various methods for calculating the material properties are devised. In the next parts, the mathematical expressions for calculating total error in $\delta\varepsilon_r$ and $\delta\mu_r$ for a given set of error in the measured parameters in different methods are derived. In this appendix, four different methods based on measuring $T\parallel \& T\perp$, $\Gamma\parallel \& \Gamma\perp$, $T\parallel \& \Gamma\parallel$, or $T\perp \& \Gamma\perp$ are taken into account. In each of these methods two sets of equations among (11) to (14) are used, and $\delta\varepsilon_r$ and $\delta\mu_r$ are worked out as functions of the other parameters, ($\delta T_{t\parallel}$, $\delta T_{t\perp}$, $\delta \Gamma_{t\parallel}$, $\delta \Gamma_{t\perp}$, $\delta\theta$, $\delta\lambda$ and δd).

A12.3 Transmission method

If the measured transmission coefficients at parallel and perpendicular polarisations are used to calculate the electric and magnetic properties of a sample, equations (15) and (16) give $\delta\varepsilon_r$ and $\delta\mu_r$ respectively. In derivation of differentials of permittivity and permeability equation (11) and (12) are used.

$$\delta\varepsilon_r = \frac{f_{20}.f_{18} - f_{17}.f_{21}}{f_{20}.f_{19} - f_{17}.f_{19}} \quad ...(15)$$

$$\delta\mu_r = \frac{f_{17}.f_{19} - f_{20}.f_{16}}{f_{17}.f_{18} - f_{21}.f_{16}} \quad ...(16)$$

$$f_1 = \frac{\cos\theta \,.\, (2\sin^2\theta - \mu_r.\varepsilon_r)}{(\sqrt{\mu_r.\varepsilon_r - \sin^2\theta})(\sqrt{\mu_r.\varepsilon_r - \sin^2\theta} + \varepsilon_r.\cos\theta)^2} \quad ...(17)$$

$$f_2 = \frac{\varepsilon_r^2.\cos\theta}{(\sqrt{\mu_r.\varepsilon_r - \sin^2\theta})(\sqrt{\mu_r.\varepsilon_r - \sin^2\theta} + \varepsilon_r.\cos\theta)^2} \quad ...(18)$$

$$f_3 = \frac{2.\varepsilon_r.(\mu_r.\varepsilon_r - 1).\sin\theta}{(\sqrt{\mu_r.\varepsilon_r - \sin^2\theta})(\sqrt{\mu_r.\varepsilon_r - \sin^2\theta} + \varepsilon_r.\cos\theta)^2} \quad ...(19)$$

$$f_4 = \frac{-\mu_r^2.\cos\theta}{(\sqrt{\mu_r.\varepsilon_r - \sin^2\theta})(\sqrt{\mu_r.\varepsilon_r - \sin^2\theta} + \mu_r.\cos\theta)^2} \quad ...(20)$$

$$f_5 = \frac{\cos\theta.(\mu_r.\varepsilon_r - 2.\sin^2\theta)}{(\sqrt{\mu_r.\varepsilon_r - \sin^2\theta})(\sqrt{\mu_r.\varepsilon_r - \sin^2\theta} + \mu_r.\cos\theta)^2} \quad ...(21)$$

$$f_6 = \frac{2.\mu_r.(1 - \mu_r.\varepsilon_r).\sin\theta}{(\sqrt{\mu_r.\varepsilon_r \sin^2\theta})(\sqrt{\mu_r.\varepsilon_r - \sin^2\theta} + \mu_r.\cos\theta)^2} \quad ...(22)$$

$$f_7 = \frac{-j.\pi.d.\mu_r.P}{\lambda_o(\sqrt{\mu_r.\varepsilon_r - \sin^2\theta})} \quad ...(23)$$

$$f_8 = \frac{-j.\pi.d.\varepsilon_r.P}{\lambda_o(\sqrt{\mu_r.\varepsilon_r - \sin^2\theta})} \quad ...(24)$$

$$f_9 = \frac{-j.2.\pi.d.P.\sin\theta.\cos\theta}{\lambda_o(\sqrt{\mu_r.\varepsilon_r - \sin^2\theta})} \quad ...(25)$$

$$f_{10} = \frac{j.2.\pi.d.P.\sqrt{\mu_r\varepsilon_r \sin^2\theta}}{\lambda_o^2} \quad ...(26)$$

$$f_{11} = \frac{-j.2.\pi.P.\sqrt{\mu_r.\varepsilon_r - \sin^2\theta}}{\lambda_o} \quad ...(27)$$

$$f_{12\,thin} = \frac{(1+\Gamma_{\parallel}^2 P^2)(1-P^2)}{(1-\Gamma_{\parallel}^2 P^2)^2} \qquad f_{12\,thick} = 1-\Gamma_{\parallel}^2 \quad ...(28)$$

$$f_{13\,thin} = \frac{2.P.\Gamma.(\Gamma_{\parallel}^2 - 1)}{(1-\Gamma_{\parallel}^2 P^2)^2} \qquad f_{13\,thick} = -2.P.\Gamma_{\parallel} \quad ...(29)$$

$$f_{14\,thin} = \frac{(1+\Gamma_\perp^2 P^2)(1-P^2)}{(1-\Gamma_\perp^2 P^2)^2} \qquad f_{14\,thick} = 1-\Gamma_\perp^2 \qquad ...(30)$$

$$f_{15\,thin} = \frac{2.P.\Gamma_\perp.(\Gamma_\perp^2-1)}{(1-\Gamma_\perp^2 P^2)^2} \qquad f_{15\,thick} = -2.P.\Gamma_\perp \qquad ...(31)$$

$$f_{16} = f_7.f_{12}+f_1.f_{13} \qquad ...(32)$$

$$f_{17} = f_8.f_{12}+f_2.f_{13} \qquad ...(33)$$

$$f_{18} = \delta T_{t\parallel}-\delta\theta.(f_{12}.f_9+f_{13}.f_3)-\delta\lambda_o.f_{12}.f_{10}-\delta d.f_{11}.f_{12} \qquad ...(34)$$

$$f_{19} = f_7.f_{14}+f_4.f_{15} \qquad ...(35)$$

$$f_{20} = f_8.f_{14}+f_5.f_{15} \qquad ...(36)$$

$$f_{21} = \delta T_{t\perp}-\delta\theta.(f_{14}.f_9+f_{15}.f_6)-\delta\lambda_o.f_{14}.f_{10}-\delta d.f_{11}.f_{14} \qquad ...(37)$$

A12.4 Reflection method

In the reflection method, the measurement of reflection coefficients at two orthogonal polarisations are used to calculate the complex permittivity and permeability of a sample. Similarly, the partial differentials of permittivity and permeability can be calculated in the transmission method. In this case, equations (13) and (14) are used in the derivation. $\delta\varepsilon_r$ and $\delta\mu_r$ are given by (15) and (16), but equation (28) to (31) should be replaced by (38) to (41). Equations (34) and (37) should also be replaced by (42) and (43).

$$f_{12\,thin} = \frac{2.P.\Gamma.(\Gamma_\parallel^2-1)}{(1-\Gamma_\parallel^2 P^2)^2} \qquad f_{12\,thick} = 0 \qquad ...(38)$$

$$f_{13\,thin} = \frac{(1+\Gamma_\parallel^2 P^2)(1-P^2)}{(1-\Gamma_\parallel^2 P^2)^2} \qquad f_{13\,thick} = 1 \qquad ...(39)$$

$$f_{14\,thin} = \frac{2.P.\Gamma_{\perp}.(\Gamma_{\perp}^2-1)}{(1-\Gamma_{\perp}^2P^2)^2} \qquad f_{14\,thick} = 0 \qquad ...(40)$$

$$f_{15\,thin} = \frac{(1+\Gamma_{\perp}^2P^2)(1-P^2)}{(1-\Gamma_{\perp}^2P^2)^2} \qquad f_{15\,thick} = 1 \qquad ...(41)$$

$$f_{18} = \delta\Gamma_{t\parallel}-\delta\theta.(f_{12}.f_9+f_{13}.f_3)-\delta\lambda_o.f_{12}.f_{10}-\delta d.f_{11}.f_{12} \qquad ...(42)$$

$$f_{21} = \delta\Gamma_{t\perp}-\delta\theta.(f_{14}.f_9+f_{15}.f_6)-\delta\lambda_o.f_{14}.f_{10}-\delta d.f_{11}.f_{14} \qquad ...(43)$$

A12.5 Transmission and reflection method

If transmission and reflection coefficients at parallel polarisation are used for calculating the sample properties, equations (11) and (13) can be used for finding $\delta\varepsilon_r$ and $\delta\mu_r$. In this case equations (28) to (31) should be replaced by (44) to (47). Equations (34) and (37) should be replaced by (46) and (47). If the measured transmission and reflection coefficients at perpendicular polarisation are used, equations (12) and (13) are used for calculating $\delta\varepsilon_r$ and $\delta\mu_r$ and (28) to (31) are modified to (48) to (51), and (34) and (37) should be replaced by (52) and (53).

$$f_{12\,thin} = \frac{(1+\Gamma_{\parallel}^2P^2)(1-P^2)}{(1-\Gamma_{\parallel}^2P^2)^2} \qquad f_{12\,thick} = 1-\Gamma_{\parallel}^2 \qquad ...(42)$$

$$f_{13\,thin} = \frac{2.P.\Gamma_{\parallel}.(\Gamma_{\parallel}^2-1)}{(1-\Gamma_{\parallel}^2P^2)^2} \qquad f_{13\,thick} = -2.P.\Gamma_{\parallel} \qquad ...(43)$$

$$f_{14\,thin} = \frac{2.P.\Gamma_{\parallel}.(\Gamma_{\parallel}^2-1)}{(1-\Gamma_{\parallel}^2P^2)^2} \qquad f_{14\,thick} = 0 \qquad ...(44)$$

$$f_{15\,thin} = \frac{(1+\Gamma_{\parallel}^2P^2)(1-P^2)}{(1-\Gamma_{\parallel}^2P^2)^2} \qquad f_{15\,thick} = 1 \qquad ...(45)$$

$$f_{18} = \delta T_{t\parallel} - \delta\theta.(f_{12}.f_9 + f_{13}.f_3) - \delta\lambda_o.f_{12}.f_{10} - \delta d.f_{11}.f_{12} \quad \ldots(46)$$

$$f_{21} = \delta\Gamma_{t\parallel} - \delta\theta.(f_{14}.f_9 + f_{15}.f_6) - \delta\lambda_o.f_{14}.f_{10} - \delta d.f_{11}.f_{14} \quad \ldots(47)$$

$$f_{12\,thin} = \frac{(1+\Gamma_\perp^2 P^2)(1-P^2)}{(1-\Gamma_\perp^2 P^2)^2} \qquad f_{12\,thick} = 1-\Gamma_\perp^2 \quad \ldots(48)$$

$$f_{13\,thin} = \frac{2.P.\Gamma_\perp.(\Gamma_\perp^2-1)}{(1-\Gamma_\perp^2 P^2)^2} \qquad f_{13\,thick} = -2.P.\Gamma_\perp \quad \ldots(49)$$

$$f_{14\,thin} = \frac{2.P.\Gamma_\perp.(\Gamma_\perp^2-1)}{(1-\Gamma_\perp^2 P^2)^2} \qquad f_{14\,thick} = 0 \quad \ldots(50)$$

$$f_{15\,thin} = \frac{(1+\Gamma_\perp^2 P^2)(1-P^2)}{(1-\Gamma_\perp^2 P^2)^2} \qquad f_{15\,thick} = 1 \quad \ldots(51)$$

$$f_{18} = \delta T_{t\perp} - \delta\theta.(f_{12}.f_9 + f_{13}.f_3) - \delta\lambda_o.f_{12}.f_{10} - \delta d.f_{11}.f_{12} \quad \ldots(52)$$

$$f_{21} = \delta\Gamma_{t\perp} - \delta\theta.(f_{14}.f_9 + f_{15}.f_6) - \delta\lambda_o.f_{14}.f_{10} - \delta d.f_{11}.f_{14} \quad \ldots(53)$$

Appendix 13

Total error simulation program

The total error in permittivity and permeability of a slab can be computed by a computer program. This program is based on calculating the partial differentials of permittivity and permeability ($\delta\varepsilon_r$ and $\delta\mu_r$) with respect to changes in the measured parameters, then integrating them over the required range. This method delivers good accuracy if $\delta\varepsilon_r$ and $\delta\mu_r$ are sufficiently small. In calculating the total error, the integration is carried out numerically. In order to keep the accuracy sufficiently high, $\delta\varepsilon_r$ and $\delta\mu_r$ are calculated for small $\delta\Gamma_t$, δT_t, $\delta\theta$, $\delta\lambda$ and δd. In practice, the transmission and reflection coefficients are measured in *dB* and *degree*. The calculation is based on derivations of $\delta\varepsilon_r$ and $\delta\mu_r$ presented in appendix 12. In calculating the total error, $\delta\Gamma_t$ and δT_t are complex numbers given equations (1) and (2).

$$\delta T_t = T_t\,(\,-0.30103\delta|\,T_t\,|+0.0174533j\delta\angle T_t\,) \qquad \ldots(1)$$

$$\delta \Gamma_t = \Gamma_t\,(\,-0.30103\delta\,|\Gamma_t|+0.0174533j\delta\angle\Gamma_t\,) \qquad \ldots(2)$$

$\delta|T_t|$ and $\delta|\Gamma_t|$ are the error in the magnitude of transmission and reflection coefficients expressed in dB. The error in the phases of transmission and reflection coefficients (in degree) are given by $\delta\angle T_t$ and $\delta\angle\Gamma_t$.

Appendix 14

Total error simulation results

In this appendix, the results obtained from simulating error sensitivity in the different free-wave methods are presented and discussed. The simulation is based on a computer program integrating $\delta\varepsilon_r$ and $\delta\mu_r$ for a given range of changes in the measured parameters. Since presenting the results as a set of curves is virtually impossible, the average rate of change in the material properties are listed to compare the error sensitivity in different techniques. In free-wave measurements the error mechanisms are quite complicated, and the error in μ_r and ε_r cannot be regarded a criteria in the error assessment. Therefore, the product of $\mu_r\varepsilon_r$ and ratio of ε_r/μ_r are considered as figures of merit in different methods.

The use of transmission coefficient at two polarisations for calculating the sample properties is referred as *Method 1*. In *Method 2,* reflection coefficients at two polarisations are used to calculate the complex permittivity and permeability of the sample. *Methods 3* and *4* are denoted to the cases that the sample properties are calculated from the measured transmission and reflection coefficients at parallel and perpendicular polarisations respectively.

Table TA14.1 shows the error sensitivity in sample 1 (ε_r=*2.6, d=10 mm*) treated as a *thick* slab. It can be concluded that the ratio of ε_r/μ_r can be measured more accurately than $\varepsilon_r\mu_r$ from the reflection measurement (*Method 2*). If the transmission and reflection coefficients in one polarization are used for calculating the permittivity and permeability of the slab (*Methods 3 and 4*), the error in the product of $\varepsilon_r\mu_r$ and the ratio of ε_r/μ_r are optimised. The results obtained from simulating the error sensitivity of sample 3 (ε_r=*7.5-j0.5*, μ_r=*0.8-j0.15* and *d=10 mm*) are shown in table TA14.2. Similarly, the same conclusion can be made for this sample.

	Method 1		*Method 2*		*Method 3*		*Method 4*	
	$\Delta(\varepsilon_r.\mu_r)$	$\Delta(\varepsilon_r/\mu_r)$	$\Delta(\varepsilon_r.\mu_r)$	$\Delta(\varepsilon_r/\mu_r)$	$\Delta(\varepsilon_r.\mu_r)$	$\Delta(\varepsilon_r/\mu_r)$	$\Delta(\varepsilon_r.\mu_r)$	$\Delta(\varepsilon_r/\mu_r)$
$\Delta\lvert T_{\parallel}\rvert$/dB	+0.1%	202%			0.008%	0.008%		
	2.58°	-3.1°			1.17°	0.28°		
$\Delta\angle T_{\parallel}$/1 °	-0.45%	-0.50%			0.308%	-0.075%		
	-0.08°	8.88°			0°	0°		
$\Delta\lvert T_{\perp}\rvert$/dB	-0.121%	-62.2%					0.008%	-0.008%
	-0.14°	0.04°					1.17°	-0.28°
$\Delta\angle T_{\perp}$/1 °	0.163%	0.662%					-0.308%	0.075%
	-0.076°	-8.68°					0°	0°
$\Delta\lvert \Gamma_{\parallel}\rvert$/dB			-10.8%	-2.98%	-0.0004%	6.05%		
			0°	0°	0.0375°	0.009°		
$\Delta\angle \Gamma_{\parallel}$/1 °			-0.016%	-0.018%	-0.008%	-0.039%		
			-0.008°	0.24°	-0.0004°	0.48°		
$\Delta\lvert \Gamma_{\perp}\rvert$/dB			7.43%	10.2%			-0.004%	21.4%
			0°	0°			0.36°	-0.086°
$\Delta\angle \Gamma_{\perp}$/1 °			1.2%	-0.074%			-0.082%	-0.13%
			3.1°	0.78°			-0.005°	1.58°
$\Delta\Theta$/1 °	0.67%	-3.9%	-6.44%	0%	-0.67%	2.98%	-0.67%	-2.58%
	-0.027°	-0.01°	0°	0°	0°	0°	0°	0°
ΔFreq/	-0.54%	0.26%			-0.536%	-0.128%	-0.536%	0.128%
100 MHz	0.002°	-0.001°			0°	0°	0°	0°
Δd/mm	-14%	9.3%			14%	-3.88%	-14%	4.04%
	0.084°	-0.06°			0°	0°	0°	0°

Table TA14.1 Simulated error in sample 1 (ε_r=2.6 d=10 mm) treated as a thick slab.

	Method 1		*Method 2*		*Method 3*		*Method 4*	
	$\Delta(\varepsilon_r.\mu_r)$	$\Delta(\varepsilon_r/\mu_r)$	$\Delta(\varepsilon_r.\mu_r)$	$\Delta(\varepsilon_r/\mu_r)$	$\Delta(\varepsilon_r.\mu_r)$	$\Delta(\varepsilon_r/\mu_r)$	$\Delta(\varepsilon_r.\mu_r)$	$\Delta(\varepsilon_r/\mu_r)$
$\Delta\lvert T_{\parallel}\rvert$/dB	-1.15%	234%			-0.158%	0.046%		
	2.9°	3.94°			0.81°	0.067°		
$\Delta\angle T_{\parallel}$/1 °	-0.512%	-2.12%			-0.214%	-0.018%		
	-0.124°	8.6°			-0.014°	-0.004°		
$\Delta\lvert T_{\perp}\rvert$/dB	0.313%	-60%					-0.16%	0.046%
	0.89°	-2.74°					0.81°	-0.06°
$\Delta\angle T_{\perp}$/1 °	0.38%	-0.568%					-0.214%	0.018%
	-0.012°	-8.72°					-0.014°	0.004°
$\Delta\lvert \Gamma_{\parallel}\rvert$/dB			-54.4%	11.8%	-00.174%	0.25%		
			5.34°	0.7°	0.308°	1.43°		
$\Delta\angle \Gamma_{\parallel}$/1 °			-6.02%	-0.254%	-0.0676%	-0.506%		
1°			-7.56°	8.84°	-0.016°	1.764°		
$\Delta\lvert \Gamma_{\perp}\rvert$/dB			-57.1%	29.2%			-0.433%	67%
			-164°	1.03°			1.15°	1.70°
$\Delta\angle \Gamma_{\perp}$/1 °			-10.4%	12.6%			-0.236%	-0.946%
			-0.5°	1.9°			-0.0468°	3.82°
$\Delta\Theta$/1 °	-0.214%	-8.52%	60%	0%	-0.276%	3.82%	-0.276%	-3.2%
	-0.194°	-0.434°	2.08°	0°	-0.04°	-0.058°	-0.04°	0.058°
Δf/	-0.61%	0.22%	%	%	-0.611%	-0.05%	-0.61%	0.053%
100 MHz	0.011°	0.05°	°	°	0.007°	-0.007°	0.008°	0.008°
Δd/mm	-16.1%	7.54%	%	%	-16.0%	1.64%	-16.0%	1.66%
	0.35°	1.57°	°	°	0.24°	-0.24°	0.241°	0.241°

Table TA14.2 Simulated error in sample 3 (ε_r=7.5-j0.5, μ_r=0.8-j0.15 and d=10 mm) treated as a thick slab.

In *thin* samples, the multiple reflections within the sample contribute to the reflected and transmitted waves. Therefore, the simple argument used in *thick* sample measurement is not entirely applicable for *thin* samples. The ratio of ε_r/μ_r mainly depends on the reflection coefficient from the front surface of the slab, Γ. Since the contribution of Γ to the total transmission and reflection coefficients is a function of material properties and the electrical length of the sample, the degree of dependence of the total reflection coefficient on the ratio of ε_r/μ_r changes with frequency and the material properties, chapter 7.

If the multiple reflections within the sample are ignored, transmission coefficient is mainly defined by P (propagation coefficient). P is mainly a function of $\varepsilon_r\mu_r$, but total reflection or transmission coefficient is a function of P and Γ. Tables TA14.3 shows the error sensitivity in sample 1 treated as a *thin* slab at the optimum thickness. As can be deduced from this table, total error increases if the multiple reflections within the slab are taken into account.

The expected error in sample 3 treated as a *thin* slab is shown in table TA14.4. The presented results in Tables TA14.3 and TA14.4 show that the product of $\varepsilon_r\mu_r$ can be measured more accurately than the ratio of ε_r/μ_r, while the ratio can also be measured relatively accurately from the reflection method. In this case, the measurement of transmission and reflection coefficients at one polarisation are less sensitive to error.

The error in the incident angle, frequency and the slab thickness can also cause error in the sample properties. In all cases except the reflection method in *thick* samples, the most significant impact of the error in the incident angle is on the ratio of ε_r/μ_r. In practice, the error in measuring the frequency or the sample thickness can be ignored.

	Method 1		*Method 2*		*Method 3*		*Method 4*	
	$\Delta(\varepsilon_r.\mu_r)$	$\Delta(\varepsilon_r/\mu_r)$	$\Delta(\varepsilon_r.\mu_r)$	$\Delta(\varepsilon_r/\mu_r)$	$\Delta(\varepsilon_r.\mu_r)$	$\Delta(\varepsilon_r/\mu_r)$	$\Delta(\varepsilon_r.\mu_r)$	$\Delta(\varepsilon_r/\mu_r)$
$\Delta\lvert T_{\parallel}\rvert$/dB	-2.97%	187%			0.58%	15.6%		
	2.12°	69.4°			1.11°	2.76°		
$\Delta\angle T_{\parallel}$/1°	-0.39%	-4.4%			-0.28%	-0.69%		
	-0.10°	9.44°			0.057°	0.9°		
$\Delta\lvert T_{\perp}\rvert$/dB	-0.08%	-64%					0.17%	58.3%
	-0.14°	1.6°					1.4.3°	15.7°
$\Delta\angle T_{\perp}$/1°	0.12%	-3.2%					-0.32%	-2.038%
	-0.094°	-8.8°					0.044°	2.62°
$\Delta\lvert\Gamma_{\parallel}\rvert$/dB			0.318%	1.49%				
1dB			-0.044°	-2.86°				
$\Delta\angle\Gamma_{\parallel}$/1°			0.01%	0.80%				
			0.028°	0.166°				
$\Delta\lvert\Gamma_{\perp}\rvert$/dB			-1.01%	-2.34%	0.04%	1.18%	0.46%	6.4%
1dB			0.23°	3.17°	0.005°	-2.26°	0.073°	-9.1°
$\Delta\angle\Gamma_{\perp}$/1°			-0.04%	-0.73%	-0.002%	0.61%	-0.036%	2.44%
			-0.088°	-0.176°	0.004°	0.126°	0.039°	0.81°
$\Delta\Theta$/1°	-0.67%	10.2%	-0.40%	6.38%	-0.67%	-2.68%	-0.62%	-3.76%
	-0.027°	-0.102°	0.174°	0.38°	-0.024°	-0.074°	-0.116°	-1.54°
ΔFreq/	-5.36%	0.313%	-0.55%	-0.26%	-0.53%	0.142%	-0.54%	0.25%
100 MHz	0.002°	0.009°	-0.01°	-0.01°	0.001°	0.005°	0.006°	0.07°
Δd/mm	-14%	11.6%	-14.4%	-7.78%	-14%	4.54%	-14.1%	7.92%
	0.1°	0.38°	-0.395°	-0.4°	-0.05°	0.2°	0.18°	2.4°

Table TA4.3 Simulated error in sample 1 (ε_r=2.6) treated as a thin slab.

	Method 1		*Method 2*		*Method 3*		*Method 4*	
	$\Delta(\varepsilon_r.\mu_r)$	$\Delta(\varepsilon_r/\mu_r)$	$\Delta(\varepsilon_r.\mu_r)$	$\Delta(\varepsilon_r/\mu_r)$	$\Delta(\varepsilon_r.\mu_r)$	$\Delta(\varepsilon_r/\mu_r)$	$\Delta(\varepsilon_r.\mu_r)$	$\Delta(\varepsilon_r/\mu_r)$
$\Delta\lvert T_{\parallel}\rvert$/dB	-0.4%	37%			0.652%	0.286%		
	0.25°	94.1°			0.375°	0.276°		
$\Delta\angle T_{\parallel}$/1°	-0.376%	-10.86%			-0.09%	-0.07%		
	-0.24°	10.48°			0.057°	0.02°		
$\Delta\lvert T_{\perp}\rvert$/dB	0.19%	-76.3%					0.61%	0.52%
	-1.04°	-7.11°					0.38°	0.45°
$\Delta\angle T_{\perp}$/1°	0.42%	-10.14%					-0.09%	-0.113%
	-0.21°	-12.9°					0.053°	0.038°
$\Delta\lvert \Gamma_{\parallel}\rvert$/dB			8.71%	74%	-0.277%	48.7%		
			7.51°	7.63°	0.471°	3.41°		
$\Delta\angle \Gamma_{\parallel}$/1°			-0.07%	-2.02%	-0.088%	-1.17%		
			1.36°	4°	-0.024°	2.72°		
$\Delta\lvert \Gamma_{\perp}\rvert$/dB			-8.8%	-42.4%			-0.96%	192%
			10.9°	-2.13°			1.92°	10.1°
$\Delta\angle \Gamma_{\perp}$/1°			-3.56%	-0.768%			-0.296%	-2.74%
			1.78°	-5.08°			-0.078°	5.56°
$\Delta\Theta$/1°	-0.21%	-11.12%	1.93%	11.76%	-0.254%	-3.18%	-0.252%	-3.12%
	-0.214°	-1.1°	1.53°	0.614°	-0.12°	0.03°	-0.174°	-0.034°
ΔFreq/	-0.62%	0.55%	-0.88%	-0.2%	-0.6%	0.05%	-0.612%	0.05%
100 MHz	0.015°	0.22°	-0.005°	-0.04°	0.009°	0.0085°	0.01°	0.01°
Δd/mm	-16.3%	16.2%	-20.4%	-6.08%	-16%	1.64%	-16.02%	1.6%
	0.4°	10.4°	2.01°	-0.062°	0.28°	0.26°	0.3°	0.3°

Table TA14.4 Simulated error in sample 3 (ε_r=7.5-j0.5, μ_r=0.8-j0.15 and d=10 mm) treated as a thin slab.

Appendix 15

Calculation methods

The aim of this appendix is to explain the process of calculating the sample properties from the measured parameters. In order to calculate the magnetic and electric properties of a specimen, a combination of four measurements of transmission and/or reflection coefficients at different polarisations, incident angles or thicknesses are required. Apart from some cases the complex permittivity and permeability of a sample cannot be expressed as functions of measured parameters explicitly, and the use of iterative numerical algorithms to find the best matched answer is inevitable. In the phase measurement the correct number of 180° is discarded, therefore a prior knowledge of the sample properties is required. If the number of measured data is more than the number of unknown, which is four for magnetic materials, an optimisation method should be used.

In the *transmission* method, the measured transmission coefficients at parallel and perpendicular polarisations ($T_{t||}$ and $T_{t\perp}$) are used to calculate the sample properties. The sample properties can be calculated from reflection coefficient at two polarisations ($\Gamma_{t||}$ and $\Gamma_{t\perp}$), *reflection* method. In the *magnitude only* method, the magnitudes of transmission and reflections at two polarisations ($|T_{t||}|$, $|T_{t\perp}|$, $|\Gamma_{t||}|$ and $|\Gamma_{t\perp}|$) are measured and the sample properties are calculated from these parameters. The phase of the transmission coefficient and the magnitude of the reflection coefficient are relatively less subject to error. These parameters ($|\Gamma_{t||}|$, $|\Gamma_{t\perp}|$, $\angle T_{t||}$ *and* $\angle T_{t\perp}$) can be used for determining the magnetic and electric properties of a slab specimen (*transmission phase-reflection magnitude*). The transmission and reflection coefficients at two polarisations (*eight data*) can be used for calculating the sample properties. In this method (*eight data*), the accuracy of the measured data is taken into account. In all the above mentioned techniques, determination of μ_r and ε_r are based on the numerical algorithms, except a few cases where ignoring the multiple reflections simplifies the calculation.

Complex permittivity and permeability of a slab can be expressed by closed mathematical expressions from the measured transmission and reflection coefficients at parallel or perpendicular polarisations ($T_{t||}$, $\Gamma_{t||}$ or $T_{t\perp}$, $\Gamma_{t\perp}$). Since this method (*transmission and reflection*) is not based on numerical iterative algorithms, the computation time is quite small and there is not a problem of converging to a wrong answer or diverging. In this technique, only the correct number of wavelengths in the sample is required. This number can be found from *a prior* knowledge or studying the rate of phase change in a frequency band for materials with rather constant properties.